# DEVELOPMENT AND INVESTIGATION OF IMPLANTABLE TABLETS FOR WOUND HEALING MODULATION AFTER TRABECULECTOMY

**Qian Ru**

**Thesis submitted as part fulfillment of the requirements for the degree of**

**DOCTOR OF PHILOSOPHY (PhD)**

**of University College London**

**UCL Institute of Ophthalmology 11-43 Bath Street**

**London EC1V 9EL**

**United Kingdom**

**May 2011**

# Plagiarism Statement

This thesis describes the research conducted at the UCL Institute of Ophthalmology, and the School of Pharmacy, University of London between October 2006 and October 2009 under the supervision of Prof. Peng T Khaw and Prof. Steve Brocchini. I certify that the research described is original and that any parts of the work that have been conducted in collaboration are clearly indicated. I also certify that the text printed in this thesis has been prepared by me and I have clearly indicated any part of this thesis that has appeared in publications.

Qian Ru

**01-09-2010**

**(Signature)** **(Date)**

# Abstract

Modulation of wound healing is required to inhibit scar formation after trabeculectomy. Mitomycin C and 5-fluorouracil (5-FU) are the anti-proliferative drugs currently used in the clinic. Their effectiveness is limited due to their toxicity and suboptimal local tissue pharmacokinetics caused by rapid clearance within the subconjunctival space. Therefore, prolonged release of anti-scarring agents is needed. Ilomastat is a matrix metalloproteinase inhibitor that has been shown to moderate favorably the wound healing response after surgery. However, due to rapid local tissue clearance, several injections are necessary in a clinically relevant animal model.

The thesis describes the development and investigation of implantable ocular tablets for wound healing modulation after trabeculectomy. A tablet would be placed in the subconjunctival space called a bleb, which is caused by the outflow through the fistula made during surgery. While the bleb volume varies, the tablet is thought to dissolve in non-sink conditions. Tablet dissolution was evaluated *in vitro* using a flow chamber that mimics the liquid outflow conditions of the bleb. The *in vitro* release studies suggest that tablet dissolution would act to prolong drug release in comparison with injections. Tablet dissolution in the subconjunctival space is affected by many factors including the physical/chemical properties of the drug and tablet, temperature, the volume and flow rate of the dissolution media, and the surface area of the tablet. The efficacy of an excipient-free ilomastat tablet was evaluated using a clinically validated rabbit model. The tablet dissolution was examined using molecular dynamics simulations to consider the molecular interactions of ilomastat and 5-FU undergoing dissolution in non-sink conditions. A mathematical model was also developed to describe the dissolution of excipient-free tablets in the non-sink conditions with 94% confidence. In conclusion, we have established methods to investigate and simulate dissolution of excipientless tablets in non-sink conditions within the subconjunctival space.

# Acknowledgments

Foremost, I would like to express my sincere gratitude to Prof. Peng T Khaw and Prof. Steve Brocchini, for giving me the opportunity to undertake the research on this fantastic project. Without their constant encouragement, support and guidance, I would not have been able to complete my PhD.

I would like to thank Dr. Mire Zloh for his invaluable guidance on the molecular dynamics simulation and computational mathematical model.

I would like to thank Prof. Guoxiong Wu, Mr. Qiang Sun, and Mr. Chung Li for their invaluable help, guidance and advice with the mathematical model.

I would like to thank Dr. Simon Gasford, Prof. Clive Roberts, Prof. Xinyong Chen, and Dr. David Scurr for their valuable help in thermal and surface analysis.

I would like to thank Mr.John Frost and, Mr.Phill Ball for their valuable help with the design and manufacture of the flow chamber and punch and die sets.

I also would like to thank Dr. Hardyal Gill,for his valuable support with HPLC studies.

Thanks also to all my colleagues, Dr. Stylianos Georgoulas, Mr. Daniel Paull, , Dr. James Ellis, Dr. Hala Fadda, Dr. Ashkan Khalili, and Dr. Sumit Dingra for their invaluable help, encouragement and support.

My sincere thanks to Fight for Sight and the Engineering and Physical Sciences Research Council (EPSRC) for the Dorothy Hodgkin Postgraduate Award which funded my fees and stipend for my PhD.

Last but not least, I would like to thank my parents, Mr. Peng Song, Mr. Zuohe Ru, and all other family members, for their love, support, and encouragement.

献给我最爱的人——

爸爸，妈妈，宋鹏。

# Table of contents

# List of Figures

***Chapter I***



***Chapter II***

***Chapter III***

# List of Tables

# List of Abbreviations Used

| | |
|---|---|
| AFM | Atomic force microscopy |
| ARVO | Association for research in vision and ophthalmology |
| ASA | Accessible surface area |
| BSS | BSS PLUS® sterile intraocular irrigating solution |
| ACN | Acetonitrile |
| $CO_2$ | Carbon dioxide |
| DEX | Dexamethasone |
| DLD | Delay line detector |
| DMSO | Dimethyl sulfoxide |
| DNA | Deoxyribonucleic acid |
| DPPC | Dipalmitoylphosphatidylcholine |
| DSC | Differential scanning calorimetry |
| DVS | Dynamic vapour sorption |
| ECM | Extracellular matrix |
| FBR | Foreign body reaction |
| FdUMP | Fluorodeoxyuridine monophosphate |
| FdUTP | Fluorodeoxyuridine triphosphate |
| FGM | Fibroblast growth media |
| 5-FU | 5-fluorouracil |
| FUTP | Fluorouridine triphosphate |
| GB/SA | Generalized born/ surface area |
| GFS | Glaucoma filtration surgery |
| HA | Hyaluronic acid |
| HBAs | Hydrogen bond acceptors |
| HBDs | Hydrogen bond donors |
| HCL | Hydrochloric acid |
| HPLC | High-performance liquid chromatography |
| HPLC-MS | High-performance liquid chromatography-mass spectrometry |
| HTFs | Human tenon’s fibroblasts |

| | |
|---|---|
| ILO | Ilomastat |
| IOP | Intraocular pressure |
| KCl | Potassium chloride |
| $KH_2PO_4$ | Monopotassium phosphate |
| LTP | Laser trabeculoplasty |
| MCMM | Monte carlo multiple minimum |
| MD | Molecular dynamics |
| MMC | Mitomycin c |
| MMP | Matrix metalloproteinase |
| MTT | 3-(4,5-dimethylthiazol-2-yl)- 2,5-diphenyl tetrazolium bromide |
| $Na_2HPO_4$ | Disodium hydrogen phosphate |
| NaCl | Sodium chloride |
| nanoLTA | Nano local thermal analysis |
| NaOH | Sodium hydroxide |
| NAP | Naproxen |
| NSAIDS | Non-steroidal anti-inflammatory drugs |
| NZW | New zealand white |
| OTC | Optical coherence tomography |
| PBS | Phosphate buffered saline |
| PCPP-SA | Bis (carboxyphenoxy) propane and sebacic acid |
| PGA | Poly(glycolic acid) |
| PLA | Poly(lactic acid) |
| PLGA | Copolymer of poly(lactic acid) and poly(glycolic acid) |
| POE | Poly (ortho ester) |
| PVA | Polyvinylalcohol |
| PVP | Polyvinylpyrrolidone |
| QDs | Quantum dots |
| RHC | High heating and cooling |
| RNA | Ribonucleic acid |
| TEA | Triethanolamine |

| | |
|---|---|
| TFA | Trifluoroacetic acid |
| TM | Tapping mode |
| Tof-SIMS | Time of flight secondary ion mass spectrometry |
| TRI | Triamcinolone |
| UV | Ultraviolet |
| W/W | Weight by weight |
| XPS | X-ray photoelectron spectroscopy |

# *Chapter I Introduction*

## 1.1. Anatomy of the eye and glaucoma filtration surgery (GFS)

### 1.1.1. Glaucoma

Glaucoma is the second leading cause of blindness in the world (Resnikoff et al. 2004). It is the term used for a group of diseases with a characteristic type of optic nerve damage with visual field loss. Damage to the optic-nerve can cause irreversible blindness (Schuman 2000). It was estimated that more than 60 million people worldwide would suffer from glaucoma in 2010; and this population will increase to approximately 80 million by 2020 (Quigley & Broman 2006). Hence, the development of glaucoma therapies is very important.

As glaucoma is often associated with high intraocular pressure (IOP, usually higher than 21 mm Hg), one of the aims of treatment is to lower the IOP, which is caused by the imbalance in the production and drainage of ocular fluid. The ocular fluid, which is also called aqueous humor, is produced by the ciliary body. It flows into the anterior chamber through the pupil, and then leaves the eye through the trabecular meshwork (shown as the "angle" in Figure 1.1). The blockage of this "angle" obstructs the exit of the aqueous outflow and leads to high IOP. Methods of lowering the IOP usually include reducing the production or enhancing the outflow of ocular fluid. These will be discussed in the following sections.

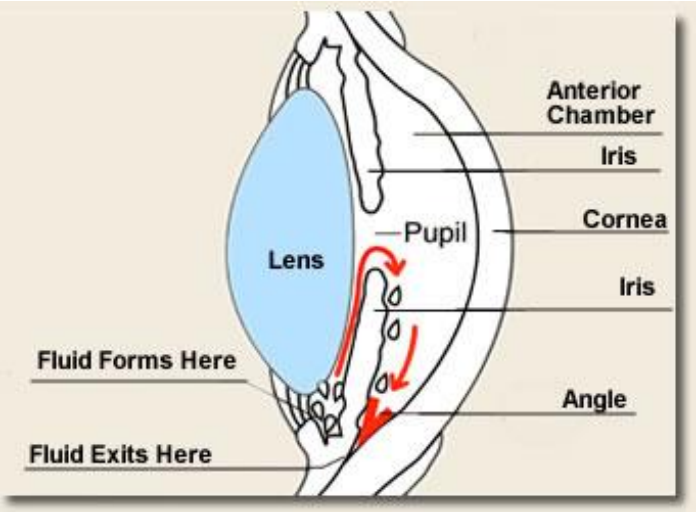


Figure 1.1. Normal intraocular fluid drainage from the eye. (Image from: www.kellyeyecenter.com/whatisglaucoma.htm)

### 1.1.2. Treatment of glaucoma

Treatment of glaucoma usually includes medication and surgery.

#### 1.1.2.1. Medication

Medical treatments of glaucoma lower IOP by reducing the production of the aqueous or enhancing uveoscleral/trabecular outflow. These medications include topical β-adrenergic antagonists (e.g. timolol, betaxolol), carbonic anhydrase inhibitors (e.g. dorzolamide, brinzolamide), cholinergics (e.g. pilocarpine), α-adrenergic agonists (e.g. brimonidine), prostaglandins (e.g. latanoprost, travoprost), and prostamides (bimatoprost) (Noecker 2006). Most of these medications are provided as topical eyedrops, with the exception of some carbonic anhydrate inhibitors that are given as oral tablets or intravenous injection (acetazolamide) (BNF 2009). Most of the glaucoma treatments start with eye drops. Surgery is required when eye drops are not effective enough in lowering the IOP.

#### 1.1.2.2. Surgical procedure

***Laser surgery***

Laser surgery, which is also called laser trabeculoplasty (LTP), is a non-invasive technique for lowering IOP that has been used for more than 30 years (Pollack & Patz 1976;Ticho 1977;Ticho & Zauberman 1976;Wise 1981;Wise & Witter 1979). The aim of LTP is to increase aqueous outflow from the trabecular meshwork to improve aqueous filtration and to lower the IOP. Originally argon lasers were most commonly used. In more recent years krypton, diode, excimer, and Nd:YAG lasers have been developed rapidly for LTP (Barkana & Belkin 2007;Wilmsmeyer et al. 2003). In early cases of open angle glaucoma, LTP treatment might be able to delay, decrease, or replace medical treatments. However, significant tissue disruption and coagulation damage caused by LTP can result in a mechanical stretching of the surrounding uveoscleral trabecular meshwork and widening of Schlemm's canal (Stein & Challa 2007). Rolim *et al* found that trabeculoplasty is less effective than trabeculectomy in controlling IOP at both six month and two year follow-ups. They also revealed that the effectiveness of LTP is less than contemporary medication (prostaglandin analogues, topical anhydrase inhibitors and alpha2-agnosts) and surgical techniques (Rolim, Paranhos, & Wormald 2007).

***Filtration surgery***

Glaucoma filtration surgery (GFS) is the most commonly used term in relation to the operation called trabeculectomy. It was first described about 50 years ago (Cairns 1968), and is still regarded as the "gold standard" for glaucoma surgery (Moura Filho & Sit 2009). The aim of the surgery is to open a new drainage channel for the outflow of aqueous humor through the sclera so that the aqueous humor can be eliminated from the conjunctiva (illustrated in Figure 1.2).

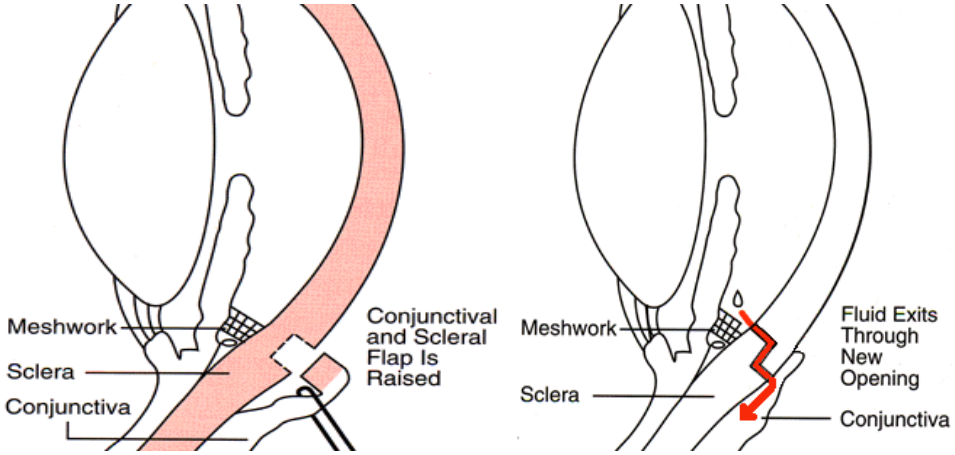


Figure 1.2. Mechanism of GFS in human eyes.

GFS in human eyes is further illustrated in Figure 1.3. (Reznick, Noecker, & Lathrop 2007). During this surgery, a pocket is firstly created under the conjunctiva. Then mitomycin C (MMC) or 5-fluorouracil (5-FU) soaked sponges are placed in the subconjunctival space for a few minutes. The reasons for using these sponges will be discussed later. Then a partial thickness scleral flap is dissected anteriorly into the peripheral corneal stroma. A window through the anterior chamber is opened by removing portion of sclera, Schlemm's canal, and trabecular meshwork. This step is called sclerostomy. Following sclerostomy, a small peripheral iridectomy is created to avoid iris incarceration in the opening. The scleral flap and the conjunctiva are then closed by sutures. Details of the surgery, such as the anesthetic, choice of limbal-based or fornix-based conjunctival flaps, and scleral flap shapes, may vary depending on the surgeons. After the surgery, visible accumulations of aqueous humor beneath the conjunctiva are expected to be observed in the subconjunctival space. This is called a bleb. The aqueous humor is excreting from the bleb (Figure 1.4. a). The surgery fails if

adequate flow cannot be achieved to maintain the IOP at a level to stop progression of glaucoma.

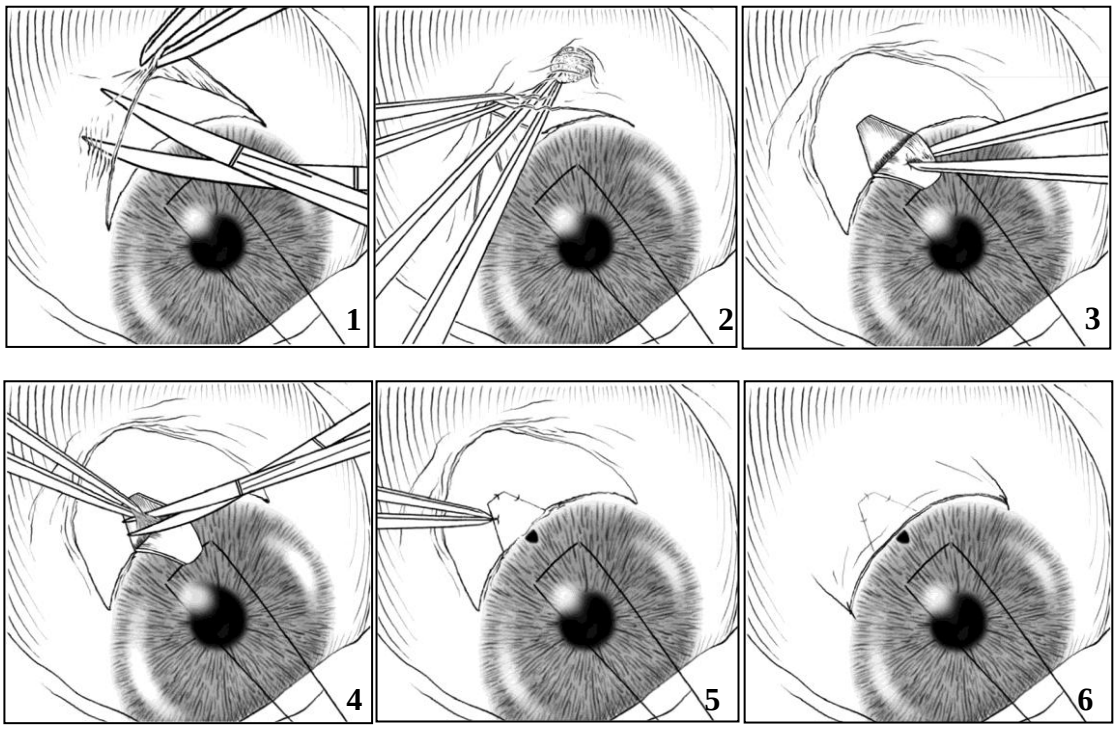


Figure 1.3. Illustration of trabeculectomy in human eyes, images are from *Reznick et al* (Reznick, Noecker, & Lathrop 2007). 1. An initial conjunctival dissection is performed to create large posterior pocket; 2. Mitomycin C or 5-FU soaked sponges are placed subconjunctivally away from the limbal region for about 2-3 minutes; 3. A half-thickness scleral flap is dissected anteriorly in the peripheral corneal stroma; 4. After creation of the sclerostony, a small peripheral iridectomy is created to prevent iris incarceration in the opening; 5. The scleral flap is secured by the sutures, and the knots buried to avoid possible erosion through the conjunctiva occurring later; 6. The conjunctiva is closed by sutures to provide tension at the limbus and avoid leaks postoperatively.

Despite complications such as hypotony, choroidal effusions, over filtration and endophthalmitis following the immediate period of the surgery, the long term success of surgery is closely associated with alterations in bleb morphology. Formation of scar tissue in the bleb is the main complication which obstructs the outcome of the aqueous humor and consequently leads to the failure of the surgery (Figure 1.4. b). Therefore, to improve the outcome of the surgery, the wound healing process in the bleb needs to be modulated. In order to find a drug that can inhibit scar formation in the bleb, a significant amount of research has been carried out. Currently MMC or 5-FU are used

clinically to stop/reduce the formation of scar tissue (Lama & Fechtner 2003).

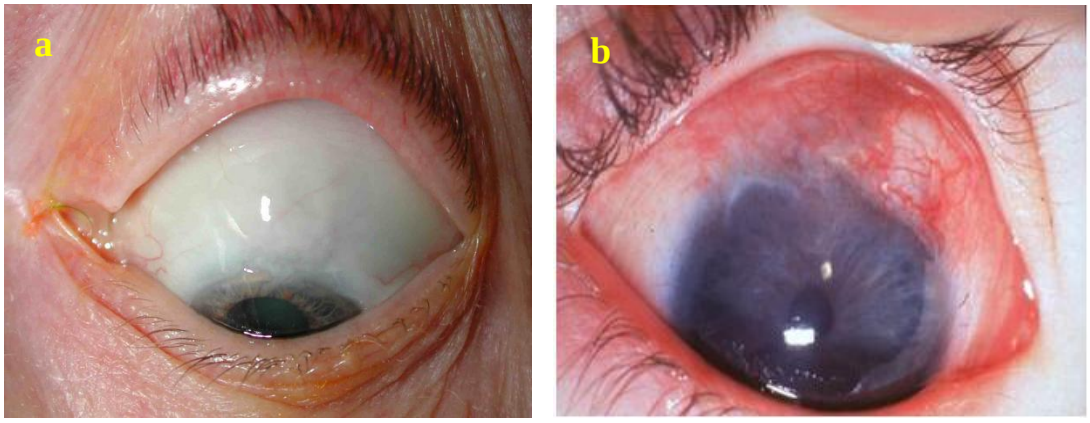


Figure 1.4. Bleb formation in the human eye after a successful (a) and failed (b) trabeculectomy. (Images from P T Khaw, Moorfields Eye Hospital, London)

However, the effectiveness of the current anti-scarring agents is limited due to their toxicity and associated side effects. Effectiveness is also severely compromised by the quick clearance of the drugs from the bleb area. Tissue pharmacokinetics are suboptimal because upon injection into the bleb area, the drug is quickly cleared at the subconjunctival space. Research has been carried out in recent decades with the aim of developing drugs and formulations that have a longer effect and lower toxicity. The effect of new drug candidates or formulations is usually evaluated using animal models including primates, rabbits and dogs (summarized in Appendix I). As the wound-healing response in rabbits is known to be usually fairly aggressive, it is believed that a rabbit model could be equivalent to high-risk eyes in humans, with surgical failure results within 1-2 weeks (Grisanti et al. 1999;Miller et al. 1989). Therefore, trabeculectomy on rabbits has become a clinically validated *in vivo* model for evaluating the effects of anti-scarring formulations (Khaw et al. 1993).

GFS in a rabbit eye is illustrated in Figure 1.5. Similar to the GFS in the human eyes, a conjunctival flap is first created. But instead of sclerostomy, a cannula is inserted through the sclera from 2 mm behind the limbus until it becomes visible under the cornea. Then the cannula is trimmed and fixed by sutures at the sclera end. Finally, the conjunctival incision is closed with sutures. The reasons for using a cannula in this

model are 1) the failure of sclerostomy can occur due to the aggressive healing process seen in rabbits and 2) the insertion of a cannula is also a relatively easy and consistent technique in comparison to sclerostomy, and is less difficult for in-experienced surgeons. In this model, the aqueous humor escapes though the cannula. Similar to GFS in human beings，the aqueous humor leaves the eye through the new subconjunctival space (bleb) created by the surgery. The morphology of the bleb often changes as healing and scarring occur and it can be affected by the effect of the anti-scarring and anti-inflammatory agents. A successful bleb in a rabbit eye is shown in Figure 1.6.

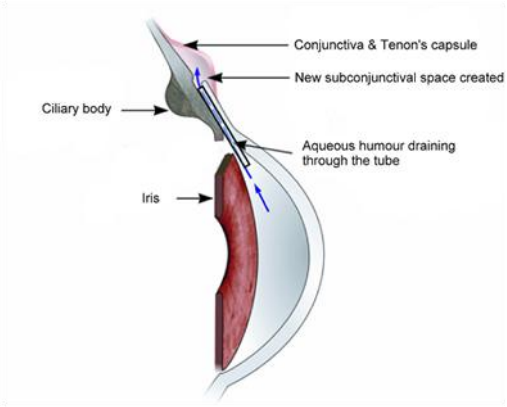


Figure 1.5. Illustration of trabeculectomy in a rabbit eye. (Image from www.blebs.net/html/introduction.html)

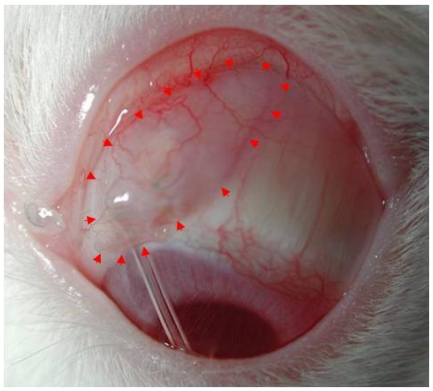

Figure 1.6. A successful bleb in a rabbit eye (circled by red arrows) (Georgoulas 2010) .

## 1.2. Wound healing in glaucoma filtration surgery

### 1.2.1. Wound healing pathway

As scar formation is part of the wound healing process, to inhibit the scar formation the wound healing pathways need to be understood. Wound healing is a complicated process that involves two distinct procedures. One is regeneration, which means the restoration of the original tissue structure without any trace of injury. Complete regeneration can only be achieved by tissues like the kidney, liver and other glandular organs (Benigni, Morigi, & Remuzzi 2010;Michalopoulos & DeFrances 1997). The other is replacement, which occurs in most tissue injury, and leads to the replacement of damaged cells by the formation of scar tissue at the site of restoration. As with skin, the healing process of the conjunctiva involves both replacement and regeneration (Lama & Fechtner 2003).

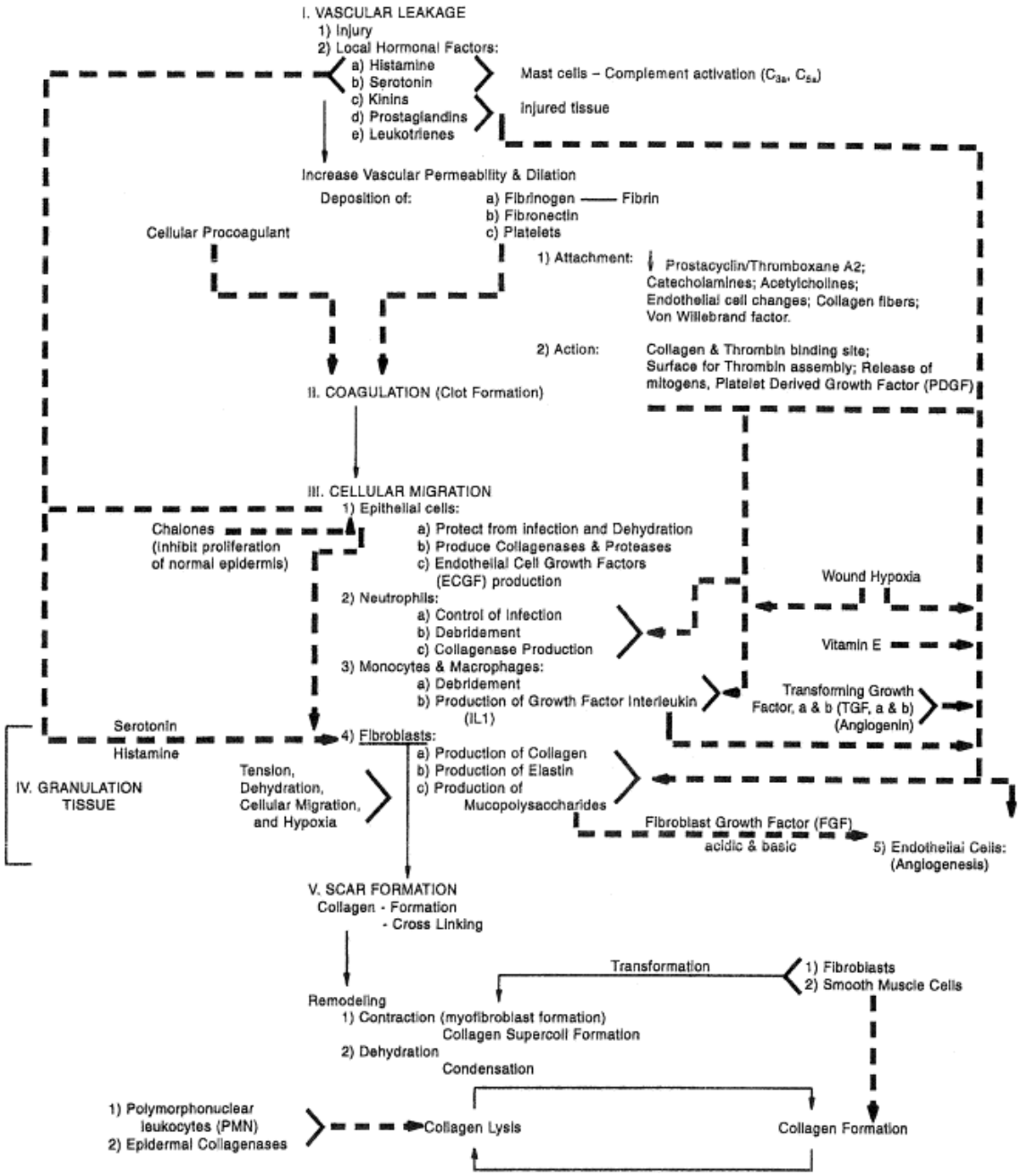


Figure 1.7. Flow chart of the wound healing pathway. (Reprinted from The Glaucomas, ed 2, 1996, with permission of Mosby) (Lama & Fechtner 2003;Tahery & Lee 1989)

The replacement process in wound healing includes several phases: coagulative and inflammatory, proliferative, and post- proliferative remodeling. As shown in Figure 1.7., each phase is associated with many cellular and humoral factors.

Following hemorrhage and tissue damage caused by injury, clotting factors and hormones are released (Lama & Fechtner 2003). The inflammatory phase then begins. The vascular permeability is increased by many local hormonal factors including

cytokines, growth factors, kinins, prostaglandins, leukotrienes, histamine, and serotonin. These factors act as chemo-attracttants to white blood cells (Albert & Jakobiec 2000). During this time, inflammatory cells, capillaries, and fibroblasts start to migrate to the fibrin-fibronectin matrix built at the injury site (Desjardins, Parrish II, & Folberg 1986;Dvorak 1986;Goodman, Alvarado, & Stern 1987;Seetner & Morin 1979). Many growth factors that stimulate cell migration, the production of matrix, and matrix degradation enzymes are produced by the inflammatory cells simultaneously (Cordeiro et al. 2000a). In this stage, steroids and non-steroidal anti-inflammatory drugs (NSAIDS) are used postoperatively to modulate tissue inflammation at the early stage of wound healing (Cordeiro et al. 2000b;Khaw et al. 2001).

In the proliferative phase, fibroblasts play a key role because they are the major producer of connective tissue including interstitial collagens, elastin, mucopolysaccharides, and glycosaminoglycans. The activity of fibroblasts increases to maximum at 3 to 5 days after injury and then starts to decrease afterwards (Albert & Jakobiec 2000). Budding and expansion of existing vascular endothelial cells lead to angiogenesis. The granulation tissue, which is composed of young fibrovascular connective tissue, is formed (Desjardins, Parrish II, & Folberg 1986;Dvorak 1986). The wound is finally closed by reepithelialization and contraction of myofibroblasts (Albert & Jakobiec 2000). However, the wound closure does not mean the deactivation of fibroblasts. In the remodeling phase, fibroblasts fabricate matrix metalloproteinases (MMPs), which plays an important role in the process of tissue remodeling and contraction (Cordeiro et al. 2000a;Daniels et al. 2003). Hence, anti-fibrotic agents are used in the proliferative and post-proliferative phases to inhibit scarring after GFS.

### 1.2.2. Clinical drugs for wound healing modulation

The varied types of cellular and humoral factors involved in the wound healing process suggest that there are many different ways to modulate the wound healing response. Cordeiro *et al* summarized the agents that could be used to modulate the wound healing process at different phases after GFS (Figure 1.8.) (Cordeiro et al. 2000b). A comprehensive list of wound healing modulation targets for GFS has been summarized

recently (Khaw P et al. 2009).

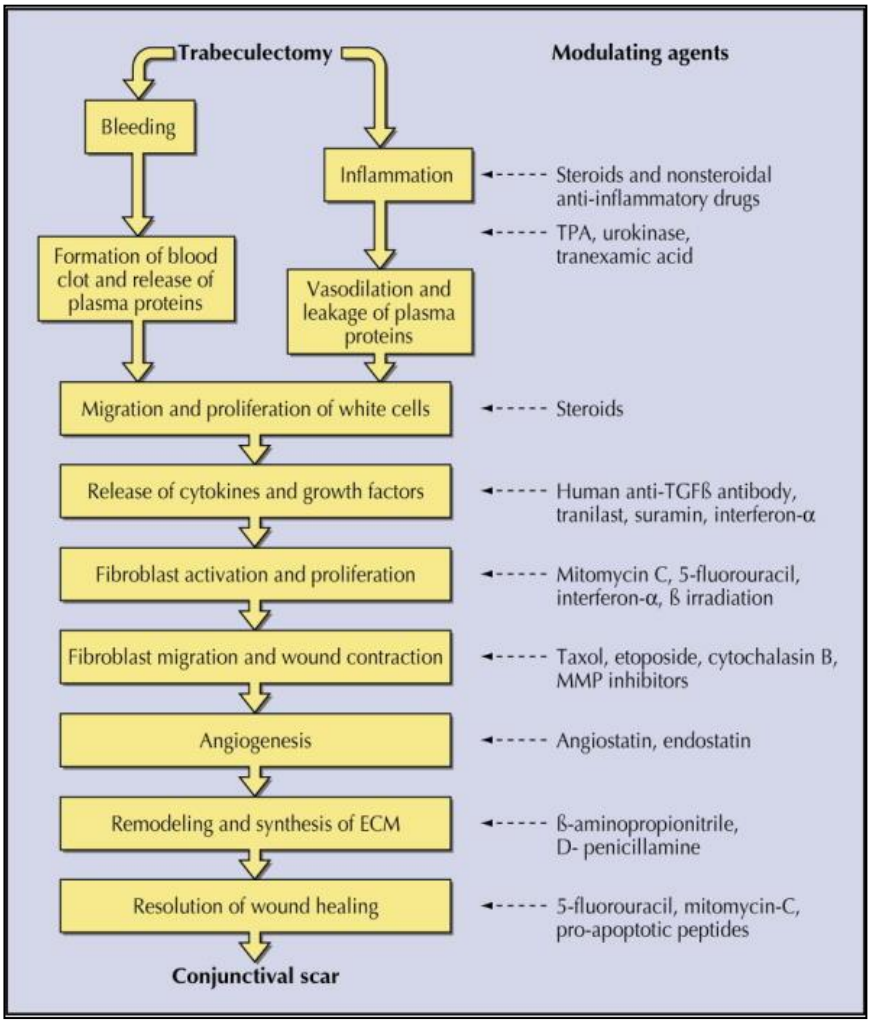


Figure 1.8. Targets for wound healing modulation following glaucoma trabeculectomy (Cordeiro et al. 2000b).

Although there is a list of wound healing modulation agents, currently there is no licensed medicine that is registered to treat fibrosis in the eye. 5-FU (Figure 1.9) and mitomycin C (MMC, Figure 1.10) are the most commonly used two drugs after GFS (Palanca-Capistrano et al. 2009;Singh et al. 1997;Wollstein et al. 2000;Wudunn et al. 2002). They are both toxic anti-cancer drugs that administered to inhibit fibroblast proliferation, with a narrow therapeutic window.

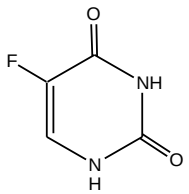


Figure 1.9. Chemical structure of 5-FU.

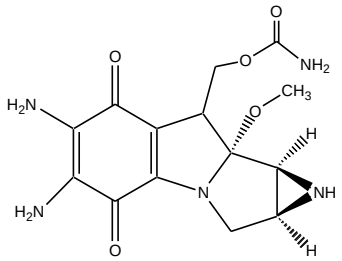


Figure 1.10. Chemical structure of MMC.

***5-Flurouracil (5-FU)***

5-FU (2, 4-Dihydroxy-5-fluoropyrimidine, Mw: 130.08 g/mol) is a fluorinated pyrimidine analog which act as a thymidylate synthase inhibitor. Its aqueous solubility is 11.1 mg/mL (pH 4.0, 22 ℃) (Yalkowsky & He 2003). After being converted intracellularly, it has three main metabolites: fluorodeoxyuridine monophosphate (FdUMP), fluorodeoxyuridine triphosphate (FdUTP) and fluorouridine triphosphate (FUTP). These metabolites inhibit thymidylate synthase and disrupt DNA/RNA synthesis in the cells (Longley, Harkin, & Johnston 2003).

***Mitomycin C (MMC)***

MMC (Mw: 334.33 g/mol) is an antibiotic agent derived from the soil fungus *Streptomyes caespitosus* by Wakaki in 1958. It is 10 times less soluble than 5-FU (0.912 mg/mL) (Yalkowsky & He 2003). It blocks DNA synthesis, inhibits cell mitosis, and causes cell cycle arrest by producing cross-linking of the DNA molecules between adenine and guanine.

Both 5-FU and MMC are anti-proliferative compounds, but 5-FU leads to less direct DNA damage than MMC and is more cell cycle specific (Crowston et al. 1998;Falck, Skuta, & Klein 1992;Gilman AG, Rall TW, & Nies AS 1990). They are both used intraoperatively for GFS in the clinic. Currently sponges soaked with MMC (0.2-0.5 mg/mL for 2-3 minutes) or 5-FU (50 mg/mL for 5 minutes) were placed in the subconjunctival space then removed before the closure of conjunctival flap (Palanca-Capistrano et al. 2009;Singh et al. 1997;Wollstein et al. 2000;Wudunn et al. 2002). Many researchers have compared the effectiveness of these two compounds. For

a five minute intraoperative application, it is generally believed that these drugs have comparable efficacy (Palanca-Capistrano et al. 2009;Singh et al. 1997;Wollstein et al. 2000;Wudunn et al. 2002). However, the effectiveness of 5-FU may be more transient than MMC (Khaw et al. 1993). But MMC is more toxic than 5-FU as MMC was shown to be toxic to vascular endothelial cells (Smith, D'Amore, & Dreyer 1994) and ciliary body (Levy et al. 2001;Mietz 1996;Schraermeyer et al. 1999). In addition, it was suggested that MMC might led to an over expression of MMPs, thus causing abnormal remodeling of the scleral matrix (Hanyu 1999).

### 1.2.3. The limitation of current therapeutics

There are many factors that are related to the success of GFS. Preoperative factors (include previous topical therapy, race, age, uveitis, anterior segment neovascularization *etc*) are associated with the outcome of the surgery, and surgical techniques (Jones, Clarke, & Khaw 2005), the use of anti-inflammatory agents, fibrinolytics and anti-proliferative agents (Atreides, Skuta, & Reynolds 2004) are also important. Although highly skilled surgery followed by the application of anti-inflammatory agents has increased the success rate of GFS, maintaining the morphology of the bleb is vital for the long term halt in the progression of glaucoma. However, the efficacy of the two drugs (5-FU and MMC) most often used clinically is limited due to their toxicity, narrow therapeutic window, and short retention time.

It was reported that about 80% of trabeculectomies need bleb manipulation after GFS, even when a five minute application of MMC or 5-FU was applied intraoperatively (King et al. 2007). Almost half of blebs require massage or tissue removal. One third of the patients need at least one 5-FU injection and a quarter requires at least one needling plus one 5-FU injection. On average, the first intervention for massage, structure removal, 5-FU injection and needling plus 5-FU injection were carried out on days 1, 14, 14 and 43 respectively (King et al. 2007). This indicates that a few minutes application of 5-FU or MMC is not sufficient to maintain the long term outcome of GFS. However, the improvement offered by the use of these medicines does suggest that more extended periods of exposure of the drug to the bleb area may be advantageous. Clearly if this is

to be accomplished, it may be necessary to use less toxic drugs with larger therapeutic windows.

The need for multiple subconjunctival injections of 5-FU after GFS indicates that the residence time of 5-FU or MMC administrated during surgeries short and that the pharmacokinetics of subconjunctival injection are suboptimal. It has been reported that 5-FU reached its peak concentration 30 minutes after subconjunctival injection, and that the 5-FU concentration decreased by more than 10 times after one hour (Rootman, Ostry, & Gudauskas 1984).

Since the intraoperative plus the post operative applications of 5-FU or MMC do not provide ideal long term effects on scar inhibition, new anti-scarring medicines are needed to provide longer term residence time in the bleb and to lower the drug toxicity.

## 1.3. Development of prolonged release drug delivery systems for GFS

### 1.3.1. Analysis of the bleb

A bleb refers to all the structural elements that define an area of subconjunctival filtration of aqueous humor. To develop an anti-scarring drug which will be placed in the subconjunctival space, it is important to understand the conjunctiva, the bleb, and the aqueous humor.

The conjunctiva is a thin, transparent membrane which has a sponge like structure. It is usually divided into three layers. The outer epithelium is the first layer, which is a permeability barrier. The layer in the middle is substantia propria which contains nerves, lymphatics and blood vessels. The inner layer, which attaches to the sclera, is called submucosa or Tenon’s capsule (Sunkara & Kompella 2003). The aqueous in the bleb escapes through conjunctival vascular channels, lymphatics, and transconjunctival egress (Azuara-Blanco & Katz 1998).

Bleb morphology indicates the function of the bleb. It is associated with the surgical

complications and changes considerably after GFS. The preferred appearance is with moderate elevation, paucity of vessels, large surface area, the absence of a distinct demarcation between filtering and non-filtering areas, and the presence of conjunctival microcysts (Filippopoulos et al. 2009;Picht & Grehn 1998). The morphology and function of the bleb as well as the aqueous pathway can be investigated *in vivo* using confocal microscopy (Amar et al. 2008;Guthoff et al. 2006;Labbe et al. 2005). In histology, clear intraepithelial spaces between morphologically normal epithelial cells and clear spaces within loose subepithelial connective tissue, which are referred to as microcysts, were observed in functional blebs, and loosely arranged connective tissue was observed by confocal microscopy. In contrast, non-functioning blebs showed fewer intraepithelial microcysts and denser subepithelial connective tissue. Observations from confocal microscopy have shown that successful blebs in the early postoperative stage have some features including a trabecular connective tissue pattern, a high density of stromal cystic spaces, numerous stromal round cells, and small vessel diameters (Guthoff et al. 2006).

The estimated bleb volume can vary. New techniques, such as 3-D optical coherence tomography (OCT), have been used to evaluate the bleb volume. However, some of the results do not seem to be accurate enough. Kawasaki et al have reported that the bleb volume evaluated by OCT is approximately 6.27 $mm^3$ (Kawasaki et al. 2009). As this volume is similar to the volume of some of the inserts listed in Appendix I, it is believed that the bleb volume is larger than the results reported above. Theelen *et al* haves reported a more reasonable bleb volume which is approximately 50-100 μl (Theelen et al. 2007). The average temperature of bleb in good and poor controlled IOP eyes are 35.4 and 35.8 ℃ respectively (Kawasaki et al. 2009).

Table 1.1 Inorganic and organic substances of the anterior aqueous humor in humans and rabbits. (Kaufman P.L. & Alm A. 2003)

| **Substances** | | **Human** | **Rabbit** | **PBS** |
|---|---|---|---|---|
| Inorganic substances | Bicarbonate (μmol/mL) | 20.2 | 27.7-33.6 | |
| | Chloride (μmol/mL) | 131.0 | 105.1-105.77 | 4.15 |
| | Oxygen (mm Hg) | 53 | 30-55 | |
| | Phosphate (μmol/mL) | 0.62 | 0.86-0.89 | 9.57 |
| | Calcium (μmol/mL) | | 1.7 | |
| | Potassium (μmol/mL) | | 5.1-5.2 | 4.15 |
| | Magnesium (μmol/mL) | | 0.8 | |
| | Hydrogen ion (pH) | | 7.6 | |
| | Sodium (μmol/mL) | | 143-146 | 153.2 |
| Organic substances | Ascorbate (μmol/mL) | 1.06 | 0.96 | |
| | Citrate (μmol/mL) | 0.12 | 0.38-0.46 | |
| | Glucose (μmol/mL) | 2.8 | 4.9-6.9 | |
| | Hyaluronate (μg/mL) | 1.1 | | |
| | Lactate (μmol/mL) | 4.5 | 9.3-12.1 | |
| | Protein (mg/100ml) | 23.7 | 25.9 | |
| | Creatinine (μmol/mL) | | 0.11 | |
| | Urea (μmol/mL) | | 6.3-7.0 | |

The aqueous humor is composed of many organic and inorganic substances (summarized in Table 1.1). It also contains more than 10 different amino acids (Kaufman P.L. & Alm A. 2003). From Table 1.1 it can be seen that aqueous humor of rabbits is similar to that of humans. However, compared to the human or rabbit aqueous humor, PBS has higher concentration of ions. An OXOID PBS tablet contains NaCl (8.0g/L), KCl (0.2g/L), $Na_2HPO_4$ (1.14g/L), and $KH_2PO_4$ (0.2 g/L). These ions therefore lead to the high ion strength of PBS (0.165). Therefore, theoretically PBS is not an ideal buffer for the *in vitro* investigation of the formulation. But in the literature, it is the most frequently used buffer in the *in vitro* studies of ocular drugs (See Appendix I). This is because PBS is easy to be made and stable in room/body temperature. The rabbit aqueous contain more types of organic and inorganic substances than humans aqueous. Aqueous humor has a pH of 7.6 (Maren 1973). In normal human eyes, the average flow rate of aqueous humor is between 2.2-3.1 μL/min (McLaren 2009). The aqueous flow decreases with the age by approximately 4% per decade of life (Brubaker, Nagataki, & Townsend 1981;Toris et al. 2002). The aqueous appears to have the highest flow rate in the morning and decreases to almost half of the rate during sleep (Koskela

& Brubaker 1991;Reiss et al. 1984). But it does not vary much during the day time. It is also known that the aqueous flow appears to be independent of transient changes in intraocular pressure but it can be suppressed by some pharmacological agents. In abnormal eyes with different intraocular pressure, the aqueous flow rate does not seem to be affected significantly (McLaren 2009).

### 1.3.2. Ocular drug delivery

To develop a prolonged release anti-fibrotic drug for GFS, ocular drug delivery systems must be understood. Drug transportation in the eye is fairly restricted because the eye is well protected by several membrane barriers including the cornea, conjunctiva, iris-ciliary body, lens epithelium, and retina. Hence, ocular drug delivery is a big challenge in pharmaceutical science.

An ideal ocular drug delivery system should be able to deliver the drug to the targeted site with a defined range of therapeutic concentration without causing permanent tissue damage. Additionally, the residential time of the drug needs to be maintained for a certain period to achieve its pharmacological effects without causing any severe toxic/side effects. Ocular drugs can be delivered by topical administration (eye drops, ointments, contact lenses, and some ocular devices), systemic administration, periocular/intraocular injections, and ocular inserts. Topical administration is the most straightforward and convenient way of ocular drug delivery. However, it is well known that the majority of the drug delivered by this way is eliminated through nasolacrimal drainage. Drugs delivered systemically barely reach the eye due to the presence of blood-retinal barrier. Additionally, there can be undesirable systemic side effects.

Ocular drug delivery usually targets either the anterior segment (the cornea, iris, ciliary body, and lens) or the posterior segment (the vitreous humor, retina, choroid, and optic nerve) of the eye. For the targeted sites like subconjunctival space or the vitreous body, injections or inserts are the most direct approach for delivering the drug. But the local drug pharmacokinetics in these two parts of the eye are different. Due to the gel like structure of the vitreous body, the diffusion and movement of the drug molecules are

restricted. While in the subconjunctival space, the flow of the aqueous humor promotes the release and diffusion of the drug. Therefore, the half lives of the intravitreally delivered drugs are usually longer (hours or days) than the subconjunctival injections. Delivery of 5-FU by subconjunctival injections is not ideal because 1) the drug is delivered in a small volume (100 μl) with high concentration (50 mg/mL) which can lead to severe toxicity effects to the eye and 2) the drug residence time is short. Therefore, a prolonged release anti-scarring drug is highly desirable. The drug is ideally delivered as a semi-solid/solid insert with excellent biocompatibility which can be placed in the subconjunctival space. However, a recent review on ocular drug delivery systems has shown that most of the clinically used ocular inserts are designed either for the conjunctival sac or for the vitreous cavity. Few of them are designed specifically for subconjunctival space (Kearns & Williams 2009).

### 1.3.3. Development of prolonged release drug delivery systems for anti-scarring agents post GFS

Many research groups have tried to develop prolonged release anti-scarring agents that can be placed in the subconjunctival space (summarized in Appendix I). These drugs were incorporated in different drug carriers include liposomes, collagen sponges, matrix disks/pellets containing various polymers and injectable microspheres or semi-solid materials. The duration of the drug release time varies from days to months. However, most of these studies were at the preclinical stage with exception of Surodex (Chang et al. 1999;Kimura & Ogura 2001;Seah et al. 2005;Tan et al. 1999).

Polymers that have been frequently used include polyanhydride, poly (ortho ester) (POE), poly (lactic acid) (PLA), poly (glycolic acid) (PGA), and their copolymers (PLGA). Polyanhydride and POE usually undergo a surface erosion process when releasing the drugs. PLA, PGA, and PLGA are the polymers that release the drug through bulk erosion (Kimura & Ogura 2001). These polymers are used in many local administrated dosage forms including viscous solutions, particle systems, and semi-solid/solid dosage forms. They can improve the therapeutic efficacy by controlling drug release, prolonging drug retention, reducing the dosage frequency and hence

reducing the transient overdose, enhancing drug bioavailability, and reducing the systemic side effects.

Polyanhydrides with different molecular weight are synthesized by different methods. One of the typical high molecular weight polyanhydride is synthesized using bis (carboxyphenoxy) propane and sebacic acid (PCPP-SA) (Rabowsky et al. 1996). The ratio of the two monomers is highly related to the breakdown of the polymer. The hydrolysis and metabolism of PCPP-SA are shown in Figure 1.11. Since the breakdown products of PCPP-SA are acids, it can be seen that polyanhydride degradation can be slower in acidic medium. Bioerodible disks which are made of polyanhydride (diameter 3 mm thickness 1 mm) containing daunorubicin for GFS were developed by Rabowsky *et al* (Rabowsky et al. 1996). They found that by day 13 around 90% of control blebs failed, and in comparison only 20% of daunorubicin treated blebs failed. However, conjunctival erosions were observed in some of the daunorubicin treated eyes.

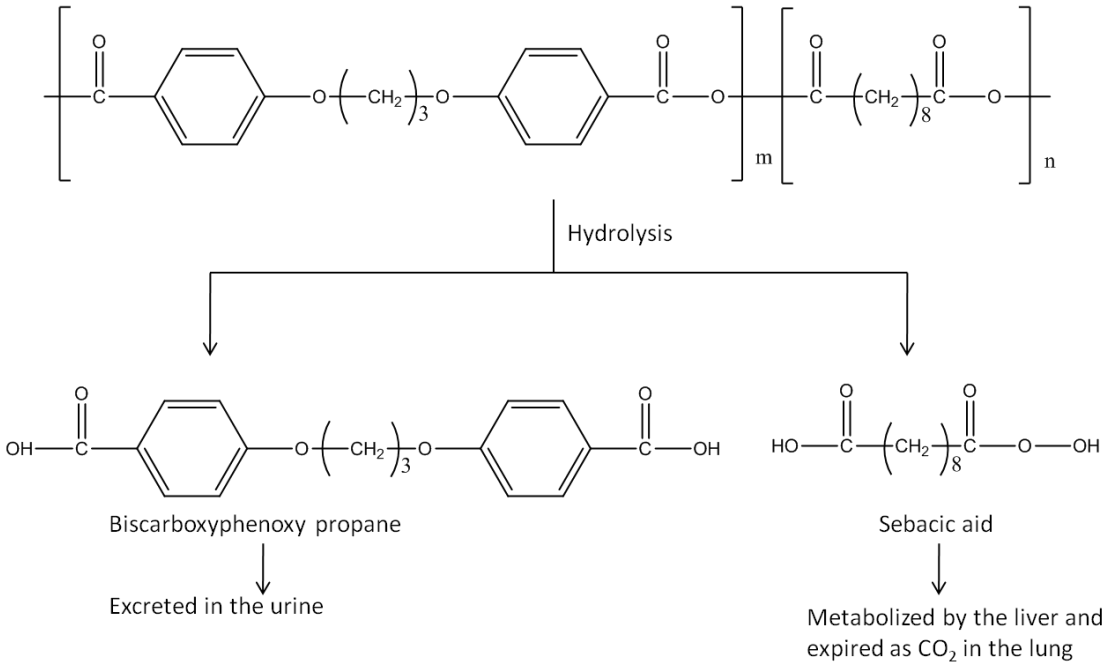


Figure 1.11. The hydrolysis of poly[bis(p-carboxyphenoxy) propane:sebacic acid](PCPP-SA) and its metabolism.

Poly (ortho esters) (POE) have been extensively examined for ocular use. Much work has been done with these polymers for the delivery of 5-FU. They have been studied for more than 30 years. Currently POE has four different families (POE I, II, III, and IV,

Figure 1.12.). Their development, synthesis, characterization, and application were summarized in detail by Heller *et al* (Heller et al. 2000;Heller et al. 2002;Heller 2005). The mechanism of the breakdown of POE is different in each of these families. POE III and IV have shown excellent controlled release of 5-FU and good biocompatibility in subconjunctival, intravitreal, intracameral, and suprachoroidal injections (Heller 2005). Injectable POE containing anti-proliferative agents have been developed by Gurny et al (Bernatchez et al. 1994;Einmahl et al. 2003;Einmahl et al. 2001;Heller et al. 2000;Heller et al. 2002;Merkli et al. 1994;Polak et al. 2008;Zignani et al. 1997;Zignani et al. 1998;Zignani et al. 2000a;Zignani et al. 2000b). It was found that the polymer was able to release the drug for 2-7 days *in vitro*. In the *in vivo* studies, the polymer was not able to be identified 10 days after surgery. Although the polymers appeared biocompatible in their early studies (Bernatchez et al. 1994), hyperemia and chemosis triggered by POE alone were observed for 3 days post surgery (Zignani et al. 2000a).

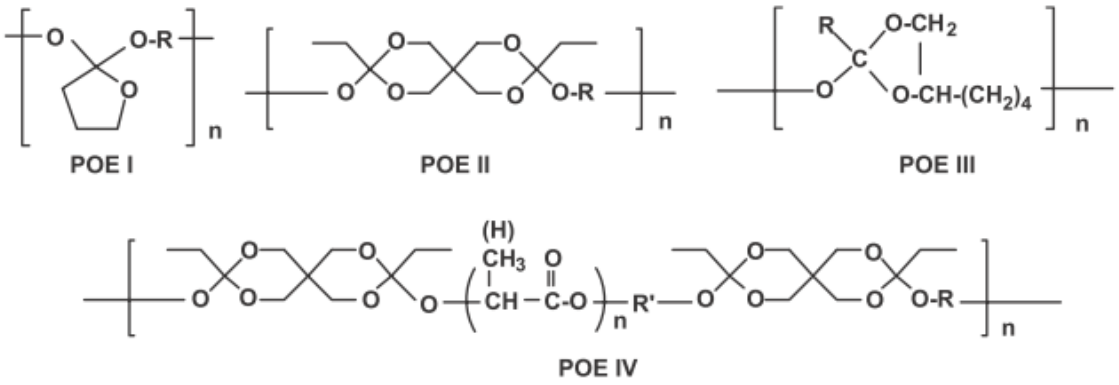


Figure 1.12. Poly (ortho ester) families (Heller 2005) .

PLA and PLGA are also the most popular biodegradable polymers that have been examined in controlled release in recent years. PGA is usually not used in controlled drug release systems due to its high sensitivity to hydrolysis. The mechanism of breakdown of PLGA is shown in Figure 1.13. Lactic and glycolic acids are the degradation products of PLA and PLGA. They are metabolized to carbon dioxide and water via Kreb's cycle. Cui et al developed subconjunctival PLA disks (diameter 3 mm thickness 1 mm) containing 5-FU microspheres for GFS. The implantation of the disks resulted in bleb survival for more than 30 days without any toxic reaction in the conjunctival biopsy. 5-FU was found to have been released for at least 91 days (Cui et al.

2008). However, there have been reports showing the toxic effects of PLA/PLGA nanoparticles to the ocular tissue, including tissue inflammation, corneal opacities and epithelial erosion, and transient hyphema *etc*. (Chang et al. 1999;Gould et al. 1994;Huhtala et al. 2009;Kimura et al. 1992;Kimura & Ogura 2001;Seah et al. 2005;Tan et al. 1999). In addition to their toxicity, we are not using PLA/PLGA here because they are very expensive materials.

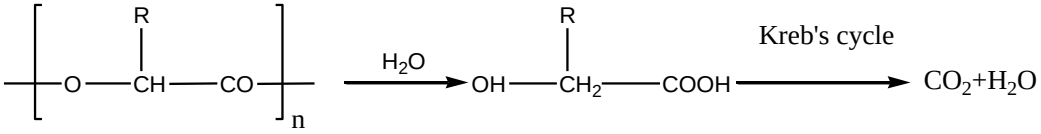


$R=CH_3$ or H

Figure 1.13. Mechanism of breakdown of PLGA in an aqueous humor.

It is shown in Appendix I that more than 70% of cited studies were conducted with cytotoxic agents such as 5-FU, and that all the drug carriers contain polymers. Most of the dosage forms led to mild inflammation. Some of them induced other complications such as hyphema, hyperemia, conjunctivitis and corneal edemas/opacities. There are some papers which claimed that no significant irritation or toxicity were observed, but the histology results were not provided (Chiang et al. 2001;Zignani et al. 2000a). In addition, only a few reports have mentioned the termination of the formulations, which is important because some of the papers have reported the encapsulation of the formulations (Cui et al. 2008;Tilleul et al. 1997). Although many *in vitro* release studies have demonstrated the long term release of the drugs, it is not well known whether the release of the drug will be stopped or slowed due to the formation of the capsule or the physical change of the formulations. It is also not clear whether the formation of a capsule can lead to wound closure in a bleb.

The prolonged release drugs summarized in Appendix I improved the outcome of GFS in animal models, but few of them have been through clinical trials because the intraoperative application of MMC has been found to have long efficacy in scarring inhibition. However, it was confirmed that MMC led to some complications after GFS such as avascular and atrophic blebs, postoperative hypotony, and pathologic changes of

the ciliary epithelium, which did not recover over time (Falck, Skuta, & Klein 1992;Mietz et al. 1994;Mietz et al. 1996;Mietz 1996). Due to the complications caused by either the drug or the polymers, the anti-scarring medicines reported previously were not ideal. New drug candidates with low toxicity and long term effect in scar inhibition are needed.

### 1.3.4. Non-sink conditions and ocular drug delivery

***Non-sink condition and the bleb***

Before *in vivo* studies, the release profiles of drugs need to be evaluated *in vitro*. Orally taken tablets are usually evaluated in sink conditions using rotating paddle methods (Aulton 1998). Due to the significant difference of the volume between the gastric-intestinal fluid and aqueous humor, a drug that is placed locally in the bleb may demonstrate a completely different release profile as a function of its dissolution rate when compared to orally administered tablets. Hence, we could not evaluate the release of drugs in the bleb using the same method as the one used for orally taken tablets. A sustained release formulation in the bleb needs to be evaluated in non-sink conditions.

To evaluate the localized release of a drug placed in the bleb, it is important to understand how non-sink conditions of flowing aqueous in the bleb environment can be exploited. To understand sink and non-sink conditions, one should first understand the dissolution process. The simplest process of solid dissolution described by Noyes–Whitney is shown in Figure 1.4. (Aulton 1998). $C_s$ is the saturated concentration on the surface of the solid. C is the concentration of the bulk solution. The relationship between the diffusion rate of solid molecules or ions through a static diffusion layer ($dm/dt$), transformation area (A), and concentration gradient ($\Delta C$) is shown in Equation 1.1. D is known as the diffusion coefficient with the unit of $m^2/s$ and h is the thickness of the boundary layer.

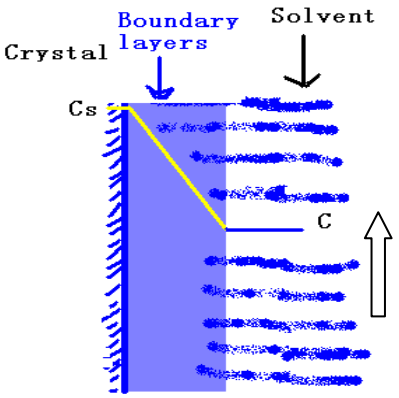


Figure 1.14. Diagram of the boundary layers and concentration change surrounding a dissolving particle.

$$\frac{dm}{dt} = \frac{DA(C_s - C)}{h} \quad 1.1.$$

$$\frac{dm}{dt} = \frac{DACs}{h} \quad 1.2.$$

If the solute passes from the dissolution medium into the bulk at a higher rate than it passes into the boundary layer (which means the solute is diluted immediately to a very low concentration), Equation 1.1 can be approximated by Equation 1.2. Similarly, if the volume of the dissolution medium is large enough ($C \leqslant C_s/10$), ($C_s$-C) can be approximated to $C_s$. Either of these two conditions can be defined as 'sink conditions'. In contrast, if $C > C_s/10$, then this is described as a 'non-sink' condition. Partitioning of the solute between the solid and dissolved state can occur. Non-sink conditions are useful for characterizing the release profile of drugs that are applied topically and are diffused or transported into local tissues.

Complete dissolution or release of an active ingredient by partitioning requires that once the partitioned volume becomes concentrated in the solute there is a mechanism for dilution of the solute. When a semi-solid or solid dosage form is placed in the bleb, it starts to release free drug molecules due to the presence of aqueous humor. Due to the small volume of the bleb (50-200 μL), the free drug molecules cannot be diluted quickly and consequently start accumulating on the surface of the formulation. When more drug molecules are released, the drug solution becomes concentrated; meanwhile, partition between the solid and dissolved state occurs. Although the turnover of aqueous humor (2 μL/min) contributes to the dilution of the drug solution in the bleb, complete

dissolution or release of the drug cannot be achieved instantly due to insufficient dilution (the rate of dilution is 1-4% per minute only). Hence, for a solid or semisolid dosage form, the concentration gradient between the drug surface and the bleb is significant. Therefore, a sustained release formulation in the bleb can be described as non-sink conditions.

***Considerations for investigating drug release in non-sink conditions***

**1) Bleb volume and aqueous flow**

Equation 1.1 suggests that the dissolution of a drug is related to the diffusion coefficient of the drug (D), the transformation area (A), the thickness of the boundary layer (h), and the gradient concentration of the drug ($C_s$-C). For localized drugs placed in the bleb, D and h are related to the dissolution/release of the drug, which is dependent on the drug and the formulation. For a given formulation, D and h are considered constant. Then the transformation area (A) and the gradient concentration ($C_s$-C) become the key factors that affect the drug release rate. Since the formulations were to be placed in the bleb with a small volume, it is assumed that drug saturation would occur in the bleb. However, this has not been confirmed because the presence of the aqueous flow may affect the drug concentration. Hence, we believed that, in the non-sink condition of the bleb, the surface area of the formulation, the bleb volume and the aqueous flow rate can greatly affect the release of the drugs. However, how these factors can affect drug release in quantity can be hardly found in the literature.

**2) Physical properties of the dosage form**

Since there is a turnover of aqueous humor in the bleb, drugs that exist in solid or semi solid states are expected to be exposed to moisture at body temperature. This may lead to the change of the physical properties of the drugs and/or the drug carriers and consequently lead to the change of drug release profile. Hence, to understand the long-term release of the drug, the physical properties of the dosage forms need to be investigated before implantation.

**3) Investigation using an *in vitro* model**

When developing a prolonged release formulation, it is important to investigate whether

the local drug concentration is in the therapeutic window. Before conducting *in vivo* studies, evaluation of the drug release profiles is required. Hence, an *in vitro* model that simulates the bleb would be very helpful in screening the dosage forms as well as in predicting the local drug concentration and drug residential time. Most of the *in vitro* release profiles in the studies listed in Appendix I were obtained by placing the formulations in a small closed tube containing 1-2 mL dissolution media, which does not simulate the bleb because 1) there is no flow in the tube, and 2) the volume of the dissolution media is much larger than the real bleb *in vivo*. Gurny et al designed special thermo stated cells to investigate the drug release profile. They placed the polymers loaded with the drug into the cells into which PBS was ciceluated at the rate of 8-10 mL/h (equal to 133-167 μL/min). These cells did simulate the flow in the bleb, but the volume of the cells was not mentioned. In addition, the flow rate was more than 60 times higher than the real condition (Merkli et al. 1994;Zignani et al. 2000a).

**4) Correlation between *in vitro* and *in vivo***

Although all the dosage forms were usually investigated using *in vitro* and *in vivo* models, few studies correlated the *in vitro* and *in vivo* models. This suggests that the release studies of the *in vitro* models could not properly predict the *in vivo* release because the *in vitro* models did not simulate the bleb very well. Wang et al developed a subconjunctival implant which released 5-FU for more than 8 days (Wang et al. 1996). In this paper, the *in vitro* and *in vivo* studies showed a good correlation. However, the implants were placed directly into the subconjunctival space without performing GFS in the rabbit eyes; the *in vitro* studies were conducted in 10 mL of PBS with samples (2 mL) taken at pre-determined time point. Both the *in vivo* and *in vitro* studies did not fully simulate the bleb after GFS due to the lack of constant liquid turnover. Therefore, after improving the *in vitro* model, further studies are needed to correlate the *in vivo* and *in vitro* models.

**5) Formation of capsules in the bleb**

It is understood that even a good *in vitro* model cannot fully represent the *in vivo* conditions. With exception of the two factors (bleb volume and aqueous flow rate) mentioned above, another key point is that the dissolution media usually used (PBS) in

the *in vitro* model is not identical to aqueous humor. The differences between aqueous humor and PBS are shown in Table 1.1. It can be seen that PBS has neither inorganic substances nor protein or amino acids. Since these substances and fibroblasts are absent, one of the results that cannot be predicted by the *in vitro* model is the encapsulation of the formulation. It has been known that foreign body reaction (FBR) is a common wound healing response following any implantation of a medical device (Anderson, Rodriguez, & Chang 2008). With no exception, a formulation will also be susceptible to be encapsulated after being placed in the bleb.

A few studies have mentioned encapsulation of dosage forms (Cui et al. 2008;Gould et al. 1994). They suggested that a drug that exists as a solid or semi solid form could possibly be encapsulated if it stays in the bleb for a long time. But most of the *in vivo* studies did not mention or predict the termination of the dosage forms. It is unclear whether capsule formation can affect the drug release and hence reduce the anti-scarring effect in long term. Although a good *in vitro* model is helpful in predicting the termination of the dosage forms, the release profiles in the *in vivo* conditions may be altered due to the capsule formation. Hence, further studies on capsule formation are needed.

### 1.4. Matrix metalloproteinase (MMP) inhibitors

Since most of the anti-scarring agents studied previously were cytotoxic drugs, many studies were conducted with new drug candidates with low toxicity. One group of agents is matrix metalloproteinase (MMP) inhibitors (Atreides, Skuta, & Reynolds 2004;Wong et al. 2002). MMPs are a family of proteolytic enzymes that are tightly regulated and capable of degrading components of the extracellular matrix (ECM). They play an important role in mediating proteolytic activities during the tissue repairing process. In the inflammatory phase, large amounts of MMP-9 are secreted by the leakage plasma components. During the subsequent migration of neutrophils, lymphocytes, and macrophages, MMP-9 stored in macrophages and neutrophils granules is released. In the proliferative phase, MMP-1, 3 and 9 have all been shown to be over-expressed at the wound healing edge. In the post-proliferative phase, which is

also called the remodeling phase, the migration of fibroblasts through the surrounding ECM and wound bed are facilitated by MMPs. In addition, fibroblast–mediated collagen contraction, which leads to wound closure, is associated with increased production of MMPs (Wong et al. 2002). Therefore, MMP inhibitors can potentially be used to interrupt the wound healing process.

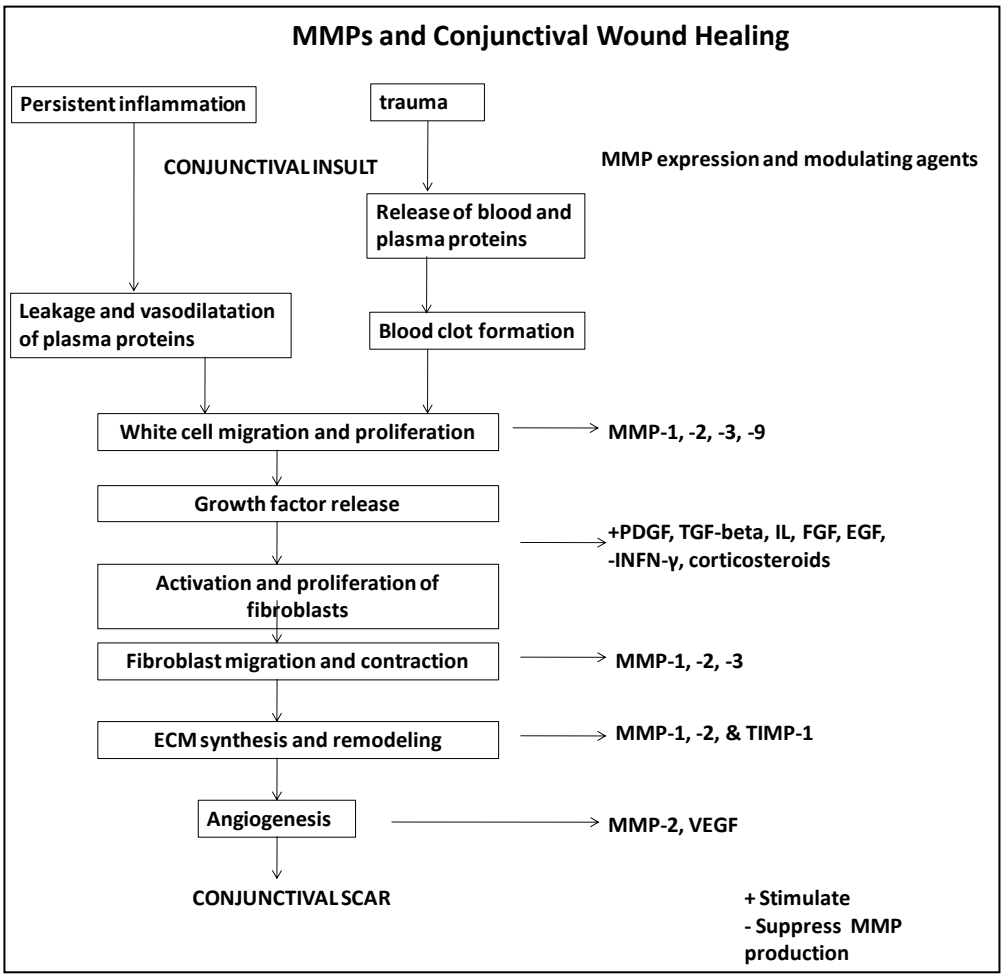


Figure 1.15. MMPs and inflammatory cytokines influence the outcome at each step of the wound healing event. PDGF, platelet derived growth factor; TGF-beta, transforming growth factor beta; PGF, fibroblast growth factor; EGF, epidermal growth factor; IFN-γ, interferon gamma; VEGF, vascular endothelial growth factor. (Figure adapted from Occleston NL and Khaw P. T) (Wong et al. 2002).

Ilomastat (N-[(2R)-2-(Hydroxamidocarbonylmethyl)-4-methylpentanoyl]-L-tryptophan methylamide, Mw: 388.5, alternative name is Galardin or GM6001) is a MMP inhibitor that has been evaluated on a rabbit model of GFS (Wong, Mead, & Khaw 2005) (Figure 1.16.). Ilomastat is a broad-spectrum MMP inhibitor which inhibits MMP 1, 2, 3, 8 & 9. It has been found to be active in a number of inflammation and cell invasion animal

models. Its inhibitory effectiveness on corneal ulceration has been studied in clinical trials (Fini et al. 1991;Galardy et al. 1994). It has been later found that ilomastat was able to inhibit post operative scarring *in vitro* and *in vivo* (Daniels et al. 2003;Wong, Mead, & Khaw 2003). Additionally, it was established that post-subconjunctival injections of ilomastat (0.1 mL of 100 μM) has a similar effect to intraoperative MMC (0.2 mg/mL) in long term scar inhibition. The results showed that, 21 days after surgery, all the blebs in the control group had failed but no bleb failures were observed on ilomastat or MMC groups. Some MMC and ilomastat treated blebs survived (57% and 29% respectively) till the end of the study (60 days post surgery). In the histology studies, ilomastat treated tissue appeared normal while MMC resulted in subconjunctival hypocellularity (Wong, Mead, & Khaw 2005). The histology results indicate that ilomastat is less toxic than MMC. However, it is noticed that the subconjunctival injections were given daily for the first 9 days post surgery, followed by twice weekly injections for 2 weeks and weekly injections for a further 2 weeks. The need of multi-injections suggests that the pharmacokinetics of ilomastat is suboptimal due to rapid clearance of the drug solution. This problem could be resolved if ilomastat were to be incorporated in a slow released solid or semi-solid dosage form. Hence, the development of prolonged release formulations for ilomastat becomes important in future studies.

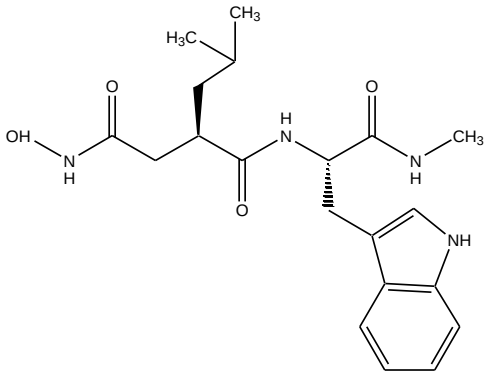


Figure 1.16. Chemical structure of ilomastat

## 1.5. Hypotheses and aims

From the literature and current clinical practice, we understand that scar inhibition plays an important role in determining the success of GFS in halting the progression of

glaucoma. The anti-cancer drugs 5-FU and MMC are unlicensed for ocular use, but are commonly used in clinical practice; currently there is no licensed medicine. The effectiveness of 5-FU and MMC is limited due to their narrow therapeutic window, severe side effects and suboptimal pharmacokinetics. Hence, there are two broad clinical needs: (1) a need for less toxic agents to inhibit the scaring after GFS and (2) a need to increase the local bleb tissue exposure of the drug beyond that which is possible by subconjunctival injection. One MMP inhibitor, ilomastat, has a potential to work as a good anti-scarring agent due to its low toxicity compared to 5-FU and MMC. However, its residence time in the bleb needs to be prolonged. Due to the small volume of the subconjunctival space and the existence of the aqueous flow, a formulation that is placed in the bleb will potentially clear more quickly than in the back of the eye. But due to the small volume, prolonged residence time may be possible. Therefore, drug release profiles in the bleb need to be studied specifically. We hypothesize that 1) the long term inhibition of scarring with low toxicity can be accomplished by placing a prolonged release formulation in the bleb, 2) the release profiles of the formulation can be evaluated *in vitro* using a flow chamber that mimics the bleb, 3) the efficacy of the formulation can be evaluated in a clinically validated rabbit model, and 4) the dissolution of the formulation in non-sink conditions can be simulated computationally.

Therefore, we aim to fabricate and develop a prolonged release formulation that is less toxic than the currently used therapeutics. This formulation is preferred to be a small implantable tissue tablet. Before placing the tablet in the bleb, its release profile will be evaluated using a flow chamber. Following the *in vitro* studies, the effectiveness of the tablet will be evaluated *in vivo* using a clinical validated rabbit model. In addition, the dissolution of the tablet and the release rate of the drug in non-sink conditions will be simulated using molecular dynamics simulation as well as a computational mathematical model.

# *Chapter II Prolonged release of 5-Florouracil*

## 2.1. Introduction

As mentioned in the introduction (1.2.3), the need for bleb maintenances (massage, needling, and 5-FU subconjunctival injections) after GFS indicates that the long term efficacies of 5-FU or MMC are not sufficient for long term scar inhibition. Bleb needling augmented along with 5-FU has been confirmed as a safe and effective way of rescuing failing blebs (Broadway et al. 2004). As summarised in Appendix I, in the last two decades much work has been done to prolong the drug residential time by incorporating these drugs into polymers. However, the efficacy has not been ideal due to the side effect caused by the drug carrier. Therefore, we decided to examine how to prolong the residential time of 5-FU using polymers that are clinically used in commercial products..

Polymers used in commercial ophthalmic products, such as polyvinylalcohol (PVA), polyvinylpyrrolidone (PVP) (K 29/30/32/90), dextran, hydroxypropylmethylcellulose, hydroxyethylcellulose, methylcellulose, polyacrylic acid, sodium hyaluronate, and sodium alginate (U.S. Food and Drug Administration), play an important role in the ophthalmic formulations as their viscosity can prolong the drug residential time and increase the mucoadhesion. We have chosen two polymers as carriers for 5-FU: hyaluronic acid (HA, Figure 2.1) and PVP (Figure 2.2.). According to the criteria of FDA, PVP K 29/30/32/90 has been used in the ophthalmic formulations. Here we choose K30 as it was widely used in both ophthalmic solutions and suspensions.

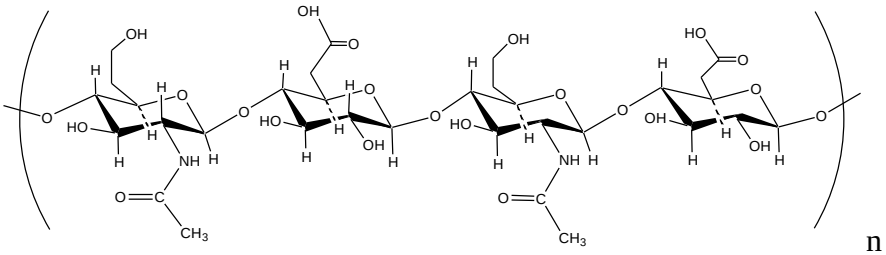

Figure 2.1. Chemical structure of hyaluronic acid.

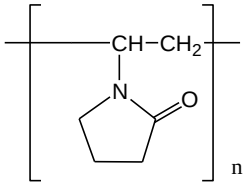

Figure 2.2. Chemical structure of polyvinylpyrrolidone (PVP).

HA is a polysaccharide composed of disaccharide units linked by glycosidic bonds (Kim et al. 2003). It is a natural product of mammals and human beings, and is one of the most important components of the vitreous body. HA has been registered as an intra-articular and intra-ocular medicine. It has many advantages over other commonly available polymers including a high molecular weight, high viscosity, as well as non-toxic, non-inflammatory, and non-antigenic properties. In addition, it does not cause a foreign body response (Reinmuller 2003). It is also effective in atraumatic manoeuvres, for controlling and keeping tissues separated. Furthermore, it has been found that HA is able to form a large coiled, porous meshwork which can entrap drug molecules (Hascall & Laurent 2007). Accordingly, HA could be used as a vehicle for anti-proliferative drugs in the treatment of GFS.

Healon® is a marketed ocular HA product. It is a steam-sterilized solution of sodium hyaluronate 5000 dissolved in a physiological buffer (pH 7.0-7.5). There are three different Healon® products available, all with different concentrations of sodium hyaluronate: Healon® (10mg/mL), Healon® GV (14 mg/mL), and Healon® 5 (23 mg/mL). They all have a fairly similar osmolality and pH to aqueous humour, but more than 20,000 times the viscosity. Although highly viscous (viscosity: 3,000,000 mPas), Healon® is easy to inject because the viscosity decreases considerably when ejected through a cannula, whereas the viscosity is restored immediately after injection (Pharmacia 2007). As a result, Healon® GV has been widely used in clinic including in trabeculectomy (Goa & Benfield 1994). In our study, HA was used as a vehicle for the delivery of anti-scarring agents due to its very high molecular weight and high viscosity. In the preliminary studies we used Healon®, but in the tablet fabrication we used different source of HA (purchased from Sigma). It is understood that the HA contained in Healon® might be different from the ones purchased from Sigma but we believe they are similar as they both were extracted from rooster combs. We decided to purchase some HA instead of freeze drying Healon® because 1) Healon® is relatively expensive, and 2) we do not want to include any salt in the tablet since Healon® is a HA solution in a biological buffer.

Although HA has a very good biocompatibility, it is relatively expensive compared to many other polymers. PVP is a nonionic, water soluble polymer which is widely used in pharmaceutical products. It is used as an excipient in artificial tears. Its rheology does not change significantly when mixed with artificial tears (Hartmann & Keipert 2000). Hence, it is hoped that PVP can prolong the residential time of 5-FU by increasing the viscosity of the aqueous humor in the bleb and delaying the diffusion and elimination of the drug. Therefore, we decided to use PVP and HA to prolong the residence time of 5-FU.

## 2.2. Materials and methods

### 2.2.1. Materials and instrumentation

5-fluorouracil (5-FU), hyaluronic acid sodium salt from human umbilical cord (Cat No. H1876), PBS (phosphate buffered saline) tablets (OXOID), sodium hydroxide (NaOH) and triethanolamine (TEA) were purchased from Sigma-Aldrich (UK). Polyvinylpyrrolidone (PVP, Mw approx 44,000) was purchased from BDH. Healon® (10mg/mL), Healon® GV (14 mg/mL), and Healon® 5 (23 mg/mL) was made by Pharmacia (Switzerland). The Discovery® HS F5 HPLC column (15 cm×4.6 mm, 5 μm) was purchased from Sigma-Aldrich (UK). The syringe pump (PHD2000 model) was manufactured by Harvard Apparatus. The multi-channel peristaltic pump was manufactured by ISMATEC (Switzerland). The tubing used on the peristaltic pump (inner diameter 0.25mm, color code: orange/blue) was purchased from ISMATEC. The manual hydraulic press was manufactured by Specac Orpingham (UK). The punches and dies used for tablet compression were manufactured by iHolland Ltd (UK). The Turbula® T2C / T2F Heavy-Duty Shaker-Mixer was manufactured by the Willy A. Bachofen (WAB) company (German company manufacturing these units in Switzerland). The flow chambers were made by Mr. John Frost in the workshop of the London School of Pharmacy. The Pyris 1 differential scanning calorimetry (DSC) instrument was purchased from PerkinElmer Ltd. The high performance DSC was purchased from TA instruments.

### 2.2.2. Preparation of phosphate buffer at pH 7.6

Phosphate buffer pH 7.6 was made from PBS tablets. Ten tablets were dissolved in 1 L of deionized water (NaCl 8.0 g/L, KCl 0.2 g/L, $Na_2HPO_4$ 1.15 g/L, $KH_2PO_4$ 0.2 g/L ), the pH of the solution was then adjusted to 7.6 by 0.1 M NaOH. The solution was filtered using a 0.22 μM syringe filter (purchased from Millipore) to remove bacteria before use.

### 2.2.3. Preparation of 5-FU powder suspended in HA gel

Healon® GV (50 mg) was firstly injected into the flow chamber. Then 5-FU (6 mg) was deposited on the Healon® GV. Another addition of Healon® GV (50 mg) was injected into the chamber on top of 5-FU. This was followed by a gently stirring of the viscous suspension using a glass stick for approximately 15 seconds.

### 2.2.4. Preparation of tablets

#### 2.2.4.1. Preparation of 5-FU HA tablets

5-FU (45 mg) and HA (9 mg or 45 mg, 5-FU: HA=5:1 or 5:5, W/W) were dissolved in 10 mL deionized water and stirred overnight. The solutions were then lyophilized for 48 hours. The freeze dried solid mixture was compressed into tablets under the pressure of 5 bars. Each tablet was 3 mm in diameter. Tablet weight and thickness varied according to the different ratios of excipients (Table 2.1).

#### 2.2.4.2. Preparation of 5-FU PVP tablets

***Direct blended 5-FU PVP tablets***

5-FU (3 g) and PVP (3 g) were put in a 50 mL amber glass jar and then mixed by Turbula® heavy-duty shaker-mixer for 30 minutes. The solid mixture was then compressed into tablets directly using a pressure of 5 bars. Tablet weight and thickness is illustrated inTable 2.1.

***Freeze dried blended 5-FU PVP tablets***

5-FU (100 mg) and PVP (100 mg) were dissolved in 10 mL deionized water and the solution stirred overnight at room temperature. The solution was then lyophilized for 48 hours. After lyophilization, the mixture was compressed into tablets using a pressure of 5 bars. Tablet weight and thickness is illustrated inTable 2.1.

Table 2.1 Weight and thickness of the 5-FU HA and 5- FU PVP tablets.

| **Tablets** | **Weight (mg)** | **Thickness (mm)** |
|---|---|---|
| 5-FU HA (5:5, W/W) | 10.1 ±0.2 (n=3) | 1.31 ±0.02 (n=3) |
| 5-FU HA (5:1, W/W) | 6.1 ±0.2 (n=3) | 0.78 ±0.02 (n=3) |
| 5-FU PVP (1:1, freeze dried blended) | 11.1 ±0.6 (n=3) | 1.16±0.06 (n=3) |
| 5-FU PVP (1:1, direct blended) | 11.4 ±1.3 (n=3) | 1.24 ±0.12 (n=3) |

#### 2.2.4.3. Tablet fabrication by compression

The lower punch was firstly put into the die. The drug or mixture of drug and polymer were weighed using a small weighting boat and gently placed into the space between the lower punch and the die. The upper punch was placed on the die. The tip of the upper punch was pushed down until it was in contact with the drug or the mixture. The assembled punch and die sets were placed in the manual hydraulic press. A pressure (5-14 bar) was applied for 10 seconds. Finally, both the upper and lower punches were removed, and the tablet ejector inserted into the die to gently push the tablet out. The diameter of the tablets was 3 mm. Tablets with or without excipients were compressed using the same punch and die sets.

#### 2.2.4.4. Preparation of excipient-free 5-FU tablets

The 5-FU tablet was compressed using the method described in 2.2.4.3. 5-FU was compressed into tablets directly using a pressure of 14 bar. The excipient-free 5-FU tablets weighed approximately 5.1 ± 0.4 mg (n=12). The thickness of the tablets was approximately 0.55 ±0.06 mm (n=12).

### 2.2.5. Use of a flow chamber to obtain release profiles: evaluation of the release profiles of the formulations

After the formulated tablets were placed inside, the flow chambers were sealed and connected to a syringe pump or a multi-channel ISMATEC dispensing pump. Each chamber contained one formulation only. Then the PBS solution was pumped into the chamber at a flow rate of 100, 50, 20 (provided by syringe pump) or 2 (provided by multi-channel pump) µL/min. The accuracy of the flow was validated by evaluating the volume of the collected liquid using pipette (volume collected = flow rate (volume/time) × time). The fluid that flowed out of the chamber was collected at predetermined time

points and analyzed by HPLC. Each sample was injected 3 times. The amount of drug released at each time point was calculated by multiplying the volume and the concentration of the outgoing fluid (Figure 2.1, Table 2.2).

### 2.2.6. HPLC instrumentation and conditions

The HPLC methods were developed with the guide and discussion with Dr. Hardyal Gill at London School of Pharmacy. HPLC analysis was performed on an Agilent Technology 1200 series system consisting of a separation module for solvent and sample delivery, a UV detector and chemstation software for data acquisition and analysis. The UV wave length was set at 260 nm following the HPLC methods for 5-FU in the literature(Chu et al. 2003;Gamelin et al. 1997). Since 5-FU is a polar compound, a 15cm × 4.6mm I. D., 5μm particle size Discovery® HS F5 HPLC column was used for compound separation. The mobile phase was 20mM ammonium acetate buffer with 0.6% TEA (pH 5.0). 5-FU was eluted at a flow rate of 1.0 mL/min. The chromatography was performed at 40 ℃. The injection volume for each sample was 10μl.

### 2.2.7. Testing tablet content uniformity

Each tablet (5-FU HA and 5-FU PVP) was put in 10 mL of de-ionized water and then stirred until the tablet was completely dissolved. The solution was injected in to the HPLC column to analyze the concentration of 5-FU. Each sample was injected three times. The amount of 5-FU contained in the tablet was calculated by multiplying the 5-FU concentration with the volume of the water (10 mL) that was used to dissolve the tablet.

### 2.2.8. Examination of the biological effects of an excipient-free 5-FU tablet on Human Tenon's Fibroblasts

***Culturing and counting of the cells***

Human Tenon's Fibroblasts (HTFs) were grown to confluency in a T75 Flask (Fisher, UK) containing 12 mL of fibroblast growth media (FGM) with 10% FBS (fetal bovine serum, Sigma, UK), 100 U/mL Penicillin/Streptomycin and 2mM L-Glutamine (both Invitrogen, UK). Flasks were incubated at 37 ℃ in 5% humidified $CO_2$. The culture medium was replaced every 3 days until confluency was reached. Cells were used

between passage 2 and 8.

Cells were removed from the flask via trypsinisation. To accomplish this the media was aspirated from the flask and the flask was then washed with 5-10 mL of PBS (Invitrogen, UK). The PBS was then aspirated and 2 mL of 1X Trypsin solution (Invitrogen, UK) added. The flask was then placed in an incubator for 2 minutes, after which it was checked for complete HTF detachment using phase-contrast microscopy (Leica) and a x4 objective lens. FGM (5 mL) was then added to the flask and the base washed several times before all liquid was transferred to a 15 mL falcon tube (Fisher, UK) and centrifuged at 1000 RPM for 5 minutes. The cell pellet was then re-suspended in 1 mL of FGM before being counted.

Cell counting was undertaken using Trypan Blue (Invitrogen, UK) whereby 20 μL of cell suspension was mixed in a 1:1 ratio with Trypan Blue. Cells were then plated onto a Neubauer plate (10 μL). The number of cells was calculated by taking an average from 4, 4 × 4 squares. Cells that were colored blue were not included in total cell number count, as the blue indicated a ruptured membrane and therefore a dead or dying cell.

***5-FU treatment I***

HTFs were plated into 6 well plates at a concentration of 1×105 cells per well. Cells were allowed to attach to the plates for 24 hours prior to 5-FU treatment. Then 5-FU (6 mg/mL, 2 mL per plate) was added to each of the wells for 8 hours. Following treatment the wells were washed three times with PBS (200 μl per well). Afterwards, HTFs were removed, counted and seeded into 96 well plates at a concentration of 2×104 cells per well. Cell viability and proliferation were investigated 0, 24, 48, 72 hours after being plated in the 96 well plates.

***5-FU treatment II***

HTFs were plated into the wells of 96 well plates at a concentration of 2×104 cells per well. Cells were allowed to attach to the plates for 24 hours prior to the 5-FU treatment.

Then 5-FU (6 mg/mL, 200 µl per plate) was added to each of the wells for 8 hours. Following the treatment the wells were washed for three times using PBS (200 µl per well). Cell viability and proliferation were investigated 0, 24, 48, 72 hours after treatment.

***Measuring cell viability and proliferation***

Cell viability and proliferation was measured using MTT (3-(4,5-dimethylthiazol-2-yl)-2,5-diphenyl tetrazolium bromide; Sigma; 5 mg/mL stock in PBS), following previously published procedures. The assay is dependent on the production of purple formazan crystals from a methyl tetrazolium salt in the mitochondria of active cells.

At the predetermined time points, MTT solution (10 µL) was added to each well and incubated for 4 hours at 37 ℃. Following the incubation the solution was carefully removed. The wells were carefully washed once with PBS, taking care not to disturb the formazan crystals at the bottom of each well. The crystals were then dissolved in a mixture of DMSO and ethanol (50:50, 200 µL per well). The plates were placed on a rocker for 10 minutes to ensure all the crystals had dissolved. The absorbance of the colored solution was then measured using a Tecan Safire spectrophotometer (test wavelength: 570 nm; reference wavelength 630 nm). The spectrophotometer was operated using the XFluor 4 software and results were extracted as an Excel formatted spreadsheet. To take a back ground for each condition, media was added to a well without cells before being washed and 200 µL of DMSO/ethanol added. This background reading was accounted for and used in calculation of the results. Cell viability/proliferation was then calculated through the reading and the use of statistical tests.

### 2.2.9. DSC measurements of the tablets

The DSC samples were all weighed using a METLER TOLEDO XS105 balance (d = 0.01 mg). The DSC measurements of the 5-FU PVP tablets and 5-FU excipient-free tablets were made with a Pyris 1 DSC (PerkinElmer Ltd.). Samples (2–5 mg) were sealed in non-hermetic aluminum pans and measured with a nitrogen purge gas (25

m/min). Samples were firstly heated from 25 to 120 ℃ at a rate of 100 ℃ $min^{-1}$, then held at 120 ℃ for 3 minutes to remove the moisture. Finally the samples were quenched at -10 ℃ and heated to 300 ℃ at a rate of 100 ℃/min.

The 5-FU HA tablets were measured with a high heating and cooling DSC (TA instruments) with nitrogen purge gas (25 mL $min^{-1}$). Samples (approximately 0.1 mg) were sealed in non-hermetic aluminum pans. They were firstly heated from 25 to 120 ℃ at 500 ℃ /min, then held at 120 ℃ for 3 minutes to remove the moisture. Following this step the samples were quenched to -50 ℃ and heated to 300 ℃ at a heating rate of 500 ℃ /min. In all the DSC experiments, an empty pan was used as a reference and the instrument was calibrated for temperature and enthalpy with indium (melting point 156 ◦C and H = 28.4 J/g).

## 2.3. Results and discussion

### 2.3.1. Designing the *in vitro* model

When developing a new formulation, the release of the drug usually needs to be evaluated using some *in vitro* models before conducting the *in vivo* studies. Although it is appreciated that an *in vitro* model can never perfectly predict *in vivo* conditions, it is still expected to be able to provide some useful information. As mentioned in Chapter 1, the bleb forms a non-sink condition for the formulations, but few studies have paid much attention to the importance of the *in vitro* model. As a result, the *in vitro* and *in vivo* studies were not correlated well. Therefore, we developed an *in vitro* model mimicking the bleb. It is hoped that the experimental data obtained using this model correlates well with *in vivo* studies in the future.

Since the volume of the bleb has been estimated at approximately 50-100 μl (Theelen et al. 2007), we designed two types of flow chambers with different volumes. One with a volume of 50 μl, which is the minimum volume used for most of the formulations studied previously (Appendix I). Theoretically the other volume should be around 100 μl but we made it 200 μl. By enlarging the volume we are able to more fully investigate

how the chamber volume affects drug release. Ideally the liquid in the flow chamber would be similar to the aqueous humor. However, it was mentioned in Chapter 1 that the aqueous humor is composed of many different organic/inorganic substances as well as amino acids; so it is difficult to make a solution that is exactly the same as the aqueous humor because proteins and amino acids are unstable. PBS with a pH that is similar to aqueous humor was usually used in the *in vitro* release studies in the literature (). It is appreciated that PBS is not the buffer that is most similar to aqueous humor because its ion strength is much stronger than aqueous humor; BSS or Kreb's buffer for example are more similar to aqueous humor. But the flow in the chamber did not seem to be constant when using BSS or Kreb's buffer because of the presence of the carbon dioxide bubbles generated from the bicarbonate. Therefore, PBS was used as the dissolution media in our preliminary study.

It is also understood that a drug released into the aqueous humor will be eliminated from the capillaries and lymphatics in the conjunctiva (Azuara-Blanco & Katz 1998). Hence, ideally a piece of conjunctiva should be placed on the top of the chamber to stop the undissolved drug particles coming out of the chamber. But this is difficult because 1) the presence of conjunctival stops the flow as it causes high back pressure in the chamber and 2) the thickness of the conjunctiva varies in different parts of the eye or among individual animals. Therefore, a sponge was placed on the inner top of the flow chamber to prevent the drug particles from being flush out before they had chance to dissolve. However, a few types of sponges were tested but they all led to failing of the experiment again due to the back pressure brought by the sponge. Therefore, it was decided that the drug solution would be collected directly without placing a piece of tissue. Although this flow chamber does not mimic the bleb perfectly, we believe that the approximation from the *in vitro* model will give us some trends and information with regard to the retention of the formulation as well as the drug release profile.

It has been predicted that tablets placed in a flow-through cell may have different release behavior caused by the varied liquid flow (Kakhi 2009). Although in our case

the flow rate of aqueous humor is as low as about 2 μL/min, the release rate of the drug may vary on the formulation because the boundary layer will be disturbed by the liquid flow. In the *in vivo* condition, this problem may also exist as the volume and shape of the blebs are varied among the individuals. To obtain consistent results from the flow chamber, we try to avoid dead spaces as much as possible. Hence, the flow chamber was made in round shape. We also make sure that 1) the formulation is placed constantly right at the same place of the chamber (usually the center) 2) the fluid entrance was designed to be near the bottom of the chamber, and the fluid exit at the top of the chamber as far away from the entrance as possible (Figure 2.3, Figure 2.4, & Figure 2.5). In addition, tubing with a small inner diameter (0.92 mm) was used as the out-going channel. This tubing was also designed to be as short as possible to ensure it does not significantly enlarge the volume of the chamber. The volume of the outgoing tubing was approximately 10% of the chamber volume. To mimic the temperature of the eye, the chambers were placed in a 37 ℃ oil bath. By collecting the liquid that flows out of the chamber and determining the concentration of the drug at different time points, the amount of the drug that flows out of the chamber can be evaluated (Figure 2.3). The calculation of accumulate drug that flows out of the chamber is demonstrated in Table 2.2. It is understood that the flow chamber is not perfect in predicting the *in vivo* conditions, but we believed that this *in vitro* model is able to give us some trends. By testing the formulations in the flow chamber, we are able to make sure that 1) the retention of the formulation in the bleb is prolonged, 2) the formulation and drug is stable before the drug release is completed, and 3) the release profile of the drug can be estimated approximately.

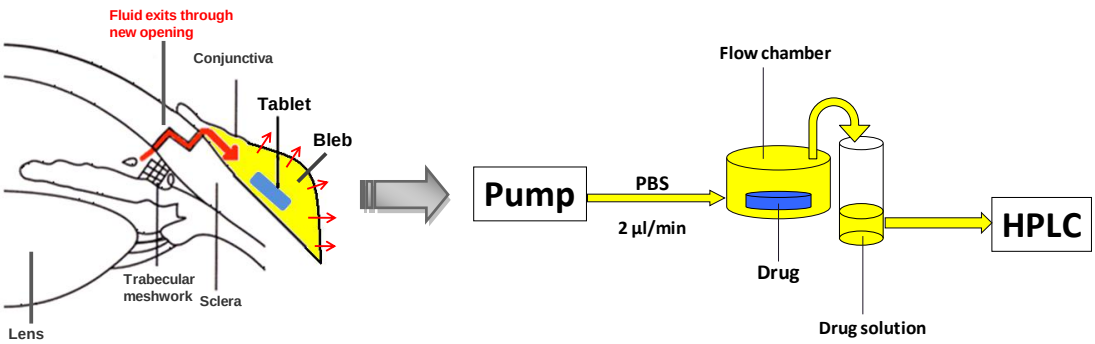


Figure 2.3. Design of the *in vitro* model for the release studies of the drug formulation.

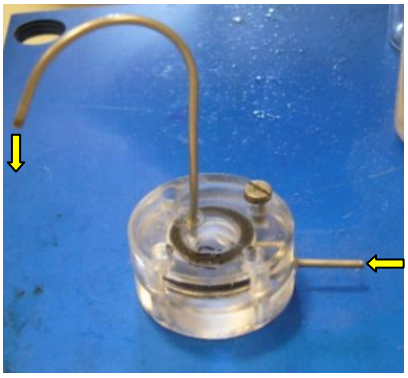

Figure 2.4. A flow chamber that simulates the bleb. Arrows in the figure illustrate the flow of the liquid.

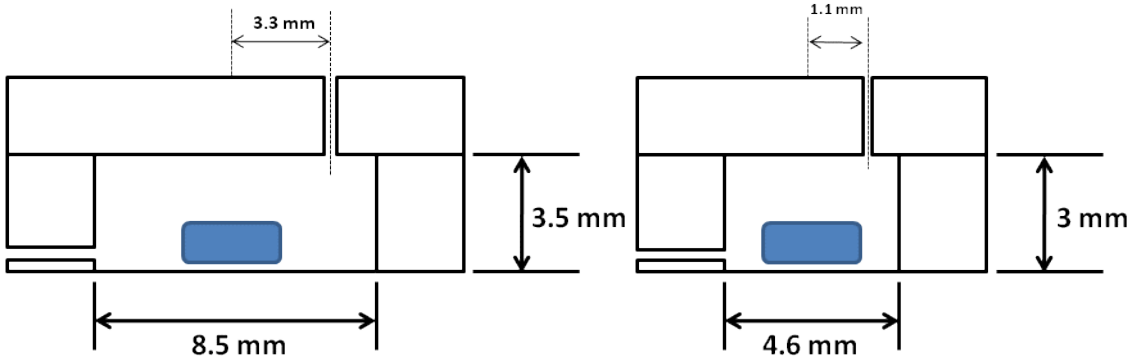


**a** **b**

Figure 2.5 The dimensions of the 200 µL (a) and 50 µL (b) flow chamber.

Table 2.2 Calculation of the accumulate drug that flows out of the chamber.

| **Time point** | **Volume of the liquid collected** | **Drug concentration** | **The amount of drug that came out of the chamber** | **Accumulation of the drug that came out of the chamber (%)** |
|---|---|---|---|---|
| 0 | 0 | 0 | 0 | 0 |
| $t_1$ | Flow rate $\times t_1$ | A | $a \times t_1$ | $a \times t_1/m_0$* |
| $t_2$ | Flow rate $\times(t_2-t_1)$ | B | $a \times t_1+b \times (t_2-t_1)$ | $[a \times t_1+b \times (t_2-t_1)]/ m_0$* |
| … | … | … | … | … |
| $t_n$ | Flow rate $\times(t_n-t_{n-1})$ | X | $a \times t_1+b \times (t_2-t_1)+\ldots+x \times (t_n-t_{n-1})$ | $[a \times t_1+b \times (t_2-t_1)+\ldots+x \times (t_n-t_{n-1})]/ m_0$* |

*m: total amount of the drug contained in the formulation.

### 2.3.2. Preliminary studies: 5-FU solution mixed with Healon®

It is understood that the pharmacokinetics of 5-FU are not sufficient when it is delivered as a solution. Hence, it was suggested that the elimination of 5-FU could be delayed if the viscosity of the solution was increased. In order to see whether the presence of polymer

could prolong the release of 5-FU, a preliminary study was conducted in the 50 μL chamber with HA (Shen.Y. 2004;Wong et al. 2006). Different concentrations of HA (Healon® 10 mg/mL, Healon® GV 14 mg/mL) and 50 mg/mL 5-FU solution (1:1 W/W) were injected into the flow chamber and then manually mixed by stirring. In the preliminary studies, the flow of PBS was initially provided by a syringe pump. As the syringe pump could not provide any accurate flow rate that is less than 20 μL/min, studies were conducted using the flow rate of 20 μL/min. Since our aim is to see whether the polymer viscosity can prolong the drug retention time, it is believed that the 5-FU retention time in the bleb will definitely be prolonged if it can be prolonged at a flow rate *in vitro* that is 10 times higher than the human average aqueous flow rate (2 μL/min).

The results show that, at a flow rate of 20 μL/min, 5-FU solution was eliminated completely within one hour (60 minutes). But 5-FU was slowly released for more than 3 hours (180 minutes) when mixed with HA solutions (Figure 2.6.). Complete release of 5-FU was not shown in this figure because the experiment was not conducted till the time when all the 5-FU was released. It is believed that, due to the high viscosity of HA, complete release of 5-FU will need another few hours. This suggests that 5-FU release was prolonged at least two fold by Healon® due to the high viscosity of HA.

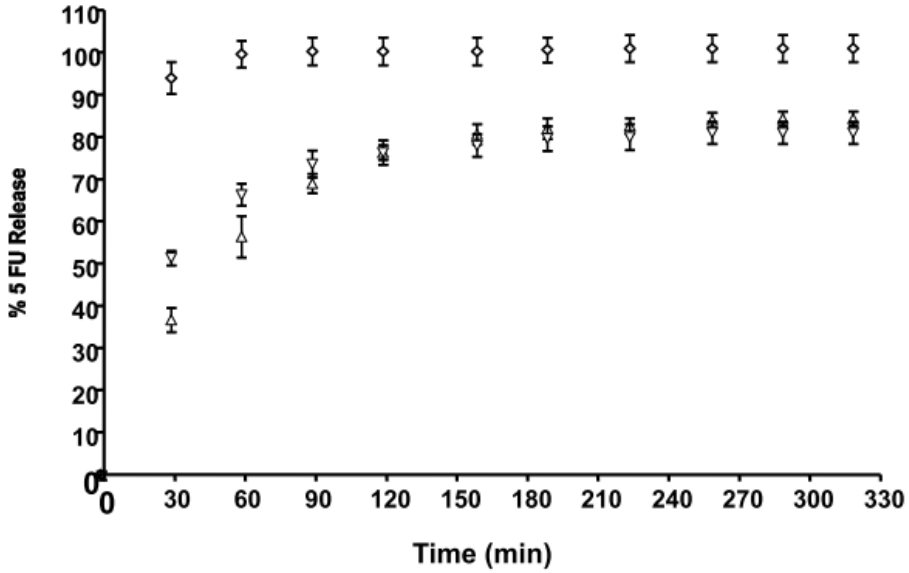


Figure 2.6. 5-FU concentrations released from Healon® mixed with the 5-FU solution (50 mg/mL) at ambient temperature and a flow rate of 20 μL/min (n=3, error bars indicates standard deviation) (Wong et al. 2006). ◇5-FU solution only ▽Healon® (10mg/mL HA) with 5-FU solution △Healon® GV (14 mg/mL HA) with 5-FU solution. Data suggest that the residence time of 5-FU was prolonged when the 5-FU solution was mixed with Healon®.

### 2.3.3. 5-FU powder mixed with Healon®

The above study has shown that the release of 5-FU can be slowed down when mixed with HA solution because the presence of HA increases the viscosity of the solution inside the chamber. But the water contained in the 5-FU solution could still decrease the HA viscosity. Therefore, to avoid the dilution of HA caused by the water contained in the 5-FU solution and to obtain a longer drug residential time, 5-FU powder was simply mixed to the most concentrated HA solution (Healon® GV). Using this method, it is believed that the release of 5-FU will be more prolonged because 5-FU would need to dissolve in the HA solution and then eliminated slowly by diffusion. Meanwhile, to understand whether the 5-FU release rate will be affected by different flow rates, the release of 5-FU was evaluated using different flow rates (20, 50, and 100 μL/min). The results indicate that the 5-FU release rate was decreased with a decreasing of the flow rate (Figure 2.7). When the flow rate was 100 μL/min, 5-FU was completely released after 5 hours. Meanwhile, about 80% of 5-FU was released when the flow rate was set at 20 μL/min. These studies further confirmed that HA is able to prolong the release of 5-FU. However, it is understood that the results of this study may show significant variability due to the difficulties of reproducibly formulating the 5-FU powder which

suspended in Healon®. Results will also be affected by factors such as stirring techniques, particle size, and polymorph of 5-FU. The release profiles of 5-FU with different particle size can be vary because the particle size is associated with the surface area which greatly affects the dissolution rate of a material, whilst the particle size of the 5-FU powder can vary from different manufacturer or even in different batch from the same manufacturer. As different crystal forms of 5-FU may have very different dissolution rate, the polymorph of 5-FU also needs to be defined. Hence, further studies on 5-FU HA suspensions were not conduct since this is only a preliminary study.

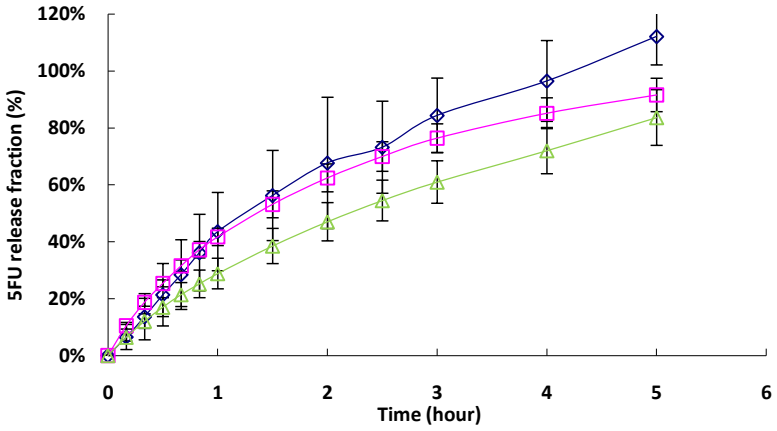


Figure 2.7. Release profiles of Healon® GV mixed with 5-FU powder under different flow rate in the 200 µl chamber at ambient temperature (n=3, error bars indicates standard deviation). ◇ 100 µL/min, □ 50 µL/min △ 20µL/min. Data suggest that the residence time of 5-FU will be reduced when the flow rate increases.

### 2.3.4. Fabrication of a mini tablet

Since it was established that HA was able to prolong the release of 5-FU, it was considered that the release of 5-FU could be further prolonged if the drug was incorporated into the polymer and then compressed into a tablet. Hence, we decided to make 5-FU tablets using HA as an excipient. Based on findings from previous studies (Chapter 1), it was felt that a mini tablet with 3 mm diameter and maximum 1 mm thickness is suitable for the bleb. To make these mini tablets, a punch and die set was designed (Figure 2.8.). As the diameter of the punch is only 3 mm, one of the most important issues in this design is that the punches must be well protected from bending and damage under high pressure. Therefore, we had several discussions with Mr. J frost from the workshop at the School of Pharmacy and specialists in tablet compression

from iHolland Ltd. In accord with these discussions, the upper and lower punches were designed to be as short as possible to minimize the risk of distortion on compression. They were attached to a strong base with a large surface area with radian so that the pressure could be applied evenly during tablet compression. The tools were designed so that a 0.2 mm safety gap is maintained between the upper and lower punch. This is to ensure that they do not collide during compression if there is insufficient material to fill the die space. Due to the absence of lubricants, the tablets were sometimes found to stick to the die after compression. A tablet ejector was therefore made to push the tablet out (Figure 2.8.).

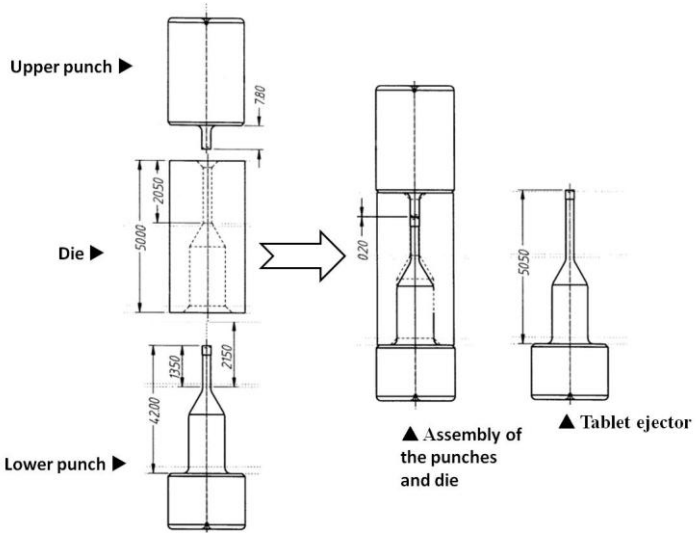


Figure 2.8. The punches and die used for compressing tablets.

### 2.3.5. 5-FU HA tablets

Having carefully designed the punch and die sets, we started to make tablets. We first used HA as the excipient for the 5-FU tablet. It is hoped that 5-FU could be well dispersed in the polymer, and that the residence time of 5-FU would be prolonged due to the viscosity of the polymer. To make reproducible tablets, it was important to ensure that the polymer and drug are well mixed. In other words, a good content uniformity was required before testing the tablet release profiles. As the HA purchased from Sigma was fleecy, its compressibility was poor. In addition, it was not possible to mix 5-FU powder directly with the fleecy HA. Therefore, to obtain a good content uniformity, HA was dissolved in 5-FU solution. The solution was then lyophilized to get a proper mixture of 5-FU and HA. This mixture appeared to have a better compressibility than

HA, so the 5-FU HA tablets were made from this lyophilized mixture.

To simulate flow of the aqueous humor, a peristaltic dispensing pump was purchased to ensure that the flow rate was set as the average flow rate of human aqueous humor (2 µL/min) (McLaren 2009). To gain some understanding on how the release rate could be affected by different proportion of HA, two types of tablets containing the same amount of 5-FU but different amounts of HA (50% and 16.7%, W/W) were fabricated and evaluated using the *in vitro* model.

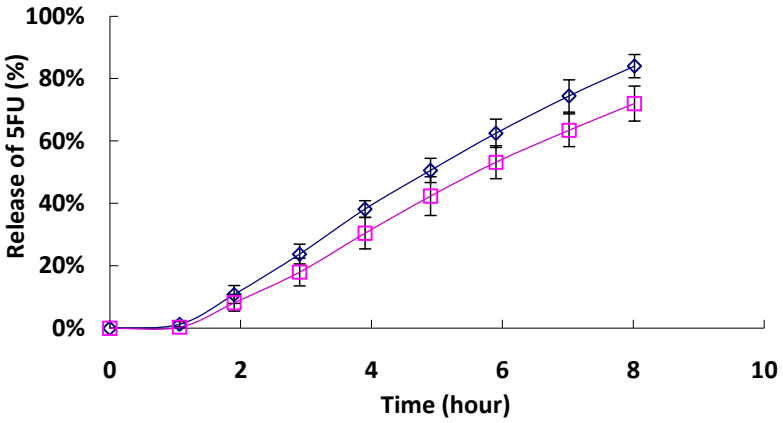


Figure 2.9. Release profiles of 5-FU HA tablets in the 200 µl chamber at ambient temperature (n=3, error bars indicates standard deviation). ◇ represents 5-FU: HA = 5:5 (W/W), □ represents 5-FU: HA=5:1 (W/W). Data suggest that with the decreasing of the proportion of HA the release rate of 5-FU as well as the 5-FU concentration in the flow chamber will be decreased.

The accumulate release (in %) of the tablets in 8 hours is shown in Figure 2.9. A lag time of tablet dissolution was observed in both tablets, led by the water absorption process of the tablet. After 8 hours, approximately 80% of 5-FU was released from the tablets containing 50% HA; meanwhile, less 5-FU (70%) was released from the other type of tablets which contained 16.7% HA. The peak concentration of 5-FU, which appears at around 3-4 hours, was around 6-7 mg/mL. The 5-FU concentration was found to be nearly zero after 24 hours (data not shown). This indicates that with the same flow rate (2 µL/min), tablets containing the higher proportion of HA (50%) released 5-FU more quickly.

### 2.3.6. 5-FU PVP tablets

Although HA did prolong 5-FU release, the price of HA is relatively high. Other water soluble polymers that are used in the commercial ophthalmic products could also be good excipients for a prolonged release 5-FU tablet. PVP is a good candidate because 1) it is frequently used as a tablet binder 2) it is water soluble and 3) its solution is viscous. Hence, PVP was also mixed with 5-FU and compressed into tablets. As PVP is a powder, it could be directly blended with the 5-FU powder. 5-FU and PVP mixture could also be obtained by freeze drying their aqueous solution. Therefore, 5-FU and PVP were dissolved in water and then lyophilized. The 5-FU PVP tablets were made from the lyophilized mixture. The release profiles of the different type of 5-FU PVP tablets were investigated using our *in vitro* model.

The release profiles of 5-FU PVP tablets blended using different methods were compared. The results show that PVP prolonged the release of 5-FU for more than 8 hours (Figure 2.10.). After 8 hours, 75% of 5-FU was released from freeze dried blended tablets; meanwhile, only about 50% of 5-FU was released from the directly blended tablets. This suggests that 5-FU is released more quickly if it was freeze dried blended with PVP, probably because lyophilization leads to the formation of amorphous 5-FU, which dissolves faster than the 5-FU crystals.

Although the 5-FU tablets containing HA and PVP did prolong the release of 5-FU in comparison with the 5-FU solution, all the tablets released 100% of the 5-FU within 24 hours, even when the proportion of the polymers was increased. Although the highly viscous polymer solution obstructed the diffusion of 5-FU solutions in the flow chamber, the wettability and dissolution rate of 5-FU was enhanced by the hydrophilicity of PVP and HA. It was also believed that the residence time of 5-FU would not be significantly prolonged unless the compression force of the tablet is increased considerably. A high compression force may delay the hydration time of the tablets; as once the tablet is fully hydrated, the release profiles cannot be significantly changed. However, we did not try any higher compression force because we are not sure whether the punch and die sets

will be damaged if a high pressure (more than 30 bar) is applied.

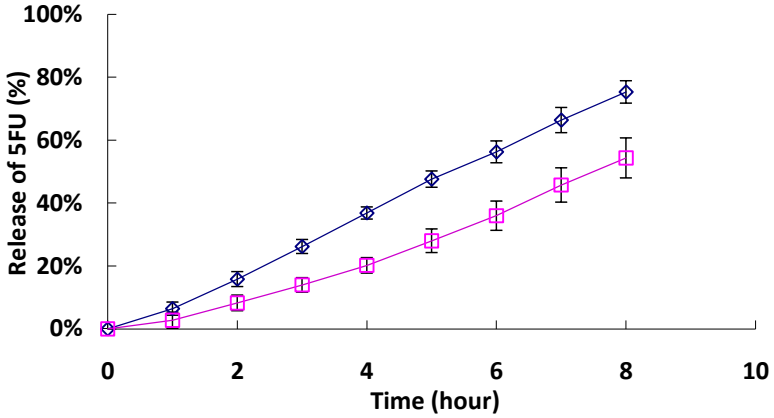


Figure 2.10. Release profiles of 5-FU PVP (1:1 W/W) tablets in the 200 µl chamber at ambient temperature (n=3, error bars indicates standard deviation). □ Direct blended ◇Freeze dried blended. Data suggest that with the decreasing of the proportion of PVP the release rate of 5-FU as well as the 5-FU concentration in the flow chamber will be decreased.

### 2.3.7. Excipient-free 5-FU tablets

***Excipient-free 5-FU tablets in different chamber volumes***

When analyzing the release profiles of the 5-FU tablets with PVP and HA, it was found that tablets containing larger amounts of polymer demonstrated a faster release rate than the ones containing smaller amounts of polymer. Although both HA and PVP prolonged the release of 5-FU due to their viscosity, they also improved the 5-FU dissolution process because their hydrophilicity and potential wettability brought more contacts between water and the dispersed 5-FU. So it was considered that the release of 5-FU might be slower without the presence of hydrophilic polymers. Thus, excipient-free 5-FU tablets were also fabricated and evaluated. Fabrication of excipient-free tablets means that the tablets contain only the solely pure drug. This brings us some unique advantages include 1) batch to batch difference caused by the excipients can be avoided 2) reworking and recovery of the drug material is possible when problems occur. However, batch to batch difference induced by inconsistencies associated with the drug such as polymorph and the water content of the material should always be considered and investigated.

The evaluations were conducted in both the 200 and 50 µl chambers at a flow rate of 2 µL/min. As with the tablets tested before, the 5-FU excipient-free tablets also

disappeared overnight. But they exhibited the slowest release rate compared to all the previous studied tablets. In the 200 μl chamber, less than 50% of 5-FU was released after 8 hours. After 24 hours, the 5-FU concentration in the chamber was still around 1.6 mg/mL. The release profiles appeared almost as first order. In the 50 μl chamber, it was found that the release of 5-FU was significantly accelerated (Figure 2.13.). This is because the fresh PBS around the surface of the tablets was replaced more frequently when the tablet was placed in a relatively small chamber (Figure 2.11). As a result, the boundary layer at the tablet surface becomes thinner in the small chamber due to the relatively faster diffusion of the 5-FU solution.

***Tablets placed at different positions inside the 200 μl chamber***

Based on results that the tablets dissolved faster when placed in a smaller chamber, it was suggested that the direction of the liquid may also have an effect on the tablet release. It was therefore considered that the tablet release behavior might change if the tablet is placed at different positions in the chamber. Hence, the same 5-FU tablets were evaluated again by placing them at different positions in the 200 μl flow chamber (centre, side, near the outgoing tube or in going tube, Figure 2.12). The release profiles are shown in Figure 2.13. However, it is difficult to tell by eyes whether there is any difference between the release profiles of the tablets placed in different positions. Hence, a two way between-groups analysis of variance was conducted to explore the impact of position (centre, side, in going and outgoing Figure 2.13) and time on the levels of drug release. Subjects were divided in to 9 groups according to the different time points (Group 1: 1 hour, Group 2: 2 hours, …, Group 9: 9 hours). The results show that there is a statistically significant change with time ($F(8, 68) = 62.86$, $P < .0005$). Also there was a statistically significant main effect for position ($F(3, 68) = 7.21$, $P < .0005$). But the release profile of the group in the center did not differ significantly from the groups on either side or by the out-going tube ($F(2, 50) = 2.52$, $P = .091$). The group by the in-going tube was significantly different from all the other three groups. These results indicate that 5-FU is released more quickly when the tablet is placed near the in going tube in the chamber. On reflection, these results suggest that, when placing the tablet *in vivo*, a faster drug

release of the drug might be achieved if the tablet is placed near the exit of the aqueous humor.

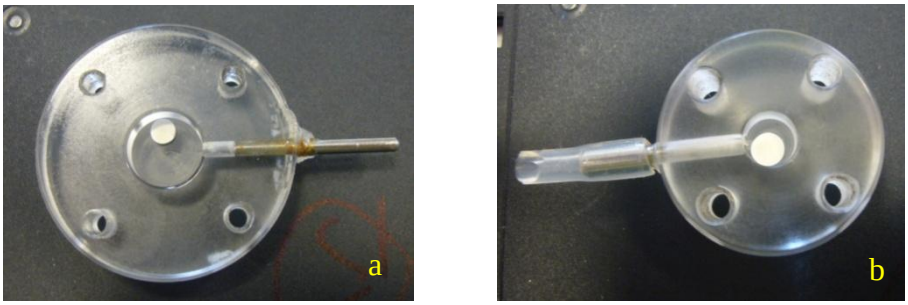


Figure 2.11. The same tablet (3 mm diameter, 0.5 mm thickness) placed in 200 µl (a) and 50 µl (b) chamber.

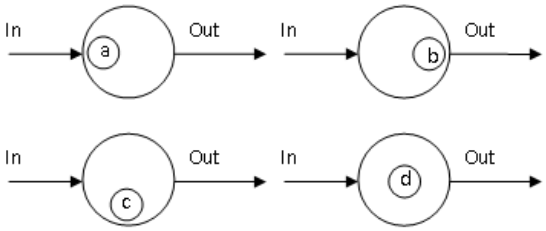


Figure 2.12. Illustration of 5-FU tablets placed in different position in the flow chamber. a. near the in going tube; b. near the out going tube; c, the side of the chamber; d, the centre of the chamber.

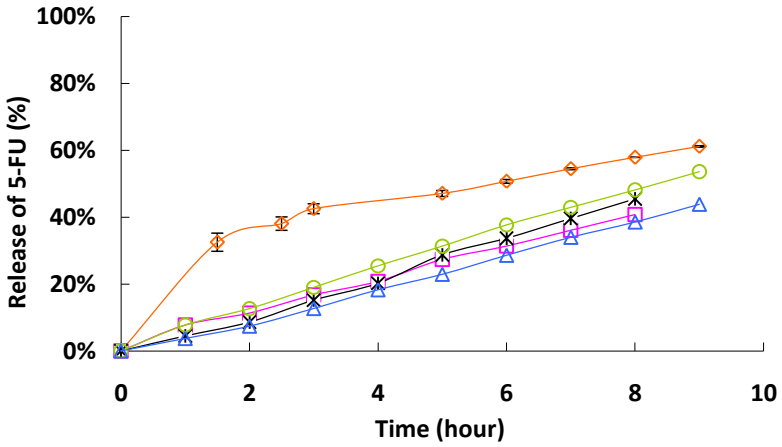


Figure 2.13. Release profiles of excipient-free 5-FU tablets at ambient temperature (n=3, error bars indicates standard deviation). ◇ Tablets in the 50 µL chamber □ Tablets at the centre of the 200 µL chamber △ Tablets placed in the 200 µL chamber close to the in going tube ○ Tablets placed in the 200µL chamber close to the out going tube ∗ Tablets at the side of the 200 µL chamber. Data suggest that 1) the release rate of 5-FU and the 5-FU concentration will be increased when the tablet is placed in the 50 µL chamber and 2) in the 200 µL chamber the release rate of 5-FU will be higher when the tablet is near the in going tube.

***The excipient-free 5-FU tablets released at different temperatures***

As a real bleb in the body is not at ambient temperature, there was a need to find out

whether temperature significantly affected tablet release. Hence, tablet release studies were conducted again in the 200 µl chamber at 37 ℃. It was found that the 5-FU release rate became double at 37 ℃ than at ambient temperature (Figure 2.14.). This is because 5-FU dissolved faster when the temperature was increased. However, a saturated concentration of 5-FU (11.1 mg/mL) was still not observed even when the release study was conducted at a higher temperature. Assuming a complete mix of 5-FU and PBS exists in the flow chamber, this suggests that the 5-FU dissolution, not the drug solubility, is the rate limiting step for the release of the drug. Hence, the release profiles of the 5-FU tablets cannot be calculated directly using its intrinsic solubility.

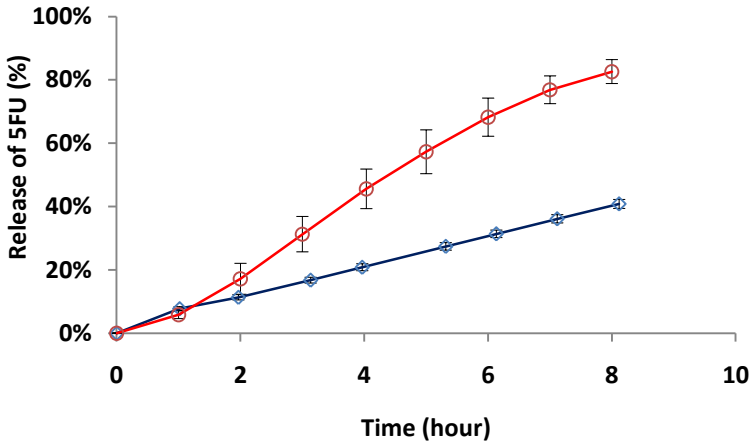


Figure 2.14. Comparison of 5-FU release profiles at different temperature in 200 µl chamber (n=3, error bars indicates standard deviation). ◇ Ambient temperature ○37 ℃. Data suggest that the release rate of 5-FU and the 5-FU concentration will become significantly higher at 37 ℃ than at ambient temperature.

### 2.3.8. The biological effect of the excipient-free 5-FU tablets

Our studies highlight the difficulties in prolonging the release of 5-FU using hydrophilic polymers. Although there have been many reports of successful sustained release of 5-FU for GFS using hydrophobic polymers, side effects caused by the drug carriers were frequently reported (Appendix I). An excipient-free 5-FU tablet will not cause excipient mediated side effects but the toxicity of the excipient-free 5-FU tablets remains unclear.

Khaw *et al*. found that HTFs were "growth arrested" after 1 day of treatment with high concentrations (0.1 and 1 mg/mL) of 5-FU (Khaw et al. 1992;Khaw 1995). When the HTFs were constantly treated with 1 mg/mL 5-FU for 3 days, the whole population of

the cells died gradually in a 30 day period. However, our results suggest a potential different way of the 5-FU treatment. In our *in vitro* release studies at 37 ℃, the concentration of 5-FU were determined from the solutions that flushed out of the chamber. It was found that the 5-FU concentration increased to 6 mg/mL after 3 hours and then decreased gradually to 2.5 and 0 mg/mL at 8 and 24 hours respectively. This means an excipient-free 5-FU tablet is different from all the formulations reported in the literature because the fibroblasts will be exposed to a range of 5-FU concentrations that are all less than 25 mg/mL (0- 6 mg/mL), for a period which is longer than 5 minutes but less than 24 hours. Since Khaw *et al* found that HTFs were still alive after 1 day treatment of 1 mg/mL 5-FU, it is possible that HTFs will be alive and "growth arrested" after exposure to an excipient-free 5-FU tablet in the flow chamber. Therefore, it would be interesting to see how HTFs behave in a flow chamber which mimics the bleb. However, growing cells in a flow chamber was not practical for a number of reasons. One of the biggest obstacles is the maintaining of the humidified 37 ℃ $CO_2$ which is required for the cell growth. To maximize the possible toxicity of the excipient-free 5-FU tablets, further biological studies on HTFs were conducted using the peak concentration (6 mg/mL) of 5-FU observed in the *in vitro* release study. Hence, we decided to treat the HTFs with 6 mg/mL 5-FU for 8 hours. These biological studies were mainly conducted in collaboration with our colleagues (Mr. Daniel Paull).

#### 2.3.8.1. 5-FU treatment I

The HTFs were seeded in 6 well plates and then treated with 5-FU for 8 hours. After that, the cells were removed from the plate. The number of the live cells was examined using Trypan blue (a stain that selectively colors dead cells). Most of the cells were found alive after 8 hours of treatment with 6 mg/mL of 5-FU. To examine the proliferation of the treated cells, the cells were re-seeded into the 96 well plates. Cell viability and proliferation was measured using the MTT assay. Proliferation of HTFs was still observed within 24 hours post treatment, but significant differences in cell number was found between the control group and treated group after 3 days (Figure 2.15.). The cell number of the treated group was half that of the control group. This indicates that 8 hours treatment with 6 mg/mL of 5-FU will inhibit the proliferation of HTFs.

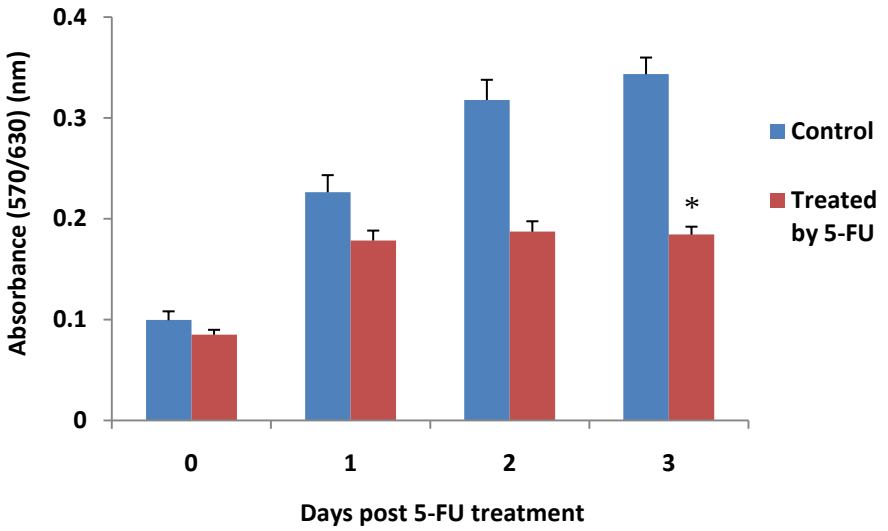


Figure 2.15. HTFs viability and proliferation after 8 hours of 5-FU treatment in the 6 well plate. * P<0.0001. Data suggest that proliferation of HTFs was still observed within 24 hours post treatment but cell number decreased significantly compared to control group.

#### 2.3.8.2. 5-FU treatment II

To confirm the above findings and to understand whether the 5-FU treatment have killed some of the HTFs, we plated the cells in the 96 well plates directly. Cell viability and proliferation were measured directly using the MTT assay. It was found that, although approximately 25% of HTFs were killed by the 5-FU treatment, cell proliferation were still able to occur after 5-FU was removed. Three days post 5-FU treatment, the cell number of the treated group was significantly lower than that of the control group (Figure 2.16).

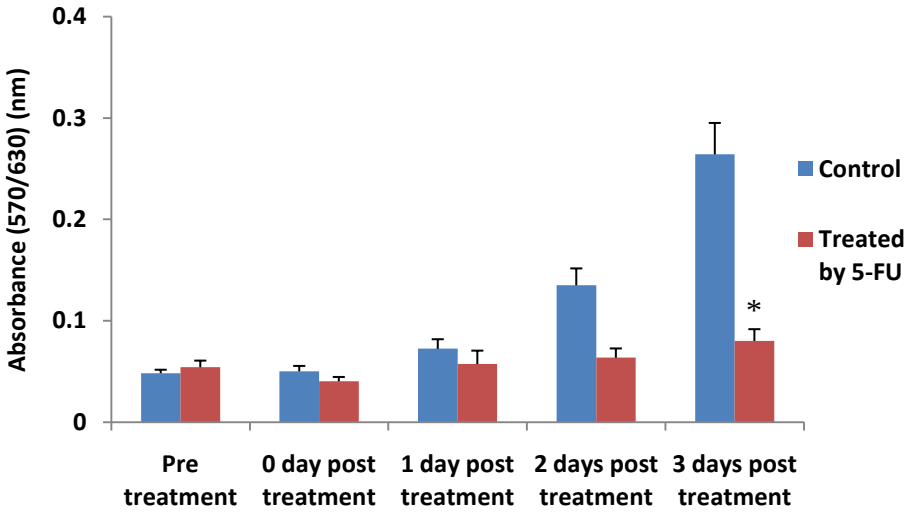


Figure 2.16. HTFs viability and proliferation before and after 5-FU treatment in the 96 well plates. *P<0.0001. Data suggest that proliferation of HTFs was still observed within 24 hours post treatment but cell number decreased significantly compared to control group.

### 2.3.8.3. Cell morphology before and after the 5-FU treatment

The morphology and proliferation of the HTFs were also observed under a microscope. The density of the cells was found reduced slightly after the 8 hour 5-FU treatment (Figure 2.17. A & B). Cell proliferation was observed in both control and treated group after the 5-FU treatment. But proliferation in the treated group was not as confluent as the control group (Figure 2.17. C & D).

The above studies reveals that an 8 hour treatment of high concentrated 5-FU (6 mg/mL) is able to inhibit the proliferation of HTFs for at least 3 days. Investigation into its long term effect on cell proliferation and inhibitory effect on the collagen gel contraction are currently being conducted by our colleagues. Although an 8 hour treatment at a concentration of 6 mg/mL does not exactly equal the release of an excipient-free 5-FU tablet, the preliminary studies above provided us with some positive indications. They suggest that an excipient-free 5-FU tablet is possibly as effective as a 5 minute application of 25 mg/mL 5-FU in inhibiting the proliferation of HTFs.

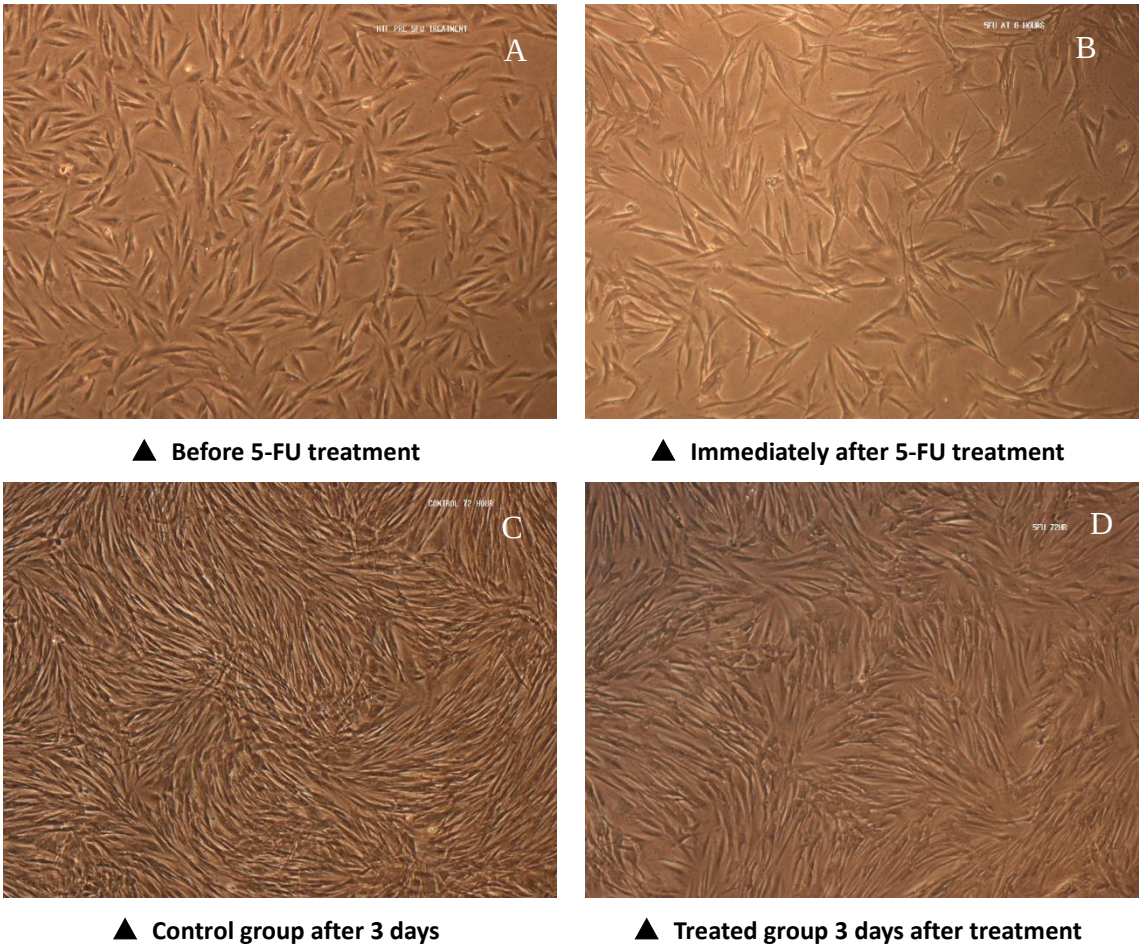


Figure 2.17. Morphology of HTFs before and after an 8 hour 5-FU treatment. It suggests that the number of the cells decreased slightly after 5-FU treatment. Cell proliferation was observed 72 hours after 5-FU treatment, but the proliferation in the treated group is not as confluent as the control group.

### 2.3.9. Preliminary characterizations of the 5-FU tablets

Since our results have shown that the polymers can affect the 5-FU release rate, we then investigate the interactions between the drug and polymers. It is hoped that by evaluating the tablet physical properties, the release mechanism of the tablet can be understood. To study the physical properties of the tablets, one of the most commonly used methods is differential scanning calorimetry (DSC). Hence, DSC analysis was conducted on the 5-FU PVP, 5-FU HA, and the 5-FU excipient-free tablets.

***5-FU excipient-free tablets***

The analysis was conducted firstly on excipient-free 5-FU tablets to see if there are any polymorphic transitions induced by compression. Figure 2.18 shows that 5-FU powder has a sharp melting peak with an onset temperature of 283 ℃. This agrees with the

melting point of 5-FU reported in the Merck Index. But the excipient-free 5-FU tablet has the same onset temperature of melting with a few melting peaks overlaid. These peaks could indicate degradation of 5-FU since the decompositions of 5-FU above 280 ℃ have been well confirmed (Liu et al. 2008;Singh et al. 2009). In addition, the initial temperature cycling and annealing at 120 ℃ could have lead to conversion of less stable polymorphs back into the most stable polymorph. Although there is only one crystal structure of 5-FU reported in the literature (Fallon III 1973;Hulme, Price, & Tocher 2005), it is unknown whether these peaks can be attributed to the formation of different polymorphs of the 5-FU crystals, since new polymorph of 5-FU have recently been predicted by computers using molecular dynamics simulations (Hamad et al. 2006;Hulme, Price, & Tocher 2005;Karamertzanis et al. 2008). Therefore, to fully understand the formation of 5-FU polymorph after compression, our studies are far from enough. But we did not continue this investigation because it is unsure whether the 5-FU tablets will be applied *in vivo*.

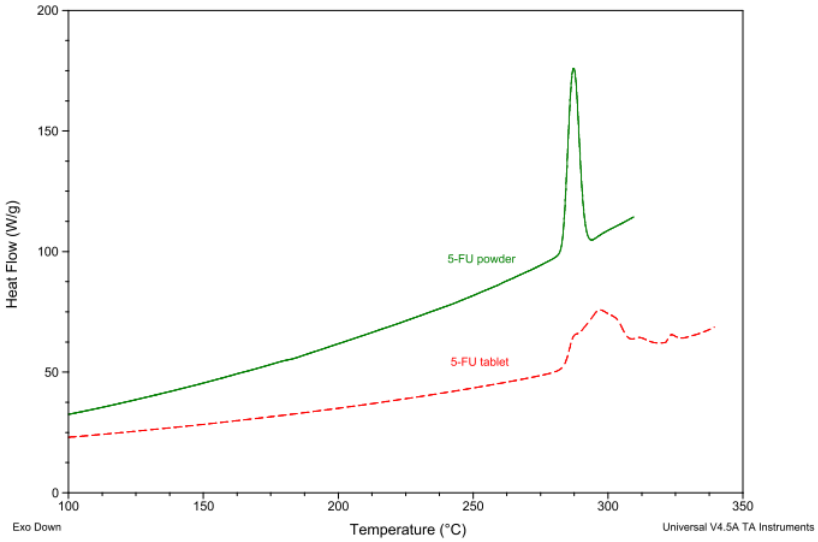


Figure 2.18. DSC curves of the 5-FU powder (solid line) and 5-FU excipient-free tablet (broken line) in a nitrogen atmosphere, flow rate 25 mL/min, heating rate 100℃/min. Data indicates the degradation of 5-FU at its melting point.

***5-FU PVP tablets***

From Figure 2.18 it can be seen that the 5-FU powder purchased from the provider was crystallized. Figure 2.19 shows the interactions between 5-FU and PVP. It can be seen that freeze dried 5-FU shows two melting peaks (283 and 304 ℃). This could be caused

by the degradation of 5-FU. When PVP alone was analyzed using the same heating rate, a fairly weak glass transition was observed at 167 ℃ (Figure 2.20 A), which is close to the reported Tg of PVP (160 ℃) in literature (Turner & Schwartz 1985).

When 5-FU was mixed directly with PVP, both melting of 5-FU (at 283 ℃, Figure 2.19) and a weak Tg of PVP (at 167 ℃, Figure 2.20 B) were observed. However, the freeze dried blended 5-FU PVP tablet did not show any melting peak around 283 ℃; whilst a glass transition and a melting/degradation peak were clearly observed at 152 and 260 ℃ respectively (pointed by red arrows in Figure 2.19). Since the Tg of PVP appears fairly weak in our results, it is felt that the Tg of PVP could not be well determined using this heating rate. However, the DSC curve of freeze dried 5-FU PVP tablets shows different from the direct blended ones. This suggests that 5-FU and PVP might become amorphous clusters after lyophilization. Further investigation needs to be conducted. But currently this has not been done since we are not planning to use these tablets *in vivo*.

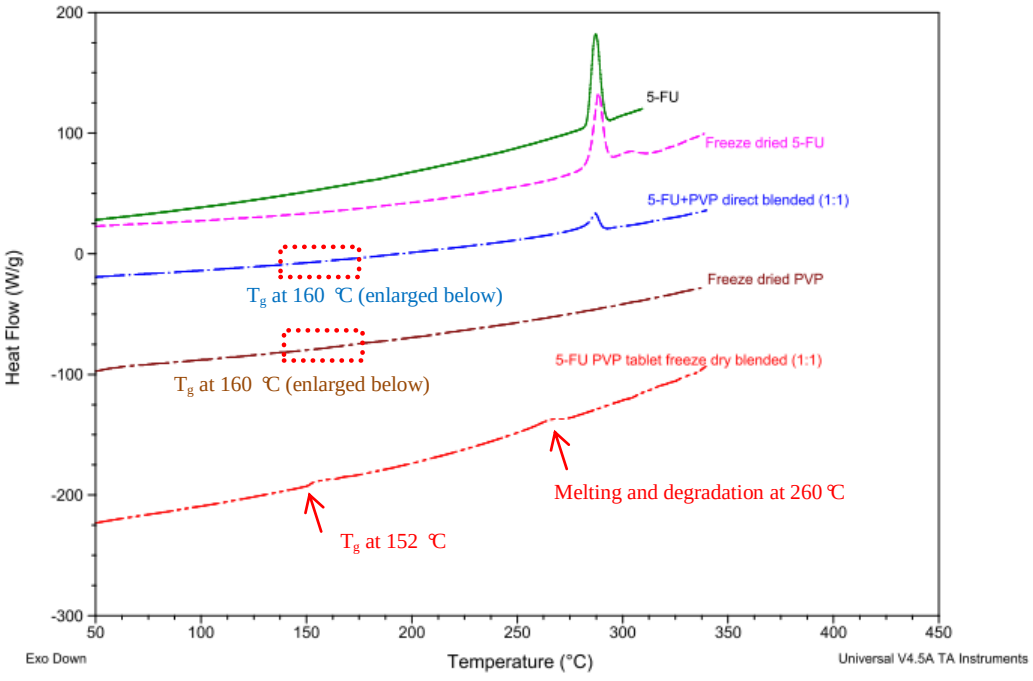


Figure 2.19. DSC curves of 5-FU powder, freeze dried 5-FU, directly blended 5-FU&PVP (1:1), freeze dried PVP, and the 5-FU PVP tablet (freeze dry blended, 1:1) in a nitrogen atmosphere, flow rate 25 mL/min, heating rate 100℃/min. Data suggest that 5-FU became amorphous after being mixed with PVP by lyophilization.

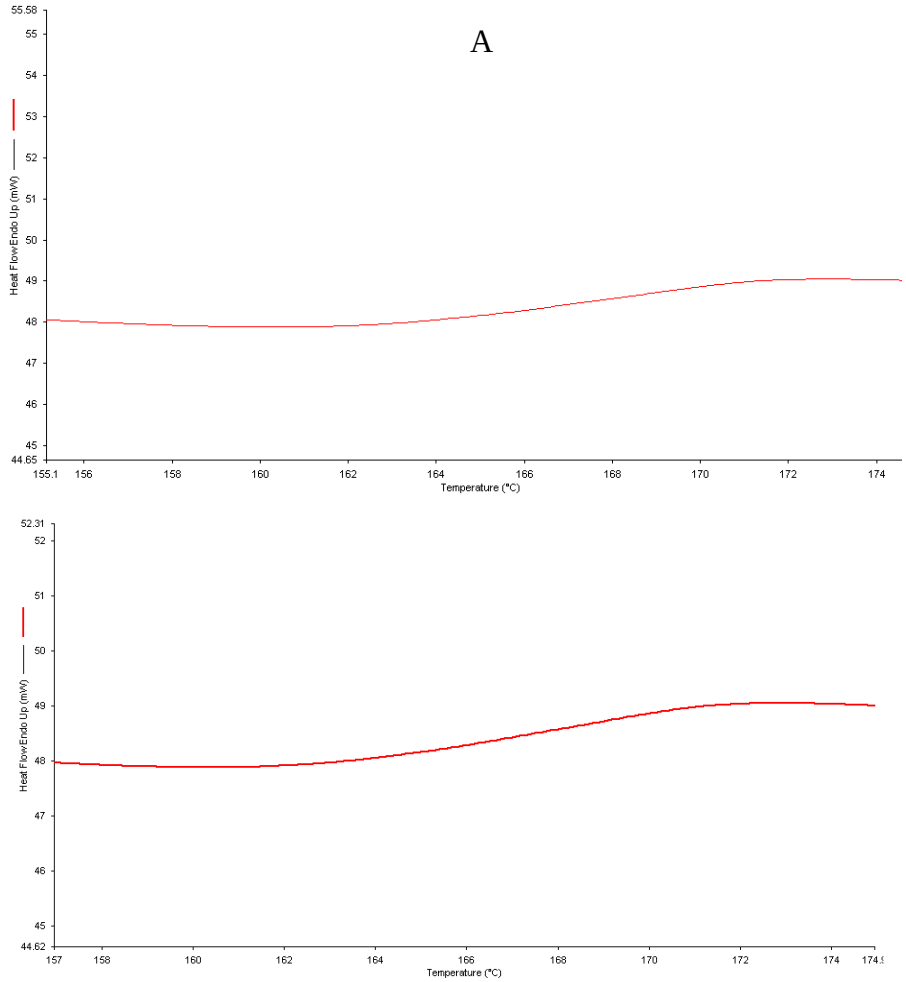


Figure 2.20 Glass transition of PVP alone (A) and 5-FU PVP directly blended tablets (B).

***5-FU HA tablets***

In a manner similar to the 5-FU PVP tablets, the 5-FU HA tablets were also analyzed. However, identification of the glass transition of HA was fairly difficult using either normal DSC, or the high heating and cooling rate DSC because HA has very high molecular weight (Mw > 1,000,000). Some of the curves seem to suggest that HA was in semi-crystallized state, but the results were not reproducible. The glass transition of solid HA can hardly be found in the literature as most of the thermal analysis was conducted on HA hydrogels. The DSC curves of HA show that degradation starts around 250 ℃. When 5-FU and HA were physically mixed without lyophilization, the 5-FU melting peak over laid that of the HA degradation (Figure 2.21).

On the DSC curve of freeze dry blended 5-FU and HA (1:1, W/W, ), a small sharp

melting peak with an onset temperature of 281 ℃ was observed, which is similar to pure 5-FU (283 ℃). This suggests that a small fraction of 5-FU was crystallized after lyophilization with HA. The peaks before the 5-FU melting peak could be attributed to the glass transition of the amorphous 5-FU HA clusters and degradation of HA. To interpret these peaks, further studies need to be conducted. But as with the excipient-free 5-FU tablets, it was felt that tablet dissolution would not be significantly affected as the 5-FU HA tablets would absorb water immediately after being placed in the bleb. This water absorption process actually made the tablet become a HA gel containing 5-FU. The release of 5-FU then mainly depends on the diffusion of the 5-FU solution within the flow chamber.

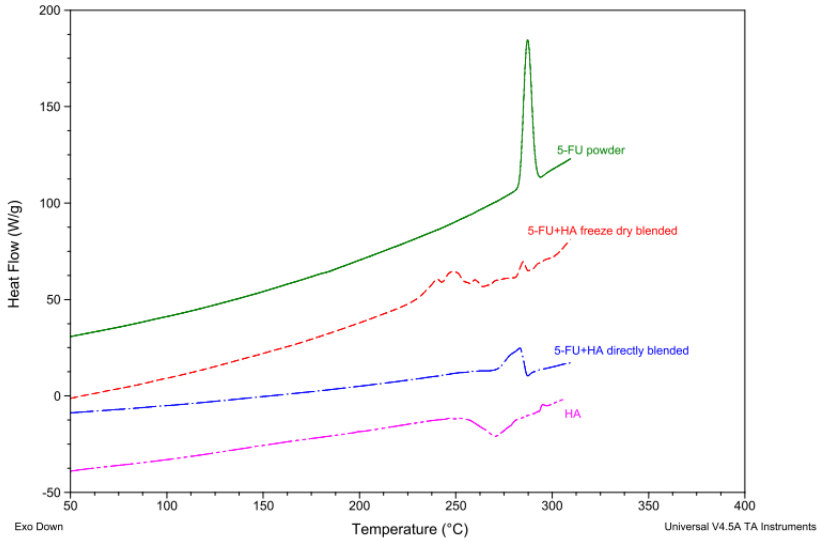


Figure 2.21. DSC curves of 5-FU powder, freeze dry blended 5-FU & HA (1:1), directly blended 5-FU & HA (1:1), and HA in a nitrogen atmosphere, flow rate 25 mL/min, heating rate 500℃/min. Data suggest that part of 5-FU was in crystal forms after being mixed with HA by lyophilization.

The DSC analysis of the 5-FU tablets showed that 1) the 5-FU powder was crystallized and 2) that 5-FU tends to become amorphous after being lyophilized with PVP or HA. This is one possible explanation for the observed higher release rate seen with the freeze dried blended 5–FU PVP tablets compared to the direct blended ones. It also suggests that the hydrophilic polymers accelerated 5-FU release by enlarging its surface area and enhancing its wettability.

## 2.4. Conclusions

We have developed an *in vitro* model with a flow chamber, which can mimic the bleb. Also, a punch and die set that can compress small tablets with 3 mm diameter was designed and fabricated. From the *in vitro* experiments conducted using the flow chamber, we understand that

1) Polymers with high viscosity can prolong the residential time of 5-FU, but hydrophilic polymers can also accelerate the 5-FU dissolution;
2) The release rate of 5-FU can be enhanced when the flow rate is increased;
3) At the same flow rate, the release rate of 5-FU can be enhanced when the volume of the flow chamber is decreased;
4) The release rate of 5-FU can be affected by the position of the tablet. The tablet demonstrates the highest release rate when it is near the entrance of the liquid flow;
5) An excipient-free 5-FU tablet is possibly as effective as a 5 minute application of 25 mg/mL 5-FU on inhibiting the proliferation of HTFs.

# *Chapter III Prolonged release of ilomastat*

## 3.1. Introduction

The excipient-free 5-FU tablets were able to prolong drug release in the flow chamber for more than 8 hours at 37 ℃. But they had not been studied *in vivo*, as it had not been confirmed whether they are able to inhibit fibroblast proliferation for longer than subconjunctival injections. From the preliminary studies on the excipient-free 5-FU tablets, we learned that 1) it is possible to make a small tablet without excipients that could potentially be placed in the subconjunctival space and 2) the release profiles of an excipient-free tablet in a non-sink condition in the bleb are mainly correlated to the solubility and dissolution rate of the drug. Since it has been established in pre-clinical studies that post-operative subconjunctival injections of ilomastat were more effective and less toxic than intraoperative MMC (Wong, Mead, & Khaw 2005), it was thought that ilomastat could possibly be fabricated into a tablet which is similar to the 5-FU tablet. Since ilomastat is a poorly water-soluble compound, we considered using some hydrophobic materials as the tablet excipients. However, the hydrophobic excipients used in the literature usually cause unintended inflammatory effects. Since it is possible to make an excipient-free 5-FU tablet, before seeking for new excipients it is worth trying to compress ilomastat into an excipient-free tablet directly. If an excipient-free ilomastat tablet can be fabricated successfully, we then do not need to worry about the side effects brought by the excipients. Since the dissolution rate of 5-FU has been found to be the rate-limiting step of the release of the drug, it suggests that, when placed under the same conditions (50-200 μl volume with liquid turnover at a flow rate of 2 μL/min), an ilomastat tablet could provide a longer release than 5-FU because ilomastat has much lower aqueous solubility (0.039 mg/mL,(Millipore 2010)) than 5-FU (11.1 mg/mL, (Yalkowsky & He 2003)). Therefore, we started to make the excipient-free ilomastat tablets.

## 3.2. Materials and methods

### 3.2.1. Materials

Ilomastat was supplied by Europa Bioproducts, Cambridgeshire, UK. Acetonitrile (ACN) was purchased from Sigma-Aldrich (UK). The Discovery® HS C18 HPLC column (15 cm×4.6 mm, 5 μm) was purchased from Sigma-Aldrich (UK). The guard

column (C18 4×3.0 mm) was purchased from Phenomenex.

### 3.2.2. Preparation of ilomastat tablets

The ilomastat tablets were made by direct compression using method described in 2.2.4.3. The weight of the ilomastat tablets was 4.1 mg, 4.8 mg (preliminary *in vitro* study), and 2.1-2.3 mg (*in vivo* studies). Their thicknesses were 0.54, 0.64, and 0.33 mm respectively.

### 3.2.3. Evaluation of the release profiles of ilomastat tablets

The release of ilomastat was evaluated using the method described in 2.2.5. The PBS flow rate was set to 2 or 4 μL/min.

### 3.2.4. Application of the tablets *in vivo*

#### 3.2.4.1. Glaucoma filtration surgery in rabbits

All experiments conformed to the ARVO Statement for the Use of Animals in Ophthalmic and Visual Research (ARVO Animal Policy). To anaesthetize the rabbits, Ketamine (50 mg/kg) and Xylazine (10 mg/kg) were given by intramuscular injections. Initially, a partial thickness 8-0 silk corneal traction suture (Ethicon) was used at the 12 o'clock position to gain access to the superior conjunctiva. A fornix based conjunctival flap was then raised and blunt dissection of subconjunctival area was performed. Following this, a partial thickness scleral tunnel was created with an MVR blade starting 2 mm behind the limbus and continuing until the blade was visible in the anterior chamber. Then a 22G/25 mm Veflon in a cannula was passed through the scleral tunnel until the cannula needle was visible in the clear cornea. During this process the cannula needle entered the anterior chamber, was advanced to the mid puppilary area and then withdrawn. The cannula was trimmed and bevelled at its scleral end so that it protruded 1 mm from the insertion point. The tube was fixed to the scleral surface using a 10-0 nylon suture on a B/V 100/4. The conjunctival incision was closed with two interrupted sutures as well as with a central mattress type 10-0 nylon suture on a B/V 100/4 needle to form a water-tight closure. One drop of Atropine Sulphate 1% (Martindale Pharmaceuticals, Romford, UK) and Betnesol N ointment was administrated at the end of the surgery (Wong, Mead, & Khaw 2005;Wong, Mead, & Khaw 2003).

### 3.2.4.2. Preliminary *in vivo* study

***Experimental design***

A random, one block study design was performed, with four rabbits undergoing GFS to the left eye. Animals were observed for a period of 30 days. The experiment was performed as a randomised, blind, controlled study with masked observers. Each observer was used to assess clinical data.

***Animals***

Four female New Zealand White (NZW) Rabbits (Harlan UK Ltd; 2-2.2 kg, 12 - 14 weeks old) were used. Animals were housed in the BRU Unit of the UCL Institute of Ophthalmology and were allowed an acclimatization period of 7 days, as is normally required.

***Treatment regimen***

Animals were randomly assigned to two selected groups, as shown in Table 3.1. Rabbits underwent GFS (described in section 3.2.4.1) in the left eye, and the right eye was used as control. Animals in Group A received an ilomastat excipient-free tablet and Group B an ethylcellulose tablet, which is the control. Ethylcellulose is an excipient that does not swell or dissolve in aqueous solution and hence we expected the size of the ethylcellulose tablet to remain unchanged during the 30-days of the *in vivo* experiment. This control tablet was the same size as the ilomastat tablet in order to establish if the effect of ilomastat itself and not just the placement of an external body (tablet) kept the bleb area functioning.

The ilomastat and ethylcellulose tablets were placed subconjunctivally just before conjunctival closure at the end of GFS. Tablets were placed only in the left eyes (one tablet per eye).

Table 3.1 Description of the groups for a preliminary *in vivo* study in which the anti-scarring effect of an excipient-free ilomastat tablet was tested.

| Group | Treatment | Tablet characteristics | Left eye | Right eye | Study end |
|---|---|---|---|---|---|
| A (3 rabbits) | Ilomastat tablets | Weight: 2.1-2.3 mg<br>Diameter: 3 mm<br>Thickness: 0.4 mm | Place one tablet in the left eye during GFS | No treatment | Day 30-all rabbit eyes to histology |
| B (1 rabbit) | Ethylcellulose tablet | Weight: 1.5 mg<br>Diameter: 3mm<br>Thickness: 0.4 mm | | | |

### 3.2.4.3. Second *in vivo* study

***Experimental design***

A randomized, prospective, masked-observer study with 24 female NZW rabbits was conducted to evaluate the potential therapeutic effect of these tablets. The 24 rabbits were divided into three different treatment groups (8 rabbits in each group) as shown in Table 3.2, the ilomastat tablet treatment group, the positive control group treated with sponges with 0.2 mg/mL MMC and the negative control group treated with sponges with sterile water. Rabbits underwent GFS (described in section 3.2.4.1) in the left eye and the right eye was used as control. As in the previous *in vivo* study, the rabbits (24 Female NZW Rabbits) were bought from the same provider (Harlan UK Ltd) and were of similar size and weight (2-2.2 kg, 12 - 14 weeks old).

Endpoints, clinical examination, measurement of IOP and study termination are described in section 3.2.4.4,3.2.4.5, and 3.2.4.6.

Table 3.2 Description of the groups for a second (randomized, blind, control) study *in vivo* study in which the anti-scarring effect of ilomastat tablet were tested.

| Group # | Treatment | Tablet/ sponge characteristics | Left Eye | Right Eye | Study End |
|---|---|---|---|---|---|
| A (8 rabbits) | Ilomastat tablet | Weight: 2.1-2.3 mg Diameter: 3mm Thickness: 0.4 mm | Placement of one pellet in the subconjunctival area of the left eye at the end of the GFS just before conjunctiva closure | No treatment | On day 30 all rabbit eyes to histology |
| B (8 rabbits) | 0.2 mg/mL MMC sponges for 3 minutes | Sponges removed after 3 minutes | Placement of the sponge in the subconjunctival area of the the left eye d at the end of the GFS just before conjunctiva closure | | |
| C (8 rabbits) | Sponges with sterile water for 3 minutes | Sponges removed after 3 minutes | Placement of the sponge in the subconjunctival area of the the left eye d at the end of the GFS just before conjunctiva closure | | |

***Aqueous, vitreous and blood samples***

At the end of the *in vivo* study and prior to the killing of the rabbits, samples of aqueous humor and cardiac blood were taken from each rabbit. Blood was obtained from the heart of the rabbits by cardiac puncture. The bloods were placed in lithium heparin polypropylene tubes and spun using centrifuge at 4000 rpm for 10 minutes. The plasma was collected and was placed in 15 mL polypropylene tubes. The amount of ilomastat contained in the samples was determined by HPLC (method described in 3.2.7.1).

### 3.2.4.4. Endpoints and clinical examination

Clinical assessments of the following parameters were undertaken every 2-3 days from day 0 to day 30:

- Bleb size (width, height and length) using callipers,
- Bleb capacity (width × height × length),
- Bleb vascularity (very hyperaemic = 3, hyperaemic = 2 , normal vascularity = 1, avascular = 0)
- Bleb location (top, nasal, temporal),
- Anterior chamber inflammation (0 = quiet, 1 = many cells, 2 = fibrin, 3 = hypopyon),
- Anterior chamber depth (deep, swallow or flat),

- Corneal epitheliopathy (0 = nil, 1 = <25 %, 2 = 50 %, 3 = 75 %, 5 = up to 100%).

#### 3.2.4.5. Measurement of IOP

Measurements of intraocular pressure in both eyes were carried out using a Mentor tonopen. IOP was measured after the topical administration of 0.5 % Proxymetacaine HCl a local anesthetic. The tonopen was lowered perpendicularly onto the corneal surface and a recording made. Five recordings per eye were made per time point and all the readings, were documented and the mean calculated.

#### 3.2.4.6. Termination of the *in vivo* study

All animals were sacrificed on day 30 of the experiment. This was carried out using a lethal intracardial injection of pentobarbitone (4 mL), administered under general anesthetic.

### 3.2.5. Thermal and surface analysis of tablets

#### 3.2.5.1. DSC measurements of ilomastat tablets

***Preparation of the ilomastat tablets***

An ilomastat tablet was placed in the flow chamber with PBS (flow rate 2 μL/min) at 37 ℃. After 48 hours, the tablet was taken out and washed three times with 200 μl de-ionized water. The tablet was then dried in a 37 ℃ oven overnight. The control tablet was not incubated in the flow chamber. The tablets were crushed gently using motor and pestle before analysis.

***DSC measurements***

Due to the limited amount of samples, DSC measurements of the ilomastat tablets were conducted on a high heating and cooling (RHC) DSC (mentioned in 2.2.9) because the amount of sample required for RHC DSC is small. The DSC samples were all weighed using a METLER TOLEDO XS105 balance (d = 0.01 mg). Samples (approximately 0.1 mg) were sealed in non-hermetic aluminium pans and heated from 25 to 300 ℃ at 500 ℃ $min^{-1}$ with a nitrogen purge gas. In all the DSC experiments, an empty pan was used as a reference and the temperature and enthalpy of the instruments calibrated with indium.

#### 3.2.5.2. Surface analysis of the ilomastat tablets

All the surface analyses were conducted by Prof. Xinyong Chen, Dr. David Scurr, and

Prof. Clive Roberts at Laboratory of Biophysics and Surface Analysis, School of Pharmacy, The University of Nottingham.

***Preparation of the ilomastat tablets***

- **Ilomastat tablets for AFM and nanoLTA**

An ilomastat tablet was placed in the flow chamber with PBS (flow rate 2 μL/min) at 37 ℃. After 24 hours, the tablet was taken out and washed three times with 200 μl de-ionized water. Then the tablet was dried in a 37 ℃ oven overnight. The control tablet was not incubated in fluid.

- **Ilomastat tablets for XPS and Tof-SIMS**

An ilomastat tablet was incubated in the 200 μl flow chamber for 9 hours at 37 ℃. Simulated aqueous fluid (Hanks buffer containing $CaCl_2$, 10% serum and 0.5% $NaN_3$) was pumped into the flow chamber at a flow rate of 2 μL/min. The tablets were then taken out and washed three times with 200 μl de-ionized water. Then the tablets were dried in a 37 ℃ oven overnight. The control tablet was not incubated in fluid.

***Atomic force microscopy (AFM) and nano-TA localized thermal analysis (nanoLTA)***

Atomic force microscopy (AFM) and Nano local thermal analysis (nanoLTA) were used to determine topographic, adhesive, stiffness and thermal changes of the tablet both before and after incubation in the flow chamber.

A Veeco MultiMode AFM with a NanoScope V controller in HarmoniX mode using HMX probes (k = 4 N/m) was used for AFM imaging. The same MultiMode AFM with an Anasys Instruments nano-TA attachment using AN2-200 thermal probes were used for nanoLTA. The same probes were used for tapping mode (TM) imaging to identify areas with relatively high or low phase contrast and for the nanoLTA measurement after area of interest were located.

***XPS and TOF-SIMS analysis***

XPS (X-Ray Photoelectron Spectroscopy) spectra were recorded using a Kratos Axis Ultra spectrometer employing a monochromated Al $K_\alpha$ X-ray source ($h\nu$ = 1486.6 eV), hybrid (magnetic / electrostatic) optics, hemispherical analyzer and a multi-channel plate and delay line detector (DLD) with a collection angle of 30 °and a take off angle of 90 °.

X-ray gun power was set to 100 W. All spectra were recorded using an aperture slot of 300 × 700 microns with a pass energy of 80 eV for survey scans and 20 eV for high-resolution core level scans. All XPS spectra were recorded using the Kratos VISION II software; data files were translated to VAMAS format and processed using the CASA XPS$^{TM}$ software package (Version 2.3.2 and later). During experiments charge compensation was used (Kratos AXIS Nova charge neutralization system: a coaxial low energy electron source within the field of the magnetic lens)) and samples were earthed via the stage using a standard BNC connector. Binding energies were charge corrected by setting the C 1s aliphatic carbon signal from adventitious carbon contamination to 285 eV.

Secondary ion mass spectrometric analysis was carried out using a SIMS IV time-of-flight instrument (ION-TOF GmbH., Münster, Germany) equipped with a Bismuth liquid metal ion gun and a single-stage reflectron analyser. Typical operating conditions utilised a primary ion energy of 25 kV and a pulsed target current of approximately 1.0 pA. Low energy electrons (20 eV) were used to compensate for the surface charging caused by the positive primary ion beam on insulating surfaces.

### 3.2.6. Preparation of ocular tissue for ilomastat extraction

Ocular tissues (cornea, bleb conjunctiva, sclera under the bleb, iris, and vitreous body) were dissected from rabbit eyes and soaked in ilomastat solutions (100 μM). The tissues were freeze-dried and then digested in Collagenase D (1.0 mL, 2mg/mL) for up to 48 hours. The liquid was then analyzed for ilomastat concentrations using the HPLC method described in 3.2.7.2. The same method was then used to detect levels of Ilomastat following the creation of an artificial bleb in an ex-vivo model. A tablet was placed under an artificial bleb and a flow (2 μL/min) passed through the subconjunctival space using a pump. Eyes were maintained for either 4 or 24 hours before tissue digestion and ilomastat detection.

### 3.2.7. HPLC instrumentation and conditions

The HPLC methods were developed with the guide and discussion with Dr. Hardyal Gill at London School of Pharmacy. HPLC analysis was performed on an Agilent Technology 1200 series system consisting of a separation module for solvent and sample delivery, a UV detector and Chemstation software for data acquisition and analysis. The UV wave length was set at 280 nm according to the maximum absorption of ilomastat shown on the UV scan. Both C8 and C18 column were tested. It was found that the C18 column demonstrated better retention and separation than the other. Therefore, a Discovery® HS C18 HPLC column (15cm × 4.6mm I. D., 5μm particle size) was used with a guard column for compound separation.

#### 3.2.7.1. HPLC method for *in vitro* release of ilomastat tablets

The mobile phase was 20 mM ammonium acetate buffer with 0.1% TEA (pH 5):ACN (75:25). Samples were eluted at a flow rate of 1.0 mL/min. The injection volume was 10 μl. Chromatography was performed at 40 ℃. The retention time of ilomastat was found to be 6.5 minute.

#### 3.2.7.2. HPLC method for detection of ilomastat in ocular tissues

The mobile phase was 20mM ammonium acetate buffer with 0.1% TEA (pH 5):ACN (75:15). Samples were eluted at a flow rate of 1.2 mL/min. The injection volume was 100 μl. Chromatography was performed at 40 ℃. The retention time of ilomastat was found to be 25.6 minute.

## 3.3. Results and discussion

### 3.3.1. *In vitro* release profiles of ilomastat tablets

Since there is no excipient in the ilomastat tablets, we need to find out whether ilomastat can be compressed into tablets that are robust enough for handing and transportation. So a number of different pressures (1, 2, 4, 5 bar) were tested during tablet compression. It was found that at least 5 bar was required to fabricate an ilomastat tablet which can keep its integrity during handling and transportation. According to the regulatory in industry, friability of the ilomastat tablets compressed under this pressure needs to be investigated. But it was felt that this should be investigated after the efficacy and dose of the tablets are confirmed due to the limit availability of ilomastat. Therefore,

we needed to decide how much drug the tablet should contain. Previous studies on 5-FU showed that a 5 mg excipient-free 5-FU tablet could stay in the flow chamber for approximately 8 hours at 37 ℃. However, during the release studies on the 5-FU tablets, the concentration of the drug was not constant; it changes along with the time as a result of the changing of tablet surface area and the presence of aqueous flow. Similarly, the concentration of ilomastat is expected to change if a saturation of ilomastat cannot be observed. Therefore, the dissolution of a 5 mg ilomastat tablet could not simply be predicted using its intrinsic solubility alone because it is unknown whether saturation of ilomastat will occur in the flow chamber. To understand the dissolution profiles of the ilomastat tablets, we investigated the ilomastat tablets using the same *in vitro* model that was used for the 5-FU tablets.

The release profiles of the ilomastat tablets were evaluated at different flow rate (2 and 4 μL/min, Figure 3.1.) and at different temperatures (ambient temperature and 37 ℃, Figure 3.2.) using the flow chambers. It was observed that the tablet kept its integrity during the *in vitro* dissolution experiments. Although the experiments were not repeated three times due to the limited availability of ilomastat, Figure 3.1. shows that the ilomastat tablets dissolved much slower than 5-FU tablets. After one month at ambient temperature, approximately 70% of the ilomastat was released under a flow rate of 4 μl; whilst only about 46% of ilomastat was released when the flow rate was 2 μl. During this period, the ilomastat concentration was kept at 60-100 μM with the low flow rate (2 μL/min); but when the flow rate was doubled (4 μL/min) the ilomastat concentration dropped below 20 μM after 20 days. This is probably because the surface area of the tablet decreased more quickly when the flow rate was increased. Hence, the results suggest that the dissolution rate of the ilomastat tablets increased with an increase in the flow rate. Meanwhile, the ilomastat concentration seemed to decrease more rapidly with an increase in flow rate, which is probably the result of a fast diffusion of the drug solution at a high flow rate of the dissolution media.

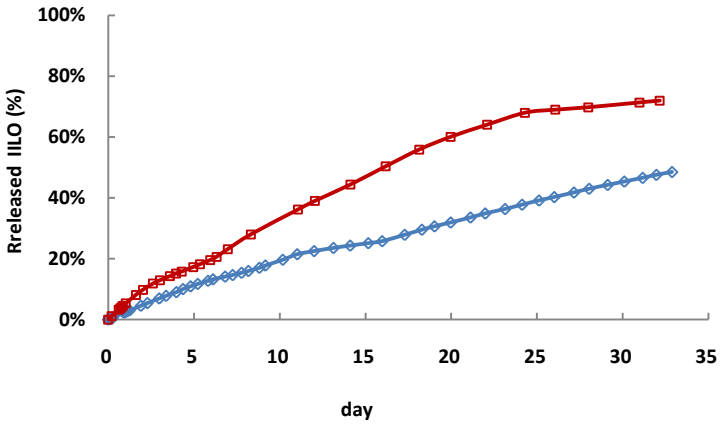


Figure 3.1. Release profile of ilomastat (ILO) tablets in 200 µl chamber in ambient temperature at different flow rate. ◇ 2µL/min □ 4 µL/min. Data suggest that the release rate of ilomastat would be enhanced when the flow rate is increased.

The dissolution of the ilomastat tablet was significantly increased at 37 ℃. More than 40% of the ilomastat was released from the tablet after 2 days at 37 ℃ compared to less than 10% of the ilomastat at ambient temperature (Figure 3.2.). Due to the limited availability of ilomastat, evaluation of the ilomastat tablet at 37 ℃ was conducted for 2 days only because we wanted to use the remaining tablet for thermal analysis. The concentration of ilomastat in the flow chamber reached around 200 µM at 37 ℃, which is twice as high as the one at ambient temperature. However, this concentration is still far below the saturated concentration of ilomastat in pH 7.4 PBS at 37 ℃ (574.1 µM, Dr. Hala Fadda), which again confirmed that the dissolution rate of ilomastat, not the solubility, is the rate limiting step for the dissolution of the ilomastat tablet.

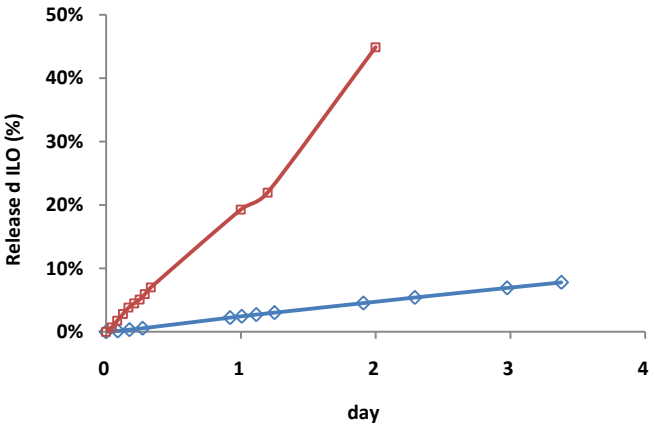


Figure 3.2. Comparison of ilomastat (ILO) release profiles in 200 µl chamber at 2 µL/min in ambient temperature (◇) and 37 ℃ (□). Data suggest that the release rate of ilomastat will be increased with the increasing of temperature.

Unlike the 5-FU tablet which disappeared in the flow chamber after 8 hours, the ilomastat tablet still remained in the flow chamber after 48 hours. Although the above studies were not done in triplicate due to the limited availability of ilomastat, it still suggests that the residence time of an ilomastat tablet is significantly longer than the 5-FU tablets. This is encouraging because we believed that when the ilomastat tablet is placed in the bleb its anti-proliferative effect would possibly last for at least 2 days, which is longer than an intraoperatively used sponge or subconjunctival injections. However, before the *in vivo* studies, we needed to find out whether the ilomastat tablet is as effective as the ilomastat solution at scar inhibition. To confirm this, we needed to ensure that 1) there is no degradation of ilomastat during the tablet incubation period and 2) the ilomastat concentration in the flow chamber is in the therapeutic window.

It has been established that ilomastat degrades in aqueous solutions at a ratio of 1% per month at 4 ℃. At 37 ℃, the degradation increases to 1% per day (Millipore 2010). Since the tablet will be exposed to an aqueous environment at the body temperature for a long period of time, it is possible that ilomastat could start to degrade within the bleb before it joins in the blood/lymphatic circulation. Therefore, the degradation of ilomastat was investigated using HPLC. To ensure that the degradation product does not have the same retention time as ilomastat, fully degraded ilomastat solution was injected into the HPLC. No peak could be seen at 6.5 minute (the retention time of ilomastat). This suggests that the degradation product will not produce a peak on the HPLC that overlays with ilomastat. Hence, we can evaluate the degradation of ilomastat by observing the presence of extra peaks on the HPLC chromatograms. When we evaluated the ilomastat solution collected from the 37 ℃ flow chamber at different time point by HPLC, no extra peaks were observed in comparison to the ilomastat powder. This suggests that the ilomastat released at 37 ℃ did not degrade in the flow chamber. In the *in vitro* study at ambient temperature, after 30 days the remaining ilomastat tablet was dissolved in pH 7.6 PBS and injected into the HPLC. No extra peaks were observed either. This suggests that the ilomastat solid which was exposed to moisture for 30 days did not degrade. Hence, it was confirmed that no chemical decomposition of ilomastat

had occurred in the flow chamber. This provides us with a positive indication that ilomastat will probably be stable when the tablet is placed in the bleb.

### 3.3.2. Sterilization of the ilomastat tablets

Before the ilomastat tablets could be implanted in a bleb, they had to be sterilized. Since no data has been published on the degradation of ilomastat following sterilization, we needed to confirm whether the sterilization process could cause any degradation of ilomastat. Following the guidelines of European and the US pharmacopoeias**,** the ilomastat tablets were irradiated by either gamma radiation (28.8 kGys) or electronic beams (28.0-29 kGys) and then dissolved in pH 7.6 solutions. The degradation of ilomastat was evaluated by injecting the solutions into the HPLC. As shown in Figure 3.3., a new peak was observed at 7.4 minute on the irradiated ilomastat, which represents the degradation products of ilomastat. These peaks account for a 0.55% (gamma radiation) and 0.47% (electronic beams) degradation of the ilomastat in the tablets respectively, which is less than 1% of degradation after irradiation. These results meet the criteria of the American and European Pharmacopoeia (less than 1% degradation).

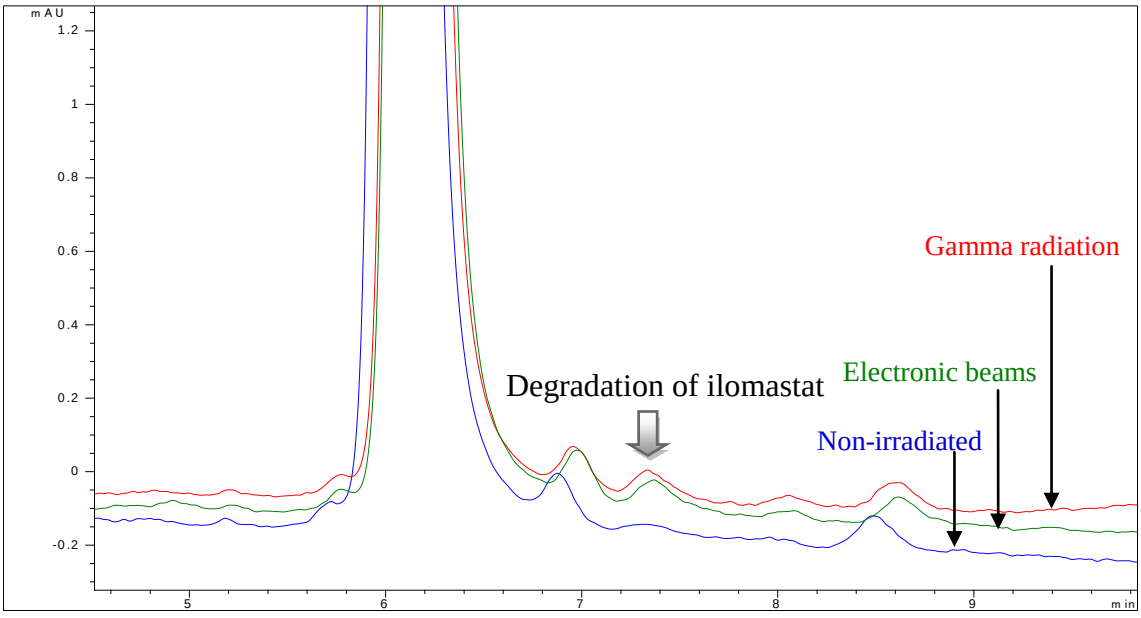


Figure 3.3. HPLC chromatograms of the non-irradiated (blue), gamma radiation (red) and electronic beams (green) irradiated ilomastat. The degradation peak appears at 7.4 min. Data suggest that gamma or electronic beam radiation can cause a small amount of ilomastat degradation.

It was then necessary to establish whether a sterilized ilomastat tablet is able to inhibit the Human Tenon's Fibroblasts (HTF) populated collagen I gel contraction for more than 7 days. Thus, the inhibitory contraction of non-irradiated ilomastat and ilomastat released from irradiated tablets were compared (by Dr. Stylianos Georgoulas). The results showed that the efficacy on HTF gel contraction of the irradiated tablet is similar to the non-irradiated ilomastat powder (Figure 3.4., provided by Dr. Stylianos Georgoulas), thus confirming that the sterilized ilomastat tablet is as effective as the non-irradiated ilomastat. So the *in vivo* studies of the ilomastat tablets could be conducted.

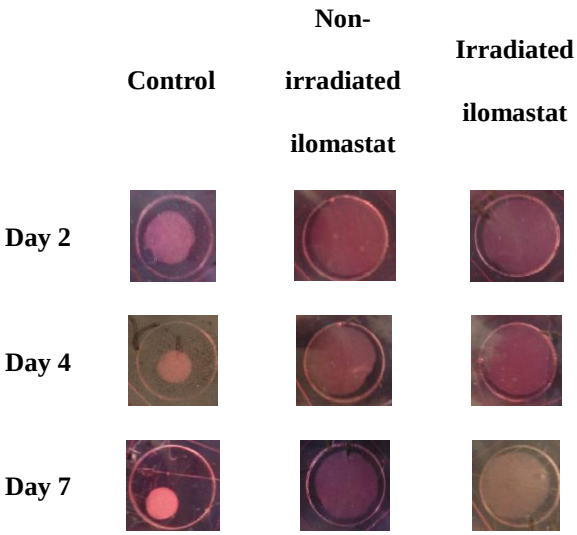


Figure 3.4. HTF populated collagen I gels treated with normal media without ilomastat (negative control), media in which non-irradiated ilomastat powder was dissolved without DMSO (positive control) and media in which irradiated ilomastat tablet was dissolved without DMSO. The concentration of ilomastat in the positive control and the media in which the ilomastat tablet was dissolved was tested with HPLC and was adjusted to be at the same level (65 μM). The results indicate that the efficacy on HTF gel contraction of the irradiated tablet is similar to the non-irradiated ilomastat powder.

### 3.3.3. *In vivo* release of ilomastat tablets

#### 3.3.3.1. Preliminary *in vivo* experiment

To evaluate the anti-scarring effect of the ilomastat tablet, the tablets needed to be placed in the bleb. Since the *in vivo* studies require filtration surgeries on the rabbit eye, the studies was conducted in collaboration with a clinician (Dr. Stylianos Georgoulas). All the surgeries were performed by Dr. Georgoulas. A preliminary *in vivo* experiment was conducted on four rabbits. To establish that the formation of the bleb is not a result

of spacer effect caused by the tablet, an ethylcellulose tablet which has the same size as the ilomastat tablet was designed as a control. Since ethylcellulose is insoluble, inactive and does not swell in the bleb, we were able to compare the effect of the ilomastat tablets and the inert tablet on the morphology of the bleb. The other three rabbits were all treated with the ilomastat tablets (weight approximately 2.3 mg each). Unlike the clinically used sponges which are removed after a few minutes, all the tablets were left in the subconjunctival space before the closure of the conjunctiva. After the surgery, the bleb treated with ethylcellulose tablet failed on day 10 (Figure 3.5); while the ilomastat tablet treated blebs were still functional after 30 days (Figure 3.6). These results indicate it is the drug (ilomastat) and not the tablet itself that is responsible for scar inhibition in the bleb.

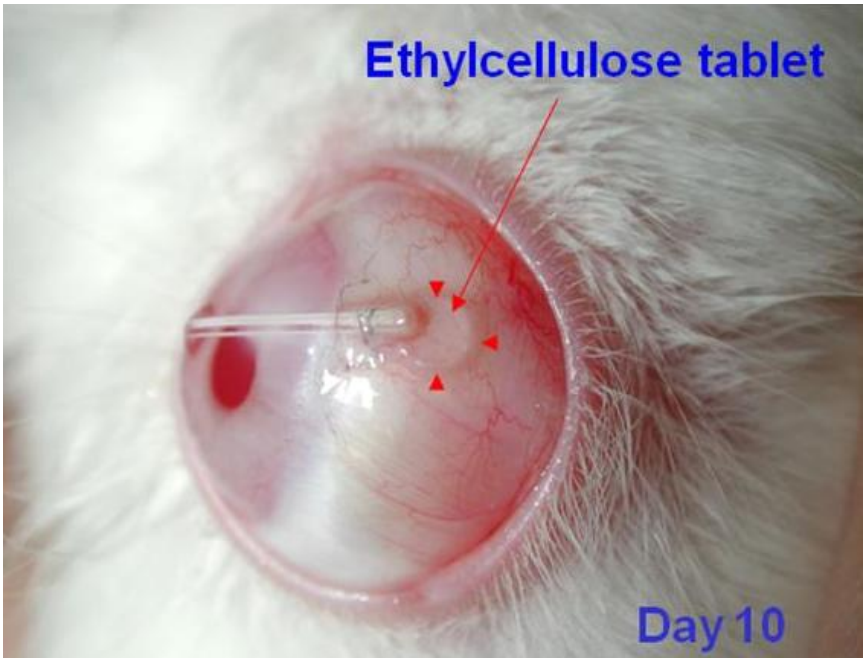


Figure 3.5. Appearance of a bleb in which an ethylcellulose tablet has been inserted after glaucoma filtration surgery. The bleb failed on day 10. This image shows the conjunctiva surrounding the tablet and the tip of the tube, possibly stopping aqueous outflow from the tube.


Figure 3.6. Appearance after 30 days of the bleb in which an ilomastat tablet was placed after glaucoma filtration surgery. The bleb remained elevated and functional throughout the experiment and it indicated that the ilomastat tablet may be effective *in vivo* in the inhibition of scarring.

#### 3.3.3.2. Second *in vivo* study

***Effect of ilomastat tablets on bleb function and morphology***

Having confirmed that the survival of the bleb was not due to the presence of a tablet but due to the anti-scarring effect of ilomastat, a second *in vivo* study was conducted to further investigate the anti-scarring effect of the ilomastat tablet. In this study, the ilomastat tablets were compared with both negative (water sponge for 3 minutes) and positive (MMC 0.2 mg/mL sponge for 3 minute) controls. It was observed that blebs treated with the ilomastat tablets (Figure 3.9) appeared larger than the MMC treated blebs (Figure 3.8). In addition, all the ilomastat tablet treated blebs remained functional for 30 days. The bleb survival curve is shown in Figure 3.10. It indicates that the scar inhibition effect of ilomastat tablets was significantly better than the MMC treatment currently used in the clinic.

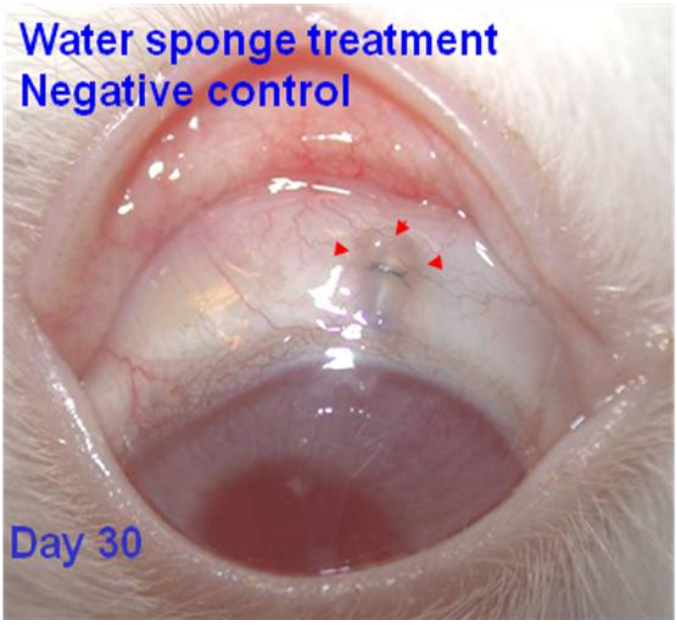


Figure 3.7. Representative failed bleb from the water sponge negative control group. The bleb is shown to be flat and to block the tip of the tube due to the development of scarring, possibly inhibiting the aqueous outflow through the tube.

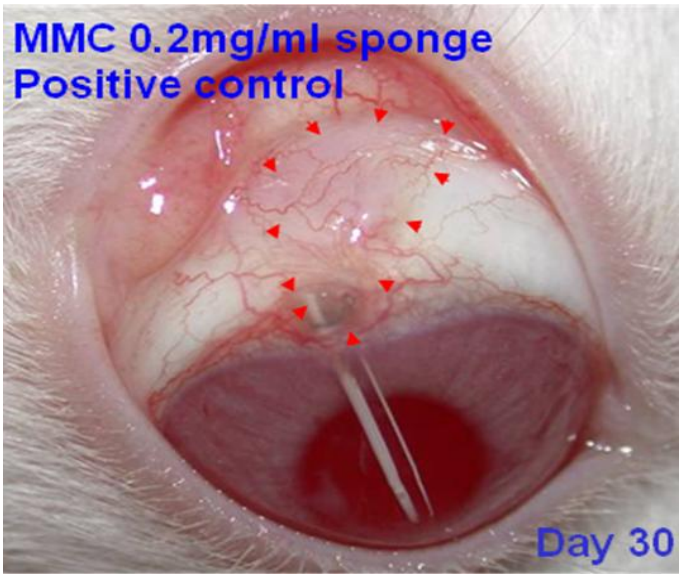


Figure 3.8. Representative functional bleb from the positive control group (MMC 0.2 mg/mL) sponge for 3 minutes). Two out of eight blebs treated with MMC remained functional throughout the experiment.

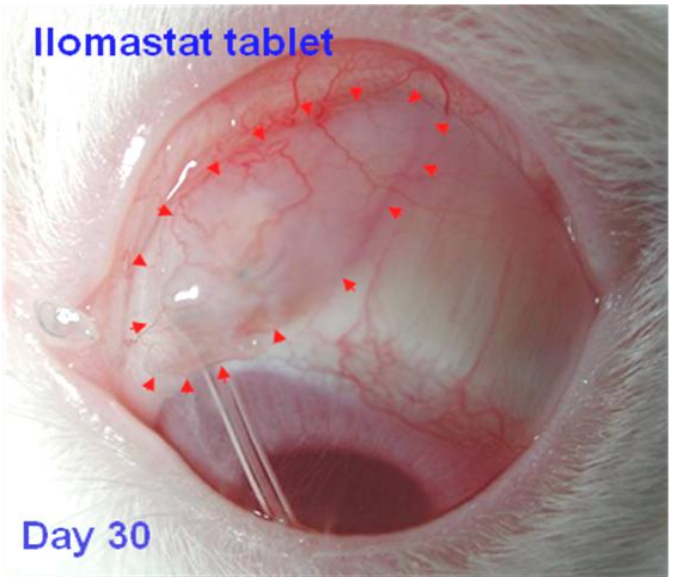


Figure 3.9. Representative functional bleb from the ilomastat tablet group. The bleb area of all rabbits treated with the ilomastat tablet remained functional and significantly elevated throughout the experiment. This outcome was significantly superior not only compared to the negative control (water sponge) but also compared to the positive control (MMC).

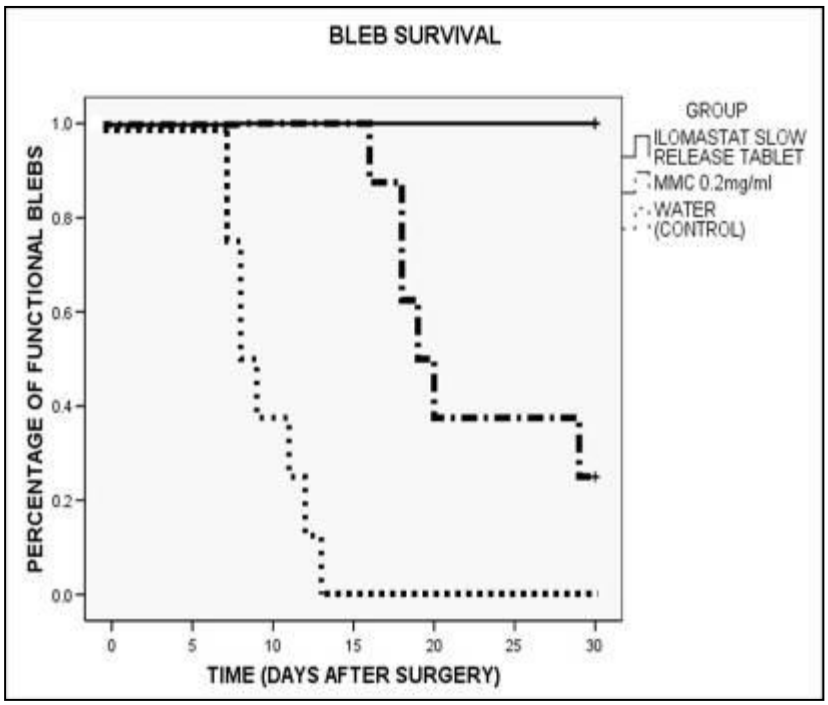


Figure 3.10. Bleb survival in the ilomastat tablet group was found to be significantly superior to the sterile water group ($P<0.001$) and the MMC group ($P<0.01$) ($n=8$) (Georgoulas S.D. et al. 2008).

***Effect of ilomastat tablets on intraocular pressure (IOP)***

As IOP is one of the most important indexes in halting the progression of glaucoma, the effect of ilomastat tablets on the IOP was also evaluated (Figure 3.11). A normal IOP was observed in all the rabbit eyes treated with the ilomastat tablets. The mean IOP of

the ilomastat treated eyes was found to be significantly lower than the negative control group on day 7, 16, 20, 23 and 27. In comparison with the positive control group, the IOP was significantly lower on days 20 and 23. No hypotony was observed in the ilomastat tablet treated eyes. In contrast, hypotony was observed in MMC treatment group on day 3.

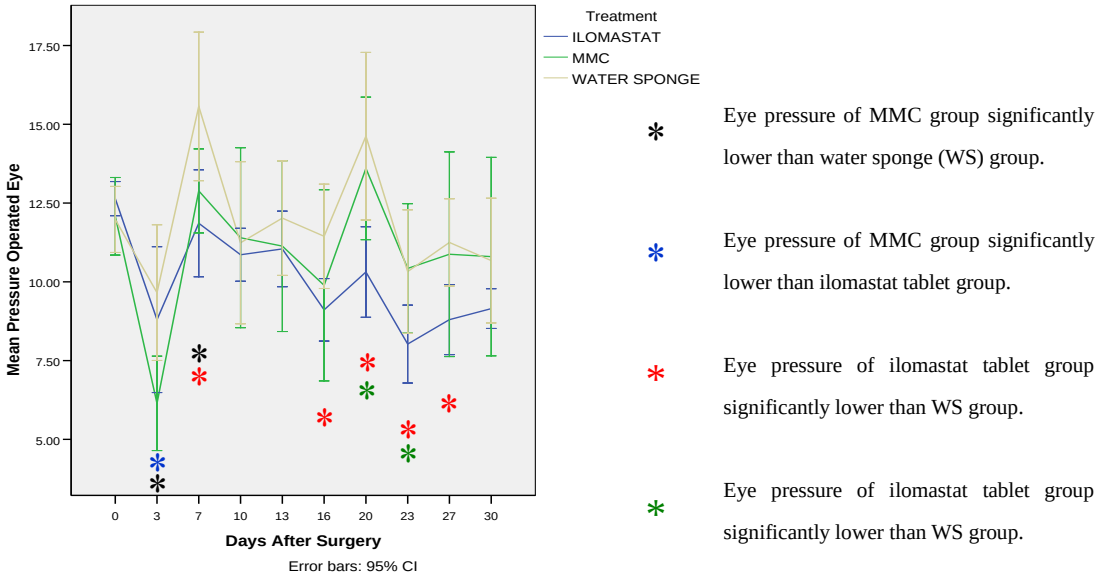


Figure 3.11. Ilomastat tablet significantly reduced IOP compared to positive and negative controls (Georgoulas S.D. et al. 2008).

The IOP was measured with a Mentor tonopen. The tonopen is based on the principle that the IOP can be gauged by the pressure necessary to flatten the central area of the cornea. The accuracy of the IOP based on this principle is influenced by corneal biochemical properties such as its thickness and rigidity. Hence, as shown in Figure 3.11, fluctuation of the measurements does occur because 1) there is variation in individual rabbit corneas, and 2) the outflow of aqueous humor, which is directly associated with the IOP, is affected by the varying bleb dimensions as well as the level of scarring in the subconjunctival space. Newer tonometry devices, including the dynamic contour tonometry and the Ocular Response Analyzer®, which take into account the biomechanical properties of the cornea, have been designed to measure the IOP more consistently (Stamper 2011). However, a Mentor tonopen was the best technique we had when the animal studies were conducted. Nonetheless, this technique has been proven to be useful in both animal and human being studies, and has been clinically validated

(Mollan et al. 2008;Rahman, Cannon, & Sadiq 2010).

***Detection of ilomastat in the aqueous humor, vitreous body and blood serum of the rabbits treated with the ilomastat tablet***

Since ilomastat may cause adverse effects (musculoskeletal syndrome) when administrated systemically at a dose of 50-100 mg/kg body weight (Dormn et al. 2010;Fingleton 2007;Li et al. 2002;Millipore 2010), it is important to examine its local and systemic toxicity. Using the HPLC method described in 3.2.7.1, no ilomastat was detected in the blood serum or the aqueous humor that was obtained at day 30 from the rabbit eyes treated with the ilomastat tablets. However, since the sensitivity of this method is low (approximately 5 μM, see the calibration curve in Table 3.3), it is possible that ilomastat exists in the blood at a concentration lower than 5 μM. As the typical dose of ilomastat in animals is 50-100 mg/kg body weight (Millipore 2010), it is believed that the systemic toxicity of the ilomastat tablet is fairly low because our tablet contains less than 5 mg of ilomastat.

Table 3.3 Calibration curve of ilomastat using the HPLC method described in 3.2.7.1 (n=3, $R^2$=0.9999). Data indicates that the lowest ilomastat concentration that can be detected using this HPLC method is approximately 3-5 μM.

| Concentration (μM) | Average Peak Area |
|---|---|
| 250 | 712.8±1.17 |
| 100 | 281.5±0.52 |
| 125 | 357.4±0.21 |
| 62.5 | 178±0.26 |
| 50 | 143.7±0.40 |
| 31.25 | 87.87±0.2 |
| 12.5 | 35.4±0.1 |
| 6.25 | 21.7±0.06 |
| 3.125 | 8.533±0.12 |

### 3.3.4. Thermal and surface analysis of ilomastat tablets

#### 3.3.4.1. Thermal analysis of tablets

Since the ilomastat tablets will stay in the bleb for days, the tablets were immersed in 35 ℃ aqueous humor for a long time. As the physical properties of ilomastat have not been studied before, the morphology of ilomastat is unknown. It is also unknown whether its morphology will change on long exposure to aqueous humor. Change in drug morphology (such as crystal forms) may affect tablet release profiles. Therefore, it

is necessary to determine the physical properties of the tablets. Due to the limited availability of ilomastat, we only evaluated two tablets use high heating and cooling rate DSC. One was the control tablet; and the other the tablet that was in the flow chamber for 48 hours.

Figure 3.12 shows the DSC curves of the ilomastat tablet before and after being incubated in pH 7.6 PBS for 48 hours. In this figure, ilomastat demonstrates crystalline form with no detectable amorphous content. However, the initial temperature cycling and annealing at 120 ℃ could have lead to conversion of less stable polymorphs back into the most stable polymorph. Therefore, further investigation was conducted by our colleague (Dr. Hala Fada) using thermal activity monitor. It was later confirmed that there is no quantifiable amorphous content in the ilomastat tablet (data not shown). The tablets demonstrated a similar melting with an onset temperature of 217.7 ℃ (before) and 216.5 ℃ (after) respectively. The melting peak is not a sharp single peak, which suggests that the overlaying peaks could come from the degradation of ilomastat. It is known that using high heating rate in DSC experiments can improve the detection sensitivity of different transitions; but the peaks could still not be resolved at a high heating rate (500 ℃/min). The color change of the material at the end of the DSC experiments confirmed the degradation of ilomastat while melting. An endothermic peak with a low heat capacity change was observed around 130 ℃ in both tablets. This peak was reversible (existed in the same position on repeated heating and cooling). The evidence suggests it is an enantiotropic solid-solid transition, which was further confirmed by performing X-ray on an ilomastat tablet heated to 150 ℃ (data not shown, experiments conducted by Dr. Hala Fadda).

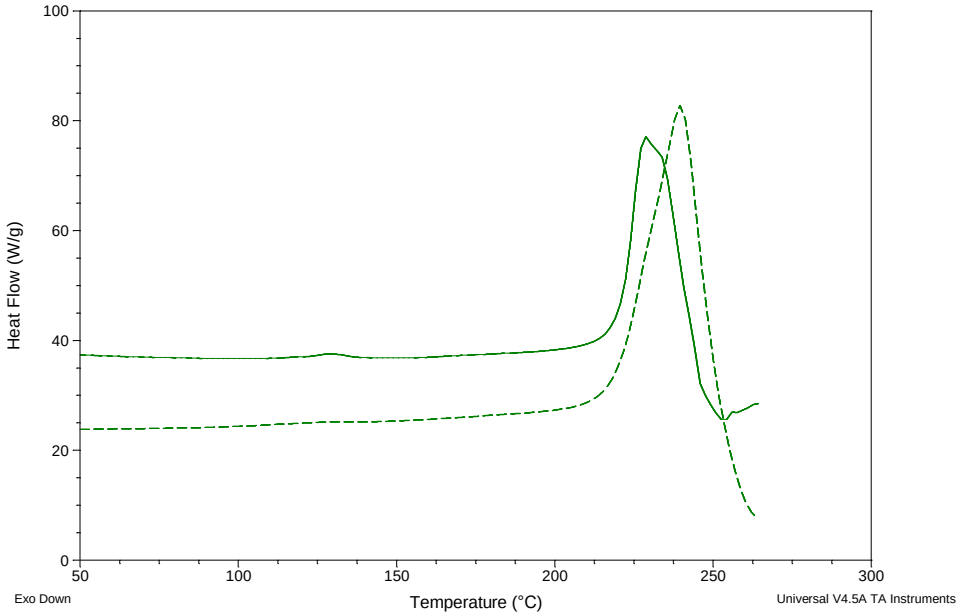


Figure 3.12. DSC curves of the excipient-free ilomastat tablets before (solid line) and after (broken line) aqueous incubation. The DSC experiments were conducted in a nitrogen atmosphere, flow rate 25 mL/min, heating rate 500℃/min. Data suggest possible formation of ilomastat polymorphs after tablet incubation.

Therefore, further investigations were conducted by our colleague (Dr. Hala Fadda). It was found that different batches of ilomastat from the same supplier demonstrated different crystal forms on an X-ray powder diffractogram (Figure 3.13). The moisture uptake of the ilomastat tablets was investigated by dynamic vapour sorption (DVS). The results show that the moisture uptake of the ilomastat tablets was 4.7% at 90% relative humidity (RH), but all moisture absorbed was displaced at 0% RH (Figure 3.14). The X-ray showed changes in the crystal habit of ilomastat on immediate exposure to a moist environment (Figure 3.15). This can have implications on the solubility and dissolution of the drug. However since these changes arise immediately on wetting, the dissolution characteristics of the tablet will not change during the course of incubation in the bleb (Fadda et al. 2010).

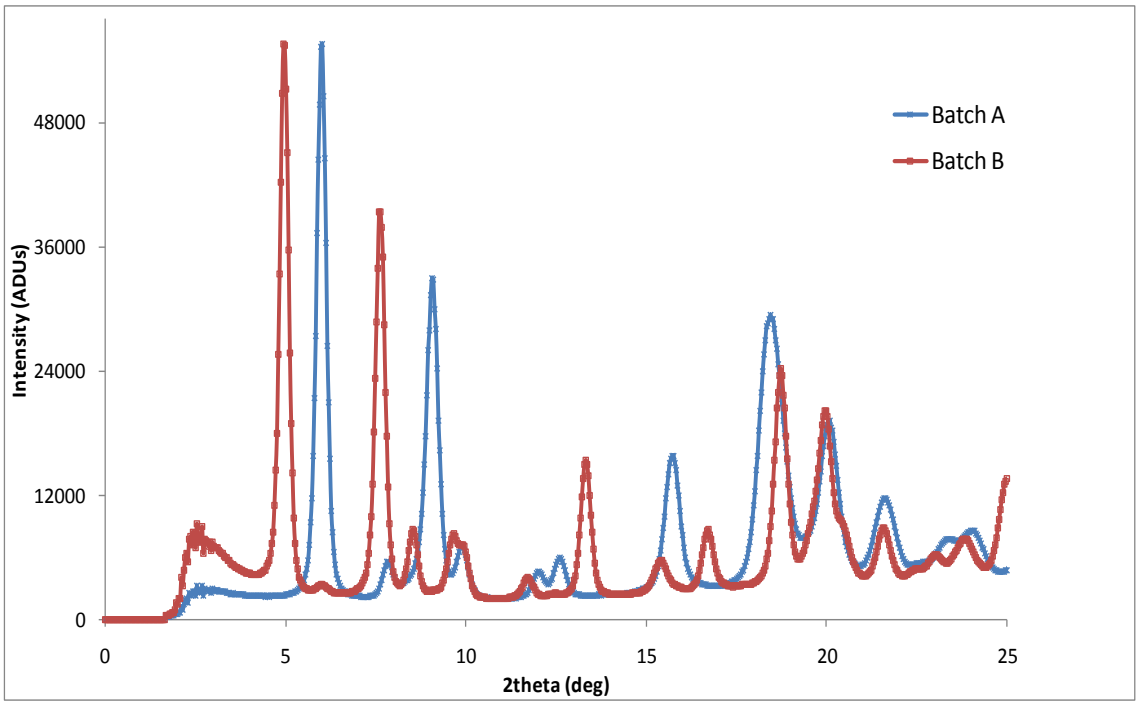


Figure 3.13. X-ray powder diffractogram of ilomastat tablets prepared from different batches obtained from the same supplier (Fadda et al. 2010). Data suggest existence of new ilomastat polymorphs from different batches of ilomastat provided by the same supplier.

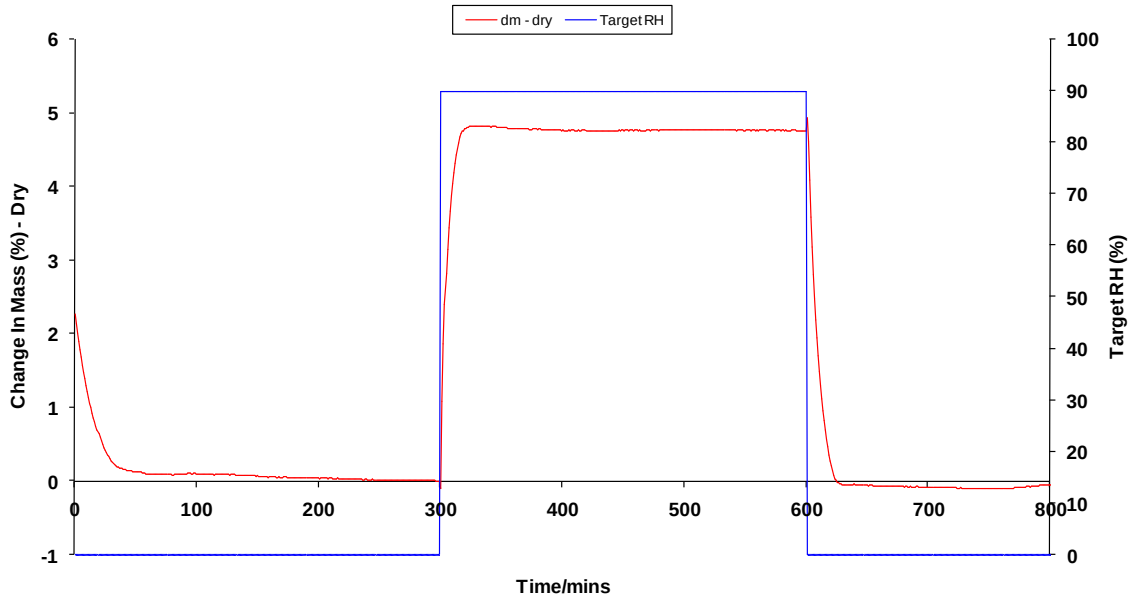


Figure 3.14. Water uptake of the ilomastat tablet as studied by dynamic vapour sorption (Fadda et al. 2010). Data suggest that the moisture uptake of the ilomastat tablets was 4.7% at 90% relative humidity (RH), but all moisture absorbed was displaced at 0% RH.

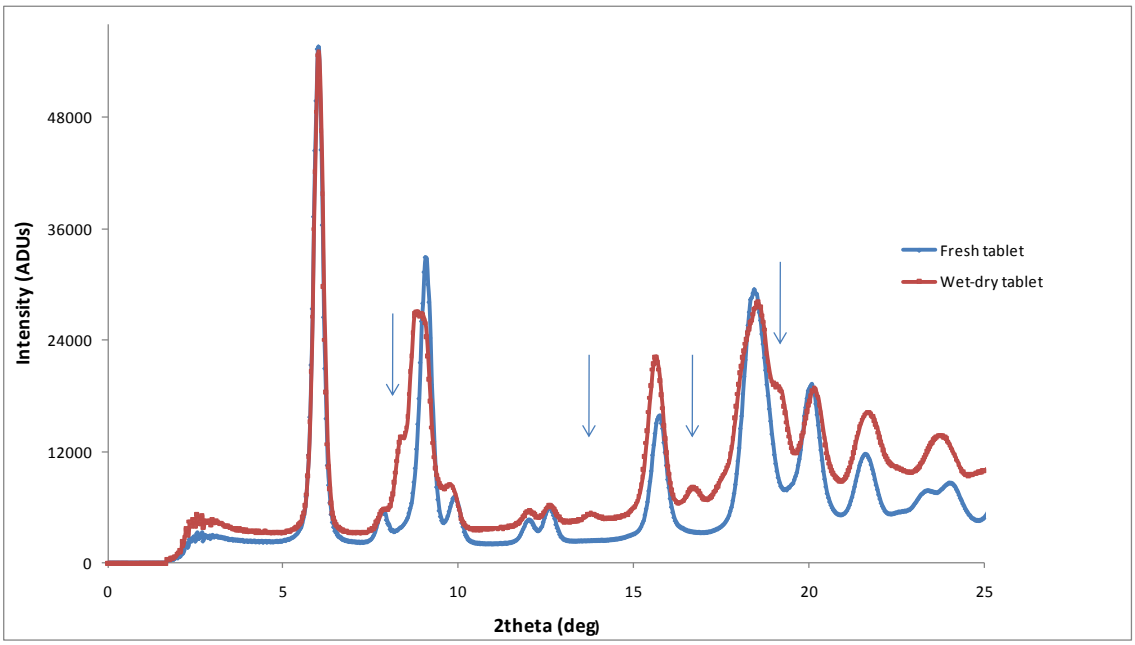


Figure 3.15. X-ray powder diffractogram illustrating changes in the crystal form of ilomastat on exposure to high humidity levels. (Arrows indicate where the changes are observed) (Fadda et al. 2010).

#### 3.3.4.2. Atomic force microscopy (AFM) and nano-TA localized thermal analysis (nanoLTA) of ilomastat tablets

Although it has been established that changes in the physical properties of the ilomastat tablets did not significantly affect the *in vitro* tablet releases profiles, it is still unknown whether the *in vivo* environment will affect the release and efficacy of the tablets. One of the probable responses from the *in vivo* conditions is the encapsulation of the tablet, which has been described in the literature (Chapter 1). In our second *in vivo* study, the tablets could still be observed on day 30 after surgery; but it was unknown whether the tablets were encapsulated. The encapsulation of the ilomastat tablet in a functional bleb was later found in another *in vivo* study. The remaining tablet was removed from the bleb and dissolved (Figure 3.16). The amount of ilomastat left in the tablet was determined by HPLC.The results showed that 57.7% ilomastat had dissolved in the bleb over 30 days, which suggests that tablet dissolution in the bleb is slower than in the flow chamber. This indicates that, once encapsulated, tablet dissolution slows down. But this does not mean the tablet will not completely dissolve. Another *in vivo* study was conducted with excipient-free lenalidomide tablets which have a similar size to the ilomastat tablets (by Dr. Ashkan Khalili). These tablets were found to dissolve in the bleb within 3 weeks. To fully understand the dissolution of the ilomastat tablet, we need

to understand the encapsulation. Although clinically the small ilomastat tablet encapsulation is less disruptive than the usual fibrosis or the fibrosis around an implant, but it is not known when the encapsulation started. It is also unclear whether the formation of the capsule will slow down or stopped the release of ilomastat. We therefore do want to ensure that the tablet will be resorbed completely.

Figure 3.16. An ilomastat tablet was encapsulated on day 30 after implantation (image provided by Dr. Sumit Dhingra).

It has been established that the encapsulation is caused by foreign body reactions (FBR), which are the end stage response of the inflammatory and wound healing responses following implantation (Anderson, Rodriguez, & Chang 2008). The FBR is carried out by macrophages and foreign body giant cells. It is believed that the biomaterial surface plays an important role in modulating the BFR in the early stages of implantation (Anderson, Rodriguez, & Chang 2008). Protein adsorption is considered to be one of the key events in FBR because the types, levels, and surfaced conformations of the adsorbed proteins are critical determinants of tissue reactions to the implants (Wilson et al. 2005). Since it has been described that implants are covered (Wilson et al. 2005), the ilomastat tablet was supposed to be covered by similar materials due to the trauma of the surgery. However, as the tablet was placed in an environment with aqueous turnover which can cause the displacement of the cells and proteins, investigation of the surface of the remaining tablet will provide us some information on the initial signals of encapsulation. But our previous studies using the flow chamber could not predict the formation of capsule as all the studies were conducted using PBS with the absence of all the other substances (e.g. fibroblasts, proteins and amino acids (Table 1.2)) existing in aqueous humor. Therefore, we incubated the ilomastat tablets at 37 ℃ with simulated

aqueous fluid (see 3.2.5.2) being pumped into the chamber at a flow rate of 2 μL/min. It is hoped that during this incubation the deposition of proteins and salts on the surface of the ilomastat tablets will simulate the *in vivo* conditions. The effect of the simulated aqueous fluid on the surface physical properties of the tablets will then be determined.

Atomic force microscopy (AFM), which is also called scanning force microscopy, is one of the most advanced tools for imaging, measuring, and manipulating materials (Giessibl 2003). Its resolution is demonstrated on nano scale, which is more than 1000 times better than the optical diffraction limit. AFM is able to "feel" the specimen surface with a mechanical probe, which is a conducting cantilever with a sharp tip (Giessibl 2003). Information about the material surface is gathered from the forces between the tip and the sample. The forces measured could be mechanical contact forces, van der Waals forces, chemical bonding, and electronic forces etc. Depending on the application, different modes can be operated in an AFM, including static (contact) modes and dynamic (non-contact) modes. In the static mode operation, the feedback signal comes from the static tip deflection; whist in the dynamic mode, the cantilever is externally oscillated (Garcia & Perez 2002).

When an AFM is attached to a thermal probe, it is able to perform local thermal analysis on the material surface on a nano scale, which is called nano localized thermal analysis (nanoLTA). In pharmaceutical science, AFM and nanoLTA are used in the investigation of drug crystal growth, particle characterization, and tablet granules/ coatings in solid dosageforms. It is hoped that this technique will be able to help us to observe the surface of the ilomastat tablets and to investigate the change in the surface physical properties of tablets after being in contact with the aqueous fluid. Of interest is the accumulation of both salt and protein on the surface of the tablet following incubation with simulated aqueous fluid. Ultimately we aim to understand the deposition behaviour of proteins in an effort to understand how the tablets may interact with tissue and cells *in vivo*.

***Optical microscope images***

The ilomastat tablets' surface was observed firstly by the AFM. Optical microscope images were captured using the basic CCD camera attached to the AFM. In all the images, the AFM cantilever might not be properly focused as the samples need to be focused on. A relatively "clean" surface was observed for the control ilomastat tablet which had not been in the flow chamber (Figure 3.17 A). The observed parallel lines are probably caused by the compression punch. These lines were not observed on the incubated ilomastat tablet (Figure 3.17 B). This change is caused by the dissolution of the ilomastat on the tablet surface.

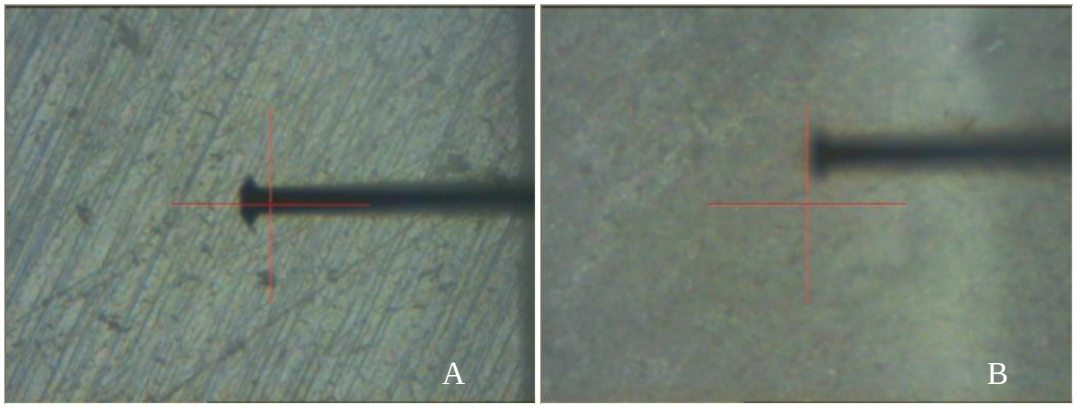


Figure 3.17. AFM optical images of the ilomastat tablets before (A) and after (B) being in the flow chamber. The control tablet appears more "clean" than the incubated tablet.

***Other surface quantitative "images"***

HarmoniX is a new AFM mode that provides true nanoscale quantitative material property mapping of adhesion, stiffness, dissipation, peak force, and average force for a wide range of materials. Unlike the previous AFM techniques, HarmoniX is able to acquire both the high-resolution imaging and high-resolution, quantitative material property maps simultaneously (Veeco 2010). In HarmoniX AFM, as well as Height and Phase images as in normal tapping mode, a number of quantitative "images" relating to surface mechanical properties or tip-sample interactions, such as surface Young's Modulus (stiffness), peak force, average force, adhesion, energy dissipation, can be simultaneously obtained. For clarification, only the most representative adhesion and stiffness images are presented together with the corresponding height and phase images

in Figure 3.18. More adhesion is observed in the control tablet (22 nN) as compared to the incubated tablet (5.3 nN) both of which are highlighted with a red square. The surface of the control tablet shows greater stiffness, 6 GPa as opposed to 0.8 Gpa. Surface component-related phase separation was obviously observed in the incubated ilomastat tablet. The "adhesion" image shows that the surface areas showing "brighter" phase data possess higher adhesion to the silicon based AFM tip. These surface areas are also slightly "harder" than the other areas, as shown in the corresponding "stiffness" image.

In the HarmoniX images of the control tablet shown in Figure 3.18, the contrast in the phase, adhesion, and stiffness images are just topography-related artefacts. 'True' phase contrast was clearly observed in another tapping mode image (Figure 3.19). This may indicate a fairly inhomogeneous surface.

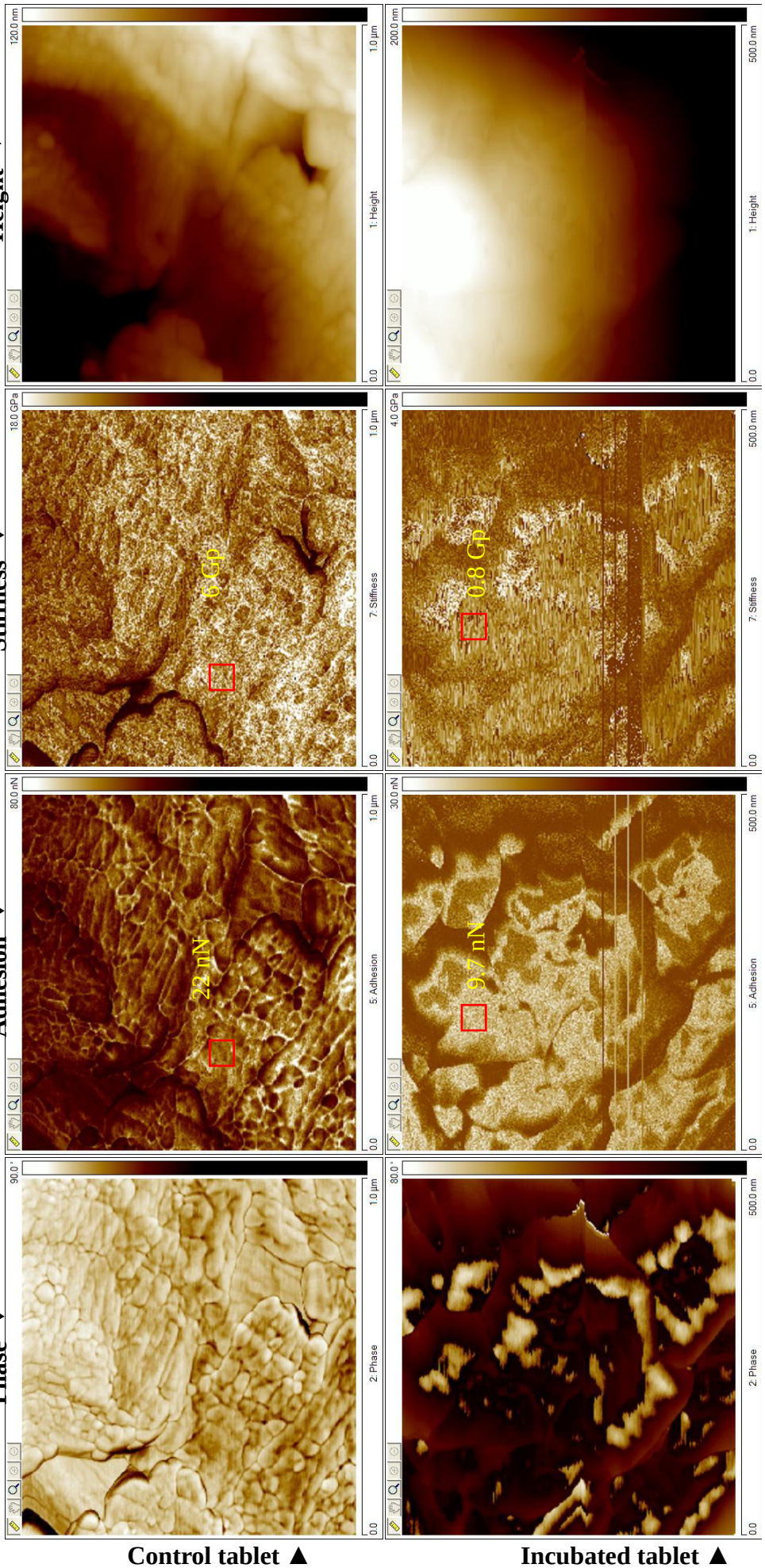


Figure 3.18. HarmoniX AFM images of the adhesion and stiffness of both control and incubated tablet surface. The brighter colour in the "adhesion" and "stiffness" images indicate higher adhesion and greater Young's modulus, respectively. More adhesion is observed in the control tablet (22 nN) compare to the incubated tablet (9.7 nN) both of which are highlighted with a red square. The surface of the control tablet also shows greater stiffness (6 GPa) as opposed to 0.8 Gpa.

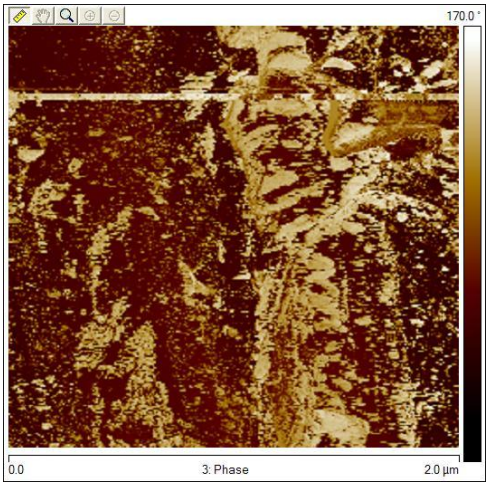


Figure 3.19. Tapping mode AFM images of the control ilomastat tablet. This indicates an inhomogeneous surface on the control tablet.

***nanoLTA results***

NanoLTA results of the ilomastat tablets are shown in Figure 3.20. For both ilomastat tablets (before and after being incubated), a sharp dropping down consistent with a melting event was observed in the ranges of about 150-190 ℃ and 130-160 ℃, respectively. Since the nano-TA thermal probe can perform normal tapping mode AFM imaging, it was used to investigate if there was any difference in the observed thermal transition temperature ($T_x$) between the surface areas with bright and dark phases (the phase images obtained by the nano-TA probe are not shown, but they are very similar to those shown in Figure 3.20). There seemed to be no significant correlation with the phase difference compared with the relatively large variation of $T_x$ itself from repeated nanoLTA measurements.

It was observed during tapping mode that imaging of the nano-TA measurements made in the high-phase areas was usually unstable. Once the scan size of the tapping mode imaging was reduced and limited to the high-phase area, the phase signal usually shifted down very quickly. Therefore, special attention was paid to avoid excessive heavy tapping (and hence applied force) on the high-phase areas before the nanoLTA was conducted. This quick change in the high-phase areas during tapping imaging may mainly result from 1) a change in the tip status because of adsorption of material from the surface or 2) that the material with the high-phase feature may be a loosely attached thin layer,

which was swept off by the nano-TA probe during TM imaging. If the latter reason is true, it may explain why the high-phase area has the similar $T_x$ to the low-phase area.

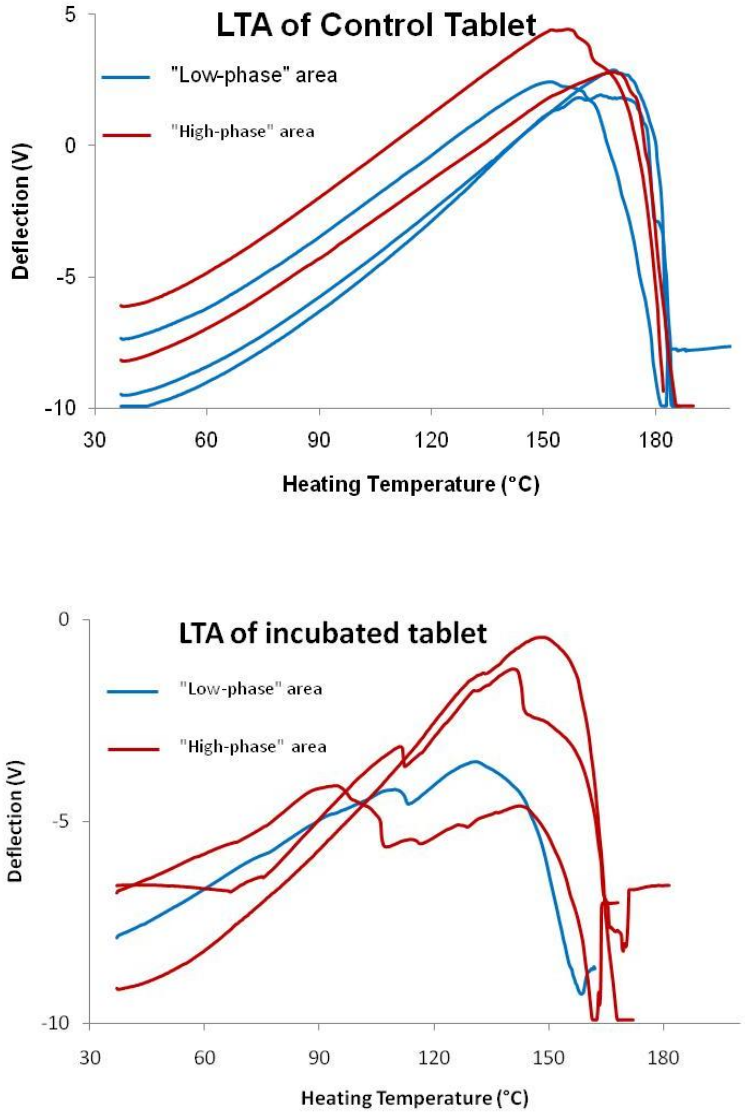


Figure 3.20. The effect of incubation on the thermal properties of the tablets using NanoLTA (localized thermal analysis) measurements with AFM. Differences in the transition temperature (Tx) were determined. The lower Tx observed following incubation suggests a softening of the tablets. The complexity of melting curve with the incubated tablet may be as a result of deposition of salts on the tablet surface.

Difference in the mechanical properties and $T_x$ were observed for both ilomastat tablets, in addition to differences in their optical image. This indicates that they are different materials, at least in terms of their surfaces. This may correlate with changes in the crystal form of ilomastat after exposure to high humidity levels (Figure 3.15). The surface of the control tablet is generally harder, more adhesive (to the silicon tip) and

has a higher $T_x$.

#### 3.3.4.3. XPS and TOF-SIMS (time-of-flight secondary ion mass spectrometry) of ilomastat tablet (ions mapping)

In addition to AFM, X-ray photoelectron spectroscopy (XPS) and time of flight secondary ion mass spectrometry (Tof-SIMS) are other surface analysis techniques that can be used to analyze the surface chemistry of a material. XPS quantitatively measures the elemental composition, empirical formula, chemical state and electronic state within a material. Tof-SIMS provides information about the chemical structure, including elements, functional groups, polymer constitutes, molecules, with very high sensitivity. It is hoped that these techniques will help us to further investigate the differences between the ilomastat tablet before and after being incubated in a simulated aqueous fluid. Specifically, the presence of proteins, which are associated with the possibility of capsule formation, can be identified by sulphur.

***Atomic composition of the ilomastat tablet surface (Ca. 8 nm)***

Surface analysis using X-ray photoelectron spectroscopy (XPS) reveals an accumulation of sodium, sulphur and increased composition of calcium on the tablet surface (Table 3.4). Figure 3.21 shows the distribution of the different positive ions deposited on the tablet surface. It was found that the ion intensities of $Na^+$, $K^+$, and $CHS^+$ on the tablet surface increased 3.7, 1.3, and 4.1 times after incubation. This data in combination with Table 3.4 suggests that the accumulation of both salts (e.g. sodium and calcium) and protein (sulphur) within 8 nm of the tablet surface.

Table 3.4. Atomic composition (%) of ilomastat tablets surface before and after incubation in a simulated aqueous fluid. Data suggest the significant increasing of $Na^+$, $K^+$, and $CHS^+$ on the tablet surface after incubation.

| Element | Control ilomastat tablet | Incubated tablet |
|---|---|---|
| Chlorine 2p | 0.28 | 0.53 |
| Carbon 1s | 74.06 | 71.09 |
| Nitrogen 1s | 12.9 | 13.28 |
| Oxygen 1s | 12.19 | 14.63 |
| Sodium 1s | 0.00 | 0.09 |
| Calcium 2p | 0.01 | 0.04 |
| Sulphur 2p | 0.00 | 0.12 |
| Silicon 2p | 0.55 | 0.23 |

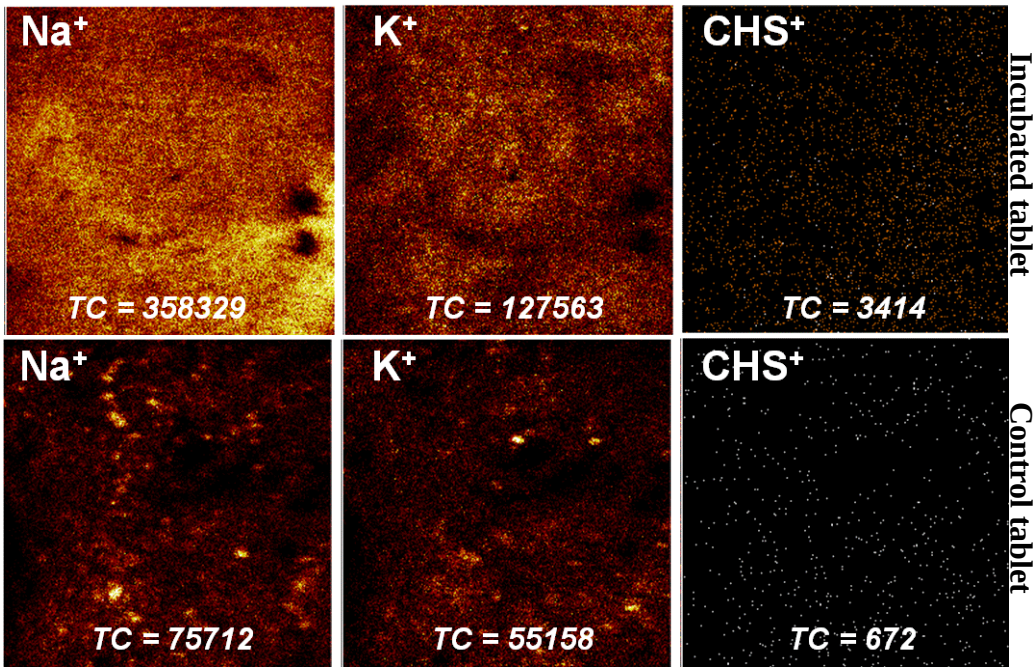


Figure 3.21. Distribution of different positive ions on the tablet surface. Data shows an accumulation of sodium (Na+) potassium (K+) and sulphur (CHS+) on the tablet surface following incubation in the rig with simulated aqueous fluid (9 hours). This in turn suggests the accumulation of both protein and salts on tablet surface. Ion intensities (TC) are given in the bottom. Higher values depict higher intensities. This data complement the XPS data shown in Table 3.4.

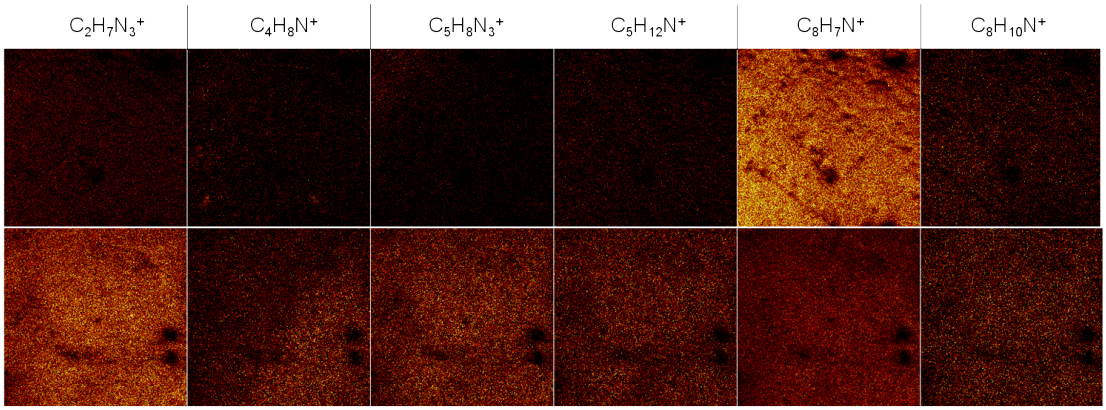


Figure 3.22. Distribution of ions associated with amino acids on the surface of the tablets. The normalized intensities (TC) suggest an increase in the deposition of all ions with the exception of $C_8H_7N^+$ which is believed to be a fragment of ilomastat.

Figure 3.22 shows the distribution of ions associated with amino acids (including isoleucine, phenylalanine, proline, arginine, and histidine) on the surface of the tablets (Wagner et al. 2002;Wald et al. 2010). An increase in the deposition of all ions with the exception of $C_8H_7N^+$ (a fragment of ilomastat) was observed. This data in combination with the ToF-SIMS and XPS data suggest that, even with a liquid turnover, the ilomastat tablets accumulate protein on their surface following incubation with serum containing proteins. This will have implications for the release rate of ilomastat from tissue tablets that will come into contact with proteins. More importantly, this indicates that capsule formation is possible within the bleb.

### 3.3.5. Determination of the accumulation of ilomastat in rabbit ocular tissue

Previous studies have demonstrated that using HPLC, ilomastat with a concentration that is higher than 5 μM could not be found in blood serum or the aqueous humor of the rabbits after 30 days of exposure to an ilomastat tablet (Georgoulas 2010). However, as the ilomastat tablet will be placed in the subconjunctival space, accumulation of ilomastat in ocular tissue is possible. It has been reported in literature that drugs delivered locally can accumulate within tissues close to the site of delivery (Wang et al. 1996). Since the toxicity of ilomastat with regards to ocular tissue remains unclear, understanding both the tissue distribution and accumulation of ilomastat within the eye will provide us valuable information for future toxicity studies.

Most studies analyzing the bio-distribution of drugs commonly involve the use of one of two markers either: (1) use of a fluorescent probe or (2) radiolabelling. In devising a method for the analysis of the bio-distribution of ilomastat in ocular tissues, both methods were fully investigated.

***Use of a Fluorescent Probe***

Ilomastat itself does not have any absorption on fluorescence spectroscopy. As previously documented, ilomastat is a relatively small molecule with a molecular weight of 388.5 g/mol. A number of commercially available fluorophores were investigated for conjugation with ilomastat, but even the smallest of the probes available (members of the Couramin family) had molecular weight of around 300. Using a probe of this size would almost double the size of ilomastat and likely impact the function of the drug.

Much smaller in size than the types of fluorophore previously discussed, quantum dots (QDs) are rapidly becoming a favored tool for both *in vitro* and *in vivo* imaging of cellular targets, cells themselves and drugs (Gao et al. 2005;Hild, Breunig, & Goepferich 2008;Orlov et al. 2008;Smith et al. 2008). The use of fluorophore and QDs with drug molecules (particularly protein antibodies) is becoming widespread (Agarwal et al. 2008;Frasco & Chaniotakis 2010;Furrer & Gurny 2010;Lu 2010). However, conjugation of either fluorophore or QD to a small molecule without affecting its efficacy is still an obstacle that needs to be overcome.

***Use of Radiolabelling***

Radiolabelling has long been used to determine drug distribution *in vivo*, particularly in ocular tissues as well as drugs currently used during GFS (Jarus et al. 1985;Rootman, Ostry, & Gudauskas 1984). To radiolabel a drug, two options are available: either creation of the drug using a radiolabelled molecule (such as carbon-14) or the substitution of a radiolabelled molecule (such as tritium) to modify a pre-existing compound. The development of a radiolabelled compound from the start using a radiolabelled molecule is very expensive and often prohibitive to many investigators. We therefore set out to

develop a method using HPLC to determine the distribution of ilomastat in ocular tissues.

Using HPLC for drug detection in ocular samples is not a novel concept, but previous studies have focused primarily on fluid samples such as the aqueous humor and blood serum, although some studies have looked at ocular tissues (Hollo et al. 2006). We sought a method that 1) would provide a high sensitivity for ilomastat detection 2) would not compromise the integrity of ilomastat, and 3) is reproducible.

***Increasing the Sensitivity of HPLC***

Using the previously described HPLC method for ilomastat (see 3.2.7.1) may not be sensitive enough for the purpose of drug detection in tissue. Therefore, we tried to improve the sensitivity of the HPLC method, which means the lowest ilomastat concentration which can be detected using HPLC. Firstly, the injection volume was increased from 10 µL to 100 µL so that the amount of ilomastat in one injection could be increased. Following this change in injection volume, the flow rate was increased to 1.2 mL/min to minimize any broadening of the peak that would occur had the initial flow rate been used. Following these small, yet important changes, the sensitivity of ilomastat detection using HPLC was increased from 5 µM (Table 3.3) to 100 nM (Table 3.5).

Table 3.5. Calibration curve of ilomastat using the HPLC method described in 3.2.7.2 ($R^2$=0.9999). Data suggest that the sensitivity of this HPLC method is approximately 100 nM.

| **Concentration (nM)** | **Average Peak Area** |
|---|---|
| 100000 | 2757 |
| 50000 | 1375 |
| 25000 | 681.2 |
| 12500 | 338.7 |
| 6250 | 163.4 |
| 3125 | 80.83 |
| 1562.5 | 39.83 |
| 781.25 | 18.57 |
| 390.625 | 10.07 |
| 195.3125 | 3.9 |
| 97.65625 | 2.7 |

***Tissue digestion***

To determine the ilomastat tissue concentration using a HPLC method, several confirmatory conditions during the digestion step were required. Firstly the ocular tissue had to be well digested, with all tissue (including fibrous regions) digested as fully as possible. Secondly, it needed to be confirmed that the digestion reagents did not cause a decomposition of ilomastat. Thirdly, it needed to be confirmed that the digestion reagents (including the tissue itself and digestion reagents) did not lead to the creation of peaks that overlay with ilomastat on the HPLC curve. This would be confirmed by HPLC (data shown below).

During method development several chemicals and enzymes were tried at different temperatures. Mechanical methods were also examined. A summary of those used are presented below in Table 3.6. Although some of the methods, including Trizol and proteinase K, provided good homogenization of the tissue, the reagents led to the decomposition of ilomastat. The only method which provided both good tissue digestions without destroying ilomastat was through the use of collagenase D.

Table 3.6 The methods used to digest the ocular tissues. It suggests that the only method which provided good tissue digestions without interfering with ilomastat was through the use of collagenase D.

| **Mechanism of Homogenization** | **Extra Products Used** | **Positive Results** | **Negative results** |
|---|---|---|---|
| Acid/Base | | | Degradation of ilomastat |
| Laemelli Buffer | | Relatively Inexpensive | Little to no degradation without some mechanical input |
| Mortar and Pestle | Homogenize directly | | Inconsistent homogenization |
| | Laemelli Buffer | | Loss of Sample |
| | Liquid Nitrogen | | |
| Homogenizer | Various sized probes | | Loss of tissue in the probe |
| | With Laemelli Buffer | | Poor homogenization in Laemelli Buffer |
| | With TRIZOL | Good homogenization in Trizol | Degradation of ilomastat due to TRIZOL |
| Centrifuge Beads | Various speeds in PBS | Rapid Tissue degradation | Sclera not homogenized |
| | Various speeds in Laemelli Buffer | Rapid Tissue degradation | Sclera not homogenized |
| TRIZOL | | Excellent tissue degradation, particularly with mechanical input | Degradation of ilomastat |
| Proteinase K | 56 $^{o}$C | Excellent tissue degradation after 24 hours | Degradation of ilomastat |
| | 37 $^{o}$C, 300 RPM | | Poor tissue degradation after 48 hours |
| Collagenase D | 37 $^{o}$C, 300 RPM | Excellent tissue digestion after max. 48 hours | |

***Internal standard***

During the extraction process, an internal standard, that is similar to the standard analyte, is normally used to correct the loss of the analyte during sample preparation prior to detection. An internal standard must have several properties similar to that of the target analyte including its molecular weight and structure. A number of databases were searched to find a compound that would act as an internal standard for ilomastat, including PubChem, ChemSpider and SciFinder. It was found that Leu-Trp (Sigma-Aldrich, UK) was the only commercially available compound that had a similar molecular weight and structure to that of ilomastat (Figure 3.23.). The solubility of Leu-Trp was unknown. Leu-Trp was later found to be soluble not in water or the HPLC mobile phase but in DMSO. Using DMSO to dissolve Leu-Trp and then mixing it with ilomastat, it was found that the ilomastat peak overlaid with one of the impurities in Leu-Trp when a gradient elution was used (Figure 3.24.). Alternative gradient methods were tried but the peaks could not be separated. The overlaying peaks were not observed when an isocratic flow (3.2.7.2) was used (Figure 3.25.).

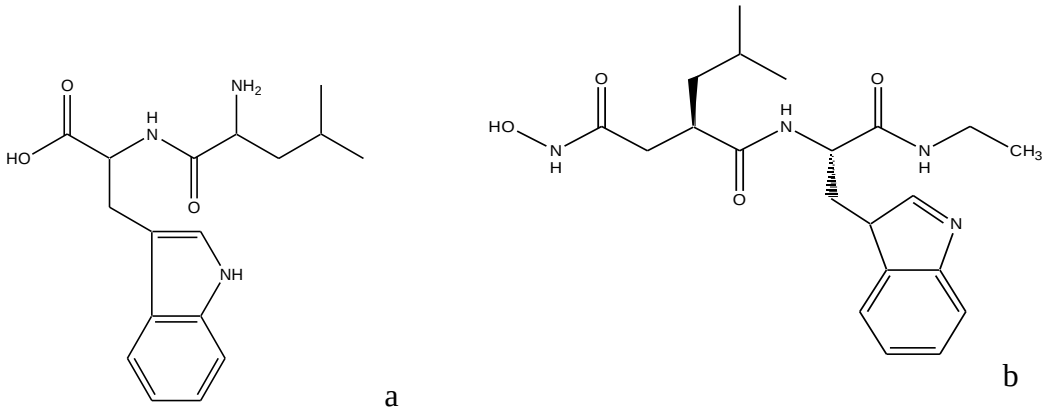


a b

Figure 3.23. Chemical structure of LEU-TRP (a) and ilomastat (b).

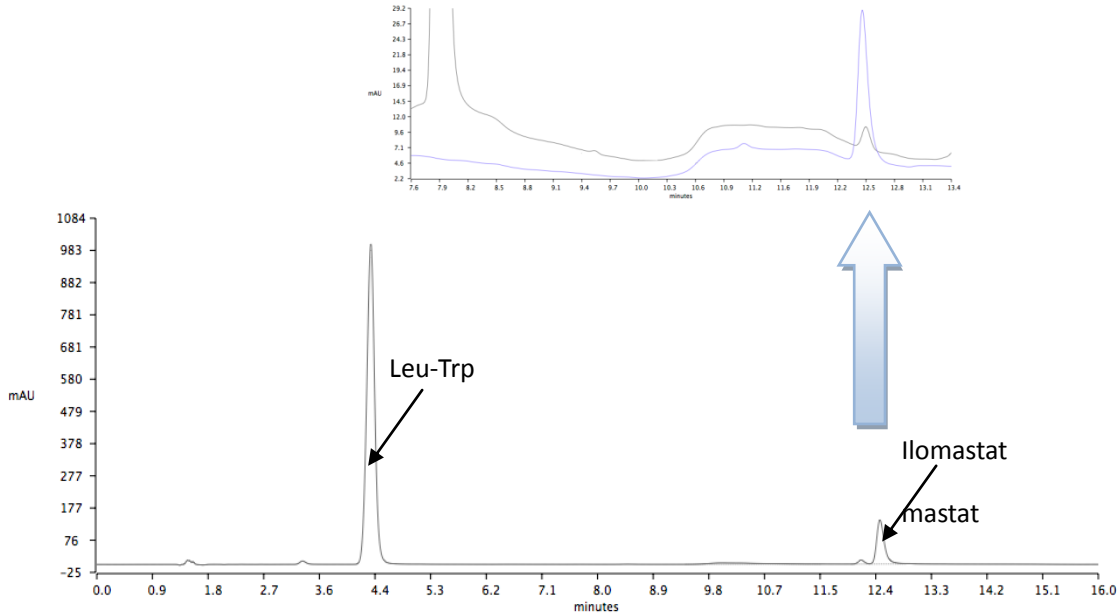


Figure 3.24. One of the impurities of Leu-Trp overlays with ilomastat peak when using a gradient method.

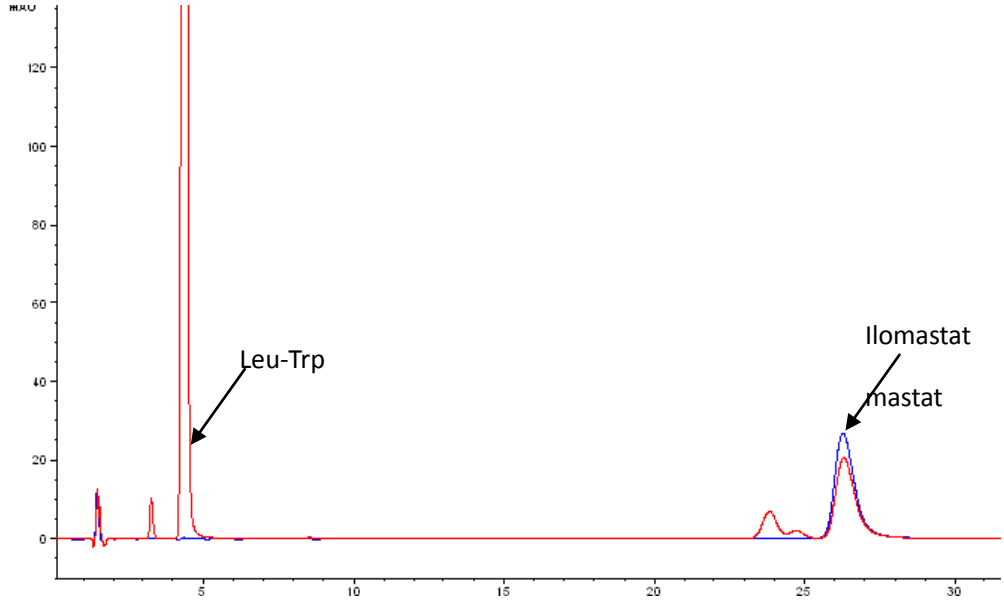


Figure 3.25. HPLC chromatograms of the ilomastat (blue) and ilomastat solution containing LEU-TRP (red) using the isocratic method. It can be seen that ilomastat peak is separated from the from the Leu-Trp impurity.

### 3.3.5.1. Tissue soaked in ilomastat solution

Following on the initial experiments that confirmed that Leu-Trp did not overlay with ilomastat on the HPLC chromatograms, we next set out to determine if ilomastat could be detected in tissue. Before conducting any *in vivo* studies, we firstly examined whether the accumulation of ilomastat can occur in dissected ocular tissue. Using rabbit eyes obtained from an abattoir (Woldsway Farm), the eyes were dissected and different

sections of ocular the tissues (cornea, conjunctiva, sclera, muscles, iris, and vitreous body) obtained. The tissues were weighed and placed and incubated in a 100 μM ilomastat solution (ilomastat dissolved in DMEM 1X (Invitrogen, UK)) overnight at room temperature. After 24 hours of soaking, each piece of the tissues was washed briefly using 1 mL 1X PBS (Invitrogen, UK) in an eppendorf tube. Tissues were then placed in 15 mL falcon tubes (Fisher, UK) followed by the addition of 1ml of Collagenase D (2 mg/mL in PBS containing $MgCl_2$) (Roche, UK). The tubes were then placed in a 37 ℃ shaking incubator, shaking at 300 RPM. Samples were checked every 6-12 hours and after 48 hours digestion of all tissues was complete. Samples were passed through a 29 gauge needle following digestion to further disrupt any small fragments.

The samples were then centrifuged at 13000 RPM for 5 minutes and the supernatant passed through a 0.22 (or 0.45) μM filter before being run on the HPLC. It was found that ilomastat could be detected in most of the tissues with the exception of the lens, and that no overlay peaks from the tissue and ilomastat were observed. However, as the amount of water contained in the tissues could not be quantified as the total volume of the sample was unknown. We therefore could not calculate the concentration of ilomastat accurately. It was felt that the problem can be solved if the supernatant of digested tissue samples could be lyophilized and then re-dissolved using a known amount of liquid. Hence, this lyophilization step was included in the design of the following experiments.

#### 3.3.5.2. Ilomastat tablets in *ex vivo* rabbit eyes

Previous studies have confirmed that 1) ocular tissues can be well digested without interfering with ilomastat 2) accumulation of ilomastat in dissected ocular tissues can occur, and 3) accumulated ilomastat is detectable by HPLC. However, the dissected ocular tissues are different from an intact eye. It is unknown how much ilomastat can accumulate in different parts of ocular tissue due to the presence of the tissue barriers and the aqueous/blood circulation. In order to simulate the *in vivo* condition, excised rabbit eyes were used to model a functioning bleb. A 5-10cm cut was made at the conjunctival/limbo edge of the eye and a pocket created posteriorly using forceps. A tablet was placed under the conjunctiva, and a tube connected to a peristaltic pump placed

at the front of the pocket. To seal the bleb, glue was used to attach the conjunctiva to the sclera below. This created a water tight bleb. To ensure that a water tight pocket can be created in an excised eye, a separate eye was subjected to the same procedure (minus the tablet) and a contrast agent (Rhodamine) injected through a tube (Figure 3.26.). The distribution of the dye showed both the formation and size of the bleb. PBS (pH 7.4) was pumped through the bleb at a flow rate of 2 μL/min. The eyes were kept moist through the use of a drip containing 0.9% NaCl (approximately one drop every 30 seconds onto the eye surface). Three eyes with ilomastat tablets were dissected after 4 hours, and a further 3 dissected after 24 hours along with 2 control eyes (no tablet). The bleb tissue (conjunctiva and sclera within the bleb) was dissected away, along with the cornea, muscle, iris, lens and vitreous body. Excluding the vitreous body all samples were briefly washed in PBS, weighed and placed into an eppendorf tube and stored at -20 ℃.

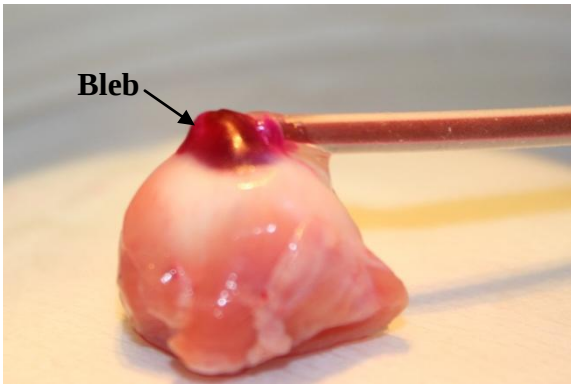


Figure 3.26. Demonstration of the formation of a "bleb" in an excised rabbit eye. Rhodamine was pumped into the pocket to prove the formation of a sealed pocket.

The tissue samples were next cut into small pieces and placed into a 15 mL round bottom falcon tube with 0.9 mL of the collagenase solution (2 mg/mL) along with 0.1 mL of the Leu-Trp solution (500 μM, dissolved in DMSO). The tubes were placed in a 37 ℃ shaking incubator for 48 hours (300 RPM). Following incubation samples were again passed through 29 gauge needles 5 times to ensure any remaining fragments were broken up. The sample solutions were centrifuged for 5 minutes (13,000 RPM). To ensure the samples were dissolved in the minimum amount of liquid possible the supernatants were lyophilized for 48 hours using a freeze-dryer set to -20 ℃. Meanwhile, an ilomastat aqueous solution was lyophilized in order to ensure

lyophilization does not cause any degradation of ilomastat (Figure 3.27).

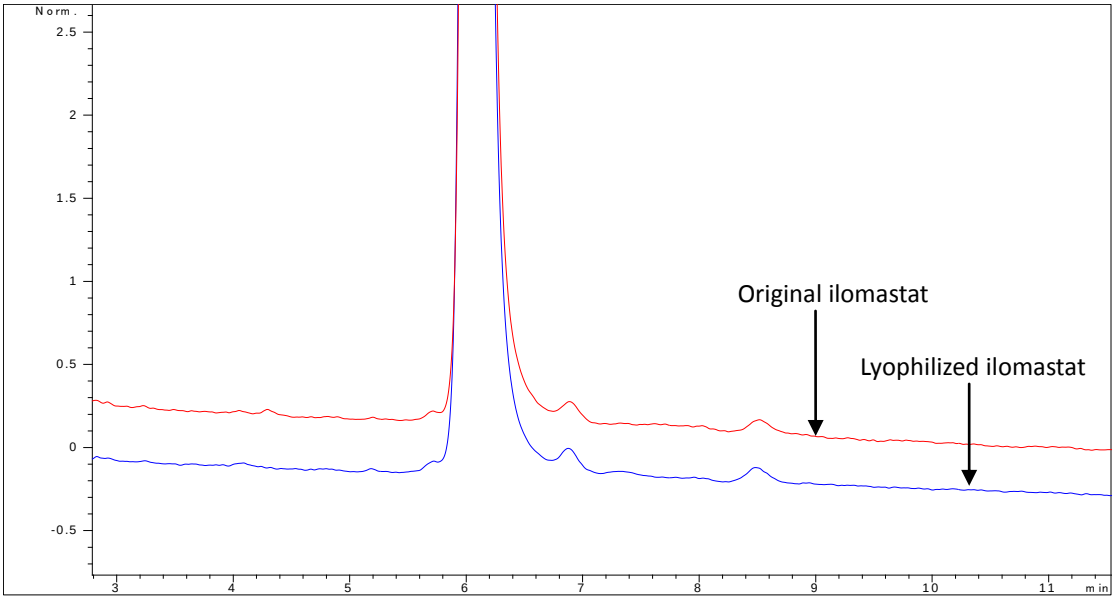


Figure 3.27. HPLC chromatograms of original ilomastat (red) and lyophilized ilomastat (blue). Data suggest that lyophilization did not cause any decomposition of ilomastat.

Following lyophilization, it was felt that DMSO would be a suitable agent for dissolving both the Leu-Trp and ilomastat. Hence, we decide to use DMSO to dissolve the samples. This way it was hoped that the amount of ilomastat contained in the samples would be as concentrated as possible because highly concentrated ilomastat is easier to detect by HPLC. However, the supernatant of the tissue samples did not dissolve well in DMSO; but it was found to dissolve well in water. The well dissolved samples were further subjected to filtration using a 0.22 μM filter and injected into the HPLC. Compounds were eluted using the isocratic method mentioned in 3.2.7.2. The HPLC chromatograms are similar to the tissues soaked in the 100 μM ilomastat solution.

Ilomastat was detected in the conjunctiva, sclera and muscle near the bleb site (Figure 3.28.). There was no significant difference in ilomastat concentrations for any individual tissue between 4 and 24 hours. The ilomastat concentration in the conjunctiva was approximately 0.5 μM per mg whilst in the sclera and muscle the concentration was 10-20 times less (Figure 3.29.). However, it should be noted that these concentration were not exact because the real concentration could not be recovered using the internal standard. As the samples were finally dissolved in water, Leu-Trp did not dissolve

completely. Therefore, the peaks of Leu-Trp on the chromatogram were not reliable. Consequently, the loss of ilomastat during the tissue preparation could not be calculated.

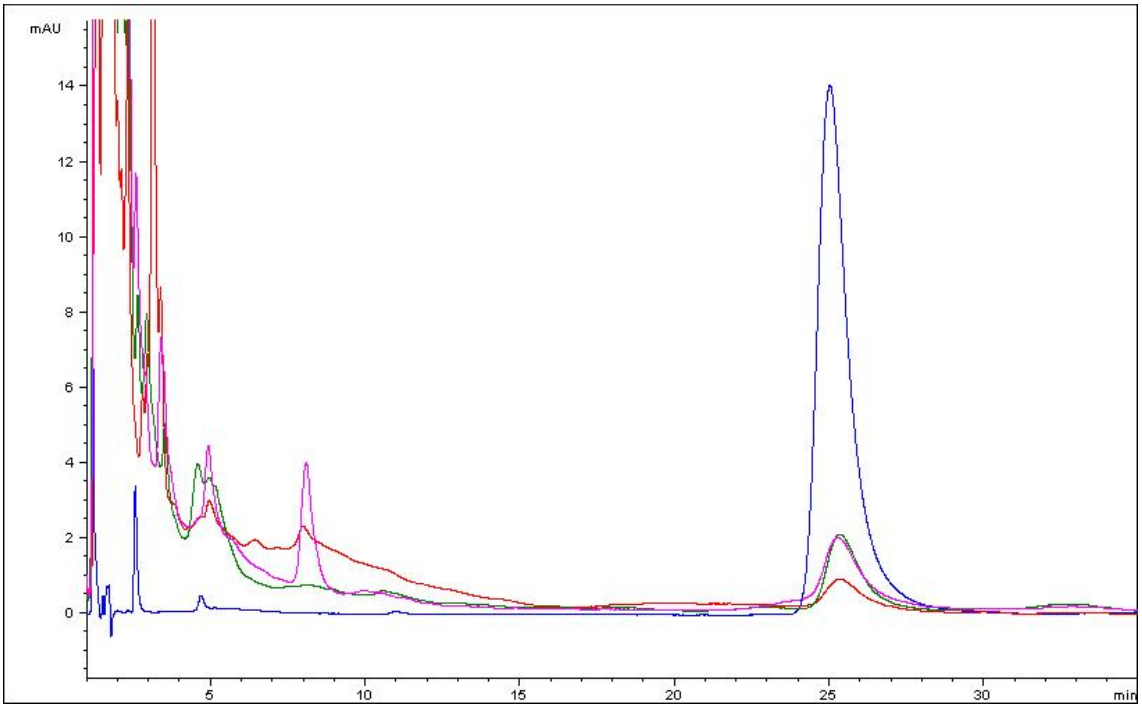


Figure 3.28. Chromatogram showing that there was no overlap between the different tissues and ilomastat. Tissues displayed on the graph are: conjunctiva (red), sclera (green) and muscle (pink). The ilomastat control (blue) is also displayed.

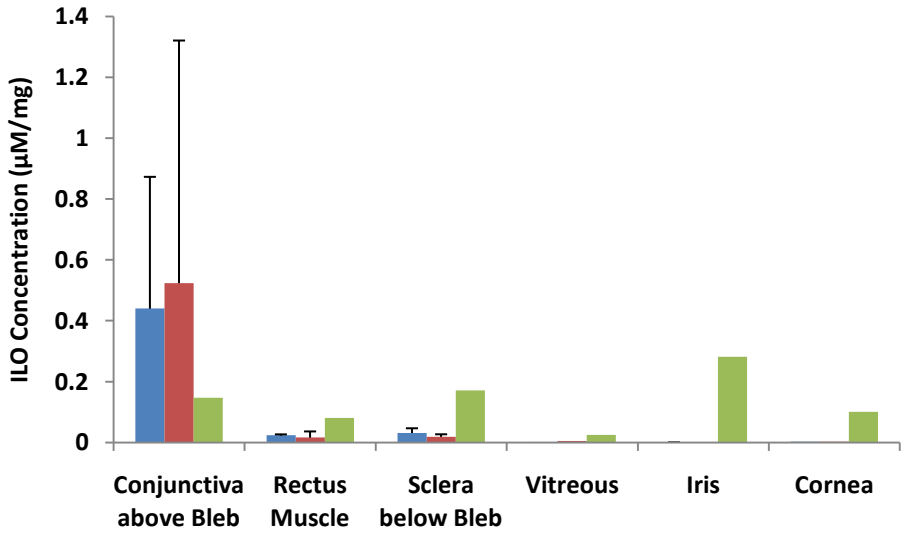


Figure 3.29. Concentrations of ilomastat (ILO) in different part of the eye. ■tissue dissected from rabbit eyes with ex vivo GFS after 4 hours (n=3, error bars indicates standard deviation) ■tissue dissected from rabbit eyes with ex vivo GFS after24 hours (n=3, error bars indicates standard deviation) ■tissue soaked in 100 µM ilomastat solution for 24 hours (n=1). Data suggest that in the *ex vivo* eye ilomastat was only detected in the conjunctiva, sclera and muscle

near the bleb site.

From Figure 3.29 it can be seen that the ilomastat concentrations in the sclera, iris, cornea and vitreous body were much higher in the tissue which was cut and soaked in the ilomastat solution, rather than in the *ex vivo* model. This suggests that in the *ex vivo* eye, probably due to the absence of blood and aqueous circulation, it was difficult for ilomastat to pass through the sclera and cornea. Accordingly, ilomastat could hardly be detected in the iris and vitreous body of the *ex vivo* eye. Ilomastat could only accumulate in the spongy conjunctival and the sclera below the bleb.

An interesting discovery was made when looking at the ilomastat concentration in the conjunctiva. Figure 3.29. shows that the ilomastat seemed to be more concentrated in the conjunctiva from the *ex vivo* eye rather than from the dissected tissue which was soaked in ilomastat solution. This is not because the ilomastat particles remaining on the conjunctiva were not washed off properly before tissue digestion. From the release profiles of ilomastat in the 200 μl chamber at room temperature (Figure 3.1.), we know that the 1) the ilomastat concentration reached approximately 90-100 μM after about 4 hours and 2) this concentration could be maintained in the flow chamber for days. However, it is estimated that the ilomastat concentration in the *ex vivo* bleb is higher than 100 μM. This is because the bleb created on the *ex vivo* eye had a volume which was less than 200 μl (50-100 μl). From the 5-FU release profiles from Chapter II, we know that, when the tablet is placed in a small chamber (50 μl), the tablet release rate and the drug concentration in the flow chamber were both increased significantly (Figure 2.13). Although the ilomastat tablet release profiles in a 50 μl chamber are not available, it is believed that the ilomastat concentration was also increased in the *ex vivo* bleb in comparison to the one in the 200 μl chamber. As the conjunctival is the main destination of the drug solution, the ilomastat concentration in the conjunctival from the *ex vivo* eye was higher than the one from the soaked conjunctiva.

Although the ilomastat concentration in the tissue was not thought to be accurate due to the precipitation of Leu-Trp, it was confirmed that a) collagenase was able to digest tough

ocular tissue without interference to ilomastat and b) ilomastat accumulated in the *ex vivo* eyes could be detected using our HPLC method with a minimum sensitivity of 100 nM.

#### 3.3.5.3. Freeze dried ocular tissue digested using collagenase

As Leu-Trp had been shown to be a poor internal standard, we had to consider whether we could detect ilomastat without using an internal standard. This is new because drug extraction from tissue without using internal standard is hardly reported in the literature. If tissue samples could be freeze dried before being digested in a known volume of collagenase, the water initially contained in the tissue could be removed. We then will be able to determine the concentration of ilomastat by injecting the supernatant of digested tissue into HPLC. However, we also understand that there is a possibility that ilomastat is bound to tissue/protein. Examining whether there is any binding between the drug and tissue will be part of the future studies.

To test the possibility of freeze drying tissue in advance of digestion, we repeated the earlier experiment of soaking tissue in a 100 μM ilomastat solution. Following 24 hours of soaking, the tissues were washed using 1ml of PBS and placed in the freeze dryer. After lyophilization, the samples were transferred to a 15 mL round bottom falcon tube with 1 mL of collagenase solution (2 mg/mL) and then shaken at 37 ℃ at 300 RPM for 48 hours. As with the previous studies, the 1 mL ilomastat solution was also freeze dried, re-dissolved in 1 mL collagenase D solution, and then shaken in the incubator for the same period of time (48 hours). The ilomastat concentration in the tissue is shown in Figure 3.29. The HPLC chromatograms are similar to the ones shown in Figure 3.28. A 10% loss of ilomastat was observed using this method, which is probably because of the degradation of ilomastat in the 37 ℃ collagenase solution.

The aim of this experiment was to determine the concentrations of ilomastat in ocular tissues using a non-radioactive/non-fluorescent method. The whole development process is summarized in Table 3.7. The most challenging obstacle was the development of a universal method for tissue homogenization. Previous studies have used a number of different methods. For example, iris and retina/choroid were homogenized with using

hydrochloric acid (pH 1.0) and centrifuged before subjecting the supernatant to solid phase extraction (Hu et al. 2007). The cornea/sclera were homogenized by an ultrasound bar and then in Sörensen phosphate buffer pH 7.4 mixed with dimethyl sulfoxide (3:7) (Knapp et al. 2003). The vitreous was homogenized with methyl-tert-butyl-ether (Knapp et al. 2003). However, if we were to digest the different part of ocular tissues using the different methods mentioned in the literature, it had to be ensured that all these methods do not led to the decomposition of ilomastat and the internal standard. In addition, depending on the types of tissue, different HPLC methods might need to be developed. This could be very complicated and time consuming. Furthermore, due to the limited availability of ilomastat, it was more convenient to develop a unique method to digest all the ocular tissues in a single protocol. As documented in Table 3.6 several methods were investigated, but for the reasons listed in the table, none could be brought forward mainly due to their effects on ilomastat.

Table 3.7 Summary of the method development for detecting ilomastat in ocular tissues.

| Experiments | Progress | Problems | Problem solving |
|---|---|---|---|
| Increase HPLC sensitivity of ilomastat | 5 μM to 100 nM | | |
| Look for commercial available internal standard | Leu-Trp was purchased | | |
| Develop HPLC method for both ilomastat and Leu-Trp | Peaks were well separated | | |
| Look for a universal method to digest all ocular tissue without interfering with ilomastat | Tissue were well digested using Collagenase D | | |
| Dissect different parts of the ocular tissue in a 100 μM ilomastat solution with Leu-Trp | Tissues were well digested; ilomastat could be detected by HPLC without showing overlay peaks with the tissue samples. | The ilomastat concentration was not accurate as the amount of water in the tissue could not be quantified. | Lyophilize the supernatant of the digest tissue samples, then re-dissolved them in known amount of liquid. |
| Ilomastat tablets were placed in artificial blebs created on excised rabbit eyes | Tissues were well digested and a known amount of Leu-Trp added in. Samples were then lyophilized. | Lyophilized samples could be re-dissolved not in DMSO but in water. Leu-Trp precipitated in water. | Not to use Leu-Trp |
| Repeat experiments by soaking tissue in 100 μM ilomastat solution | Tissue samples were first lyophilized and then digested by collagenase D. Ilomastat was detected by HPLC with 10% lost during the sample preparation process. | The accumulation of ilomastat in a live eye could be lower than an ex vivo eye. The sensitivity of the HPLC method needs to be further improved. | A HPLC-MS method is being developed. |

Using our extraction protocol, Leu-Trp was not an appropriate internal standard due to its poor aqueous solubility and also showed peaks that overlay with the tissue samples on the HPLC chromatograms. As no organic phase was used in our final extraction process, it was unclear whether the ilomastat extraction was complete during tissue breakdown or how much was lost during the preparation for HPLC. Since binding of MMPis to

extracellular matrix has been observed in literature (Zhang et al. 2008), it is possible that some ilomastat was bound to protein and consequently removed during the centrifugation step. Further interaction studies of ilomastat with proteins as well as extracellular matrix are needed. If ilomastat does indeed bind to tissue/proteins that we are unable to break apart, organic solvents will be needed to precipitate the tissue/protein. Furthermore, the sensitivity of our HPLC method, whilst good at 100 nM, may not be sufficient to detect very small amounts of ilomastat in tissue. Ideally we would prefer the sensitivity to be at least 100 times lower. Currently an HPLC-MS method with a higher sensitivity (2.57 nM) is being developed by our group (led by Dr. Hala. Fadda).

Our *ex vivo* model of the bleb does not fully represent the *in vivo* conditions. It has a few limitations. Firstly, there is no blood supply through the tissue. Due to the absence of blood circulation, it would be difficult from this data to draw conclusions about how much drug may be in tissue in a living eye. Specifically it is not possible to predict the presence of the drug at the posterior segment of the eye brought by the ocular blood circulation. Secondly, the temperature was not body temperature. Finally, PBS was used, whereas it would be aqueous humor in a living eye. Since our colleagues have found that ilomastat solubility can be as high as 574 μM in 37 ℃ PBS (pH 7.4), we believe the ilomastat will be more soluble in an *in vivo* bleb than in an *ex vivo* bleb because the *in vivo* bleb has the temperature of 35 ℃. Have considering these limitations, our findings are still encouraging. We have developed a simple method that can digest all of the ocular tissues with the exception of the lens. The detection of ilomastat in the ocular tissues can be accomplished without radiolabelling the drug or marking it with a fluorophore. Our experiments on the *ex vivo* eye suggests that the dispersal of a drug from an implanted tablet may be limited to the tissues surrounding it. Determination of ilomastat accumulation from the *in vivo* studies is currently underway.

To summarize all our studies on the method development of ilomastat determination in ocular tissue, our best method so far is summarized below. More experiments will be conducted in the group to determine if further refinement of the method is required.

1. Dissect, weigh and cut the tissue into small segments.

2. Lyophilize the tissue for 48 hours at -20 ℃.

3. Place the tissue in 1ml of the collagenase solution (2 mg/mL) for 48 hours (or until all tissue is digested) in a shaking incubator at 37 ℃ at 300 RPM in a 15 mL falcon tube.

4. Pass the digested tissue through a 29 gauge or smaller needle in order to ensure that full tissue disruption has occurred.

5. Centrifuge samples for 5 minutes at > 10,000 RPM.

6. Filter the supernatant using a 0.45 μM filter.

7. Inject the samples into the HPLC with a UV detector (λ=280 nm). The mobile phase is ammonium acetate buffer (pH 5.0) with 15% acetonitrile. The flow rate is 1.2mL/min. The injection volume is 100 μL. The ilomastat retention time is 25.6 minutes.

### 3.4. Conclusions

In conclusion, we have successfully made excipient-free ilomastat tablets. The release of ilomastat lasted more than one month in our flow chamber. In the *in vivo* studies, these tablets proved to be more effective and less toxic than 5-FU and MMC with 100% bleb survival for 30 days after surgery. This suggests that the ilomastat tablets could potentially be a better anti-scarring medicine for GFS compared to 5-FU and MMC. It was also found that ilomastat significantly reduced intraocular pressure compared to negative and positive group. To evaluate tissue accumulation of ilomastat in the eye, we have successfully developed a simple method of ocular tissue digestion that does not interfere with ilomastat detection. Using this method, the ilomastat accumulated in the ocular tissue can be detected by HPLC with a sensitivity of 100 nM. In addition, thermal and surface analyses of the ilomastat tablets were conducted. It was also found that ilomastat exists in different crystal forms, but this finding did not seem to affect the release of ilomastat in our *in vitro* model. The analysis results from AFM and nanoLTA indicate that incubation of the tablets led to changes (stiffness, adhesion, and thermal conductivity) in the tablet surface. The surface analysis by XPS and Tof-SIMS suggests that, even with presence of constant aqueous flow, deposition of salts and proteins on the tablet surface can be observed.

# *Chapter IV Molecular dynamics simulation of the dissolution of the excipient-free 5-FU and ilomastat tablets*

## 4.1. Introduction

In the previous studies, we developed two types of excipient-free tablets that can potentially be used for scar inhibition in the bleb. They were made from two different compounds. 5-FU is a hydrophilic water soluble compound; whilst ilomastat is more hydrophobic and less water soluble than 5-FU. As mentioned above, our tissue tablets will dissolve in the subconjunctival space which results in non-sink conditions due to its fairly small volume (approximately 50-100 μl). Since the drug release profile is associated with the efficacy and toxicity of the tablets, understanding the drug release behavior in the bleb becomes important. From the previous *in vitro* studies, we found that 1) saturation of the drug was not observed in the flow chamber due to the turnover liquid 2) the dissolution rate of the tablet was the rate-limiting step of the drug release process, and 3) tablet dissolution was related to the bleb volume and the aqueous flow rate. Therefore, the dissolution of the tablets cannot be simply calculated using the drug solubility. There are a number of methods other than *in vitro* models that can be used to investigate tablet dissolution. Since the tablets are excipient-free, their dissolution can be considered as the dissolution of a big drug particle. Since the dissolution of a compound in a solvent is related to its chemical structure, the dissolution of an excipient-free tablet may also be associated with the chemical structure of the compounds. Hence, we are interested in investigating the influence of the chemical structural features of the two molecules on the tablet dissolution. We also seek to investigate the dissolution of the tablet in non-sink conditions on a molecular level.

Molecular dynamics (MD) is a computational method that calculates the behavior of a molecular system with regards to time (Adcock & McCammon 2006;Morra, Meli, & Colombo 2008). It has been widely used in investigating the structure, dynamics, and thermal dynamics of proteins and biomolecules (Adcock & McCammon 2006;Dodson, Lane, & Verma 2008;Grigera 2002;Gumbart et al. 2005;Haran, Haas, & Rapaport 1994;Morra, Meli, & Colombo 2008). It is able to run “virtual experiments” with high temporal and spatial resolution in which cannot possibly be seen with lab experiments.

MD simulations help us to understand the dynamics and mechanical functions of biological molecules at the atomic and molecular level and therefore provides promising insights into the genetic, thermodynamic and functional/mechanistic behavior of biological processes (Dodson, Lane, & Verma 2008). A successful simulation that agrees with experimental observation might be able to suggest new experiments in the lab.

The dissolution of sodium chloride crystals have been examined using MD simulations (H.Ohtaki et al. 1988;Siu et al. 2006;Yong Yang, Sheng Meng, & E G Wang 2006). However, no studies have been conducted on tablet dissolution using MD simulations. Here we intend to use MD simulations to understand the dissolution of a tablet in non-sink conditions at the molecular level. It is hoped that this simulation will be able to help us to understand the dissolution of the tablets and provide us useful indications for future *in vitro* and *in vivo* experiments. To model the dissolution times of the tablets in these conditions, we conducted computational simulations using MD on both the 5-FU and ilomastat tablets.

## 4.2. Computational methods

All the MD simulations were performed using Desmond v2.2 with Maestro 8.5 as a molecular modeling graphical interface. Conformational searches were conducted using a Macromodel (Schrodinger) to generate initial systems of drug molecules inside a constrained volume.

### 4.2.1. Building a tablet

The 3D structures of 5-FU and ilomastat molecules were generated using 3D builder in Maestro 8.5. Resulting structures were optimized using Macromodel 9.11 (Mohamadi et al. 1990), MMFFs force field (Cramer & Truhlar 1995) and the Generalized Borhn/ Surface Area (GB/SA) implicit solvation model (Still et al. 1990). An exhaustive search was carried out on a small number of molecules (25 5-FU with 2 water molecules, 10 ilomastat respectively) by generating 1000 configurations for each system using the

*Monte Carlo* multiple minimum (MCMM) approach. The lowest energy configurations were chosen as a starting point for tablet modeling. The final structures of the exhaustive searches were multiplied into a rectangular shaped tablet (containing 690 and 110 molecules of 5-FU and ilomastat tablets, respectively). Tablets were then optimized and the final conformations used to examine the intermolecular packing of drug molecules without the presence of extra water molecules. It is understood that ideally the tablets should compose not amorphous drug molecules but drug crystals. But we conducted the preliminary studies using amorphous drug molecules to form a tablet because 1) our current aim is to develop a MD simulation method to investigate the dissolution of a tablet in non-sink condition, and 2) creating drug crystals of 5-FU and ilomastat using MD simulation will include quite large amount of work which may take a few years.

### 4.2.2. Tablet compression

Molecular dynamics was performed using Desmond v2.2 with Maestro 8.5 as a molecular modeling graphical interface. The initial systems generated by conformational searches were truncated by deleting molecules and forming rectangular shapes. Simulation boxes of each tablet (672 5-FU and 110 ilomastat molecules, respectively) were prepared by Desmond setup and sizes coinciding with the size of the truncated sets (Figure 4.1). The temperature of the simulation during tablet compression was set at 300 K, corresponding to the room temperature and MMFFs force field. To imitate the process of tablet compression under increased pressures, the systems were subjected to initial relaxation minimization followed by simulation at an initial pressure of 1 bar for 0.06 ns (5-FU) or 4.8 ns (ilomastat). The final structures were further simulated using constant pressures of 2, 4, 8, and 12 bars without relaxation for 0.48 ns at each pressure. Finally, a production simulation was conducted at 14 bars for 4.8 ns. An additional simulation was conducted at higher pressure of 100 bars for 4.8 ns.

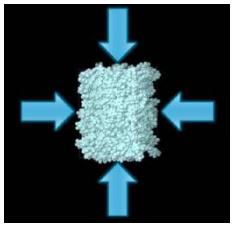

Figure 4.1. Simulation of tablet compression.

### 4.2.3. Tablet dissolution

The simulation of the tablet dissolution was performed using the final structures of rectangular shaped tablets after being compressed at 14 bars. The size of the tablets was reduced (164 5-FU and 90 ilomastat) to reduce the real CPU time of the simulations without losing the properties of tablets. By doing so, a 4.8 ns simulation usually takes about one month if everything goes smoothly. Assuming that the amorphous drug molecules will not crystallize during the tablet dissolution process, the initial simulation box systems were formed by solvating the tablets and forming all atom systems that consisted of a 5-FU or an ilomastat tablet surrounded by water molecules (12761 water molecules for 5-FU tablet and 6724 water molecules for ilomastat tablet) (Figure 4.2.). The final volume of both simulation boxes was 266966 ± 493.7 Å. In order to compare the drug dissolution from a tablet without or with the turnover of the aqueous humor, two types of simulations were performed. The first type of simulation was conducted to compare the dissolution rates of the two drugs (5-FU and ilomastat) and consisted of a production run of 4.8 ns. The simulation was conducted twice at two temperatures (300 K and 310 K, to represent ambient temperature and body temperature respectively) for both drugs. The second type was designed to examine the dissolution of the two drugs in the presence and turnover of the aqueous humor. The liquid turnover in the bleb was mimicked by eight simulating circulations. Each circulation lasted for 0.6 ns, where the released drug molecules were manually removed at the end of each step. A molecule was considered released when the contact with the tablet surfaces was lost. The manual removal of molecules at the end of each cycle was approximated to reflect the loss of molecules from the bleb by permeation. After each circulation, a new simulation box consisting of an increased number of water molecules was built, but the size of the box

was kept constant to continue the next circulation since it was assumed that the bleb volume would not change after drug release (Figure 4.3.).

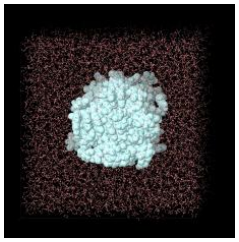

Figure 4.2. Demonstration of tablet dissolution in a box without liquid turnover.

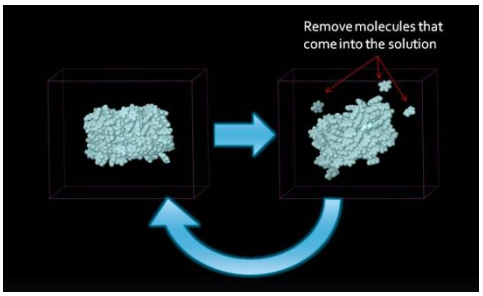


Figure 4.3. Simulation of dissolution of tablet with liquid turnover.

### 4.2.4. Tablet interaction with a biological membrane

The effect of membrane presence on dissolution rate was also investigated using the initial tablets which were used in the dissolution simulation described in the previous section. The tablet was placed on the top of a dipalmitoylphosphatidylcholine (DPPC) bilayer membrane in a simulation box that consisted of 12568 (for 5-FU) and 33578 (for ilomastat) water molecules respectively (Figure 4.4.). As we did not fix the lipid bilayer membrane, there was no static layer in the simulation. We aim to investigate whether tablet dissolution could be affected by tissue. The tissue was represented in a simplistic manner by a model of DPPC to consider the complex interactions of the polar interface and hydrocarbon chains with tablets. The volume of the simulation box was 701250 Å and 1766400 Å for 5-FU and ilomastat respectively. A 4.8 ns simulation was performed at 310 K which represents body temperature. The dissolution was monitored by calculating the change in the total molecular SA.

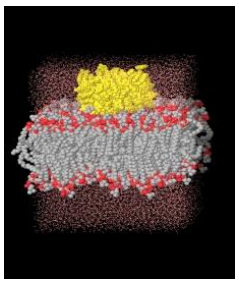

Figure 4.4. Demonstration of tablet permeation through a biological membrane.

### 4.2.5. Analysis of the results

Molecular dynamics trajectories were visualized and analyzed using Maestro and VMD (Humphrey, Dalke, & Schulten 1996). The explicit water molecules were removed within VMD to simplify the analysis. The configurations generated during the simulation were converted into pdb file format and sequentially saved for further analysis. The macromolecular properties of exported systems (surface area, molecular lipophilicity potentials (MLP), lipole) were analyzed using Vega ZZ (Pedretti, Villa, & Vistoli 2004). The estimated lipole value is calculated by projecting lipophilicity onto the surface but it depends on the conformation of the system. Molecular properties of single molecules (log P) were also calculated by Vega ZZ.

## 4.3. Results and discussion

All molecular dynamics simulations on limited size tablets were conducted to examine the dissolution of the two drug molecules with different molecular properties and solubility. It can be seen from Figure 4.5. that 5-FU has 3 hydrogen bond acceptors (HBAs) and 2 hydrogen bond donors (HBDs); whereas ilomastat has 5 HBDs and more than 3 HBAs. From literature it is known that the macroscopic aqueous solubility of 5-FU and ilomastat is 11.1 mg/mL (pH 4.0) and 0.03885 mg/mL respectively (Millipore 2010;Yalkowsky & He 2003). To understand the experimentally observed data, the dissolution simulations were correlated with the molecular properties (HBDs, HBAs, and log P) and macromolecular properties of the systems. Here the system represents an entirety that includes all the drug molecules.

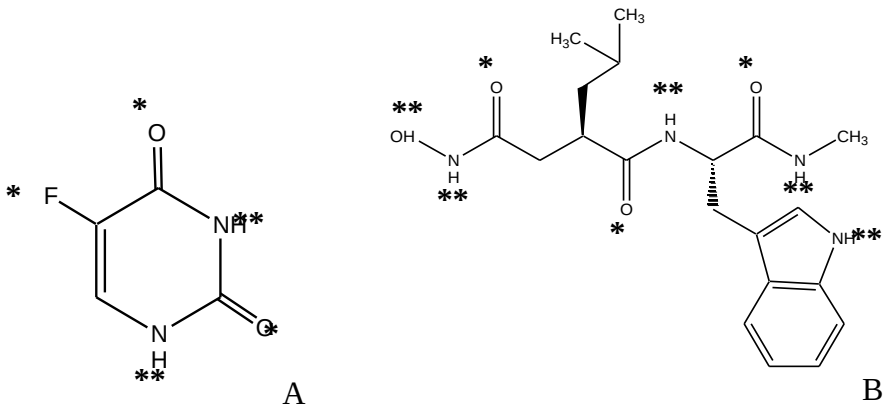


Figure 4.5. Hydrogen bond donors (HBDs, **) and hydrogen bond acceptors (HDAs, *) of 5-FU (A) and ilomastat (B).

The experimental log P of 5-FU is -0.83 (pH 4.0) (Buur & Bundgaard 1984), while the experimental log P of ilomastat was not reported. The experimental log P of ilomastat was not determined currently due to its limit availability. But to predict and compare the changes of the lipophilicity of the tablet system, we used Vega ZZ (Pedretti, Villa, & Vistoli 2004) to predict log P values of the two drugs. The predicted log P value of 5-FU and ilomastat was -1.362 and 0.652 respectively. Macroscopic values such as the lipole, a lipophilicity measure projected onto a molecular surface, can also be predicted using the same software. Lipole can be calculated for a single molecule as well as for the complexes, including the tablets. The lipole value was predicted as 0.5621 and 1.2751 for a single 5-FU and ilomastat molecule respectively. Assuming that the predicted log P value of 5-FU is similar to the experimental value, we aim to investigate the change of the tablet lipophilicity by comparing the difference of lipole values before and after dissolution.

### 4.3.1. Conformational search

The initial of 5-FU and ilomastat systems were generated by the MCMM method taking into account the solvent effects using an implicit model (GB/SA). Initial analysis of interactions between 5-FU molecules in the tablet suggests the presence of aromatic-aromatic interactions and hydrogen bonding (to a lesser extent) (Figure 4.6). Similarly, aromatic-aromatic interactions between ilomastat molecules were observed, predominantly in a face to edge orientation (Figure 4.7).

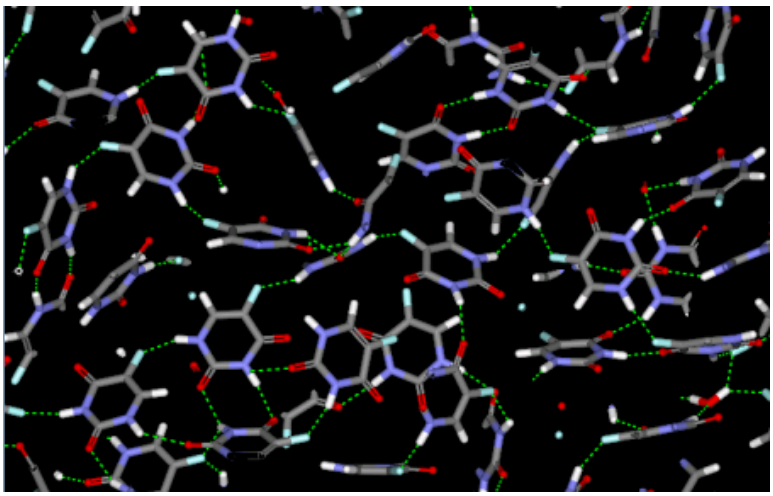

Figure 4.6. Interactions between the 5-FU molecules after conformational searches. The green broken lines represent the hydrogen bonds between the molecules. Interactions between 5-FU molecules in the tablet suggest the presence of aromatic-aromatic interactions and hydrogen bonding.

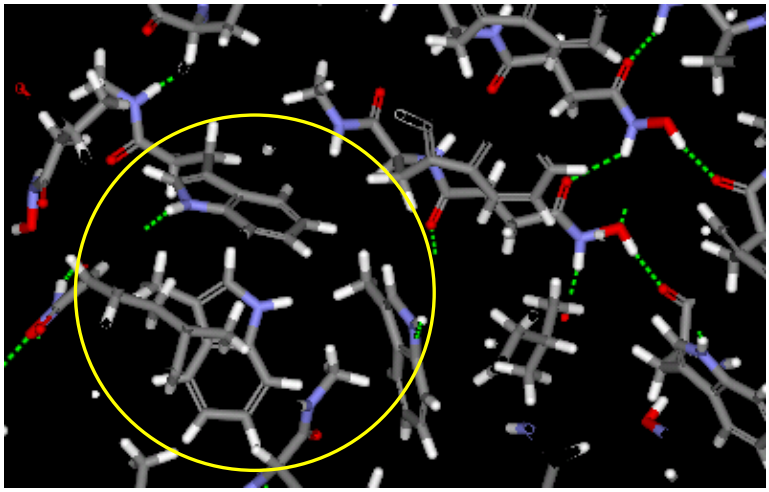

Figure 4.7. Interaction between the ilomastat molecules after conformational searches. Aromatic-aromatic interactions between ilomastat molecules were observed, predominantly in a face to edge orientation A typical face to edge orientation is shown in the circle. The green broken lines represent the hydrogen bonds between the molecules.

### 4.3.2. Simulation of tablet compression

During tablet compression, change in the tablet/material volume reflects the extent of packing. As Maestro calculates the volume of the system by adding the number of atoms without including the space between molecules, the volume of the system remains constant before and after the tablet compression. Hence, calculation of the system volume was not able to reflect tablet packing properties. Therefore, we used the accessible surface area (ASA, the surface area of a biomolecule that is accessible to a

solvent) of the system to evaluate tablet packing. It was expected that ASA will decrease after compression because the molecules packed inside the tablet will not be exposed to the solvent.

Although the 5-FU and ilomastat tablets were compressed using different pressures, no significant change in the ASA was observed between the beginning and the end of the compression (Figure 4.8.). As ilomastat is a larger molecule than 5-FU, its movement was more difficult during the conformational rearrangement. Consequently, the simulation of the ilomastat tablet compression needed more time. During the compression of the ilomastat tablet, the ASA of the ilomastat tablets increased for a short period at around 5 ns. But this does not contribute to our conclusion as it is simply the result of some ilomastat molecules moving out of the simulation box. On average, each ilomastat molecule has more H-bonds (2.3 per molecule) than 5-FU (1.6 per molecule) because ilomastat has more HBDs and HBAs. In the simulations of 14 bar or lower than 14 bar, the number of H-bonds in both tablets did not change significantly (data not shown). However, in the 4.8 ns simulation at 100 bar, the number of H-bonds slightly increased in the 5-FU tablet but not in the ilomastat tablet (Figure 4.9.). Although ilomastat does not appear to be too hydrophobic (predicted log P = 0.652), it might be that the combination of hydrophobic interactions with the hydrogen bond formation leads to its observed lower aqueous solubility.

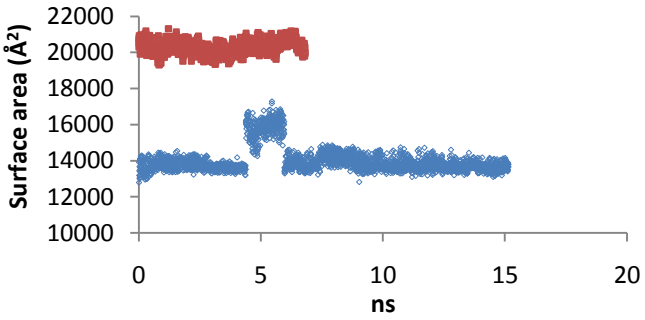


Figure 4.8. Change in the accessible surface area (ASA) after tablet compression. Data suggest that there was no significant change in the 5-FU and ilomastat tablets after tablet compression. ■ 5-FU ◇ ilomastat

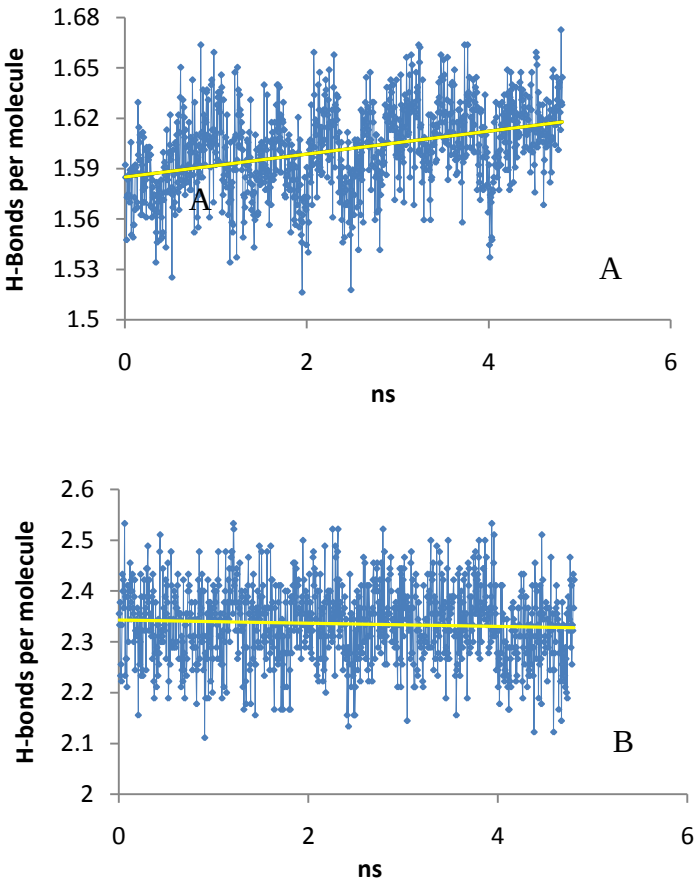


Figure 4.9. Change in H-bonds in 5-FU (A) and ilomastat (B) tablets at a pressure of 100 bar. Data suggest that the number of H-bonds slightly increased in the 5-FU tablet but not in the ilomastat tablet.

It is understood that the morphology of the drug is related to the tablet fabrication and dissolution. From the thermal analysis of the two tablets we know that both 5-FU and ilomastat exist in crystal forms. Therefore, ideally this simulation should be conducted on the drug crystals. The polymorph and thermal stability of 5-FU has been studied and predicted using computer (Hamad et al. 2006;Hulme, Price, & Tocher 2005;Karamertzanis et al. 2008); whilst the polymorph and crystal habit of ilomastat has not been well studied. As this is only a preliminary study which aims to examine the possibility of simulating tablet dissolution in non-sink conditions, we did not involve the crystal structures of the drug. Future simulations involving in the future with the drug crystals will be able to provide us with more useful information.

The compaction of pharmaceutical powder has been numerically simulated using a number of different models in recent years (Han et al. 2008;Sanchez-Castillo, Anwar, & Heyes 2003a;Sanchez-Castillo, Anwar, & Heyes 2003b). The effects of compression speeds on the deformation behavior of the powder column, the microstructure, and the integrity of the formed tablet have been investigated (Sanchez-Castillo, Anwar, & Heyes 2003b). In particular Han *et al* simulated the stress and density distributions during the tabletting process (Han et al. 2008). However, the compaction of drug crystals without excipients has never been simulated. As the drug crystals were not included, our simulation was conducted using amorphous drugs. Nevertheless, it was expected that the ASA of the particles or powders would be decreased after the compaction because this usually happens in real tablet compression. However, when the simulating system was built up before running the simulation, the molecules had to be very well packed in order to avoid adding any extra water molecules. Therefore, no significant ASA change was observed in our simulation since the initial tablet was built without allowing for empty space between molecules. Due to this fact, conformational rearrangement of the molecules became nearly impossible. Hence, no changes in packing during the compression were observed. Changes in the number of H-bonds during simulation were not significant, either.

Although a pressure of 14 bar was applied when we compress the real ocular tissue tablets, using this number in the simulation system may not represent the same compression force as in the real conditions. In fact in some MD simulations of compression, the pressure was set as hundreds or thousands of bars (Knapp et al. 2003;Suihko et al. 2000;Tilleul et al. 1997;Zahn 2004). Hence, a 4.8 ns continuous simulation of tablets compressed at 100 bars was conducted, but there was still no change to the tablet ASA. Although this might indicate that the monitoring of the molecular rearrangement during tablet formation might be variable, this approach can also be used to generate a tablet to further study its dissolution.

### 4.3.3. Simulation of tablet dissolution

#### 4.3.3.1. Simulation without the mimicking of liquid turnover

Before simulating the tablet dissolution with a liquid turnover, a 4.8 ns continual simulation was conducted in a closed box at two different temperatures (300 K and 310 K, to represent room temperature and body temperature respectively). It was found that the number of released molecules from the 5-FU tablet was considerably higher than the one from the ilomastat tablet. During this process, only one ilomastat molecule came into the solution (figure not shown). Both 5-FU and ilomastat tablets dissolved faster at body temperature (310 K) due to the higher kinetic energy of the tablet dissolution at 310 K than at 300 K (Figure 4.10.). As a result, the ASA of the tablets increased more rapidly at 310 K than 300 K (Figure 4.11.). The 5-FU tablet ASA did not increase significantly after 4 ns (Figure 4.11. A). This suggests that, without the presence of liquid flow, the solubility of 5-FU was high enough to achieve a saturated solution at around 4 ns.

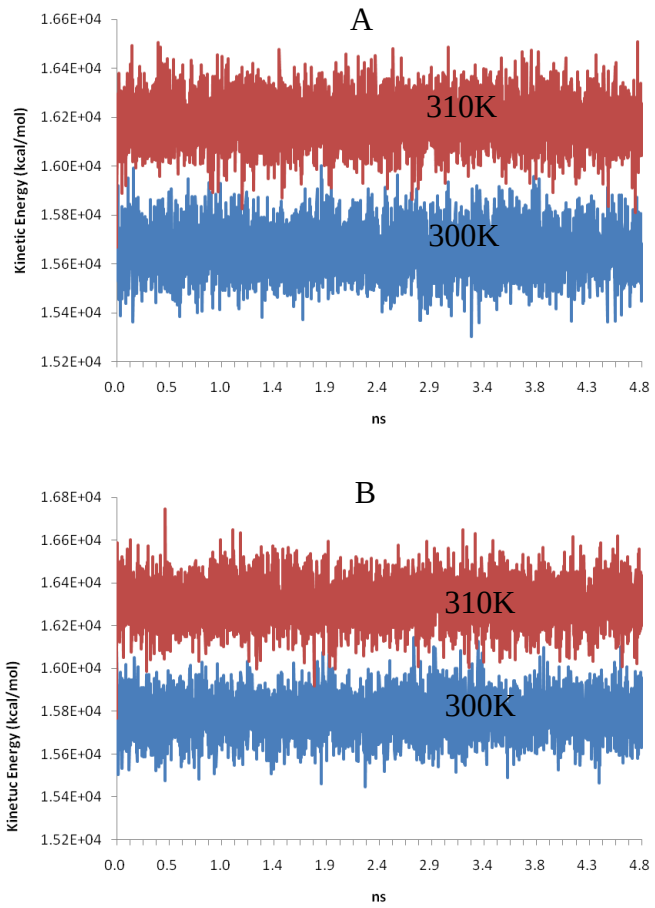


Figure 4.10. The kinetic energy of the 5-FU (A) and ilomastat (B) tablet dissolution without liquid turnover. Data suggest that both 5-FU and ilomastat tablets dissolved faster at body temperature (310 K) due to the higher kinetic energy of the tablet dissolution at 310 K than at 300 K.

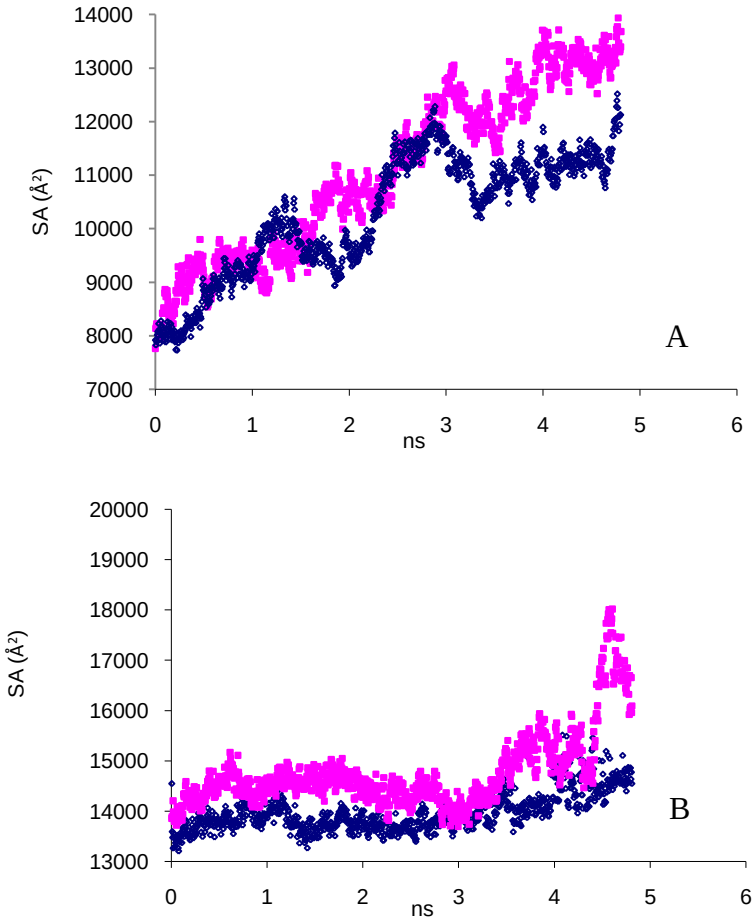


Figure 4.11. Change of ASA of 5-FU (A) and ilomastat (B) tablets in water box without liquid turnover. ■ represents 310K, ◇ represents 300K. Data suggest that the ASA of the tablets increased more rapidly at 310 K than 300 K.

In addition to the change in the ASA of the molecules, we also examined the molecular lipophilicity potentials (MLP) of the tablets. The MLP describes the hydrophobic and hydrophilic surface properties of the molecules. In our case, it represents the hydrophobicity of the tablet surface, which can be correlated with the tablet dissolution rate. The MLP of the single molecules and tablets is shown in Table 4.1. The log P values were constant during the tablet compression and dissolution. It was observed that the lipole values of the both tablets decreased after the 4.8 ns simulation. The 5-FU tablet lipole value decreased since the molecules were rearranging to decrease exposure of the hydrophobic moieties to the surrounding water. The ilomastat tablet lipole value did not reduce as significantly as 5-FU due to the lack of molecular rearrangement (caused by their large volume and complicated structure) during the simulation. When comparing

the change in the ilomastat tablet lipole value before and after the 4.8 simulation, the reduction of the ilomastat lipole value indicates that ilomastat molecules tend to expose their hydrophilic parts to the water, but the change was not as large as that seen for the 5-FU tablet.

Table 4.1 MLP of 5-FU and ilomastat molecules and tablets. Data suggest that that the lipole values of the both tablets decreased after the 4.8 ns simulation

| Drug | | Simulation time (ns) | lipole | Log P |
|---|---|---|---|---|
| 5-FU | Single molecule | - | 0.5621 | -1.362 |
| | Tablet at 300 K | 0 | 0.1658 | |
| | | 4.8 | 0.0357 | |
| | Tablet at 310 K | 0 | 0.1437 | |
| | | 4.8 | 0.0594 | |
| Ilomastat | Single molecule | - | 1.2751 | 0.6520 |
| | Tablet at 300 K | 0 | 0.9179 | |
| | | 4.8 | 0.8960 | |
| | Tablet at 310 K | 0 | 0.9983 | |
| | | 4.8 | 0.7335 | |

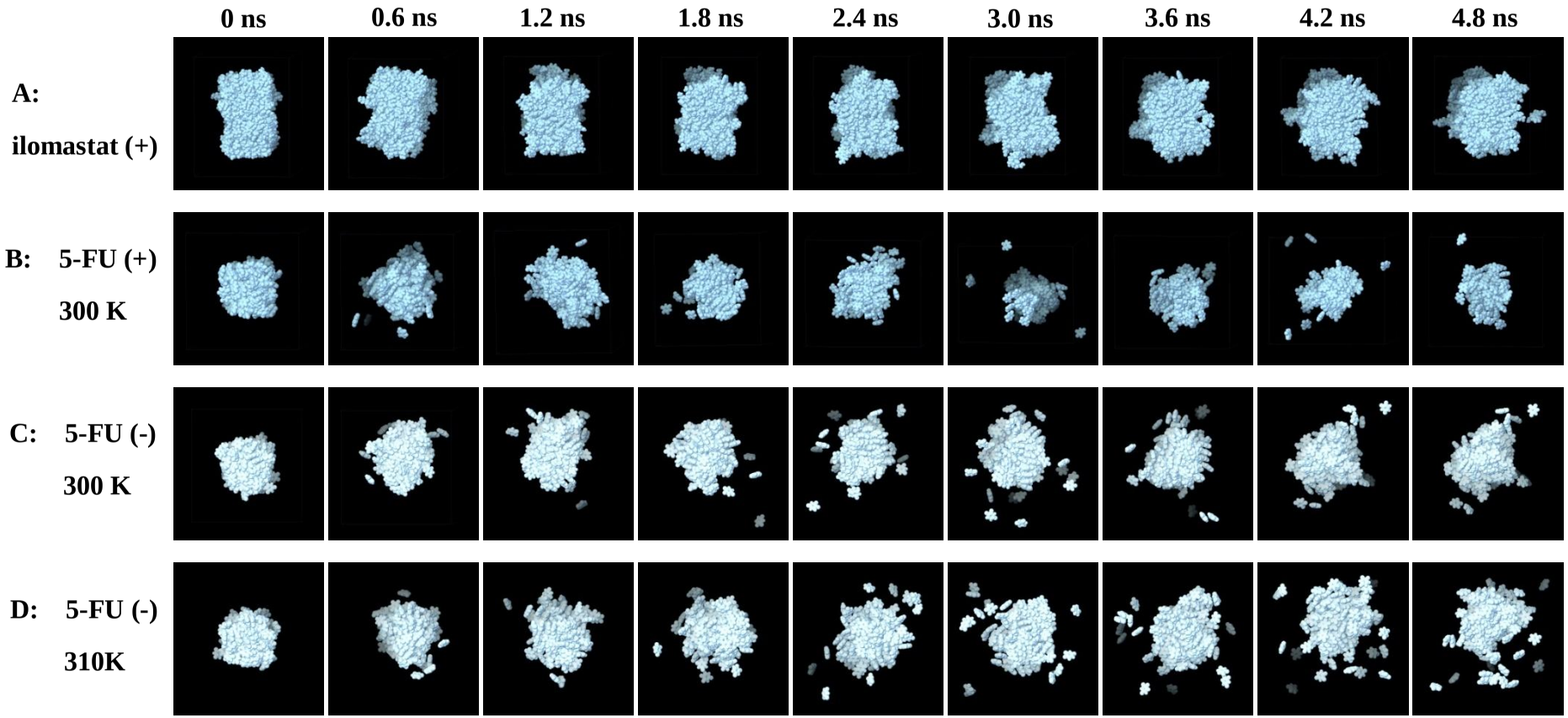


Figure 4.12. MD simulation of tablets dissolution at different time points and different temperature with (+) or without (-) the liquid turnover. Data suggest that 1) the 5-FU tablet dissolved faster than the ilomastat tablet, 2) the 5-FU tablet dissolved faster with the liquid turnover, and 3) the 5-FU tablet dissolved faster at 310 K than at 300 K.

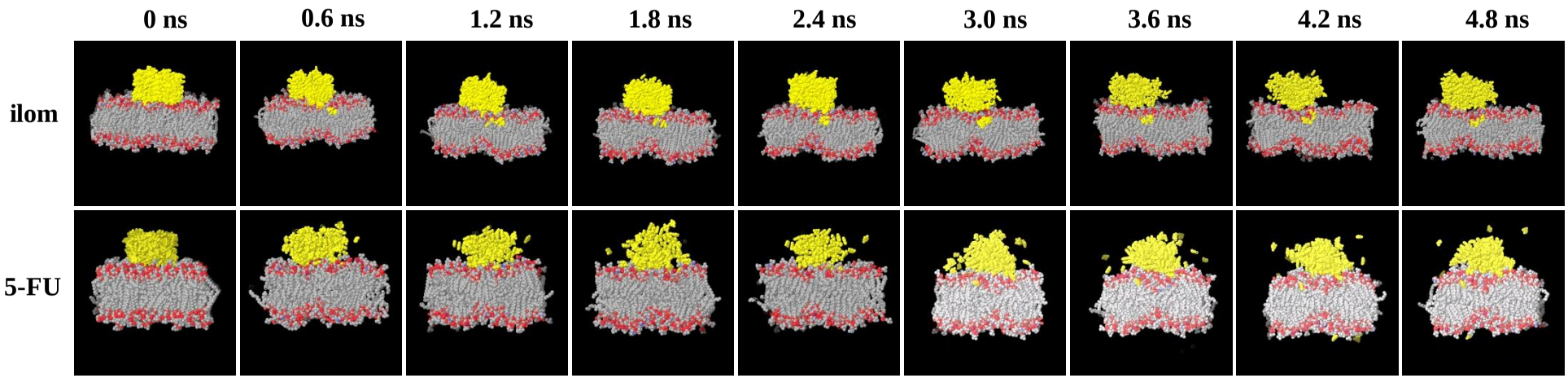


Figure 4.13. MD simulation of tablet dissolution when in contact with a simulated biological membrane at 310 K without the liquid turnover. Data suggest that, compared with 5-FU, ilomastat molecules are more likely to interact with the biological membrane. But it is difficult for both molecules to pass through the membrane (The molecules which appears to be able to pass the membrane were artefacts).

#### 4.3.3.2. Simulation with the mimicking of liquid turnover

Since the drug was eliminated due to the flow of aqueous in the bleb, the computational experiment was designed to simulate the loss of drug molecules which in reality leave the bleb. The dissolution media (water) with already dissolved molecules (molecules that have detached from a tablet) was removed and replaced manually with dissolution media at the end of each 0.06 ns circulation. In each cycle, about 10 5-FU molecules that dissolved into water were removed manually (Figure 4.12, row b). It was observed that at the beginning of each circulation, the ASA of 5-FU was increasing due to relaxation of the tablet surface (tablet swelling) and consequently the detachment of molecules from the surface. After removing the detached 5-FU molecules at the end of each circulation, the ASA initially decreased due to the smaller number of molecules left in the solution. Then the ASA of the remaining tablet increased slowly due to the further dissolution with more 5-FU molecules being released into the solution. As a result, the volume (monitored through the ASA) of the 5-FU tablets reduces gradually during each step of circulation (Figure 4.14.). However, in the simulation of the computation experiment with ilomastat tablets, only one or two ilomastat molecules were released at the end of the 8$^{th}$ circulation (Figure 4.12., row a). This indicates that 5-FU tablet dissolves much faster than ilomastat tablet.

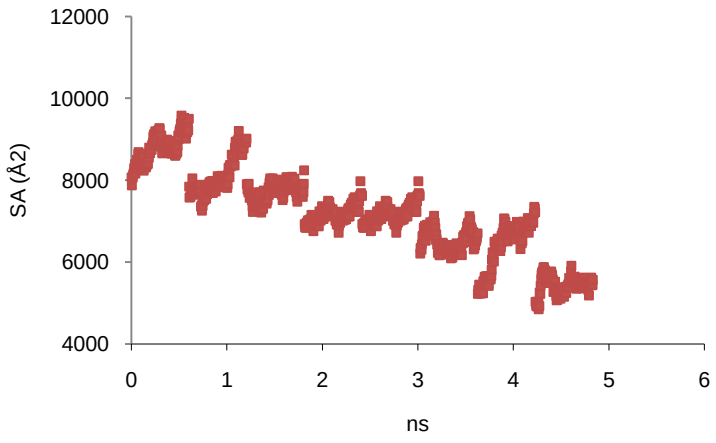


Figure 4.14. Change in the ASA of the 5-FU tablet in the presence of liquid turnover at 300 K. Data suggest that the ASA of the 5-FU tablet decreased significantly in the presence of liquid turnover.

Table 4.2 Increase of 5-FU ASA at each circulation with liquid turnover.

| No. of circulation | Increase of ASA |
|---|---|
| 1 | 14.3% |
| 2 | 15.0% |
| 3 | 4.3% |
| 4 | 9.9% |
| 5 | 9.9% |
| 6 | 7.9% |
| 7 | 38.1% |
| 8 | 8.7% |

When simulating the dissolution of the tablets, the molecule proportions of 5-FU and water were calculated to correspond to the experimental condition (5 mg 5-FU in 50 µl water, molecular ratio 1:72). To conduct a parallel study, the same size water box was set up for the ilomastat tablet. To keep the volume of water box constant, the number of the ilomastat molecules (90) was reduced compared to 5-FU (164) because the ilomastat molecules have a larger volume than the 5-FU molecules. A sudden significant increase in ilomastat tablet ASA was observed at the end of the simulation (Figure 4.11. B) as a result of some ilomastat molecules moving out of the simulation box. In order to prove that there was no mistake in the experiment setup, when the simulation was repeated, the same problem occurred. This suggests that a larger volume is needed for the dissolution of ilomastat in the future. However, this has not compromised the quality of results because we tend to evaluate the dissolution of the ilomastat molecules by observing the detachment of the molecules from the tablet. From the results we understand that the dissolution of the ilomastat tablet is much slower than the 5-FU tablets.

It was encouraging that our simulation results, which have shown that the tablets dissolved faster when the temperature was increased, corresponding to the results of *in vitro* experiments. This higher rate of dissolution at 310 K is due to the increase in kinetic energy at higher temperatures. The total number of released 5-FU molecules compared to

the number of ilomastat molecules qualitatively correlates to the ratio of their experimental solubilities. Our results indicate that the solubility of the drug is not the sole measurement of the dissolution of an excipient-free tablet. The simulation with liquid turnover suggests that the liquid flow does affect the tablet release. This effect appears more significant on hydrophilic compounds. For example, in the absence of the liquid flow, the total molecular ASA of 5-FU increased 62.5% (from 8000 $Å^2$ to 13000 $Å^2$) after 4 ns; while the total molecular ASA of ilomastat increased approximately 1% (from 14000 $Å^2$ to 15000 $Å^2$). With the presence of the liquid turnover, saturation of 5-FU could never be accomplished. Table 4.2 shows the increase of 5-FU ASA in each circulation with liquid flow. It can be seen that the increasing level of ASA (in percentage terms) decreased with time (with the exception of circulation 7). For example, the 5-FU ASA increased approximately 14-15% at the beginning; whereas this number decreased to around 8% in the $8^{th}$ circulation. This indicates that the tablet release rate decreases with the reduction of molecular ASA. These findings suggest that tablet dissolution is related to its surface area, which corresponds with the later findings in our *in vitro* model. It was also found (by Dr. Hala Fadda) that tablets containing the same amount of ilomastat but with different surface areas demonstrated significantly different release rates. Tablets with a larger surface area had a higher release rate. Therefore, in addition to the flow rate, surface area is another factor that affects the tablet release rate.

It is understood that the reported aqueous solubility of 5-FU (11.1 mg/mL) is more than 280 times higher than that of ilomastat (0.03885 mg/mL). This ratio can be changed when a different dissolution media is used. For example, in pH 7.4 PBS, the solubility of 5-FU was found to increase slightly (13.6 mg/mL), but the solubility of ilomastat increases to nearly 6 times higher (0.2230 mg/mL, by Dr. Hala Fadda). Hence, it is believed that the dissolution media dose have a significant effect on tablet dissolution. However, this was not included in our simulations since water was the only dissolution media. Hence, we seek to more closely mimic the dissolution media as a biological fluid in terms of ionic strength and proteins content.

Notwithstanding the physical and chemical properties of the tablets, our previous studies from the *in vitro* model have shown that the release profiles can be affected by temperature, chamber volume, aqueous flow rate, tablet surface area, and the dissolution media. When programming the experiments, the temperature could be adjusted for different types of simulations. The dissolution media volume could also be modulated manually by altering the size of the water box. In addition, the simulation flow rate could be adjusted by changing the frequency of the circulation. The change in total molecular ASA reflects the dissolution rate of the tablet. Hence, tablet dissolution can be further predicted and evaluated using molecular dynamics simulations. In the future, it is hoped that the simulation results can be correlated with the *in vitro* release data.

### 4.3.4. Simulation of the tablet interaction with a membrane

Considering that the tablets implanted in the eye are in contact not only with the aqueous humor but also with the tissue, including fibroblasts and collagens, the simulation was conducted in the presence of a DPPC membrane as a simplified model of a cell wall. It was observed that, in the presence of the membrane, many 5-FU molecules were released into water but only one or two ilomastat molecules were found to be released into the water. At the end of the simulation the total molecular SA of 5-FU increased by about 75%, but the total molecular SA of ilomastat did not increase significantly (Figure 4.15.). These results are consistent with the previous dissolutions findings in water without the presence of the membrane. At the end of the simulation, it appeared that in both simulations two molecules had entered the membrane (Figure 4.13.). Ilomastat molecules “diffused” into the membrane at around 0.6 ns, while 5-FU molecules did not do so until 3 ns. As 5-FU dissolved much faster than ilomastat due to its higher aqueous solubility, a larger number of isolated molecules have more chance to interact with the membrane. However, the trends of “diffusion” or “permeation” observed in the pictures are probably all artefacts. It might be very difficult for both molecules to pass through the membrane due to non-covalent intermolecular interactions between the drug molecules and the fatty acyl chains in the membrane. The results suggest that, compared with 5-FU, ilomastat molecules are more likely to interact with the biological membrane.

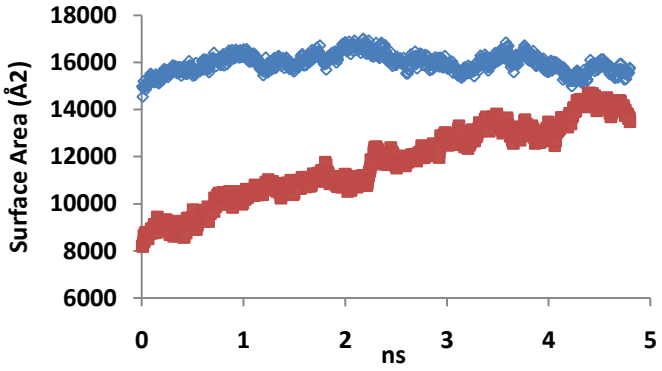


Figure 4.15. Change in the ASA of the tablets in the simulation of membrane permeation simulation. ■5-FU ◇ilomastat. Data suggest that the ASA of the 5-FU tablet increased significantly during the membrane permeation simulation, but the ASA of the ilomastat tablet did not.

In addition to the total molecular ASA, changes in the lipophilicity of the ilomastat tablet surface were also evaluated. It was found that after the 4.8 ns simulation without the presence of the membrane, the average lipophilicity of the ilomastat tablet surface decreased by about 50% in the water box. But in the presence of the membrane, the total lipophilicity of the ilomastat tablet surface decreased by only 14% because part of the tablet surface was in contact with the DPPC membrane (Figure 4.16.). This suggests that the ilomastat molecules tend to expose their polar surface when they are surrounded by water, and that the ilomastat molecules tend to expose their hydrophobic parts when in contact with the DPPC membrane.

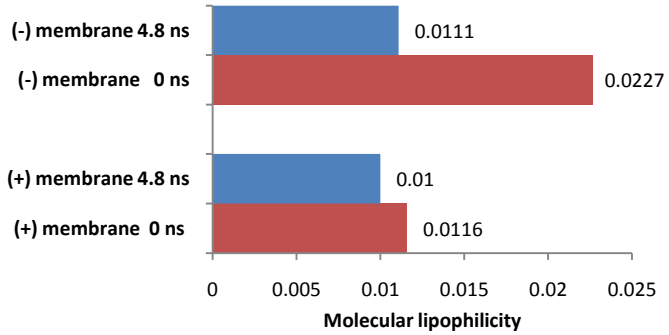


Figure 4.16. Change in the molecular lipophilicity of the ilomastat tablet with (+) or without (-) the presence of DPPC membrane before and after the simulation at 310 K. Data suggest that that the ilomastat molecules tend to expose their polar surface when they are surrounded by water, and that the ilomastat molecules tend to expose their hydrophobic parts when in contact with the DPPC membrane.

Although further simulations were not conducted due to time constraints, these

preliminary experiments give a very good indication about the effect of contacted membrane on tablet dissolution. Investigation of the interaction of ilomastat on the tissue, which is represented by DPPC membrane currently, is considered a fairly preliminary study using MD simulations. It is hoped that these studies can be further conducted in the future.

Our simulations were only conducted on two types of tablets (5-FU and ilomastat). But it has shown a new way of evaluating a tablets release profile. The advantage of this simulation is that these "virtual experiments" can run as frequently as required and without the need for any laboratory facilities. In addition to the results we have above, lots of further studies, such as tablets with various excipients and coatings, can be conducted using similar methods.

### 4.4. Conclusions

Our computational efforts indicate that the dissolution process of a tablet in non-sink conditions can be modeled using MD simulations. The fabrication and dissolution of 5-FU and ilomastat tablets were simulated. Both 5-FU and ilomastat tablets were found to dissolve faster when the temperature was increased; the release rate of 5-FU was found to be much faster than that of ilomastat. These results agree with our experimental observations. From these studies we found that 1) solubility is not the sole measurement of the dissolution of excipient-free tablet in non-sink conditions, 2) the dissolution rate is related to the chemical structural features of the drug, the temperature and the flow rate of the liquid turnover, and 3) the combination of non-covalent interactions and hydrogen bonds between the drug molecules may lead to the varied solubility of the compounds as well as the different dissolution rate of the tablet. Other factors that may affect the tablet dissolution rate, including the volume and composition of the dissolution media as well as the initial shape/surface area of the tablets may possibly be simulated by the use of computer modeling in the future.

In addition to the tablet dissolution process, the interaction between the drug molecules and a biological membrane was also investigated using MD simulations. It was found

that ilomastat is more likely to interact with a biological membrane than 5-FU. Although much work on this subject is needed in the future, we have explored a new way to examine the behavior of excipient-free tissue tablets in non-sink conditions. Hopefully the simulation results will correlate with subsequent lab experiments and will give valuable indications for future studies.

# *Chapter V Tablets derived from other compounds and development of a mathematical model to correlate drug release*

## 5.1. Introduction

### 5.1.1. Extension of excipient-free tablets for combined treatment

From previous studies we know that an excipient-free ilomastat tablet placed in the subconjunctival space could potentially provide long term scar inhibition with low toxicity. The 5-FU tablets also have shown the potential in inhibiting proliferation of fibroblasts *in vitro*. Despite the use of these two excipient-free tablets, making tablets with different compounds may provide valuable information for the future development of tablets with combined treatments. It has been established that topical, postoperative applications of anti-inflammatory agents, such as corticosteroids, are effective in suppressing the local inflammatory response of GFS and hence improving the reduction of IOP (Araujo et al. 1995;Miller et al. 1990;Roth et al. 1991;Starita, Fellman, & Spaeth 1985). Hence, it is thought that a combination of anti-inflammatory and anti-proliferative agents in our tissue tablets will be effective in long term scar inhibition after GFS. Combination of 5-FU and dexamethasone sodium phosphate (DEX-P) was attempted 10 years ago (Zignani et al. 2000a). It was found that the drug carrier (POE) alone led to a hyperemia and chemosis, but the addition of DEX-P improved the surgical prognoses and polymer tolerance due to its anti-inflammatory properties. In addition, DEX-P decreased the POE degradation rate and prolonged 5-FU release. Recently, How *et al* found that a combination of 5-FU and bevacizumab demonstrated a superior anti-fibrotic effect after GFS (How et al. 2010). These reports suggest that a combination of anti-inflammatory agents in our tablet has great potential in controlling the drug release, improving the biocompatibility of the tablet, and preventing the formation of capsules. The potential advantages of making combined tablets include not only combine treatment (e.g. anti-inflammatory and anti-fibrosis) but also the improvement of tablet fabrication and dissolution. Since our initial studies on 5-FU and ilomastat were mainly focused on the excipient-free tablets, our subsequent studies continued with excipient-free tablets and we decided to make some excipient-free tablets from clinically used anti-inflammatory compounds.

As the previous *in vitro* studies showed that tablets made of hydrophobic compounds

such as ilomastat have a long residential time in the bleb, it is important to determine the termination time of the tablets. However, although in the *in vivo* studies the ilomastat tablets have shown remarkable results in scar inhibition, the duration of the ilomastat release remains unclear. Hence, there is a need to understand the tablet dissolution and predict their termination time. Before manufacturing tablets with combined drugs, we need to obtain more general information on tablet dissolution in non-sink condition using tablets made from only one compound. We also tried to develop a computational mathematical model to mimic the tablet dissolution process. We firstly aim to correlate the current experimental data with the mathematical. If a good correlation is obtained, it was hoped that this model will be able to predict the tablet release and consequently reduce the time and cost of the laboratory experiments.

### 5.1.2. Understanding tablet dissolution

Release of the drug from a tablet is related to the manufacture and dissolution process of the tablet.

- ***Manufacturing process***

The manufacturing process of the tablets affects the tablet dissolution. Our tablets were fabricated by direct compaction, which is associated with many technical issues including the flowability, bulk density, and compatibility of the material. Since there is no filler or binder in the excipient-free tablets, a few issues need to be considered. Firstly, the flowability of the drug directly affects the accuracy of the tablet weight. For example, as 5-FU has a better flowability than ilomastat, weighing a few milligrams of 5-FU is easier and less time consuming than with ilomastat. Second, when the same amount of drug is weighed, the proportion of 5-FU that is lost during the compression process is less than that with ilomastat. Third, the compatibility of the drug directly affects the integrity and strength of the tablets. It is known that a highly compatible powder is able to form a tablet with a resistance to fracturing and without tendencies to cap or laminate. It was observed that ilomastat has better compatibility than 5-FU because the lowest pressure required for making a robust tablet (without any capping or laminate) is 5 and 14 bars for ilomastat and 5-FU respectively. The relationship between

compaction pressure and tablet tensile strength were not studied in detail due to the limited availability of ilomastat. To avoid differences in the release of the tablet caused by compression pressure, all the other tablets in the later studies were compressed using 14 bars.

- ***Dissolution process***

In addition to the manufacturing process, tablet dissolution is also highly related to the properties of the tablets as well as the dissolution medium. From a pharmaceutical point of view, dissolution of an excipient-free tablet is considered as the dissolution of a large drug particle. As most drugs exist as crystalline solids, here we restrict our discussion to the dissolution of crystalline solids. The dissolution of a solid into a liquid is usually composed of two consecutive stages: 1) an interfacial reaction which lead to the liberation of solute molecules from the solid phase to the liquid phase and 2) the migration of solute molecules from the boundary layers to the bulk of the solution (Aulton 1998). The first stage of dissolution (interfacial reaction) is dependent on the relative affinity between the molecules of the solid substances and those of the solvent. In other words, a drug molecule dissolves when the attraction of a solvent overcomes the cohesive forces of attraction between the molecules of the solid. The second stage involves the transportation of the solute from the solid/liquid interface into the bulk of the liquid phase, through either diffusion or convection. Factors that affect the dissolution of a solid include 1) the surface area of undissolved solid, 2) the solubility of solid in dissolution medium, 3) the concentration of solute in solution at time, and 4) the dissolution rate constant (summarized in Table 5.1). Similarly, when an excipient-free tablet is placed in the bleb, its dissolution will be affected by many factors including the volume and temperature of the bleb, the surface area of the tablet, the chemical structure and wettability of the drug, *etc*. These factors are summarized in the last column of Table 5.1. We have known that a small tablet placed in the bleb forms a non-sink condition. It is commonly believed that drug saturation cannot be easily observed in non-sink conditions. In the bleb this becomes true only if the aqueous flow is absent or negligible. However, our previous studies using the flow chamber have shown that the

drug solution never becomes saturated; this suggests that the influence of the aqueous flow is not negligible. As drug accumulation occurred in the flow chamber (reflected by the increasing drug concentration at the early stages of dissolution), the drug molecules must have dissolved into the media at a higher rate than they left the bleb. Therefore, the drug dissolution rate becomes the rate-limiting step of the tablet dissolution in the bleb.

Table 5.1. Factors affecting the rate of dissolution(Aulton 1998).

| **Factors** | **Explanation of the factors** | **Factors that relate to the dissolution of excipient-free tablets in the bleb** |
|---|---|---|
| **Surface area of undissolved solid (A)** | ● Size of solid particles<br>● Dispersibility/wettability of powdered solid in dissolution medium<br>● Porosity of solid particles | ● Size/shape/surface area of the tablets<br>● Wettability of the drug<br>● Porosity of the tablets |
| **Solubility of solid in dissolution medium (Cs)** | ● Temperature<br>● Nature of dissolution medium (e.g. pH)<br>● Molecular structure of solute<br>● Crystal characteristics (polymorphism and solvation) of solid<br>● Presence of other compounds | ● Temperature of the bleb<br>● The composition of aqueous humor/dissolution media<br>● Molecular structure of the drug<br>● Crystalline of the drug |
| **Concentration of solute in solution at time (c)** | ● Volume of dissolution medium<br>● Any process that removes dissolved solute from the dissolution medium | ● Volume of the bleb<br>● The flow rate of aqueous humor |
| **Dissolution rate constant (k)** | ● Thickness of boundary layer (affected by speed of stirring/shaking, size/position of stirrer, volume of dissolution medium, shape and size of the container, and viscosity of dissolution medium)<br>● Diffusion coefficient of solute in the dissolution medium | ● The shape and size of the bleb<br>● The viscosity of the aqueous humor/dissolution media |

### 5.1.3. The potential of developing of a mathematical model for mimicking tablet dissolution

The establishment of a mathematical model requires experimental data. To develop a good mathematical model, the experimental data should be representative for a wide range of drugs. Since it is known that drug dissolution rate is the rate-limiting step of the tablet dissolution in the bleb, any additional studies on excipient-free tablets should be conducted on tablets made from drugs with range of different solubilities. For the

potential development of combined treatments in the future, it is preferred that these drugs are clinically used anti-inflammatory compounds. Steroids such as dexamethasone (DEX, Figure 5.1 A) and triamcinolone (TRI, Figure 5.1 B) are commonly used anti inflammatory drugs with a fairly low aqueous solubility (Table 5.2). Naproxen (Mw 230.3, Figure 5.2.) is a non-steroidal anti-inflammatory drug (NSAID) which is commonly used to control the ocular inflammation response. Since it is practically insoluble in water, the eye drops usually contains its salt (sodium naproxen) which is more soluble than naproxen. However, the solubility of naproxen is pH dependent as it is a weak acid. Its equilibrium solubility in pH 7.4 PBS can be as high as 6 mg/mL at 37 ℃ (Amaral, Lobo, & Ferreira 2001). Here we choose naproxen for the investigation of excipient-free tablets since its solubility at pH 7.4 is lower than 5-FU but higher than ilomastat.

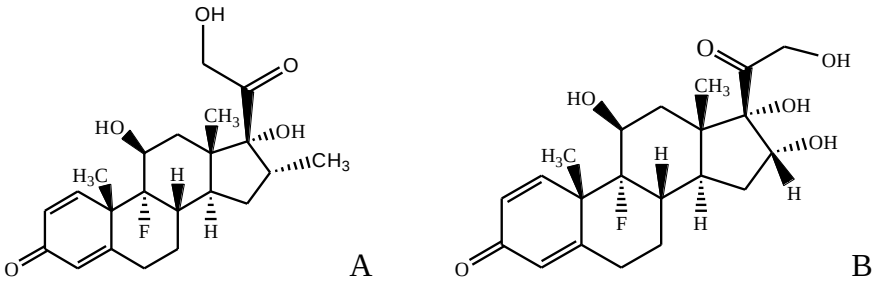


Figure 5.1. Chemical structures of triamcinolone (A) and dexamethasone (B).

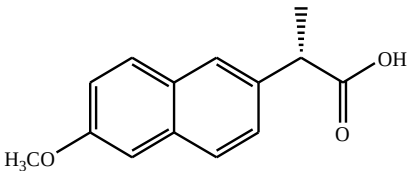


Figure 5.2. Chemical structure of naproxen.

Table 5.2. Solubility of some anti-proliferative and anti-inflammatory agents.

| **Compound** | **Solubility in water (mg/mL)** | **Solubility at pH 7.4 (mg/mL)** | **References** |
|---|---|---|---|
| 5-FU | 11.1 | > 15.4 | (Monnot et al. 1990;Singh, Singh, & Singh 2005;Yalkowsky & He 2003) |
| NAP | 0.0263 | 2.92 (25 ℃)<br>6 (37 ℃) | (Amaral, Lobo, & Ferreira 2001;Mora & Martinez 2006;Yalkowsky & He 2003) |
| Ilomastat | 0.0389 | 0.223 (at 37 ℃) | (Millipore 2010) |
| TRI | 0.08 | NA | (Yalkowsky & He 2003) |
| DEX | 0.116 | 0.14 | (Yalkowsky & He 2003) |

After recruiting the potential drug candidates, we then considered the factors that affect tablet dissolution (listed in the last column of Table 5.1) before establishing the mathematical model. Some of these factors are almost constant, such as the bleb temperature and the composition/viscosity of aqueous humor. Others such as the aqueous flow rate, the shape and size of the bleb, are difficult to predict as they vary with individual patients. Although it is understood that some of these factors may vary, there is still a need to determine the therapeutic dose of the drug for further *in vivo* studies. This can be accomplished by *in vitro* experiments. Using our flow chamber model, most of the factors mentioned above (temperature, the nature of the dissolution media, the amount of the drug and the surface area/shape of the tablet) can be manually set up. Hence, it is hoped that the *in vitro* studies using the flow chamber can help us to find some general patterns of the tablet release profiles in non-sink conditions for the future development of the mathematical model.

## 5.2. Materials and methods

### 5.2.1. Materials and instrumentation

Naproxen (NAP), triamcinolone (TRI), dexamethasone (DEX), trifluoroacetic acid (TFA), were purchased from Sigma-Aldrich (UK). The Discovery® HS C18 HPLC column (15 cm × 4.6 mm, 5 μm) was purchased from Sigma-Aldrich (UK). The Synergi Hydro-RP 80A column (150 × 3 mm, 4μm) was purchased from Phenomenex (UK).

### 5.2.2. Preparation of the tablets

The NAP, TRI and DEX tablets were made by direct compression according to the method described in 2.2.4.3 using a pressure of 14 bars. The diameter of the tablets was 3 mm. The weight of the excipient-free tablets was around 5.1 ± 0.4 mg (n=42). Their thickness was around 0.55 ± 0.06 mm (n=42).

### 5.2.3. Evaluation of the release profiles of the tablets

The dissolution profile of the tablets was evaluated using the method described in 2.2.5. The flow rate of PBS solution was set to 2 μL/min, which is the average flow rate of the

human aqueous humor.

### 5.2.4. HPLC methods for the release of the tablets

The HPLC methods were developed with the guide and discussion with Dr. Hardyal Gill at London School of Pharmacy. HPLC analysis was performed on an Agilent Technology 1200 series system consisting of a separation module for solvent and sample delivery, a UV detector and chemstation software for data acquisition and analysis. The UV wavelength was set to 254 nm, which is a universal wave length for aromatic rings. This wave length was chosen because in the future we might need to evaluate more than one compound simultaneously. To obtain the best retention and separation, a few HPLC columns, including C8, C18, and Synergi Hydro-RP 80A were tested. The best columns and mobile phase for each compounds are shown in Table 5.3. Chromatography was performed at 40 ℃. Samples were eluted at a flow rate of 1.0 mL/min.

Table 5.3 HPLC methods for the NAP, DEX, and TRI tablets.

| Compounds | Column | Mobile phase | Retention time (min) |
|---|---|---|---|
| NAP | Synergi Hydro-RP 80A | ACN: 0.1% TFA (35:65, v/v) | 6.6 |
| DEX | Discovery®HS C18 | ACN: 0.1% TFA (35:65, v/v) | 6.3 |
| TRI | Discovery®HS C18 | ACN: 0.1% TFA (25:75, v/v) | 5.6 |

### 5.2.5. DSC measurements of the tablets

***Preparation of the tablets***

The tablets were taken out from the flow chamber after 1 day (NAP) or 6 days (DEX, TRI) and rinsed three times with 200 μl de-ionized water. They were then dried in a 37 ℃ oven over night and crushed gently by motor and pestle before DSC measurement. The samples were weighed using METLER TOLERDO balance (XS105, d=0.01 mg).

***DSC measurements***

The DSC samples were all weighed using a METLER TOLEDO XS105 balance (d = 0.01 mg). DSC measurements of NAP and DEX tablets were made with a Pyris 1 DSC (PerkinElmer Ltd.). Samples (2–5 mg) were sealed in non-hermetic aluminium pans and heated from 25 to 300 ℃ at 100 ℃ $min^{-1}$ with a nitrogen purge gas (flow rate 20

mL/min).

DSC measurements of TRI tablets were made with a Q2000 DSC and a RHC DSC (TA instruments). Samples (2–5 mg for Q2000 and 0.1 mg for RHC DSC) were sealed in non-hermetic aluminium pans and heated from 25 to 300 ℃ at 100 (Q2000) and 500 ℃ (RHC) $min^{-1}$ with a nitrogen purge gas. In all the DSC experiments, an empty pan was used as a reference and the temperature and enthalpy of the instruments was calibrated with indium.

## 5.3. Results and discussion

### 5.3.1. *In vitro* release profiles of excipient-free NAP, DEX, and TRI tablets

#### 5.3.1.1. Release profiles of the excipient-free NAP tablets

The excipient-free NAP tablets were evaluated in different flow chambers (50 and 200 µl). All the tablets will be dissolved at the body temperature and not at room temperature but from a modeling perspective, the effect of temperature needs to be factored in. Hence, all the studies were conducted at two different temperatures (ambient and body temperature). It was found that NAP was completely released after approximately one week in ambient temperature (Figure 5.3). As with the 5-FU tablets, the NAP tablet was released faster when placed in the 50 µl flow chamber, compared to the 200 µl flow chamber. Six days after starting the evaluation, 84% of NAP was released in the 50 µl flow chamber; while 68% of the NAP was released in the 200 µl flow chamber. Nearly 100% of NAP was released at 37 ℃ within 5 days (Figure 5.4.).

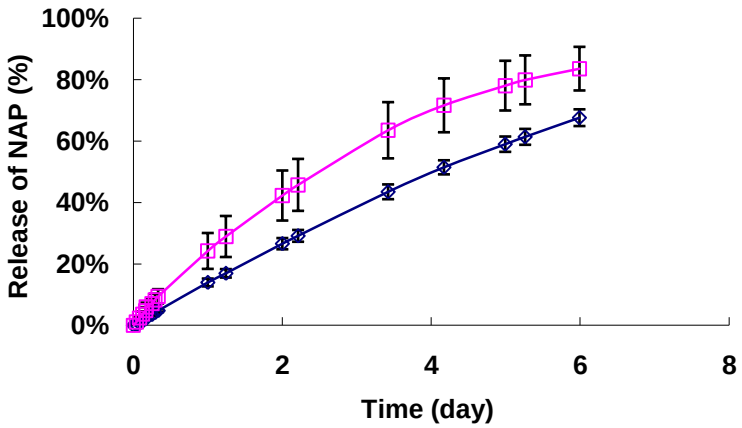


Figure 5.3 Release profiles of the excipient-free NAP tablets at ambient temperature (n=4, error bars indicates standard deviation). □ 50 µL chamber ◇ 200 µL chamber. Data suggest that the release rate of NAP as well as the NAP concentration are enhanced with the decreasing of the chamber volume.

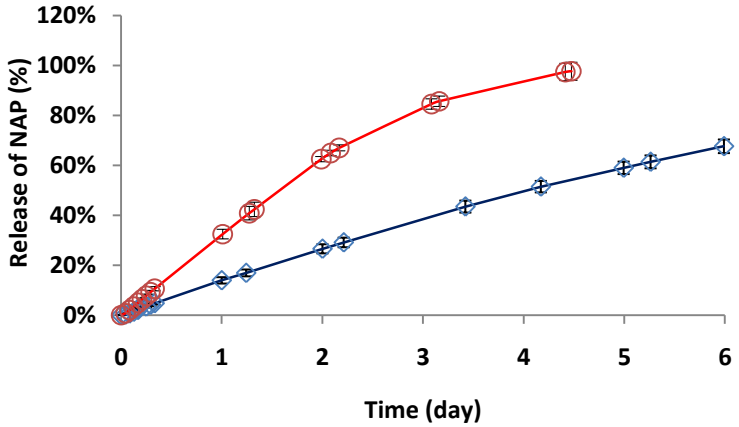


Figure 5.4. Comparison of NAP release profiles at different temperature in the 200 µl chamber (n=4, error bars indicates standard deviation). ◇ Ambient temperature ○37 ℃. Data suggest that the release rate of NAP as well as the NAP concentration are enhanced with the increasing of temperature.

### 5.3.1.2. Release profiles of excipient-free DEX and TRI tablets

As with the previous studies, the release studies of DEX and TRI tablets were conducted in parallel. In comparison to NAP, the release of DEX and TRI was much slower. After 5 days in ambient temperature, approximately 3.5% of DEX was released in the 200 µl chamber; whilst in the 50 µl chamber the release rate was double (Figure 5.5.). In the release study at 37 ℃, the DEX release rate raised to 7.5% in the 200 µl chamber (Figure 5.6.).

Since DEX and TRI have very similar chemical structures, their release profiles are very similar. The release of TRI was slightly faster than DEX as it is more soluble than DEX.

In the experiments at ambient temperature (Figure 5.5.), the release rate of TRI in the two chambers reached 6.1% and 9.3% respectively on day 5, which is slightly higher than that of DEX (3.5% and 5.7%). At 37 ℃ the accumulate release of TRI in the 200 µl chamber is approximately 1.6 times higher (12%, Figure 5.8) with respect to that of DEX (7.5%, Figure 5.6.).

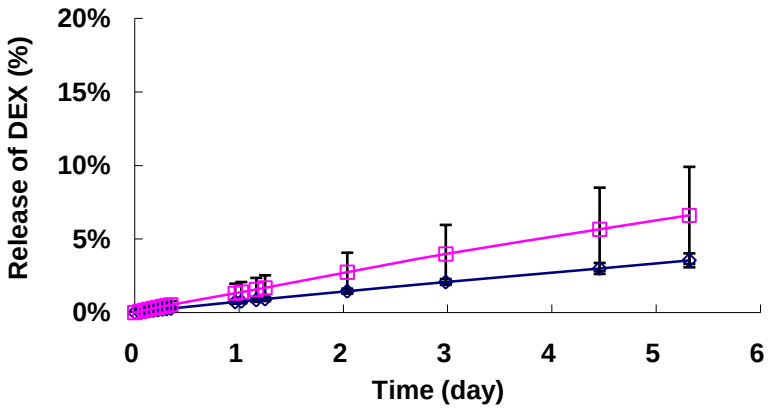


Figure 5.5. Release profiles of DEX excipient-free tablets at ambient temperature (n=4, error bars indicates standard deviation). □ 50 µL chamber ◇ 200 µL chamber. Data suggest that the release rate of DEX as well as the DEX concentration are enhanced with the decreasing of the chamber volume.

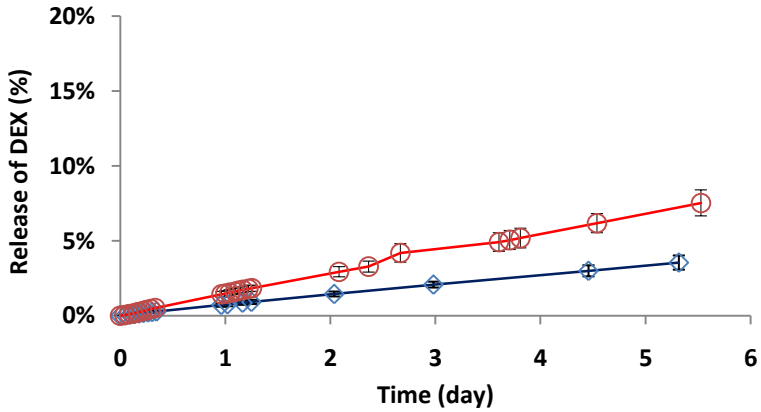


Figure 5.6. Comparison of DEX release profiles at different temperature in 200 µl chamber (n=4, error bars indicates standard deviation). ◇ Ambient temperature ○37 ℃. Data suggest that the release rate of DEX as well as the DEX concentration are enhanced with the decreasing of the chamber volume.

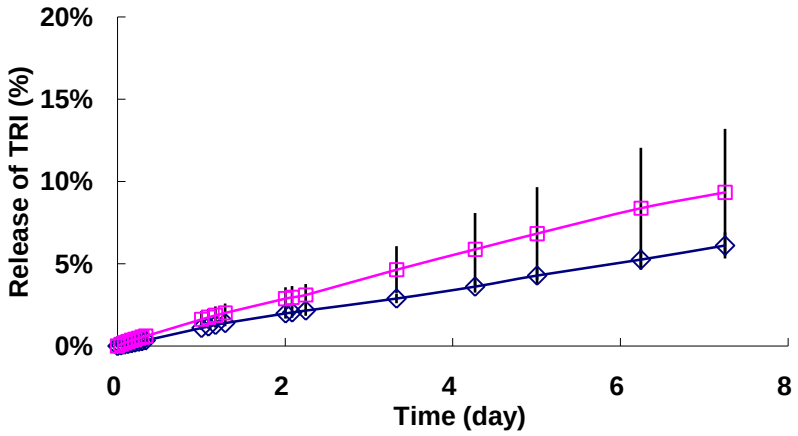


Figure 5.7. Release profiles of TRI excipient-free tablets at ambient temperature (n=4, error bars indicates standard deviation). □ 50 µL chamber ◇ 200 µL chamber. Data suggest that the release rate of TRI as well as the TRI concentration are enhanced with the decreasing of the chamber volume.

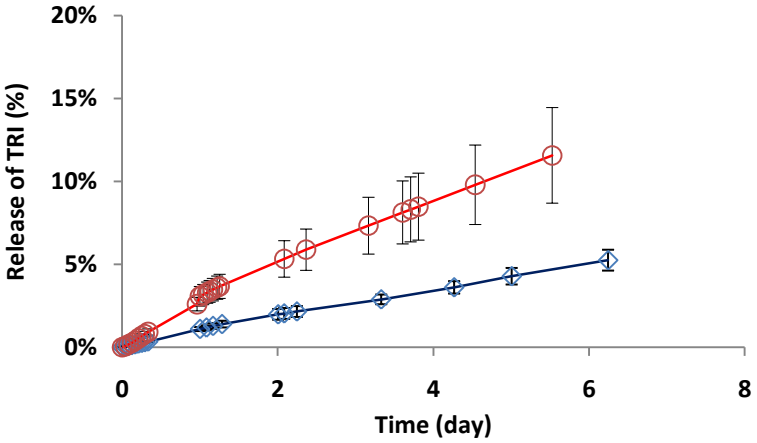


Figure 5.8. Comparison of TRI release profiles at different temperature in the 200 µl chamber (n=4, error bars indicates standard deviation). ◇ Ambient temperature ○37 ℃. Data suggest that the release rate of TRI as well as the TRI concentration are enhanced with the decreasing of the chamber volume.

### 5.3.2. Development of the mathematical model to mimic the release profile

After the evaluation of the excipient-free tablets using the flow chamber, we compared all the release profiles to see if there were any regular patterns. As mentioned before, saturation of the drug was expected to be observed for the tablets placed in non-sink conditions. However, dissolution of NAP, DEX, and TRI tablets again confirmed that the dissolution rate was the rate-limiting step in the tablet dissolution since saturation of drug in the flow chamber was never observed. It was found that these release profiles shared some common points. With no exception, the tablets dissolved faster when in the

small chamber (50 µl). This might be because, when the tablet is placed in a small chamber, the diffusion of drug from the boundary layer to bulk solution was accelerated due to the relatively high refreshment rate of PBS (2 µL/min ÷ 50 µl = 4% /min, 2 µL/min ÷ 200 µl = 1% /min). The release rate of the tablets and collected drug concentrations in the 200 µl chamber were nearly double at 37 ℃ compared to at ambient temperature, but it is unknown how this doubled concentration is mathematically related to the change in chamber volume. If we sum up all the accumulate release of the tablets, we found that the shape of the curve looks similar to a logarithm curve (Figure 5.9.). The accumulate release of ilomastat, DEX, and TRI appears to be linear over a 6 day period but this may not reflect the true picture because so little drug was released during this period. They may also look similar to a logarithm curve if the accumulate release is measured in a sufficient long time. Additionally, the drug concentration reached a peak and then decreased following a curve which is similar to an exponential curve. Due to the differences among the collected drug concentrations, we did not sum up them in one figure. Most importantly the release rate of the drugs seems to be directly proportional to drug solubility. While there appeared to be dissolution rate anomalies, we still sought a mathematical model that could describe the release behavior of the tablets by using the drug solubility.

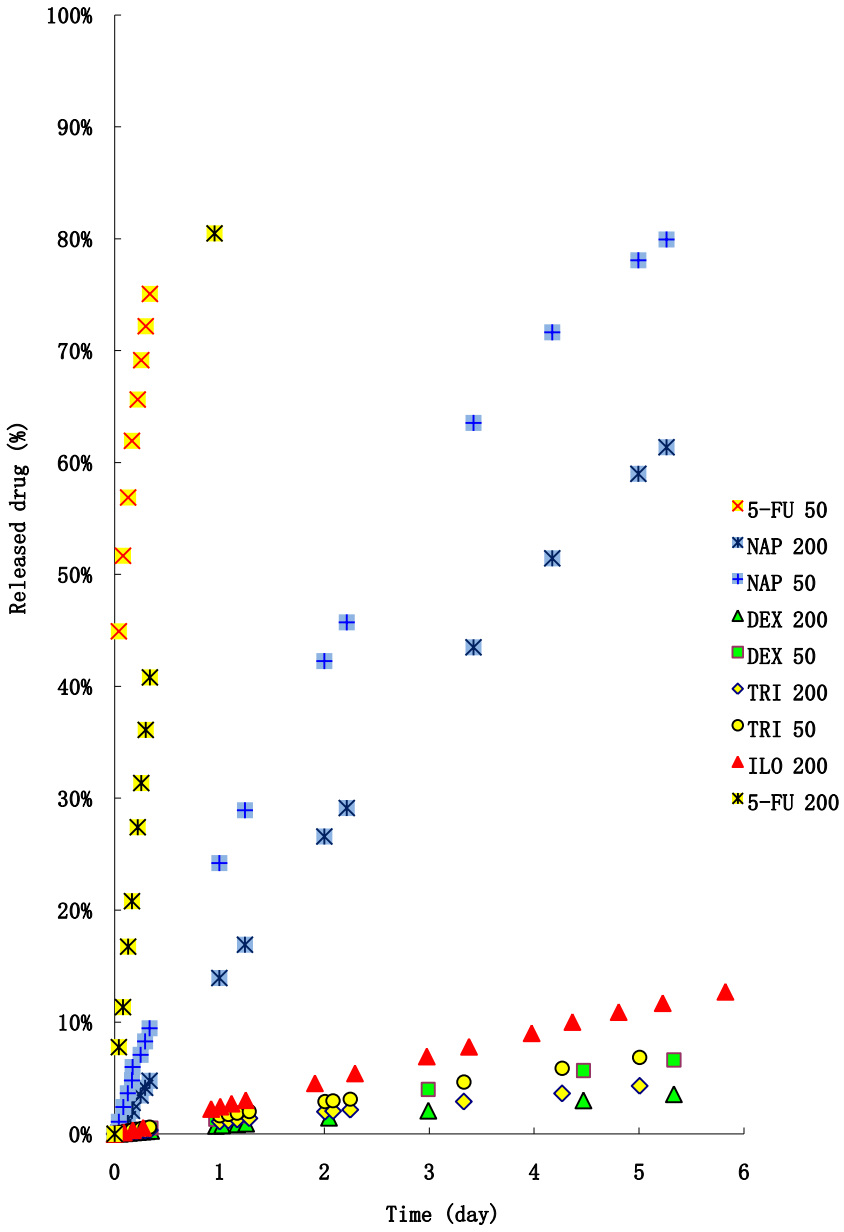


Figure 5.9. Comparison of the release fraction of all the excipient-free tablets in ambient temperature. The number 50 and 200 represent the chamber volume (µl). ILO equals to ilomastat. Data suggest that the shape of the curve looks similar to a curve of logarithm.

#### 5.3.2.1. Washington's dialysis model

When a tablet is placed in the bleb, the drug starts to dissolve in the aqueous humor. After a while the drug begins accumulate in the bleb; while simultaneously escaping slowly with the turnover of aqueous humor. Hence, during the dissolution process, the drug is distributed in three departments: the tablet, the bleb and the blood/lymphatic

circulation. As the volume of the blood in the whole body is much larger than the volume of the bleb, the whole body blood circulation is considered as a sink condition. Therefore, the tablet is placed in non-sink conditions (bleb), which is connected to a sink condition (blood circulation).

Before developing the mathematical model, a literature search was conducted on mathematical models that describe non-sink conditions. It appears that the mathematical determination of drug release profiles in non-sink conditions are less studied than those in sink conditions. The models for non-sink conditions with connection of sink conditions have not been well developed. A dialysis model (Figure 5.10.) for evaluating drug release from colloids described some concepts which are very similar to the bleb (Washington 1989). It provided us with a good starting point. Based on this model, compartment A and B can be assumed as the tablet and bleb respectively, and compartment C represents the whole body blood circulation. However, all Washington's calculations were based on the assumption that the drug accumulation in compartment B was almost zero; but in our case the released drug does accumulate in compartment B (which for us is the bleb). Therefore, we wish to explore some ways to extend its use for our ocular drug release.

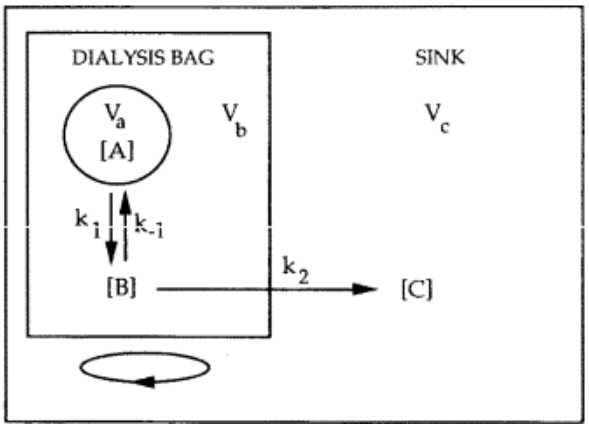


Figure 5.10. Kinetic scheme for non-sink dialysis from Washington (Washington 1989).

Ideally this model should be able to describe the tablet release *in vivo*, but currently our model is being developed based on the *in vitro* data only because the *in vivo* pharmacokinetics of the tablets have not been well established. It is hoped that, if the

correlation of the experimental data and mathematical model can be accomplished in the future, this mathematical model can be modified and used to predict the release of a tablet in the non-sink condition which is similar to the bleb. When observing the tablet release profiles, the drug distribution is similar to a typical two-step consecutive chemical reaction A→B→C (Coker & Kayode 2001)(illustrated in Figure 5.11.).

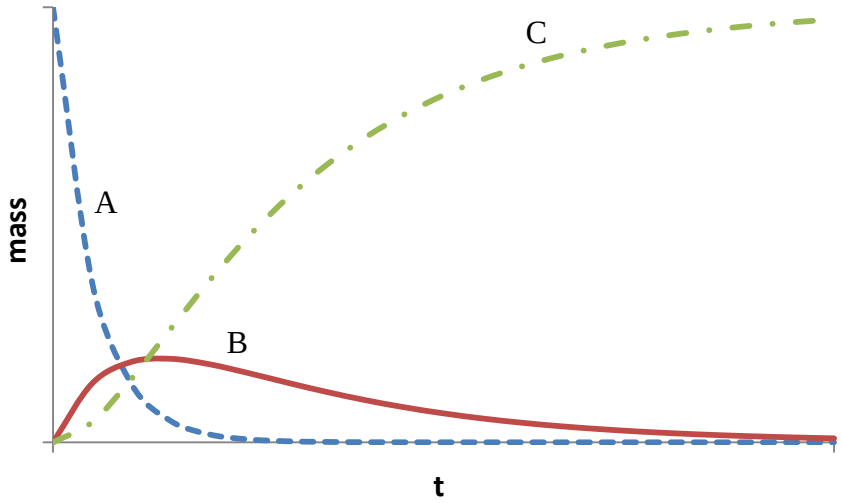


Figure 5.11. Illustration of the mass change of the reactant and product in a first order consecutive chemical reaction A→B→C.

Based on the dialysis model and the kinetics of a consecutive 2-step bidirectional first-order chemical reaction (Coker & Kayode 2001), we assume that compartment A and B represent the tablet and bleb respectively, and compartment C represents the whole body blood circulation (Figure 5.12). The tablet dissolution rate, the volume of the flow chamber, and the drug elimination rate from the bleb to the body are named as $k_1$, $V_b$, and $\lambda$ respectively. Since the saturation of the drug solution in the chamber has never been observed, it is assumed that the drug will not precipitate in the bleb. In addition, as the drug eliminated through the blood/lymphatic capillaries will be diluted immediately, after which it is assumed that the excreted drug will not come back to the bleb. Therefore, the backward reaction rate $k_{-1}$ and $\lambda_{-1}$ are assumed to be negligible (Figure 5.12).

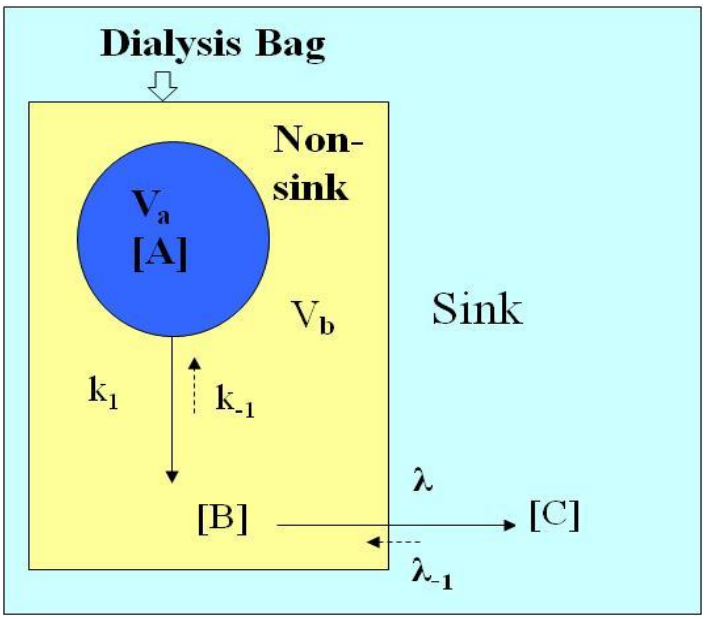


Figure 5.12 Illustration of improved dialysis model. Department (A) represents the tablet, the dialysis bag (B) represents the bleb, and the sink (C) represents the blood circulation of the body.

It is assumed that initially the amount of the drug in the tablet is $A_0$. When the drug is distributed in compartment A (tablet), B (bleb), and C (systemic circulation), the total amount of drug is then expressed by applying stoichiometric principle to the dissolution system (Equation 5.1):

$$A_0 = A_t + B_t + C_t \qquad 5.1$$

Where $A_t$, $B_t$, and $C_t$ are time dependent functions of the drug mass of A, B, and C respectively. As Equation 5.1 is based on the law of mass conservation, when t = 0 (before the tablet starts releasing drug), $B_0 = C_0 = 0$.

The drug concentration in the bleb is not uniform due to the existence of the aqueous flow. Therefore concentrations obtained from the exit of the flow chamber were close to but not equal to the real average concentration inside the flow chamber. It is very difficult to determine the real drug concentration in the chamber because at least 20-50 µl liquid need to be taken out from the flow chamber for the HPLC injections. Taking this amount of liquid from the chamber frequently can alter the concentration gradient and consequently accelerate the tablet release. Hence, we collected liquid from the out flow of the chamber. The concentrations that we determined should be lower than the average concentration in the flow chamber as the liquid collecting point was far from

the dissolution boundary layer. Hence, to simplify the conditions, we assume that drug concentration in the bleb compartment is uniform, which means there is no concentration gradient in the bleb. We also assume that the drug molecules released from the tablet will not be degraded, metabolized or bound by the tissue/proteins in the bleb. The increase of drug mass in the compartment C (systemic circulation) is then governed by

$$\frac{dC}{dt} = \lambda B \qquad 5.2$$

Where $\lambda = \frac{\text{Flow Rate}}{V_b}$. In other words, λ represents the refreshment rate of the liquid in the bleb (the flow chamber in the *in vitro* model).

Since the use of excipients can alter the tablet release mechanism, our current mathematical model is only based on the excipient-free tablets. As the tablet release profiles appear similar to a first order consecutive reaction, we used the simplest first order model to describe the dissolution of a tablet (Coker & Kayode 2001):

$$\frac{dA}{dt} = -k_1 A$$

For a standard first order consecutive reaction, the mass accumulation of the drug in department B and C at each time point *t* is calculated as follows (Helfferich 2004):

$$B_t = \frac{k_1[A]_0}{\lambda - k_1}\left(e^{-k_1 t} - e^{-\lambda t}\right) \qquad 5.3$$

$$C_t = [A]_0\left[1 + \frac{1}{\lambda - k_1}\left(k_1 e^{-\lambda t} - \lambda e^{-k_1 t}\right)\right] \qquad 5.4$$

$$\frac{C_t}{[A]_0} = 1 + \frac{1}{\lambda - k_1}\left(k_1 e^{-\lambda t} - \lambda e^{-k_1 t}\right) \qquad 5.5$$

Therefore, the drug accumulate release (%) that we obtained from the experiment can be calculated using Equation 5.5. According to Equation 5.5, the accumulate release of the drug is independent of the total amount of the drug. To investigate the real local drug concentration, we can firstly use Equation 5.3 to calculate the amount of drug released in the flow chamber ($B_t$). The local concentration of the drug is then equal to $B_t$ divided by the bleb volume ($V_b$). In this equation we need the values of $A_0$, $k_1$, and λ. $A_0$ and λ are known as the original mass of the drug and the refreshment rate of the aqueous flow repectively; but $k_1$ is unknown. By correlating our *in vitro* experimental data

(accumulate release) with the curve generated by computer using Equation 5.5 (Figure 5.13., Figure 5.14.), the value of $k_1$ can be determined (Table 5.4).

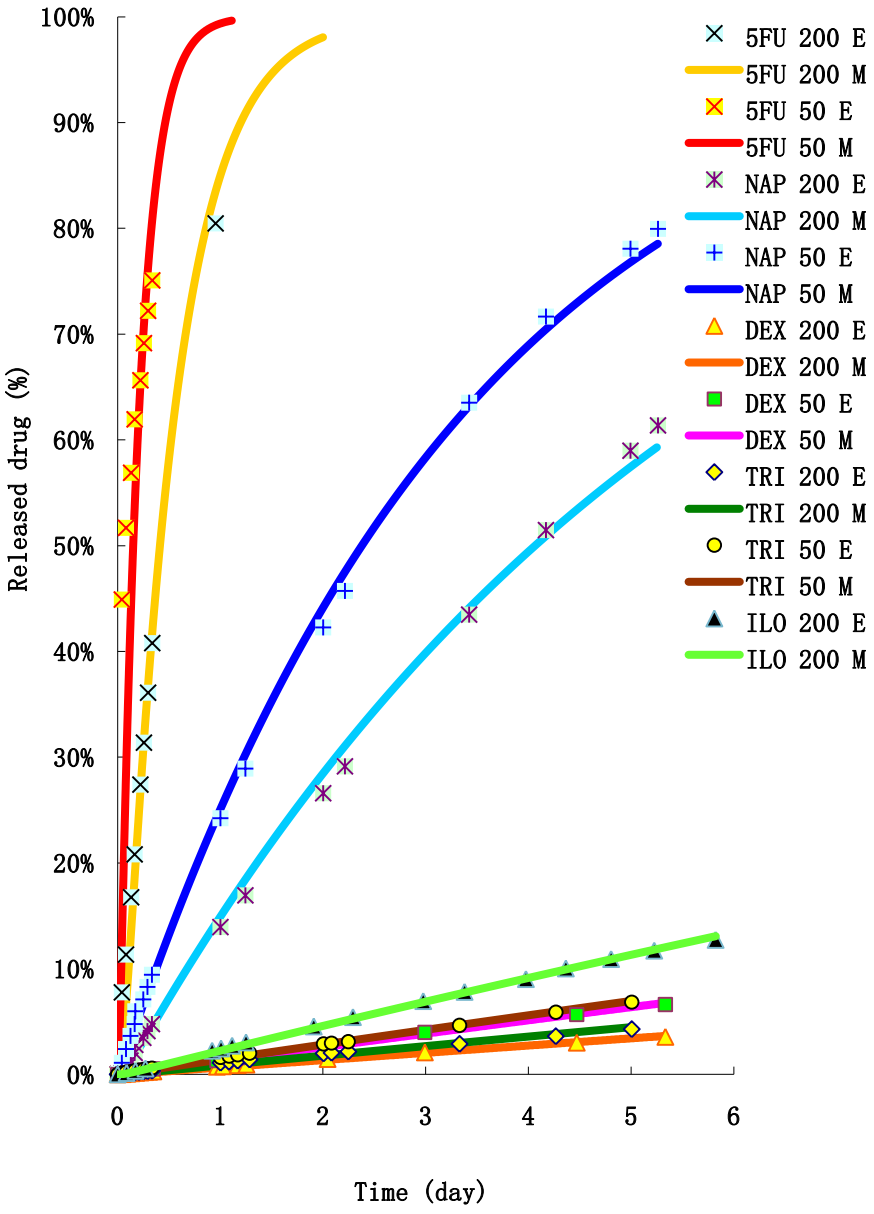


Figure 5.13. Correlation between the experimental data (scattered plots at ambient temperature) and the calculated data using Equation 5.5. ILO equals to ilomastat.

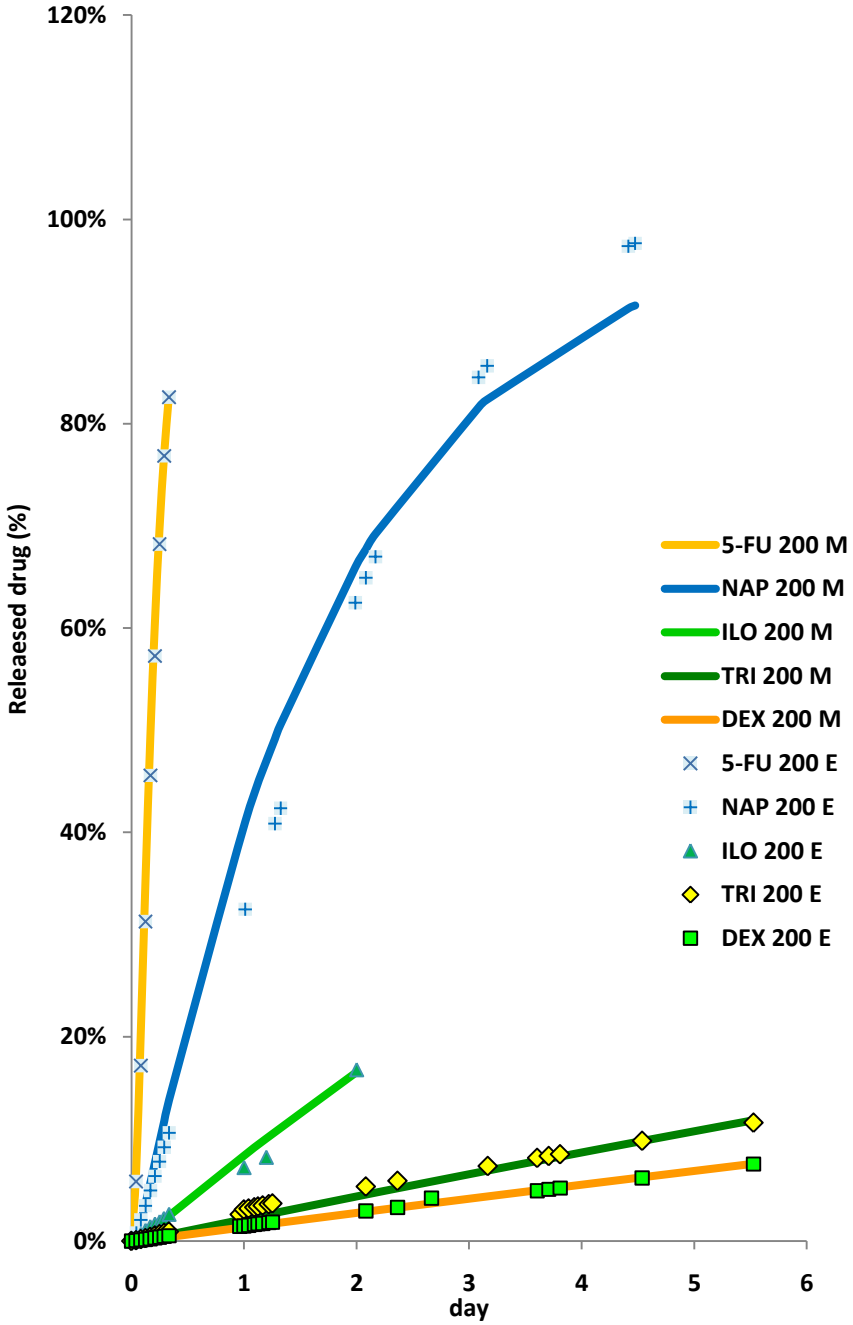


Figure 5.14. Correlation between the experimental data (scattered plots at 37 ℃) and the calculated data using Equation 5.4. ILO equals to ilomastat.

Table 5.4 The value of $k_1$ determined using the correlation between the experimental results and computational curve shown in Figure 5.13. and Figure 5.14.

| **Tablet** | **$k_1$ in 50 µl chamber (Ambient T)** | **$k_1$ in 200 µl chamber** | |
|---|---|---|---|
| | | **Ambient T** | **37 ℃** |
| 5-FU | 3.59E-3 | 1.42E-3 | 5.00E-03 |
| NAP | 2.03E-3 | 1.21E-4 | 3.50E-04 |
| Ilomastat | NA | 1.69E-5 | 6.50E-05 |
| TRI | 1.00E-5 | 6.46E-6 | 1.60E-05 |
| DEX | 9.16E-6 | 4.89E-6 | 1.00E-05 |

Using the values in Table 5.4, the amount of drug released in the flow chamber (compartment B) can be calculated using Equation 5.3 (shown in Figure 5.15.). It can be seen that the 5-FU tablets had very high peak concentrations (2 or 7 mg/mL) but decreased to zero rapidly within 1-2 days (Figure 5.15 A); while the hydrophobic drugs (ilomastat, TRI and DEX) were released much slower. From this curve we can see that the concentrations of DEX and TRI could be maintained above 0.05 mg/mL for nearly 100 days (Figure 5.15 B).

Using Equation 5.5 and the $k_1$ values shown in Table 5.4, we can calculate not only the drug concentration in the flow chamber but also the long term accumulate release of the drug. The calculated drug accumulation release at ambient temperature is shown in Figure 5.16. It suggests that the excipient-free NAP tablets will remain in the bleb for approximately 15 days; but tablets made from very hydrophobic compounds such as DEX or TRI will slowly release the drug for months even more than a year. It is unknown whether the prediction of DEX and TRI tablets is true because our *in vitro* experiments were only conducted for about a week. However, it was found that the prediction for the ilomastat tablet did not match very well with the experimental data. In our *in vitro* experiments, the ilomastat tablet disappeared in the flow chamber after about 45 days at ambient temperature; but the mathematical model suggests that the ilomastat tablet will stay in the 200 µl chamber for more than 3 months. This difference was also seen on the data at 37 ℃. This indicates that the mathematical model may have

some limitations. Therefore, this model needs to be further improved.

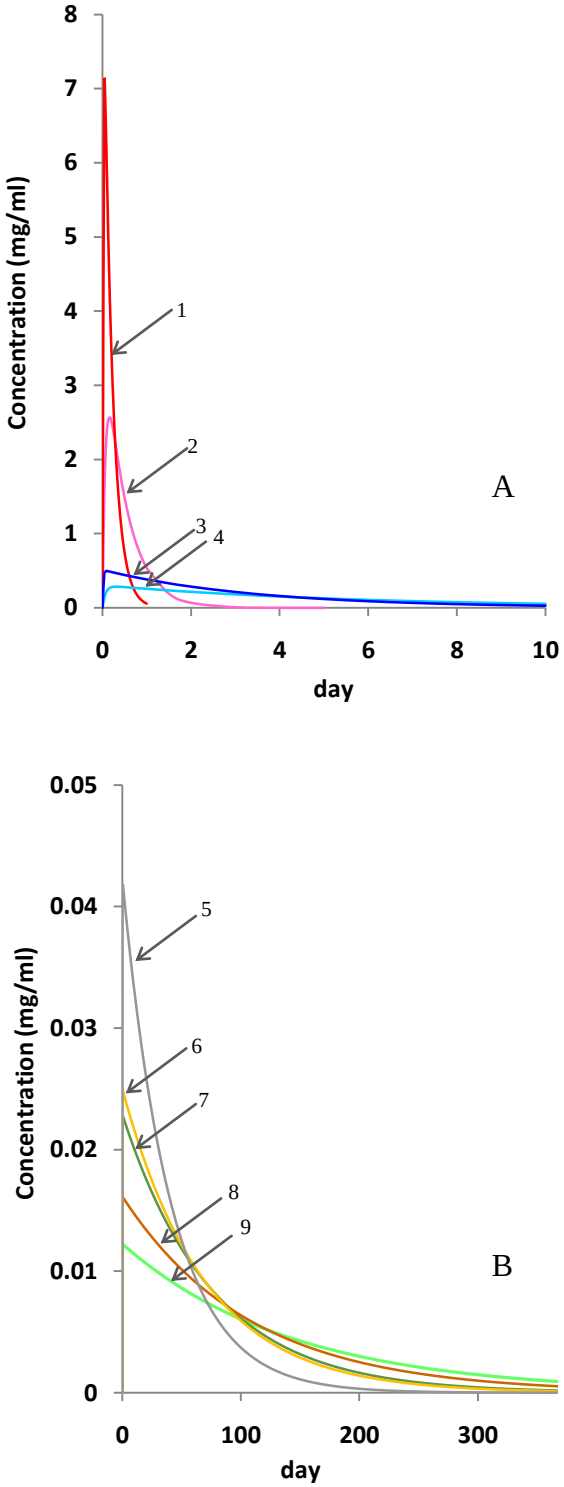


Figure 5.15. Calculated drug concentrations released for the excipient-free tablets (5 mg) in the flow chamber. 1. 5-FU in the 50 µl chamber; 2. 5-FU in 200 µl chamber; 3. NAP in the 50 µl chamber; 4. NAP in the 200 µl chamber; 5. ilomastat in the 200 µl chamber; 6. TRI in the 50 µl chamber; 7. DEX in the 50 µl chamber; 8. TRI in the 200 µl chamber; 9. DEX in the 200 µl chamber. The predicted results from the mathematical model suggest that the drug concentrations will be significantly different.

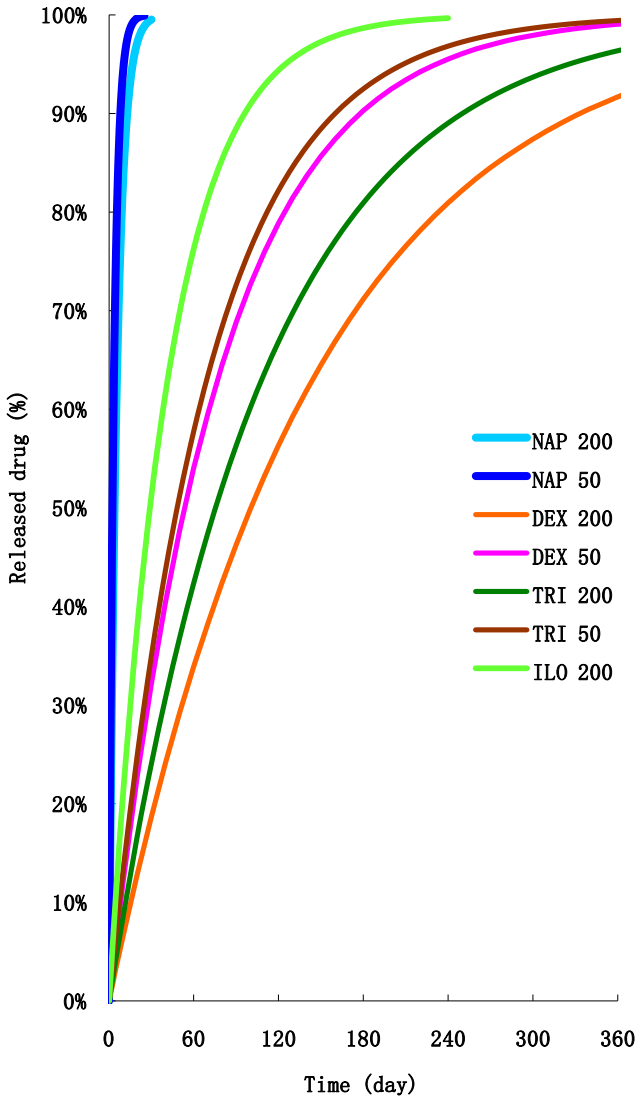


Figure 5.16. Calculated long term accumulation of drug release in the 50 and 200 µl chamber at ambient temperature using Equation 5.5. ILO equals to ilomastat. The predicted results from the mathematical model suggest that the drug release rate at ambient temperature will be significantly different.

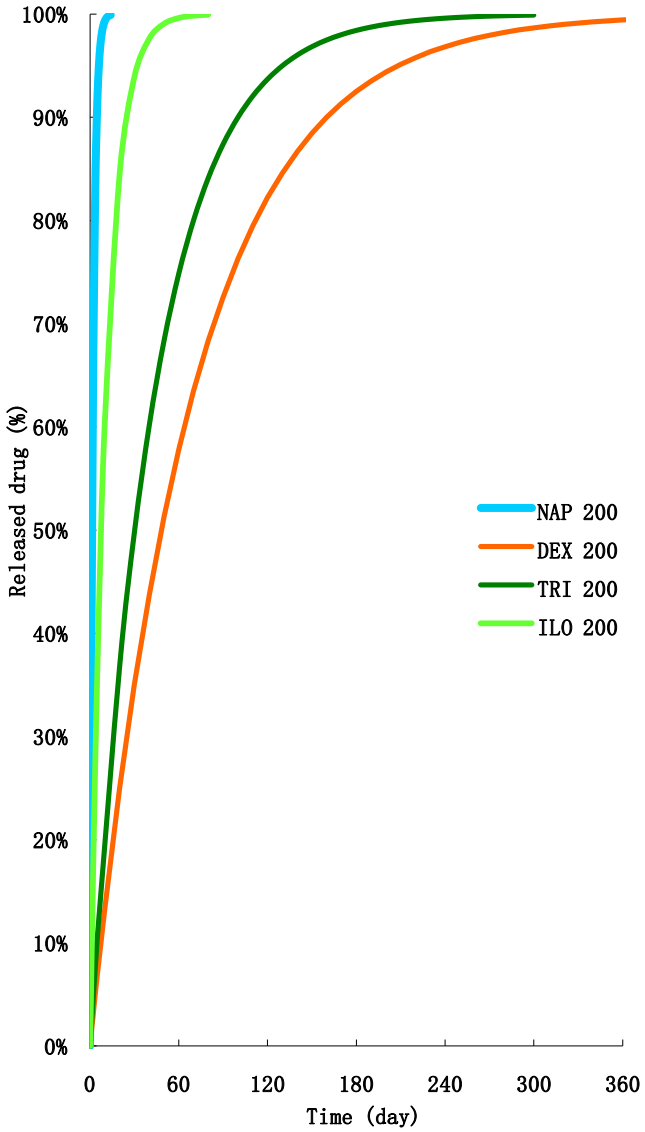


Figure 5.17. Predicted long term accumulation of drug release in the 200 μl chamber at 37 ℃ using Equation 5.5. ILO equals to ilomastat. The predicted results from the mathematical model suggest that the drug release rate at 37 ℃ will be significantly different.

From the above studies, we know that $k_1$ is the parameter that has the greatest effect on the tablet release profiles since the other two parameters ($A_0$ and $\lambda$) can be obtained directly. However, as discussed in 5.1.2, $k_1$ represent the tablet dissolution rate, which can be effected by more than one factor including temperature, tablet surface area, and the physical/chemical properties of the drug and the drug carriers. Thus, the mathematical model needs to be improved to include these factors. Therefore, a higher order mode was adapted with the collaboration with Prof. Guoxiong Wu and Mr. Qiang Sun. The higher model is expressed as follows:

$$(\frac{d}{dt}+k_1)(\frac{d}{dt}+k_2)\ldots(\frac{d}{dt}+k_n)A=0 \qquad 5.6$$

where $k_i > 0, \quad i = 1,2,\cdots,n$

If we take n=1, Equation 5.3 is then recovered. The general solution of Equation 5.6 can be written as

$$A = a_1e^{-k_1t} + a_2e^{-k_2t} + ... + a_ne^{-k_nt} \qquad 5.7$$

in which

$$a_1 + a_2 + ... + a_n = A_0 \qquad 5.8$$

because $A(0) = A_0$. From equation 5.1, we have

$$\frac{dA}{dt}+\frac{dB}{dt}+\frac{dC}{dt}=0 \qquad 5.9$$

Substituting Equation 5.2 into 5.9, we obtain

$$\frac{dB}{dt}+\lambda B=-\frac{dA}{dt} \qquad 5.10$$

The general solution of this equation can be written as

$$\begin{aligned} B &= e^{-\lambda t}\int_0^t\left(-\frac{dA}{d\tau}\right)e^{\lambda\tau}d\tau \\ &= -A + A_0e^{-\lambda t} + \lambda e^{-\lambda t}\int_0^t Ae^{\lambda\tau}d\tau \end{aligned} \qquad 5.11$$

This leads to

$$\begin{aligned} C &= \lambda\int_0^t Bdt \\ &= e^{-\lambda t}\int_0^t\frac{dA}{d\tau}e^{\lambda\tau}d\tau - \int_0^t\frac{dA}{d\tau}d\tau \\ &= e^{-\lambda t}\int_0^t\frac{dA}{d\tau}e^{\lambda\tau}d\tau - A + A_0 \end{aligned}$$

which can also be written as

$$C = -\lambda e^{-\lambda t}\int_0^t Ae^{\lambda\tau}d\tau + A_0(1-e^{-\lambda t}) \qquad 5.12$$

Substituting equation 5.7 into 5.12, we have

$$\begin{aligned} C = -\lambda[&\frac{a_1}{\lambda-k_1}(e^{-k_1t}-e^{-\lambda t})+\frac{a_2}{\lambda-k_2}(e^{-k_2t}-e^{-\lambda t})+\ldots+\frac{a_n}{\lambda-k_n}(e^{-\kappa_nt}-e^{-\lambda t})] \\ &+ A_0(1-e^{-\lambda t}) \end{aligned} \qquad 5.13$$

We replace $a_1$ in the above equation using equation 5.8. This leads to

$$C = -\lambda[\frac{A_0 - (a_2 + a_3 + \cdots + a_n)}{\lambda - k_1}(e^{-k_1 t} - e^{-\lambda t}) + \frac{a_2}{\lambda - k_2}(e^{-k_2 t} - e^{-\lambda t}) + \ldots + \frac{a_n}{\lambda - k_n}(e^{-\kappa_n t} - e^{-\lambda t})] + A_0(1 - e^{-\lambda t}) \quad 5.14$$

As mentioned above, λ in Equation 5.14 can be obtained directly from the experimental set up. It will be constant once the flow rate and $V_b$ are fixed. The other parameters $k_1$, $k_2$, …, $k_n$ are all the factors that affect the tablet release rate. At the moment our experimental data is not sufficient to define these factors corresponding to $k_1$, $k_2$, …, $k_n$ one by one. But we can investigate whether the adoption of a higher order model can improve the correlation between the experimental data and mathematical model.

As with the first order model, the coefficients $a_2$, $a_3$,…, $a_n$ and $k_1$, $k_2$,…, $k_n$ in Equation 5.14 were determined using the experimental data. To obtain these coefficients accurately, we would prefer the errors between the experimental data and the mathematical curve (generated by Equation 5.14 ) to be as small as possible. In other words, the experimental data and the computational curve from the mathematical model are expected to be as close as possible. This can usually be achieved through the least square method, which is applied to calculate the best fit between the modelled data and the observed data.

It is assumed that in the experiment the amount of drug collected in compartment C at time $t = t_j$ is E ($t_j$). We define an error function Er ($a_2$, $a_3$, …, $a_n$; $k_1$, $k_2$,… , $k_n$) as Equation 5.15.

$$Er(a_2, a_3, \cdots, a_n; k_1, k_2, \cdots, k_n) = \sum_{j=1}^{N}[C(t_j) - E(t_j)]^2 \quad 5.15$$

To ensure $Er(a_2, a_3 \cdots, a_n; k_1, k_2, \cdots, k_n)$ is minimum, we impose

$$\frac{\partial Er}{\partial a_i} = 2\sum_{j=1}^{N}\left\{[C(t_j) - E(t_j)][\frac{\lambda}{\lambda - k_1}(e^{-k_1 t_j} - e^{-\lambda t_j}) + \frac{-\lambda}{\lambda - k_i}(e^{-k_i t_j} - e^{-\lambda t_j})]\right\} = 0 \quad i \geq 2 \quad 5.16$$

$$\frac{\partial Er}{\partial k_i} = 2\sum_{j=1}^{N}\left\{[C(t_j) - E(t_j)][\frac{\lambda a_i}{\lambda - k_i}t_j e^{-k_i t_j} + \frac{-\lambda a_i}{(\lambda - k_i)^2}(e^{-k_i t_j} - e^{-\lambda t_j})]\right\} = 0 \quad i \geq 1 \quad 5.17$$

From a mathematical point of view, it is likely that the results will be considered more accurate when more factors are involved. In a preliminary study, we started evaluating the factors using the least square method with only one or two factors (n=1 or 2) included. Accordingly, we define that the errors (between experiment and mathematical model) as Er1 and Er2 respectively. The values of the coefficients ($a_1$, $a_2$, $k_1$, $k_2$) obtained with minimum errors using the best square method are shown inTable 5.8. It can be seen that when n=2, the value of $Er_2$ is equal or less than $Er_1$. The difference between $Er_1$ and $Er_2$ is shown in the last column ofTable 5.8. The higher the value is, the more significant the difference is. All these values are positive, which indicates that the accuracy can be improved when more than one coefficient is involved. This improvement has also been presented in an intuitional way (Figure 5.19 to Figure 5.23). In these figures it can be seen that, the predicted curve is able to stick more closely to the experimental data points when n=2 comparing to n=1.

Although the accuracy of the mathematical model was improved when using a higher order equation, it is unclear how these parameters can be correlated with the properties of the drug or the tablets. We could not figure out any regularity from the parameters shown inTable 5.8. Therefore, we aim to look for another way to improve the model.

We changed the unit of the drug solubility and then try to correlate them with the $k_1$ values obtained from Table 5.4. The values are listed again in Table 5.5. It was found that the solubility of the compounds appears linear to $k_1$ (Figure 5.18 and Figure 5.19.). This indicates that the solubility of the drug is probably proportional to $k_1$. Based on this assumption, we assume $k_1 = bs + c$, in which b, c, and s represent the slope, intercept (in Figure 5.18 and Figure 5.19.) and the drug solubility respectively. In this case, b changes along with λ; whilst c is a constant. Therefore, we developed the model using the drug solubility. Based on Equation 5.5, we write:

$$\frac{C_t}{[A]_0} = 1 + \frac{1}{\lambda - (bs + c)}\left((bs + c)e^{-\lambda t} - \lambda e^{-(bs+c)t}\right) \qquad 5.18$$

According to our assumption in Figure 5.18 and Figure 5.19., the value of b should be 0.012 and 0.0303 for the 200 and 50 µl chambers respectively. However, it is unknown

whether the model is accurate when using Equation 5.18 with these values. Therefore, we used the solver function in excel to find the best correlation between the experimental data and mathematical model.

Table 5.5 The relationship between the drug solubility and predicted $k_1$. Data suggest that the values of $k_1$ decreases with the decreasing of the drug solubility but increases with the decreasing of the chamber volume.

| Compound | | Solubility in the literature (mol/L) pH 7.4 | $K_1$ in 50 µl chamber | K1 in 200µl chamber |
|---|---|---|---|---|
| **5-FU** | | > 0.118395783 | 3.59E-03 | 1.42E-03 |
| **NAP** | **Ambient T** | 0.01272479 | 2.03E-03 | 1.21E-04 |
| | **37 ℃** | 0.026146829 | NA | 3.50E-04 |
| **Ilomastat** | **Ambient T** | NA | NA | 1.69E-05 |
| | **37 ℃** | 0.0005471* | | 6.50E-05 |
| **TRI** | | > 0.000202819 | 1.00E-05 | 6.46E-06 |
| **DEX** | | 0.000356723 | 9.16E-06 | 4.89E-06 |

* Determined by Dr. Hala Fadda

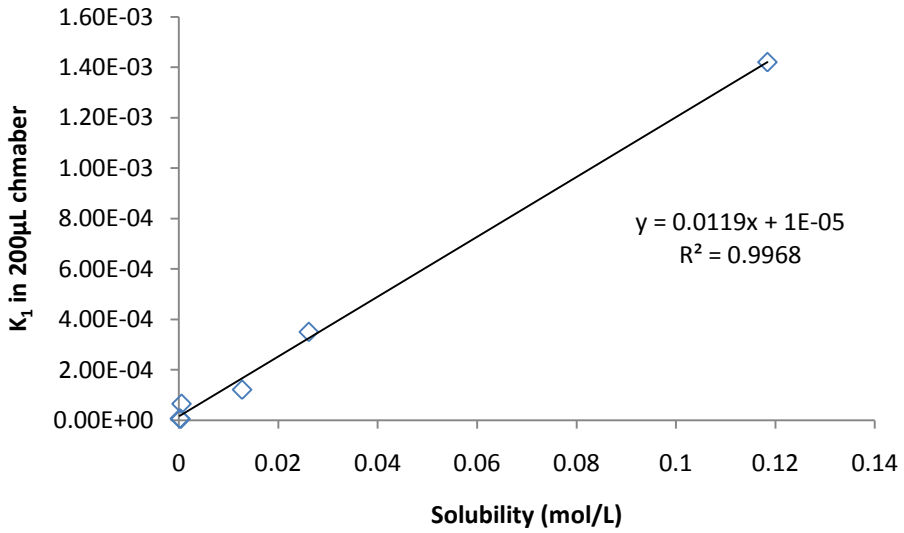


Figure 5.18. Correlation between the drug solubility (5-FU, NAP, ilomastat, DEX, TRI) and $k_1$ in the 200 µl chamber. Data suggest that the drug solubilities correlate well with $k_1$.

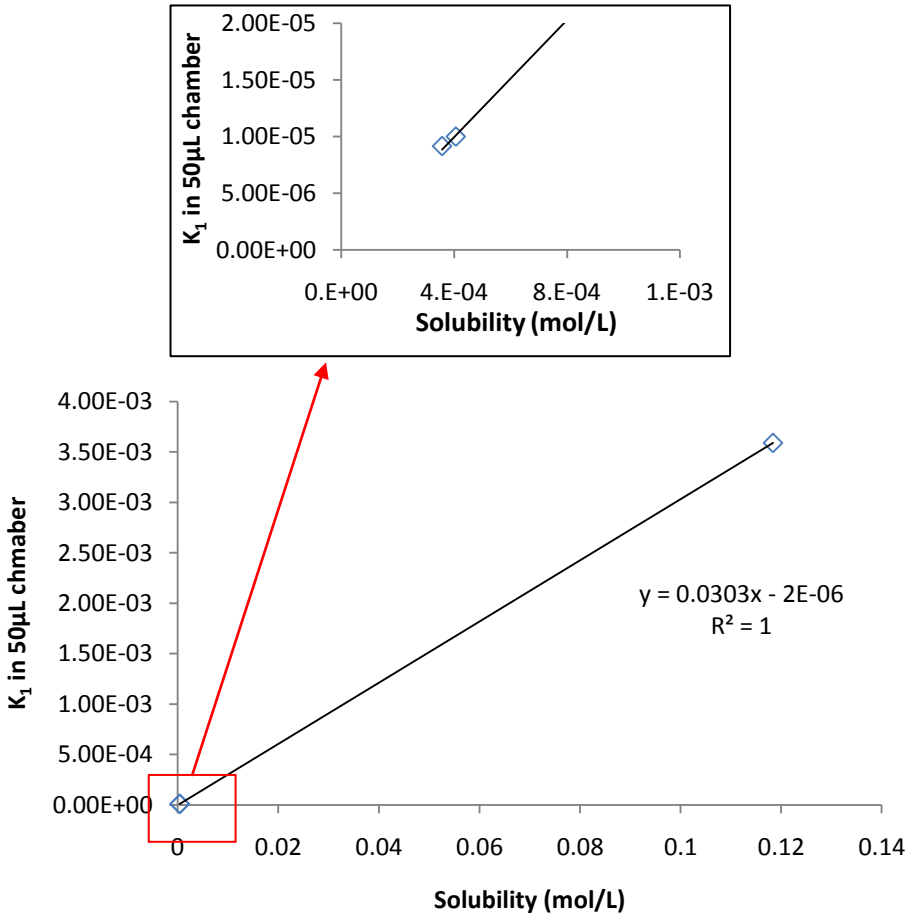


Figure 5.19. Correlation between the drug solubility (5-FU, DEX, and TRI) and $k_1$ in the 50 µl chamber. Note NAP was excluded to obtain a good correlation. Data suggest that the drug solubilities correlate well with $k_1$.

Solver is a mathematical software that solves a mathematical problem. In excel, it finds the values of certain cells in a spread sheet which optimize a certain objective. In our model, the solver function in excel will find the values of b and c that minimize the difference between the experimental data and calculated data. An example of calculation is demonstrated in Table 5.6. By running the solver, the best values of b and c were found to be 1.12 (200 µl chamber), 0.52 (50 µl chamber), and 0.0009 (Table 5.7). The correlation coefficient between the experimental data and predicted data was 0.9392 (Figure 5.20).

Table 5.6 A demonstration of calculating b and c using solver function.

**Solver calculates the values of b and c which make "total sum of difference" minimum.**

| Type of tablet | Experimental values | Calculated values using Equation 5.18 | Square difference between the experimental and calculated data | Total sum of difference | λ | Solubility of the drug (mol/L) | b (200 µl) | b (50 µl) | c |
|---|---|---|---|---|---|---|---|---|---|
| 5-FU 200 | $a_1$% | $a_1$'% | $b_1$% | m | 0.01 | 0.0118 | ? | ? | ? |
| | $a_2$% | $a_2$'% | $b_2$% | | 0.01 | 0.0118 | | | |
| | … | … | … | | 0.01 | 0.0118 | | | |
| 5-FU 50 | $c_1$% | $c_1$'% | $d_1$% | | 0.04 | 0.0118 | | | |
| | $c_2$% | $c_2$'% | $d_2$% | | 0.04 | 0.0118 | | | |
| | … | … | … | | 0.04 | 0.0118 | | | |

Table 5.7 The values of b and c calculated by excel using solver function.

| Chamber volume (µl) | Flow rate (µL/min) | λ | b | C |
|---|---|---|---|---|
| 200 | 2 | 0.01 | 1.12 | 0.000898502 |
| 50 | 2 | 0.04 | 0.52 | |

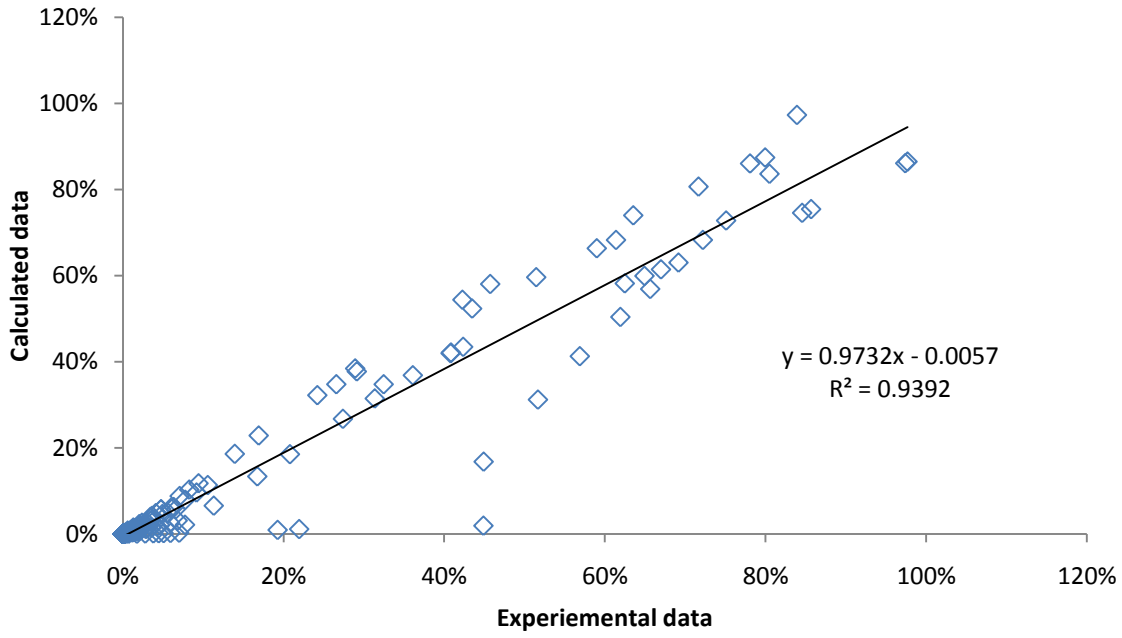


Figure 5.20. The correlation between the experimental and calculated data using Equation 5.18. Data suggest that the mathematical model correlates well with the experimental data.

The above findings suggest that the improved mathematical model is able to describe tablet dissolution in a non-sink condition with liquid turnover at a 94% confidence level. It is likely that the correlation coefficient ($R^2$) can be improved if more experimental data are available. Although it is felt that b is correlated with λ, the data we have at the moment is not sufficient to define the relationship between b and λ as we have conducted experiments with only two different values of λ (0.01 and 0.04). To further investigate the accuracy of the mathematical model and to find out the relationship between b and λ, more experimental data with different chamber volumes and different temperatures is needed.

As mentioned before, the mathematical model is also expected to be able to calculate the drug concentration. Since it has been confirmed from part of the ilomastat studies (Chapter III) that the drug concentration in the flow chamber is related to the surface area of the tablet, more experimental data with different tablet surface area are required to evaluate the accuracy of the mathematical model. However, most of our experimental data was based on tablets with nearly the same surface area (3 mm in diameter, approximately 0.5 mm thickness). Although the dissolution of the ilomastat tablets with different surface areas could provide us with some additional information, it is still not sufficient to develop a mathematical model because this data was generated from only one type of tablet. Therefore, more experimental data generated from different type of tablets with different surface areas is required in the future for the further development of the mathematical model.

Table 5.8 The predict values of $a_1$, $a_2$, $k_1$, and $k_2$ using the high order model. This suggests that the higher order mathematical model has a better correlation with our experimental data compared to the first order model.

| | n = 1 | | | n=2 | | | | | |
|---|---|---|---|---|---|---|---|---|---|
| **Tablets** | **$a_1$** | **$k_1$** | **$Err_1$** | **$a_1$** | **$a_2$** | **$k_1$** | **$k_2$** | **$Err_2$** | **$(Err_1-Err_2) / Err_1$** |
| 5-FU 50µl, ambient temperature | 1.00E+00 | 3.59E-03 | 1.06E-01 | 4.95E-01 | 5.05E-01 | 1.06E-03 | 2.31E-02 | 8.18E-03 | 92.30% |
| 5-FU 200 µl, ambient temperature | 1.00E+00 | 1.42E-03 | 8.34E-03 | 9.22E-01 | 7.82E-02 | 1.17E-03 | 6.22E-01 | 1.20E-03 | 85.60% |
| 5-FU 200 µl, 37 °C | 1.00E+00 | 4.64E-03 | 2.06E-03 | 1.66E+00 | -6.60E-01 | 6.16E-03 | 1.03E-02 | 1.07E-04 | 94.80% |
| NAP 50 µl, ambient temperature | 1.00E+00 | 2.04E-04 | 1.80E-03 | 9.97E-01 | 3.42E-03 | 2.03E-04 | 2.91E+00 | 1.73E-03 | 4.30% |
| NAP 200 µl, ambient temperature | 1.00E+00 | 1.21E-04 | 1.87E-03 | 3.18E+00 | -2.18E+00 | 1.81E-04 | 2.17E-04 | 4.84E-04 | 74.20% |
| NAP 200 µl, 37 °C | 1.00E+00 | 3.64E-04 | 2.95E-02 | 2.40E+00 | -1.40E+00 | 5.64E-04 | 8.32E-04 | 6.90E-03 | 76.60% |
| ILO 200 µl I, ambient temperature | 1.00E+00 | 1.40E-05 | 5.06E-03 | 9.80E-01 | 2.04E-02 | 1.32E-05 | 4.40E-04 | 2.03E-03 | 59.90% |
| ILO 200 µl II, ambient temperature | 1.00E+00 | 1.69E-05 | 3.53E-05 | 2.10E-02 | 9.79E-01 | 2.02E-04 | 1.45E-05 | 5.74E-06 | 83.80% |
| ILO 200 µl , 37 °C | 1.00E+00 | 1.87E-04 | 4.90E-03 | 7.78E+00 | -6.78E+00 | 3.78E-04 | 4.14E-04 | 3.28E-03 | 33.10% |
| TRI 50 µl, ambient temperature | 1.00E+00 | 1.00E-05 | 3.20E-05 | 8.83E-01 | 1.17E-01 | 4.98E-06 | 5.34E-05 | 2.00E-05 | 37.50% |
| TRI 200 µl, ambient temperature | 1.00E+00 | 6.46E-06 | 4.90E-05 | 9.94E-01 | 5.72E-03 | 5.18E-06 | 1.23E-03 | 3.61E-06 | 92.60% |
| TRI 200 µl, 37 °C | 1.00E+00 | 1.72E-05 | 8.25E-04 | 9.96E-01 | 4.28E-03 | 1.62E-05 | 1.63E-03 | 4.52E-04 | 45.30% |
| DEX 50 µl, ambient temperature | 1.00E+00 | 9.16E-06 | 1.21E-05 | 8.88E-01 | 1.12E-01 | 5.95E-06 | 3.71E-05 | 7.08E-06 | 41.50% |
| DEX 200 µl, ambient temperature | 1.00E+00 | 4.89E-06 | 7.84E-06 | 7.94E-01 | 2.06E-01 | 7.40E-11 | 2.52E-05 | 3.90E-06 | 50.20% |
| DEX 200 µl, 37 °C | 1.00E+00 | 1.01E-05 | 5.03E-05 | 2.27E-03 | 9.98E-01 | 2.95E-03 | 9.61E-06 | 2.26E-05 | 55.10% |

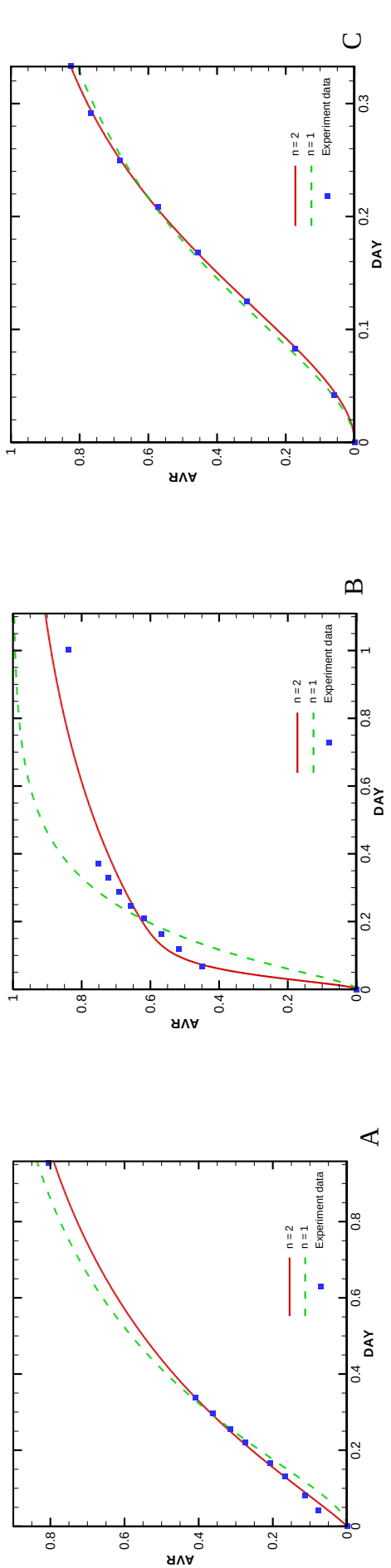


Figure 5.21. Comparison between mathematical model simulation results and experimental data of the excipient-free 5-FU tablets at ambient temperature. A tablets in the 200 µl chamber at ambient temperature; B tablets in the 50µl chamber at ambient temperature; C tablets in the 200 µl chamber at 37 ℃. This suggests that the higher order mathematical model has a better correlation with our experimental data compared to the first order model.

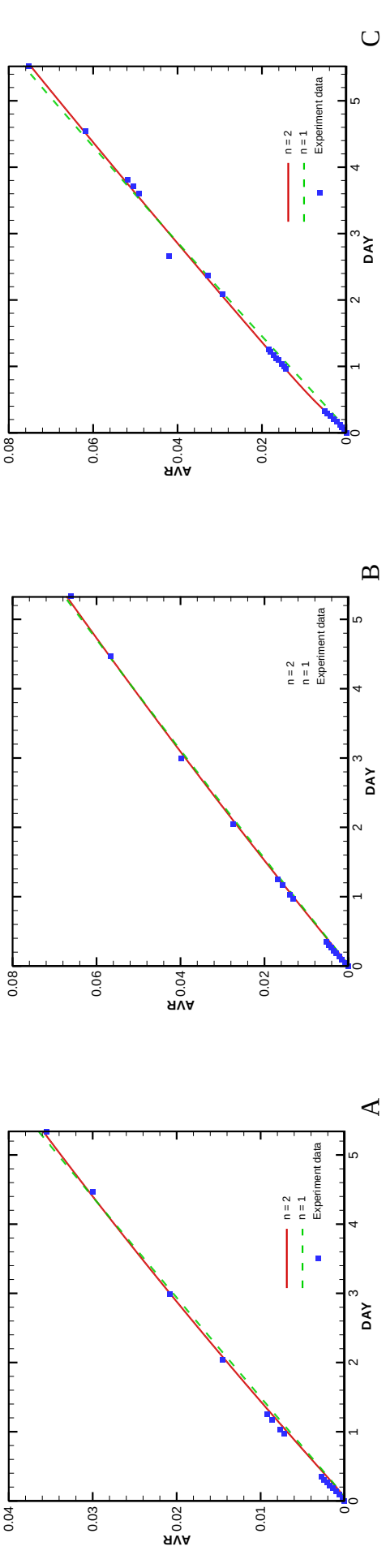


Figure 5.22. Comparison between mathematical model simulation results and experimental data of the excipient-free DEX tablets at ambient temperature. A tablets in the 200 µl chamber at ambient temperature; B tablets in the 50µl chamber. at ambient temperature; C tablets in the 200 µl chamber at 37 ℃. This suggests that the higher order mathematical model has a better correlation with our experimental data compared to the first order model.

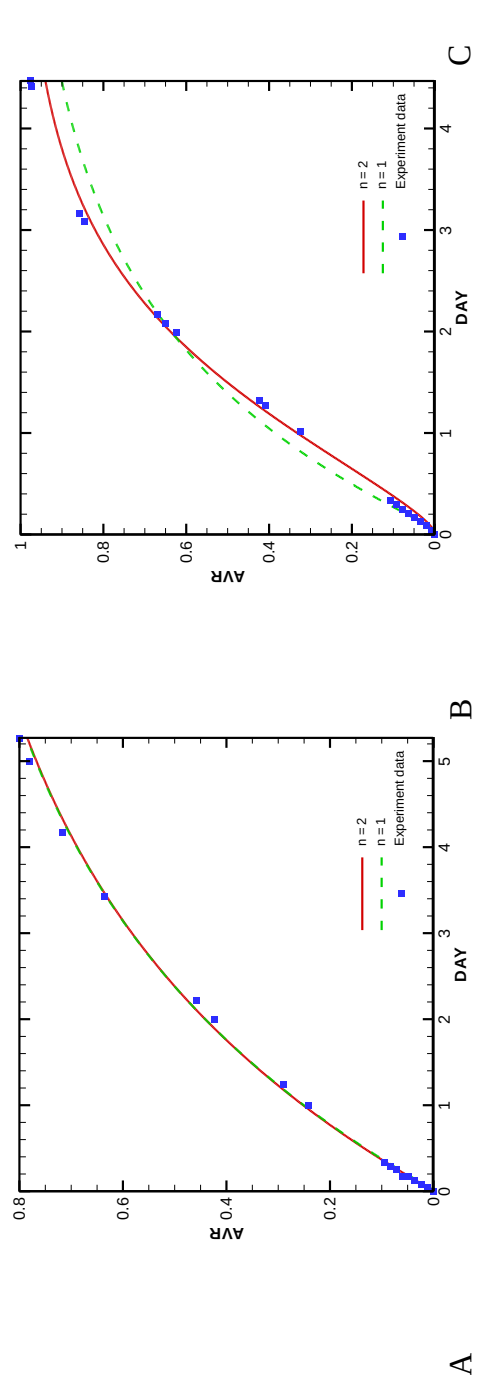


Figure 5.23. Comparison between mathematical model simulation results and experimental data of the excipient-free NAP tablets at ambient temperature. A tablets in the 200 µl chamber at ambient temperature; B tablets in the 50µl chamber at ambient temperature; C tablets in the 200 µl chamber at 37 ℃. This suggests that the higher order mathematical model has a better correlation with our experimental data compared to the first order model.

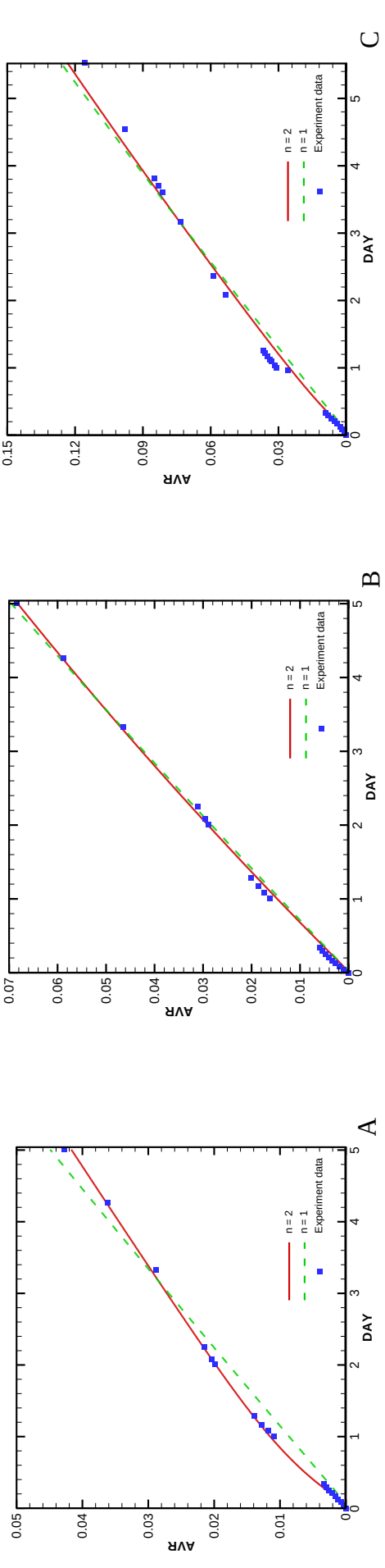


Figure 5.24. Comparison between mathematical model simulation results and experimental data of the excipient-free TRI tablets. A tablets in the 200 µl chamber at ambient temperature; B tablets in the 50µl chamber at ambient temperature; C tablets in the 200 µl chamber at 37 ℃. This suggests that the higher order mathematical model has a better correlation with our experimental data compared to the first order model.

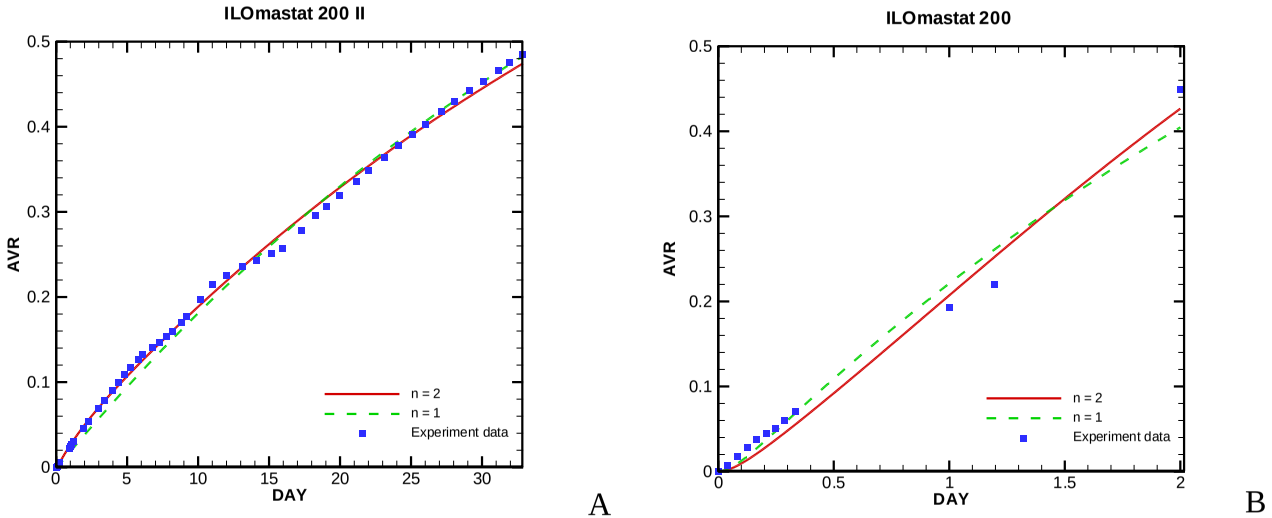


Figure 5.25. Comparison between mathematical model simulation results and experimental data of the excipient-free ilomastat tablets in the 200 µl chamber; A at ambient temperature; B at 37 ℃. This suggests that the higher order mathematical model has a better correlation with our experimental data compared to the first order model.

### 5.3.3. Preliminary characterizations of naproxen, dexamethasone, and triamcinolone tablets

We developed a mathematical model to describe the release profiles of the tablets. It should be noted that the mathematical model assumes that there is no change in the physical properties of the tablet. But the aqueous environment at body temperature may lead to changes in the physical properties and consequently cause a change in the tablet dissolution rate. Hence, as with the 5-FU and the ilomastat tablets, the physical properties of the NAP, DEX, and TRI tablets needs to be investigated. The incubated tablets were analyzed using differential scanning calorimetry (DSC).

#### 5.3.3.1. Naproxen tablets

DSC measurements were performed with NAP powder (before compression) and NAP tablets which have been in the flow chamber for 24 hours. The DSC thermogram is shown in Figure 5.26. The NAP powder showed a sharp peak with a flat baseline with the onset temperature of 157 ℃, which is slightly higher than the NAP melting point recorded in the Merck Index (152-154 ℃). This could be led by the high heating rate used in the DSC experiments. The single sharp peak shown in this figure might indicate that the NAP powder was in crystal form before compression. However, the initial temperature cycling and annealing at 120 ℃ could have lead to conversion of less stable polymorphs back into the most stable polymorph. Therefore, to confirm the polymorph of NAP powder, further analysis will be conducted when needed.

In comparison with the NAP powder, the NAP tablet has the same onset of melting temperature (157 ℃) but a hump was observed on the melting peak. Since NAP is an ionizable compound, originally it was thought that this hump could be caused by the salt of NAP. However, the melting temperature of NAP salts, such as sodium NAP, is higher than 250 ℃ (Kim & Rousseau 2004). Hence, the hump is not caused by NAP salts. This might indicate a polymorphic transition of NAP crystals during the tablet soaking in 37 ℃ PBS. But the crystal polymorphism of NAP is not well reported in literature as most studies focused on its sodium salt. To interpret whether this hump is caused by the

crystal polymorphism of NAP, further investigations are needed when necessary. The thermal analysis of the NAP tablets was not further investigated in detail because the aim of our research at the moment is focused on looking for the trend of dissolution in the non-sink condition mimicked by the flow chamber.

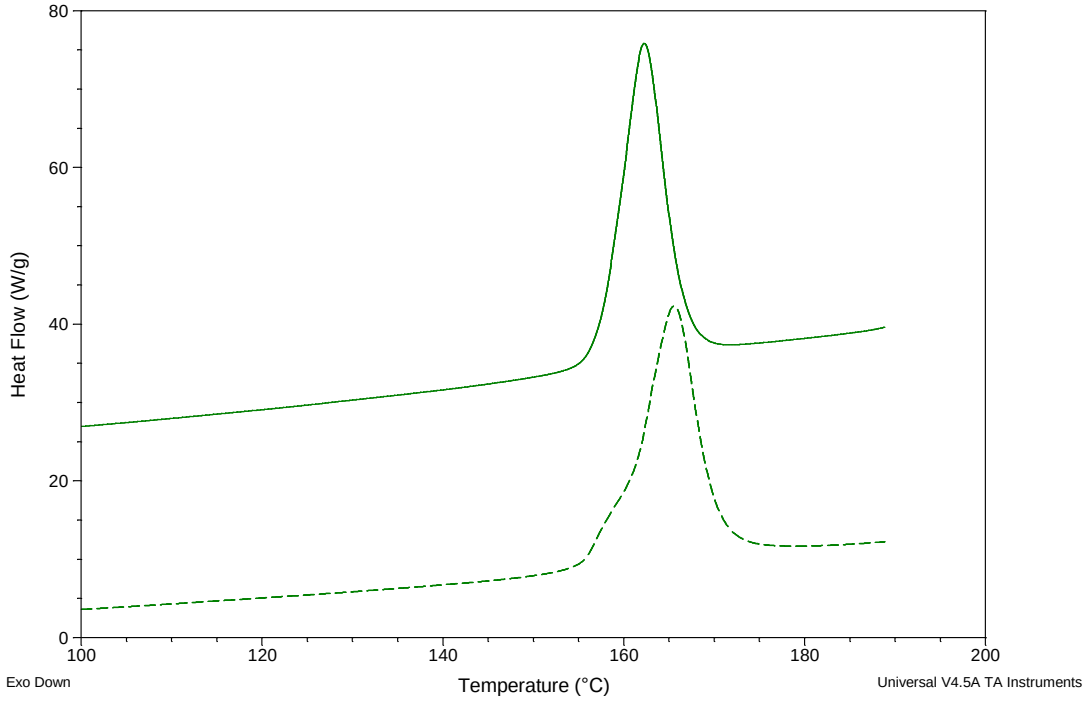


Figure 5.26 DSC curves of NAP (solid line) and the NAP excipient-free tablets after being incubated in 37 ℃ PBS (broken line) in a nitrogen atmosphere, flow rate 20 mL/min, heating rate 100℃/min, non-hermetic aluminium pans. This might indicate a polymorphic transition of NAP crystals during the tablet incubation.

### 5.3.3.2. Dexamethasone tablets

On the DSC thermograph of the DEX samples, the DEX powder has an earlier onset temperature (276 ℃) than the DEX tablet (283 ℃, Figure 5.27). These melting points are higher than the DEX melting point that recorded in the Merck Index (268-271 ℃) probably because of the high heating rate used in the experiments. It also can be seen that the melting peak of the tablet appears sharp with a flat base line, whilst a hump was observed on the melting peak of the DEX powder. In one of the recent DSC studies of pure DEX, a similar thermogram was observed (Rodrigues et al. 2009). However, the crystal polymorphism of DEX cannot be determined from the melting peaks shown in this figure as DEX melts with decomposition (British Pharmacopoeia). It is unknown yet whether there is any polymorphism of DEX since all the studies in the literature

were conducted on DEX salts (DEX sodium phosphate or DEX palmitate). In addition, the initial temperature cycling and annealing at 120 ℃ could have lead to conversion of less stable polymorphs back into the most stable polymorph. Therefore, our current DSC studies cannot yet predict any formation of DEX polymorphism. The thermal analysis of the DEX tablets was not further investigated in detail at the moment because the current aim of our research is focused on looking for the trend of dissolution in the non-sink condition mimicked by the flow chamber.

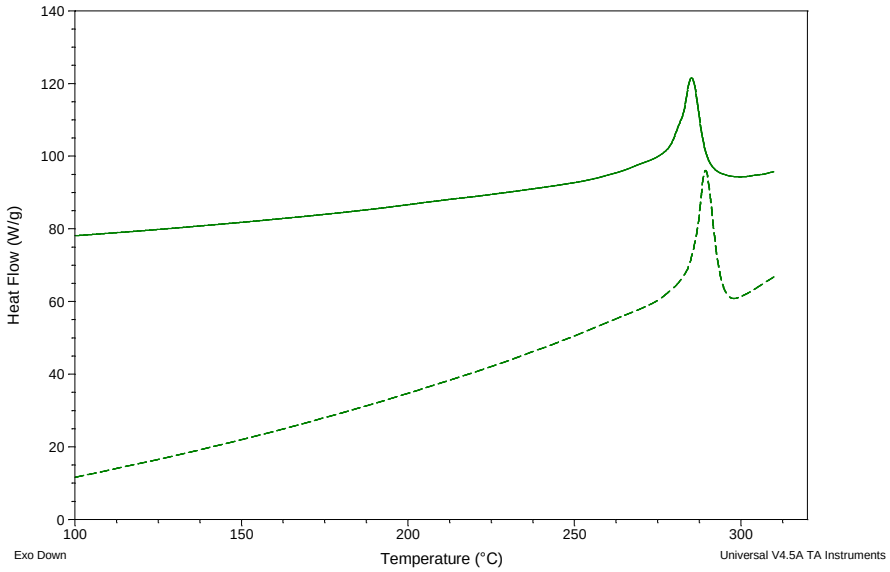


Figure 5.27 DSC curves of DEX (solid line) and the excipient-free DEX tablets after being incubated in 37 °C PBS (broken line) in a nitrogen atmosphere, flow rate 20 mL/min, heating rate 100℃/min. This indicates DEX melts with decomposition.

### 5.3.3.3. Triamcinolone tablets

The DSC thermograms of the TRI samples are shown in Figure 5.28 and Figure 5.29. It can be seen that at the heating rate of 100 ℃ $min^{-1}$, neither TRI powder nor the TRI tablets showed a sharp melting peak. Different heating rates were used, but the peaks could not be separated (data not shown). Hence, the TRI tablets were analyzed using high performance DSC with a heating rate of 500 ℃ $min^{-1}$. Figure 5.29 shows a single melting peak of TRI powder at 279 ℃, and two separate peaks of the TRI tablet at 262, 293 ℃ respectively. The onset temperatures of TRI shown in Figure 5.28 (at around 260 ℃) are consistent with the TRI melting point recorded in the Merck Index (269-271 or 260-262.5 ℃). But it also indicates the decomposition of TRI after 260 ℃, which has been reported in the literature (Dozorova et al. 1987).

The polymorphism of TRI cannot be interpreted from these experiments. But it has been studied before (Suitchmezian, Jess, & Nather 2007). Suitchmezian et al has found that triamcinolone can have two solvent free forms and a pseudopolymorphic form from monohydrate. In their studies, the monohydrate TRI demonstrated endothermic events at peak temperatures of 101, 248 and 266 ℃ when using a heating rate of 3 ℃ min-1. As the initial temperature cycling and annealing at 120 ℃ could have possibly led to the lost of water in the monohydrate or the transformation of any other unstable polymorphs, our DSC results cannot prove the existence of monohydrate. Again further interpretation of the polymorph in the tablets was not conducted because we aim to look for the dissolution trends of the tablets in non-sink conditions using the flow chamber.

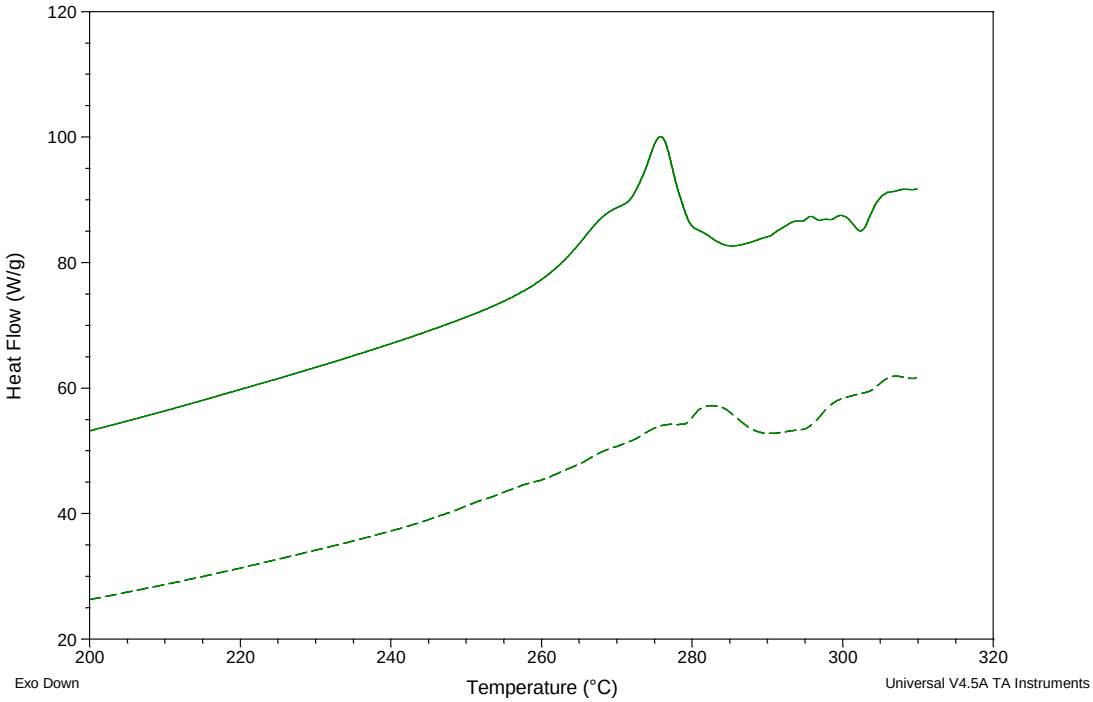


Figure 5.28. DSC curves of the TRI (solid line) and TRI excipient-free tablets after being incubated in 37 ℃ PBS (broken line) in a nitrogen atmosphere , flow rate 20 mL/min, heating rate 100℃/min. This indicates that TRI melts with degradation.

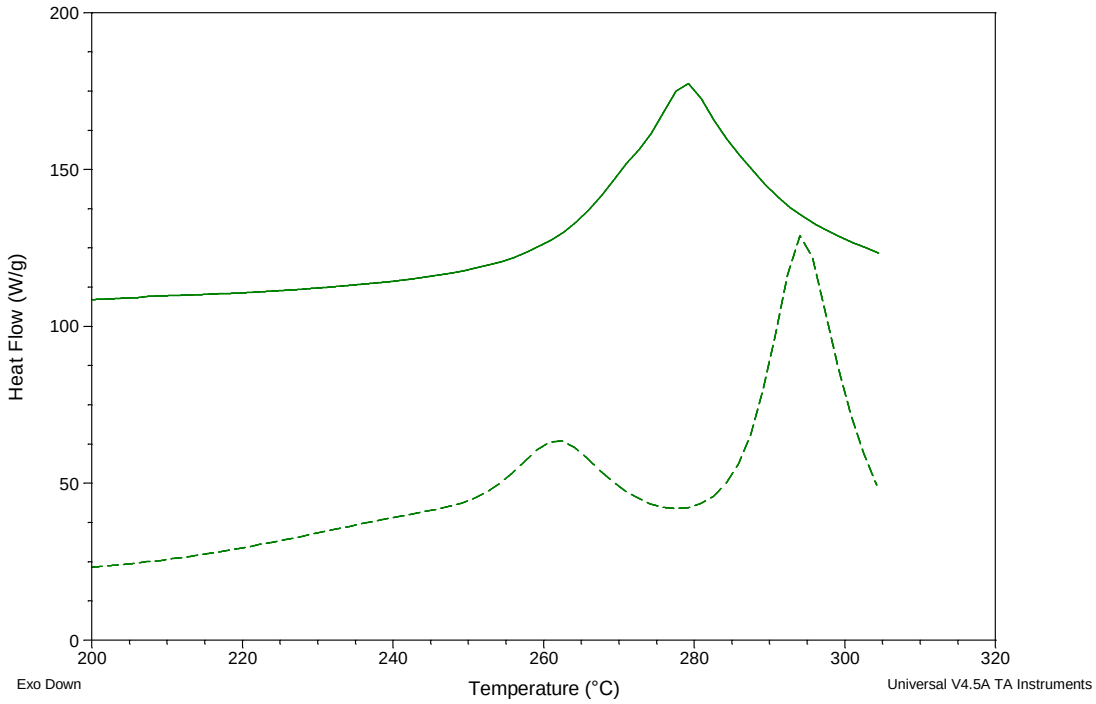


Figure 5.29 DSC curves of the TRI (solid line) and TRI excipient-free tablets (broken line) in a nitrogen atmosphere, flow rate 25 mL/min, heating rate 500℃/min. This indicates that TRI melts with degradation.

The investigation of the physical properties of the tablets was not done in depth since our current studies are mainly focused on investigating the general pattern of tablet dissolution. But our DSC studies cannot yet interpret any change of crystal forms of the drugs after the tablets are exposed to aqueous environment at different temperatures. It is understood that DSC analysis alone is not sufficient for investigating their physical properties. Further investigations using more techniques, such as X-ray crystallography, need to be conducted when necessary because 1) compounds from different suppliers can have different physical properties and 2) the change in physical properties could alter the tablet release profile. For tablets made from very hydrophobic compounds such as DEX or TRI, their physical properties need to be studied at more than one time point during the whole dissolution test.

## 5.4. Conclusions

Our dissolution studies using the flow chamber suggest that the dissolution of an excipient-free tablet is related to the solubility of the drug in the dissolution medium,

the flow rate of the aqueous media, and the volume/temperature of the flow chamber. When all these parameters are known, the tablet dissolution could be predicted using a mathematical model. The accuracy of the mathematical model needs to be improved in the future with more experimental data.

The mathematical model does not include the change of the physical properties of the tablet. Our preliminary characterizations of the tablets using DSC suggest the possible transformation of the different crystal forms during the tablet dissolution process. Further investigations are needed to confirm these findings. If the transformation of the crystal forms significantly affects the tablet dissolution profiles, it needs to be included in the development of the mathematical model.

# *Chapter VI Conclusions and future perspectives*

## 6.1. Fabricating the tablets and understanding drug release *in vitro*

We successfully fabricated some implantable ocular tissue tablets with a 3 mm diameter to modulate the wound healing process after GFS. These tablets were made from some anti-proliferative and anti-inflammatory compounds including 5-FU, ilomastat, naproxen, dexamethasone, and triamcinolone. To ensure the reproducibility of tablet fabrication process, we have successfully designed a punch and die set for tablet compression. However, fabrication of these tablets is associated with the compressibility of the drug and/or excipients. A 3 mm diameter tablet may not be the most appropriated size and shape for all the compounds. The size and shape of the tablet could be changed accordingly to adjust the need of drug delivery in the future. For example, an injectable mini rod might be preferred in dose top up post surgery. It can also be injected into the vitreous body for treatment of the diseases at the back of the eye. In addition to the shape and size, controlled release of the hydrophilic drugs might be achieved by coating the tablet in the future.

To understand the dissolution profiles of these tablets in the bleb, an *in vitro* model with a flow chamber which mimics non-sink condition in the bleb with small volume and constant aqueous flow has been developed. This model is more similar to the bleb and is able to predict the release of the drug more accurately compared to the ones reported in literature. Using the flow chambers, the 5-FU tablets were found to be dissolved completely within 10 hours; whilst the dissolution process of the other tablets was found to last for weeks or months. It was also found that 1) the solubility is not the sole measurement of the tablet dissolution in non-sink conditions and 2) the tablet release rate appears proportional to the solubility of the drug. Drug releasing from the excipient-free tablets were found dependent on many factors including the physical/chemical properties of the drug, surface area of the tablet, the volume of the bleb, the temperature, composition and flow rate of the aqueous medium. To obtain more precise and accurate results from the *in vitro* model, some issues need to be addressed in the future work: 1) a sponge or membrane need to be placed in the flow chamber to prevent small drug particles being flushed out of the chamber before they

dissolve, and 2) a better buffer system which is similar to aqueous humor need to be developed to replace PBS.

Since the tablets will be exposed to the aqueous humor at body temperature for a certain period, the release behavior of the tablets might also be altered due to the possibility of capsule formation and physical transformation of the drugs. Since degradations were observed at melting point, preliminary characterizations using DSC could not fully indicate the transformation of the drug crystal forms after the tablets being exposed to the aqueous environment. This needs to be confirmed in the future studies.

### 6.2. Potential *in vivo* application of the tissue tablets

The 5-FU tablets have shown the potential of long term inhibition of fibroblasts proliferation. Their long term inhibitory effect on collagen contraction is currently being examined by our group. The ilomastat tablets have shown remarkable efficacy of scar inhibition in a clinical validated rabbit model. The bleb survival curve was found to be significantly superior to the negative (sterile water) control group and the positive control group (MMC) with 100% bleb survival 30 days after the surgery. It was also found that ilomastat significantly reduced intraocular pressure compared to the negative and positive control groups. In addition, ilomastat in the aqueous humor and blood serum could not be detected using a HPLC method with a sensitivity of 5 μM. However, the accumulation of ilomastat in the ocular tissues is unclear. We therefore developed a simple method of ocular tissue digestion that does not interfere with ilomastat detection. Using this method, the ilomastat accumulated in the ocular tissue can be detected by HPLC with a sensitivity of 100 nM. In the future the sensitivity of the HPLC method can be further increased by HPLC-MS. It is hoped that the tissue accumulation of ilomastat in the eye will be evaluated accurately using HPLC.

In addition, thermal and surface analyses of the ilomastat tablets were conducted. Data suggest the possible existence of different ilomastat crystal forms, but this finding did not seem to affect the release of ilomastat in our *in vitro* model. The analysis results

from AFM and nanoLTA indicate that incubation of the tablets led to changes (stiffness, adhesion, and thermal conductivity) in the tablet surface. The surface analysis by XPS and Tof-SIMS suggests that, even in the presence of constant aqueous flow, deposition of salts and proteins on the tablet surface can be observed. These findings may contribute to the possible encapsulation of the ocular tissue tablets.

### 6.3. Mimicking tablet dissolution using molecular dynamics

Using the flow chamber is not the only way of examining the tablet dissolution in non-sink conditions. We have explored a new way to examine the behavior of excipient-free tissue tablets in non-sink conditions using molecular dynamics simulations. The fabrication and dissolution of 5-FU and ilomastat tablets were simulated using molecular dynamics simulation. Both 5-FU and ilomastat tablets were found to dissolve faster when the temperature was increased; the release rate of 5-FU was found to be much faster than that of ilomastat. These results agree with our experimental observations in the laboratory. From these studies we found that 1) solubility is not the sole measurement of the dissolution of excipient-free tablet in non-sink conditions 2) the dissolution rate is related to the chemical structural features of the drug, the temperature and the flow rate of the liquid turnover. In addition to the tablet dissolution process, tablet dissolution was also conducted when in contact with a simulated biological membrane at 310 K without the liquid turnover. The results suggested that, compared with 5-FU, ilomastat molecules are more likely to interact with the biological membrane. The dissolution rate of the tablet tends to be affected by the presence of the biological membrane.

In the future, the other factors that may affect the tablet dissolution rate, including the volume and composition of the dissolution media as well as the surface area of the tablets, are possibly simulated using molecular dynamics on the computer. The simulation results are hoped to correlate with more lab experiments and to give valuable indications for future studies.

## 6.4. Simulating and predicting tablet dissolution using a computational mathematical model

Our release profiles of the 5-FU, ilomastat, naproxen, dexamethasone, and triamcinolone tablets obtained from the flow chamber suggest that the dissolution of an excipient-free tablet is related to the solubility of the drug in the dissolution medium, the flow rate of the aqueous media, and the volume/temperature of the flow chamber. Based on these dissolution profiles, a computational mathematical model was developed to mimic the excipient-free tablet dissolution in non-sink conditions using the solubility of the drug in the dissolution media (with 94% confidence). The accuracy of the mathematical model needs to be improved in the future with more experimental data. It is hoped that the tablet dissolution *in vivo* can be predicted using a mathematical model in the future. To accomplish that, the *in vitro* and *in vivo* data need to be correlated. Much work on both *in vitro* and *in vivo* studies is therefore needed in the future.

The currently developed mathematical model assumes that there is no change of the physical properties in the tablets. But our preliminary physical characterizations of the tablets suggest the possible transformation of the different crystal forms during the tablet dissolution process. It is unknown whether the crystal transformations could alter drug release and tablet dissolution rate. This needs to be confirmed in further investigations. If the transformation of the crystal forms significantly affects the tablet dissolution profiles, the mathematical model needs to be further improved.

In summary, we have fabricated some implantable excipient-free tissue tablets for modulation of wound healing after trabeculectomy. The excipient-free ilomastat tablet has shown a remarkable effect on wound healing modulation on a clinically validated rabbit model. The dissolution of the excipient-free tablets can be simulated using molecular dynamics simulations and a computational mathematical model.

## Appendix I Prolonged release of anti-scriing agents after glaucoma filtration surgery

| Drug | Polymers | Dosage forms | Efficacy/prolonged time | model | Toxicity / complications | Reference | Times cited in Scopus |
|---|---|---|---|---|---|---|---|
| 5-FU and bleomycin sulfate | Highly purified bovine skin collagen cross linked with hexamethylene diisocyanate | Collagen implants (4× 4×1 mm) | 5-FU prolonged to at least 14 days, bleomycin up to 50 days | 8 rabbits | Acute inflammation in the first week | (Kay, Litin, & Jones 1986) | 15 |
| 5Fluorouridine 5'-monophosphate | Not available | Multivesicular liposomes (4 to 6 mg injected after surgery, and 3 mg injected 4$^{th}$ day postsurgery) | Avascular bleb up to 19 days | 3 monkeys | Large hyphema, prolonged hypotony, shallow anterior chamber, avascular bleb etc. | (Skuta et al. 1987) | 9 |
| 5-FU | Poly (ortho ester) | Disks 1.2 × 6.4 mm containing 5mg 5-FU | Sustained release of 5-FU for 10-60 days | *In vitro* only | NA | (Heller et al. 1987) | 30 |
| 5-FU | Liposomes consisting mainly of hydrogenated lipid phosphatides derived from egg. | Liposomes containing 5-FU injected (5 and 10 mg) | Detectable after at least 96 hours | 14 rabbits | unknown | (Simmons et al. 1988) | 10 |
| 5-fluorouridine (5-FUR) | Copolyanhydrides of l,3-bis(p-carboxyphenoxy) propane (PCPP) and sebacic acid (SA) | 3mm in diameter, 1 mm thickness, 10 mg | *In vitro* release for approximately 15 days, successful bleb for more than 36±14 days | 8 glaucomatous monkeys | No adverse effects on the retina or ciliary body but inflammation in the anterior chamber and of minor lens opacities. | (Jampel et al. 1990) | 21 |

| | | | | | | | |
|---|---|---|---|---|---|---|---|
| MMC | Coplolyanhydraide of bis(p-carboxyphenoxy) propane and sebacic acid | 3 mm in diameter and 1 mm thick containing 0.02 or 0.06 mg MMC | Released for more than 5 days *in vitro*, 70% blebs survived 20 days after surgery | 22 rabbits | Conjunctivitis and sectoral corneal haze but no significant ocular toxicity was noted | (Charles et al. 1991) | 30 |
| 5-FU | Polyvinyl alcohol (PVA; 98% hydrolyzed, 76,000-78,000 molecular weight) and Ethylene vinyl acetate (EVA) | 2.5mm diameter, 12 mg pellet | 1 mg/day for over 10 days | 14 rabbits | Moderate inflammation of the conjunctiva after implantation, which resolved after the first week No indication of impaired wound healing, coreal toxicity, inflammation, or damage to the ciliary body, | (Blandford et al. 1992) | 16 |
| Adriamycin | Poly (lactic acid), PLA | 0.2 mL subconjunctival injection of microspheres (containing 100 or 200 µg adriamycin) from the filtering site immediately after surgery | Intraocular pressure in the eyes treated with the microspheres that contained the drug was significantly lower than that in the control eyes from days 7-12 in the 100 µg group and from days 6-16 in the 200 µg group ($P < .05$) | 28 rabbits | Peripheral corneal opacities (25%) and epithelial erosion (17%) were observed in the eyes that received the 200 µg dose, but the cornea returned to normal after 4 weeks. | (Kimura et al. 1992) | 20 |

| | | | | | | | |
|---|---|---|---|---|---|---|---|
| 5-FU or bleomycin | Highly purified bovine skin collagen cross linked with hexamethylene diisocyanate | Purified absorbable collagen sponge (3×3 mm) containing 100μg of antimetabolite implanted | 78% eyes IOP lower than 21 mmHg and functional bleb after 5 years | 15 patients | No corneal toxicity | (Herschler & Sherwood 1992) | 10 |
| 5-FU | Poly (ortho ester) (POE) | Injectable semisolid (25 mg of 5-FU in 2.5g of POE) | 1-7 days | *In vitro* | NA (*in vitro* only) | (Merkli et al. 1994) | 32 |
| 5-FU | Poly (ortho ester) (POE) | Injectable semisolid (200 μl) | Unknown (mainly focused on biocompatibility) | >8 rabbit | High degree of hyperemia 3 days after injection; inflammation resolved after 10 days | (Bernatchez et al. 1994) | 17 |
| Etoposide (VP-16) | Polyanhydride1,3-bis(p-carboxyphenoxy) propane and sebacicacid(PCPP:SA) (25:75, W/W) | Disk (3 mm in diameter, 1 mm thick, 8 mg weight) | 30 ug/day, for more than 12days | 35 rabbits | Unloaded polymeric devices are non-toxic, disk was surrounded by a moderate infiltrate of acute and chronic inflammatory cells | (Uppal et al. 1994) | 10 |
| 5-FU | Poly (DL glycolic acid-lactic acid) (PGLA) polymer | Discs 0.3 mm thick and 4 mm in diameter contained 20% 5-FU by mass | 75% of 5-FU released in the first week, 80% of blebs survived 40 days post surgery | 22 rabbits | NA | (Trope et al. 1994) | 9 |

| | | | | | | | |
|---|---|---|---|---|---|---|---|
| 5-FU | Poly (DL glycolic acid-lactic acid) copolymer (PGLA) | Disks (3.6 mm wide, 0.6 mm thickness) containing 20% 5-FU | NA | 13 rabbits and 2 guinea pigs | Encapsulation was observed in both control and 5-FU groups, but 5-FU group demonstrated less inflammation. | (Gould et al. 1994) | 8 |
| MMC | Poly(hydroxyethyl methacrylate) (pHEMA) | Matrix disks (drainage device), diameter less than 1 cm | 6-90 ug/day, Over 2 months | 8 dogs | No corneal decompensation, conjunctival erosion, or significant uveitis were observed, but thick capsule and inflammation surrounding the devices in the control group were observed. | (Kiremitci-Gumusderelioglu, Gokce, & Akata 1996) | 5 |
| 5-FU | Copolymer of 2-hydroxyethyl methacrylate (HEMA) with different amounts of ethylene glycol dimethacrylate (EGDMA). | Matrix diameter 10 mm and thickness1 mm | Up to 120 h | *In vitro* | Unloaded polymeric devices was nontoxic | (Gokce, Akata RF FAU - Kiremitci-Gumusderelioglu, & Kiremitci-Gumusderelioglu) | 9 |
| 5-FU | Not available | Biodegradable implant (0.79 mm diameter, 6 mm long, 2.2 mg weight) contains 0.66 mg of 5-FU, loaded in a needle | 1.20 µg/hr for over 18 days and totally biodegraded in less than 86 days | Rabbit | No infection, inflammatory reaction or extrusion occurred. | (Hostyn et al. 1996) | 10 |

| | | | | | | | |
|---|---|---|---|---|---|---|---|
| 5-FU | Poly(D,L-lactide-co-glycolide) polymers | 2.5 mm in diameter× 1.2 mm thickness containing 5 mg 5-FU or at ratios of 9:1, 8:2, 7:3 to polymer | Prolonged release for over 200 hours | More than 6 rabbits | NA | (Wang et al. 1996) | 24 |
| Daunorubicin | Copolyanhydride P(CPP-SA) | 3.0 mm in diameter, 1.0 mm in thickness, and 8.0 mg in weight | Bleb failure in 91% of control eyes versus 22% of the treated eyes by day 13 | 23 rabbits | Conjunctival erosions occurred in four daunorubicin treated eyes | (Rabowsky et al. 1996) | 18 |
| 5-FU | Polyvinyl alcohol and ethylene vinyl acetate | Non-erodible depot | Compressed pellet of 12 mg of 5-FU coated with ethylene vinyl acetate and polyvinyl alcohol, release 20 μg per hour for about 24 days | 4 patients | Complications commonly seen in standard filtration surgeries were observed | (Smith & Ashton 1996) | 5 |
| Mitoxantrone (MTO) | Egg phospholipids, cholesterol polymers, methacrylic acid, methyl methacrylate, 2-hydroxypropyl methacrylate, and ethylene glycol dimethacrylate used for nanospheres | Solutions, nanospheres, liposomes (containing 200 μl of 0.2 mg/mL mitoxantrone) injected subconjunctivally | As with MMC, the MTO solution and liposome group showed an improved surgery outcome, the nanosphere group did not. | 66 rabbits | Corneal edemas were observed in solution, MMC, and one of the liposomal groups. Histology of one liposome group and the solution group showed no atrophy of the iris or ciliabodies. | (Tilleul et al. 1997) | 6 |

| | | | | | | | |
|---|---|---|---|---|---|---|---|
| 5-FU and dexamethasone sodium phosphate | Poly(ortho ester) (POE) | POE was injected subconjunctivally (200 µl) | *In vitro* release for 2 to 4 days | Rabbits (numbers unknown) | POE alone triggered a hyperemia and a chemosis during the forst 3 days but the eye fully recovered by day 7 with no signs of chronic inflammation | (Zignani et al. 2000a) | 22 |
| 5-FU | Poly(dl-lactide-co-glycolide) (PLG) | Microparticles (particle size 3 µm) 10 mg | *In vitro* delivery rate of 0.4 mg 5-FU/mg particles/ day | Rabbits (numbers unknown) | No ocular toxicity and no significant inflammatory response in rabbits for 2 months | (Yeh et al. 2001) | 14 |
| 5-FU | 2% acidic-collagen made from lyophilized ground corium collagen | Collagen plugs containing 1.125 mg of 5-FU placed in the silicone tubes | Improved IOP-lowering function reduced bleb wall thickness for 6 months | 16 rabbits | No cytotoxic complications | (Jacob, Lacour, & Burgoyne 2001) | 6 |
| 5-FU | Poly(dl-lactide-co-glycolide) combining lecithin as an emulsifier | 10 mg of 5-FU microspheres (containing 1 mg of 5-FU) | More than 1 week. | 20 rabbit | No significant eye irritation or toxicity was noticed | (Chiang et al. 2001) | 13 |
| Antisense TGF-β2 phosphorothioate oligonucleotides (PS-ODN) | Polyethylenimine (PEI) | Injectable microsphere suspended in Healon® (100 µL) | More than 30 days | 4 rabbits | No significant conjunctival hyperaemia was noted; also no signs of inflammation were observed | (Gomes dos Santos et al. 2006) | 21 |

| | | | | | | | |
|---|---|---|---|---|---|---|---|
| 5-FU; 5-chlorouracil (5-CU) | Poly(ortho esters) (POE) | Injectable semisolid (200 µl) | Approximately 4 weeks | 24 rabbits | 5-FU induced cell necrosis was observed *in vitro* | (Polak et al. 2008) | 2 |
| 5-FU | Poly (lactic acid) (PLA, Mw 20,000) | Disk (3 mm in diameter and 1 mm thick), each disk contained 3 mg of 5-FU | Bleb survived more than 30 days | 40 rabbits | No evidence of a toxic or inflammatory reaction was found | (Cui et al. 2008) | 2 |
| 5-FU | Poly(DL-lactide-co-glycolide); PDLGA | 0.8 mm diameter, thicknesses 0.33 mm and weight 3.5 mg | 80% of 5-FU was released during the first week *in vitro* | Rabbit (numbers unknown) | The implant induced a mild-to-moderate tissue reaction in the conjunctiva near the implantation site; | (Huhtala et al. 2009) | 0 |
| Dexamethasone | Surodex PLGA | Rod (1.0 mm in length and 0.5 mm in diameter) or pellet containing 60 µg of dexamethasone placed intrasclerally | Releases drug over 7-10 days; Average IOP maintained at 15 mmHg for 20 months post surgery | 37 patients | Transient hyphaema, hypotony, transient shallow anterior chamber | (Chang et al. 1999;Kimura & Ogura 2001;Seah et al. 2005;Tan et al. 1999) | 24, 34, 6, 43 |

# Bibliography

Adcock, S. A. & McCammon, J. A. 2006, "Molecular dynamics: Survey of methods for simulating the activity of proteins", *Chemical Reviews*, vol. 106, no. 5, pp. 1589-1615.

Agarwal, A., Tripathi, P. K., Tripathi, S., & Jain, N. K. 2008, "Fluorescence imaging: applications in drug delivery research", *Current drug targets*, vol. 9, no. 10, pp. 895-898.

Albert, D. M. & Jakobiec, F. A. 2000, "New surgical techniques in glaucoma management", *Principles and Practice of Ophthalmology.2nd Ed.* pp. 3024-3030.

Amar, N., Labbe, A., Hamard, P., Dupas, B. n. d., & Baudouin, C. 2008, "Filtering Blebs and Aqueous Pathway: An Immunocytological and In Vivo Confocal Microscopy Study", *Ophthalmology*, vol. 115, no. 7, pp. 1154-1161.

Amaral, M. H., Lobo, J. M., & Ferreira, D. C. 2001, "Effect of hydroxypropyl methylcellulose and hydrogenated castor oil on naproxen release from sustained-release tablets", *AAPS PharmSciTech [electronic resource]*, vol. 2, no. 2.

Anderson, J. M., Rodriguez, A., & Chang, D. T. 2008, "Foreign body reaction to biomaterials", *Seminars in Immunology*, vol. 20, no. 2, pp. 86-100.

Araujo, S. V., Spaeth, G. L., Roth, S. M., & Starita, R. J. 1995, "A ten-year follow-up on a prospective, randomized trial of postoperative corticosteroids after trabeculectomy", *Ophthalmology*, vol. 102, no. 12, pp. 1753-1759.

Atreides, S. P. A., Skuta, G. L., & Reynolds, A. C. 2004, "Wound Healing Modulation in Glaucoma Filtering Surgery", *International Ophthalmology Clinics*, vol. 44, no. 2, pp. 61-106.

Aulton, M. E. 1998, *Aulton's pharmaceutics : the design and manufacture of medicines*, International student ed edn, Edinburgh : Churchill Livingstone.

Azuara-Blanco, A. & Katz, L. J. 1998, "Dysfunctional Filtering Blebs", *Survey of Ophthalmology*, vol. 43, no. 2, pp. 93-126.

Barkana, Y. & Belkin, M. 2007, "Selective Laser Trabeculoplasty", *Survey of Ophthalmology*, vol. 52, no. 6, pp. 634-654.

Benigni, A., Morigi, M., & Remuzzi, G. 2010, "Kidney regeneration", *Lancet*, vol. 375, no. 9722, pp. 1310-1317.

Bernatchez, S. F., Merkli, A., Tri, L. M., Tabatabay, C., Anderson, J. M., & Gurny, R. 1994, "Biocompatibility of a new semisolid bioerodible poly(ortho ester) intended for the ocular delivery of 5-fluorouracil", *Journal of Biomedical Materials Research*, vol.

28, no. 9, pp. 1037-1046.

Blandford, D. L., Smith, T. J., Brown, J. D., Pearson, P. A., & Ashton, P. 1992, "Subconjunctival sustained release 5-fluorouracil", *Investigative Ophthalmology and Visual Science*, vol. 33, no. 12, pp. 3430-3435.

BNF 2009, *British national formulary 59*, NO.59 edn, British Medical Association and the Pharmaceutical Society of Great Britain.

Broadway, D. C., Bloom, P. A., Bunce, C., Thiagarajan, M., & Khaw, P. T. 2004, "Needle revision of failing and failed trabeculectomy blebs with adjunctive 5-fluorouracil: Survival analysis", *Ophthalmology*, vol. 111, no. 4, pp. 665-673.

Brubaker, R. F., Nagataki, S., & Townsend, D. J. 1981, "The effect of age on aqueous humor formation in man", *Ophthalmology*, vol. 88, no. 3, pp. 283-288.

Buur, A. & Bundgaard, H. 1984, "Prodrugs of 5-fluorouracil. I. Hydrolysis kinetics and physicochemical properties of various N-acyl derivatives of 5-fluorouracil", *International Journal of Pharmaceutics*, vol. 21, no. 3, pp. 349-364.

Cairns, J. E. 1968, "Trabeculectomy. Preliminary report of a new method", *American Journal of Ophthalmology*, vol. 66, no. 4, pp. 673-679.

Chang, D. F., Garcia, I. H., Hunkeler, J. D., & Minas, T. 1999, "Phase II results of an intraocular steroid delivery system for cataract surgery", *Ophthalmology*, vol. 106, no. 6, pp. 1172-1177.

Charles, J. B., Ganthier, J., Wilson, M. R., Lee, D. A., Baker, R. S., Leong, K. W., & Glasgow, B. J. 1991, "Use of bioerodible polymers impregnated with mitomycin in glaucoma filtration surgery in rabbits", *Ophthalmology*, vol. 98, no. 4, pp. 503-508.

Chiang, C. H., Tung, S. M., Lu, D. W., & Yeh, M. K. 2001, "In vitro and in vivo evaluation of an ocular delivery system of 5-fluorouracil microspheres", *Journal of Ocular Pharmacology and Therapeutics*, vol. 17, no. 6, pp. 545-553.

Chu, D., Gu, J., Liu, W., Fawcett, J. P., & Dong, Q. 2003, "Sensitive liquid chromatographic assay for the simultaneous determination of 5-fluorouracil and its prodrug, tegafur, in beagle dog plasma", *Journal of Chromatography B: Analytical Technologies in the Biomedical and Life Sciences*, vol. 795, no. 2, pp. 377-382.

Coker, A. K. & Kayode, C. A. 2001, "Reaction Rate Expression," in *Modeling of Chemical Kinetics and Reactor Design*, A. K. Coker, Ph.D., & A. K. Coker, eds., Gulf Professional Publishing, Woburn, pp. 109-217.

Cordeiro, M. F., Chang, L., Lim, K. S., Daniels, J. T., Pleass, R. D., Siriwardena, D., & Khaw, P. T. 2000a, "Modulating conjunctival wound healing", *Eye*, vol. 14, no. 3 B, pp. 536-547.

Cordeiro, M. F., Siriwardena, D., Chang, L., & Khaw, P. T. 2000b, "Wound healing modulation after glaucoma surgery", *Current Opinion in Ophthalmology*, vol. 11, no. 2, pp. 121-126.

Cramer, C. J. & Truhlar, D. G. 1995, "Continuum solvation models: Classical and quantum mechanical implementations", *Reviews in Computational Chemistry*, vol. 6, no. 1, pp. 1-72.

Crowston, J. G., Akbar, A. N., Constable, P. H., Occleston, N. L., Daniels, J. T., & Khaw, P. T. 1998, "Antimetabolite-induced apoptosis in Tenon's capsule fibroblasts", *Investigative Ophthalmology and Visual Science*, vol. 39, no. 2, pp. 449-454.

Cui, L. J., Sun, N. X., Li, X. H., Huang, J., & Yang, J. G. 2008, "Subconjunctival sustained release 5-fluorouracil for glaucoma filtration surgery", *Acta Pharmacologica Sinica*, vol. 29, no. 9, pp. 1021-1028.

Daniels, J. T., Cambrey, A. D., Occleston, N. L., Garrett, Q., Tarnuzzer, R. W., Schultz, G. S., & Khaw, P. T. 2003, "Matrix metalloproteinase inhibition modulates fibroblast-mediated matrix contraction and collagen production in vitro", *Investigative Ophthalmology and Visual Science*, vol. 44, no. 3, pp. 1104-1110.

Desjardins, D. C., Parrish II, R. K., & Folberg, R. 1986, "Wound healing after filtering surgery in owl monkeys", *Archives of Ophthalmology*, vol. 104, no. 12, pp. 1835-1839.

Dodson, G. G., Lane, D. P., & Verma, C. S. 2008, "Molecular simulations of protein dynamics: New windows on mechanisms in biology", *EMBO Reports*, vol. 9, no. 2, pp. 144-150.

Dormn, G., Cseh, S., Hajd, I., Barna, L., Knya, D., Kupai, K., Kovcs, L., & Ferdinandy, P. 2010, "Matrix metalloproteinase inhibitors: A critical appraisal of design principles and proposed therapeutic utility", *Drugs*, vol. 70, no. 8, pp. 949-964.

Dozorova, I. I., Karina, L. M., Kolchanova, L. A., Krymov, A. P., & Demchenko, B. I. 1987, "Analysis of pharmacopoeia-grade triamcinolone", *Pharmaceutical Chemistry Journal*, vol. 20, no. 6, pp. 432-433.

Dvorak, H. F. 1986, "Tumors: Wounds that do not heal: Similarities between tumor stroma generation and wound healing", *New England Journal of Medicine*, vol. 315, no. 26, pp. 1650-1659.

Einmahl, S., Ponsart, S., Bejjani, R. A., D'Hermies, F., Savoldelli, M., Heller, J., Tabatabay, C., Gurny, R., & Behar-Cohen, F. 2003, "Ocular biocompatibility of a poly(ortho ester) characterized by autocatalyzed degradation", *J.Biomed.Mater.Res.A*, vol. 67, no. 1, pp. 44-53.

Einmahl, S., Capancioni, S., Schwach-Abdellaoui, K., Moeller, M., Behar-Cohen, F., & Gurny, R. 2001, "Therapeutic applications of viscous and injectable poly(ortho esters)", *Advanced Drug Delivery Reviews*, vol. 53, no. 1, pp. 45-73.

Fadda, H., Gasford, S., Ru, Q., Khaw, P., & Brocchini, S. Understanding Changes in the Solid Phase Properties of Tissue Tablets on Exposure to Aqueous Media. Invest.Ophthalmol.Vis.Sci. 51[E-abstract 5311]. 2010.
Ref Type: Abstract

Falck, J., Skuta, G. L., & Klein, T. B. 1992, "Mitomycin versus 5-fluorouracil antimetabolite therapy for glaucoma filtration surgery", *Seminars in Ophthalmology*, vol. 7, no. 2, pp. 97-109.

Fallon III, L. 1973, "The crystal and molecular structure of 5-fluorouracil", *Acta Crystallogr.* pp. 2549-2556.

Filippopoulos, T., Hanna, E., Chen, T. C., Grosskreutz, C. L., Jakobiec, F. A., & Pasquale, L. R. 2009, "Correlation of filtration bleb morphology with histology", *International Ophthalmology Clinics*, vol. 49, no. 1, pp. 71-82.

Fingleton, B. 2007, "Matrix metalloproteinases as valid clinical targets", *Current Pharmaceutical Design*, vol. 13, no. 3, pp. 333-346.

Fini, M. E., Cui, T. Y., Mouldovan, A., Grobelny, D., Galardy, R. E., & Fisher, S. J. 1991, "An inhibitor of the matrix metalloproteinase synthesized by rabbit corneal epithelium", *Investigative Ophthalmology and Visual Science*, vol. 32, no. 11, pp. 2997-3001.

Frasco, M. F. & Chaniotakis, N. 2010, "Bioconjugated quantum dots as fluorescent probes for bioanalytical applications", *Analytical and Bioanalytical Chemistry*, vol. 396, no. 1, pp. 229-240.

Furrer, P. & Gurny, R. 2010, "Recent advances in confocal microscopy for studying drug delivery to the eye: Concepts and pharmaceutical applications", *European Journal of Pharmaceutics and Biopharmaceutics*, vol. 74, no. 1, pp. 33-40.

Galardy, R. E., Cassabonne, M. E., Giese, C., Gilbert, J. H., Lapierre, F., Lopez, H., Schaefer, M. E., Stack, R., Sullivan, M., Summers, B., Tressler, R., Tyrrell, D., Wee, J., Allen, S. D., Castellot, J. J., Barletta, J. P., Schultz, G. S., Fernandez, L. A., & Fisher, S. 1994, "Low molecular weight inhibitors in corneal ulceration", *Annals of the New York Academy of Sciences*, vol. 732, pp. 315-323.

Gamelin, E., Boisdron-Celle, M., Turcant, A., Larra, F., Allain, P., & Robert, J. 1997, "Rapid and sensitive high-performance liquid chromatographic analysis of halogenopyrimidines in plasma", *Journal of Chromatography B: Biomedical Applications*, vol. 695, no. 2, pp. 409-416.

Gao, X., Yang, L., Petros, J. A., Marshall, F. F., Simons, J. W., & Nie, S. 2005, "In vivo molecular and cellular imaging with quantum dots", *Current Opinion in Biotechnology*, vol. 16, no. 1 SPEC. ISS., pp. 63-72.

Garcia, R. & Perez, R. 2002, "Dynamic atomic force microscopy methods", *Surface*

*Science Reports*, vol. 47, no. 6-8, pp. 197-301.

Georgoulas S.D., Ru Q., Brocchini S., & Khaw P. A Novel Single Application Prolonged Release MMP Inhibitor Is Superior to Mitomycin in Preventing Scarring After Experimental Glaucoma Surgery. Invest.Ophthalmol.Vis.Sci. 49[E-Abstract 4538]. 2008.
Ref Type: Abstract

Georgoulas, S. 2010, *Novel Methods For the Modulation of Wound Healing After Glaucoma Filtration Surgery*.

Giessibl, F. J. 2003, "Advances in atomic force microscopy", *Reviews of Modern Physics*, vol. 75, no. 3, pp. 949-983.

Gilman AG, Rall TW, & Nies AS 1990, *Goodman and Gilman's the pharmacological basis of therapeutics*, 8th ed edn, New York Oxford : Pergamon, c1990.

Goa, K. L. & Benfield, P. 1994, "Hyaluronic acid. A review of its pharmacology and use as a surgical aid in ophthalmology, and its therapeutic potential in joint disease and wound healing", *Drugs*, vol. 47, no. 3, pp. 536-566.

Gokce, M. F., Akata RF FAU - Kiremitci-Gumusderelioglu, & Kiremitci-Gumusderelioglu, M. "5-FU loaded pHEMA drainage implants for glaucoma-filtering surgery: device design and in vitro release kinetics", no. 0142-9612 (Print).

Gomes dos Santos, A. L., Bochot, A., Doyle, A., Tsapis, N., Siepmann, J., Siepmann, F., Schmaler, J., Besnard, M., Behar-Cohen, F., & Fattal, E. 2006, "Sustained release of nanosized complexes of polyethylenimine and anti-TGF-beta2 oligonucleotide improves the outcome of glaucoma surgery", *Journal of Controlled Release*, vol. 112, no. 3, pp. 369-381.

Goodman, D. F., Alvarado, J. A., & Stern, W. 1987, "Liposomal incorporated 5-fluoroorotate inhibition of wound healing following posterior lip sclerectomy in the primate", *Invest Ophthalmol Vis Sci*, vol. 28, p. 271.

Gould, L., Trope, G., Cheng, Y. L., Heathcote, J. G., Sheardown, H., Rootman, D., Liu, G. S., & Menon, I. A. 1994, "Fifty:fifty poly (DL glycolic acid-lactic acid) copolymer as a drug delivery system for 5-fluorouracil: A histopathological evaluation", *Canadian Journal of Ophthalmology*, vol. 29, no. 4, pp. 168-171.

Grigera, J. R. 2002, "Molecular dynamics simulation for ligand-receptor studies. Carbohydrates interactions in aqueous solutions", *Current Pharmaceutical Design*, vol. 8, no. 17, pp. 1579-1604.

Grisanti, S., Diestelhorst, M., Heimann, K., & Krieglstein, G. 1999, "Cellular photoablation to control postoperative fibrosis in a rabbit model of filtration surgery", *British Journal of Ophthalmology*, vol. 83, no. 12, pp. 1353-1359.

Gumbart, J., Wang, Y., Aksimentiev, A., Tajkhorshid, E., & Schulten, K. 2005, "Molecular dynamics simulations of proteins in lipid bilayers", *Current Opinion in Structural Biology*, vol. 15, no. 4, pp. 423-431.

Guthoff, R., Klink, T., Schlunck, G., & Grehn, F. 2006, "In vivo confocal microscopy of failing and functioning filtering blebs: Results and clinical correlations", *Journal of Glaucoma*, vol. 15, no. 6, pp. 552-558.

H.Ohtaki, N.Fukushima, E.Hayakawa, & I.Okada 1988, "Dissolution process of sodium chloride crystal in water", *Pure and Applied Chemistry*, vol. 60, no. 8, pp. 1321-1324.

Hamad, S., Moon, C., Richard, C., Catlow, A., Hulme, A. T., & Price, S. L. 2006, "Kinetic insights into the role of the solvent in the polymorphism of 5-fluorouracil from molecular dynamics simulations", *Journal of Physical Chemistry B*, vol. 110, no. 7, pp. 3323-3329.

Han, L. H., Elliott, J. A., Bentham, A. C., Mills, A., Amidon, G. E., & Hancock, B. C. 2008, "A modified Drucker-Prager Cap model for die compaction simulation of pharmaceutical powders", *International Journal of Solids and Structures*, vol. 45, no. 10, pp. 3088-3106.

Hanyu, T. 1999, "The effects of single mitomycin C application on the expression of matrix metalloproteinase in the sclera and aqueous of albino rabbits", *Journal of Japanese Ophthalmological Society*, vol. 103, no. 3, pp. 186-192.

Haran, G., Haas, E., & Rapaport, D. C. 1994, "Molecular dynamics simulations of simple peptide models: Solvent effects and comparison with experiment", *Journal of Physical Chemistry*, vol. 98, no. 40, pp. 10294-10302.

Hartmann, V. & Keipert, S. 2000, "Physico-chemical, in vitro and in vivo characterisation of polymers for ocular use", *Pharmazie*, vol. 55, no. 6, pp. 440-443.

Hascall, V. C. & Laurent, T. C. Hyaluronan: Structure and Physical Properties. http://www.glycoforum.gr.jp/science/hyaluronan/HA01/HA01E.html . 2007.
Ref Type: Electronic Citation

Helfferich, F. G. 2004, "Kinetics of multistep reactions: Preface to second edition", *Comprehensive Chemical Kinetics*, vol. 40.

Heller, J. 2005, "Ocular delivery using poly(ortho esters)", *Adv.Drug Deliv.Rev.*, vol. 57, no. 14, pp. 2053-2062.

Heller, J., Barr, J., Ng, S. Y., Abdellauoi, K. S., & Gurny, R. 2002, "Poly(ortho esters): Synthesis, characterization, properties and uses", *Advanced Drug Delivery Reviews*, vol. 54, no. 7, pp. 1015-1039.

Heller, J., Barr, J., Ng, S. Y., Shen, H. R., Schwach-Abdellaoui, K., Emmahl, S., Rothen-Weinhold, A., & Gurny, R. 2000, "Poly(ortho esters) - Their development and

some recent applications", *European Journal of Pharmaceutics and Biopharmaceutics*, vol. 50, no. 1, pp. 121-128.

Heller, J., Ng, S. Y., Penhale, D. W., Fritzinger, B. K., Sanders, L. M., Burns, R. A., Gaynon, M. G., & Bhosale, S. S. 1987, "Use of poly(ortho esters) for the controlled release of 5-fluorouracyl and a LHRH analogue", *Journal of Controlled Release*, vol. 6, no. 1, pp. 217-224.

Herschler, J. & Sherwood, M. B. 1992, "Long-term results of trabeculectomy with collagen sponge implant containing low-dose antimetabolite", *Ophthalmology*, vol. 99, no. 5, pp. 666-671.

Hild, W. A., Breunig, M., & Goepferich, A. 2008, "Quantum dots - Nano-sized probes for the exploration of cellular and intracellular targeting", *European Journal of Pharmaceutics and Biopharmaceutics*, vol. 68, no. 2, pp. 153-168.

Hollo, G., Whitson, J. T., Faulkner, R., McCue, B., Curtis, M., Wieland, H., Chastain, J., Sanders, M., DeSantis, L., Przydryga, J., & Dahlin, D. C. 2006, "Concentrations of betaxolol in ocular tissues of patients with glaucoma and normal monkeys after 1 month of topical ocular administration", *Investigative Ophthalmology and Visual Science*, vol. 47, no. 1, pp. 235-240.

Hostyn, P., Villain, F., Malek-Chehire, N., Kuhne, F., Takesue, Y., Parrish II, R. K., & Parel, J. M. 1996, "Controlled drug release implant for 5-FU adjuvant therapy in glaucoma surgery. Experimental study", *Journal Francais d'Ophtalmologie*, vol. 19, no. 2, pp. 133-139.

How, A., Chua, J. L., Charlton, A., Su, R., Lim, M., Kumar, R. S., Crowston, J. G., & Wong, T. T. 2010, "Combined treatment with bevacizumab and 5-fluorouracil attenuates the postoperative scarring response after experimental glaucoma filtration surgery", *Investigative ophthalmology & visual science*, vol. 51, no. 2, pp. 928-932.

Hu, T., Le, Q., Wu, Z., & Wu, W. 2007, "Determination of doxorubicin in rabbit ocular tissues and pharmacokinetics after intravitreal injection of a single dose of doxorubicin-loaded poly-beta-hydroxybutyrate microspheres", *Journal of Pharmaceutical and Biomedical Analysis*, vol. 43, no. 1, pp. 263-269.

Huhtala, A., Ronkko, S., Terasvirta, M., Puustjarvi, T., Sihvola, R., Vehanen, K., Laukkanen, A., Anttila, J., Urtti, A., Pohjonen, T., & Uusitalo, H. 2009, "The effects of 5-fluorouracil on ocular tissues in vitro and in vivo after controlled release from a multifunctional implant", *Invest Ophthalmol Vis Sci*, vol. 50, no. 5, pp. 2216-2223.

Hulme, A. T., Price, S. L., & Tocher, D. A. 2005, "A new polymorph of 5-fluorouracil found following computational crystal structure predictions", *Journal of the American Chemical Society*, vol. 127, no. 4, pp. 1116-1117.

Humphrey, W., Dalke, A., & Schulten, K. 1996, "VMD: Visual molecular dynamics", *Journal of Molecular Graphics*, vol. 14, no. 1, pp. 33-38.

Jacob, J. T., Lacour, O. J., & Burgoyne, C. F. 2001, "Slow release of the antimetabolite 5-fluorouracil (5-FU) from modified Baerveldt glaucoma drains to prolong drain function", *Biomaterials*, vol. 22, no. 24, pp. 3329-3335.

Jampel, H. D., Leong, K. W., Dunkelburger, G. R., & Quigley, H. A. 1990, "Glaucoma filtration surgery in monkeys using 5-fluorouridine in polyanhydride disks", *Archives of Ophthalmology*, vol. 108, no. 3, pp. 430-435.

Jarus, G., Blumenkranz, M., Hernandez, E., & Sossi, N. 1985, "Clearance of intravitreal fluorouracil. Normal and aphakic vitrectomized eyes", *Ophthalmology*, vol. 92, no. 1, pp. 91-96.

Jones, E., Clarke, J., & Khaw, P. T. 2005, "Recent advances in trabeculectomy technique", *Current Opinion in Ophthalmology*, vol. 16, no. 2, pp. 107-113.

Kakhi, M. 2009, "Mathematical modeling of the fluid dynamics in the flow-through cell", *International Journal of Pharmaceutics*, vol. 376, no. 1-2, pp. 22-40.

Karamertzanis, P. G., Raiteri, P., Parrinello, M., Leslie, M., & Price, S. L. 2008, "The thermal stability of lattice-energy minima of 5-fluorouracil: metadynamics as an aid to polymorph prediction", *Journal of Physical Chemistry B*, vol. 112, no. 14, pp. 4298-4308.

Kaufman P.L. & Alm A. 2003, *Adler's Physiology of the Eye: Clinical Application*, 10th ed edn, Mosby, Incorporated.

Kawasaki, S., Mizoue, S., Yamaguchi, M., Shiraishi, A., Zheng, X., Hayashi, Y., & Ohashi, Y. 2009, "Evaluation of filtering bleb function by thermography", *British Journal of Ophthalmology*, vol. 93, no. 10, pp. 1331-1336.

Kay, J. S., Litin, B. S., & Jones, M. A. 1986, "Delivery of antifibroblast agents as adjuncts to filtration surgery - Part II: Delivery of 5-fluorouracil and bleomycin in a collagen implant: Pilot study in the rabbit", *Ophthalmic Surgery*, vol. 17, no. 12, pp. 796-801.

Kearns, V. R. & Williams, R. L. 2009, "Drug delivery systems for the eye", *Expert Review of Medical Devices*, vol. 6, no. 3, pp. 277-290.

Khaw P, Georgoulas S, Dahlmann A H, Ru Q, Martin B, & Brocchini S 2009, " Future Strategies," in *Glaucoma Volume Two: Surgical Management*, Shaarawy T et al., eds., Elsevier Health Sciences.

Khaw, P. T., Chang, L., Wong, T. T. L., Mead, A., Daniels, J. T., & Cordeiro, M. F. 2001, "Modulation of wound healing after glaucoma surgery", *Current Opinion in Ophthalmology*, vol. 12, no. 2, pp. 143-148.

Khaw, P. T., Doyle, J. W., Sherwood, M. B., Smith, M. F., & McGorray, S. 1993, "Effects of intraoperative 5-fluorouracil or mitomycin C on glaucoma filtration surgery

in the rabbit", *Ophthalmology*, vol. 100, no. 3, pp. 367-372.

Khaw, P. T., Ward, S., Porter, A., Grierson, I., Hitchings, R. A., & Rice, N. S. 1992, "The long-term effects of 5-fluorouracil and sodium butyrate on human Tenon's fibroblasts", *Invest Ophthalmol.Vis.Sci.*, vol. 33, no. 6, pp. 2043-2052.

Khaw, P. T. 1995, *The effects of growth factors and antiproliferative agents on ocular fibroblasts and wound healing after glaucoma filtration surgery*.

Kim, S. J., Lee, C. K., Lee, Y. M., Kim, I. Y., & Kim, S. I. 2003, "Electrical/pH-sensitive swelling behavior of polyelectrolyte hydrogels prepared with hyaluronic acid-poly(vinyl alcohol) interpenetrating polymer networks", *Reactive and Functional Polymers*, vol. 55, no. 3, pp. 291-298.

Kim, Y. S. & Rousseau, R. W. 2004, "Characterization and solid-state transformations of the pseudopolymorphic forms of sodium naproxen", *Crystal Growth and Design*, vol. 4, no. 6, pp. 1211-1216.

Kimura, H. & Ogura, Y. 2001, "Biodegradable polymers for ocular drug delivery", *Ophthalmologica*, vol. 215, no. 3, pp. 143-155.

Kimura, H., Ogura, Y., Moritera, T., Honda, Y., Wada, R., Hyon, S. H., & Ikada, Y. 1992, "Injectable microspheres with controlled drug release for glaucoma filtering surgery", *Investigative Ophthalmology and Visual Science*, vol. 33, no. 12, pp. 3436-3441.

King, A. J., Rotchford, A. P., Alwitry, A., & Moodie, J. 2007, "Frequency of bleb manipulations after trabeculectomy surgery", *Br.J.Ophthalmol.*, vol. 91, no. 7, pp. 873-877.

Kiremitci-Gumusderelioglu, M., Gokce, M., & Akata, R. F. 1996, "A novel MMC-loaded pHEMA drainage device for the treatment of glaucoma: in vitro and in vivo studies", *J.Biomater.Sci.Polym.Ed*, vol. 7, no. 10, pp. 857-869.

Knapp, S., Bertelmann, E., Hartmann, C., Keipert, S., & Pleyer, U. 2003, "Intraocular availability of topically applied mycophenolate mofetil in rabbits", *Journal of Ocular Pharmacology and Therapeutics*, vol. 19, no. 2, pp. 181-192.

Koskela, T. & Brubaker, R. F. 1991, "The nocturnal suppression of aqueous humor flow in humans is not blocked by bright light", *Investigative Ophthalmology and Visual Science*, vol. 32, no. 9, pp. 2504-2506.

Labbe, A., Dupas, B. n. d., Hamard, P., & Baudouin, C. 2005, "In Vivo Confocal Microscopy Study of Blebs after Filtering Surgery", *Ophthalmology*, vol. 112, no. 11, p. 1979.

Lama, P. J. & Fechtner, R. D. 2003, "Antifibrotics and Wound Healing in Glaucoma Surgery", *Survey of Ophthalmology*, vol. 48, no. 3, pp. 314-346.

Levy, J., Tessler, Z., Rosenthal, G., Klemperer, I., Zirkin, H. J., Kachko, L., & Lifshitz, T. 2001, "Toxic effects of subconjunctival 5-fluorouracil and mitomycin C on ciliary body of rats", *Int.Ophthalmol.*, vol. 24, no. 4, pp. 199-203.

Li, C., Cantor, W. J., Nili, N., Robinson, R., Fenkell, L., Le Tran, Y., Whittingham, H. A., Tsui, W., Cheema, A. N., Sparkes, J. D., Pritzker, K., Levy, D. E., & Strauss, B. H. 2002, "Arterial repair after stenting and the effects of GM6001, a matrix metalloproteinase inhibitor", *Journal of the American College of Cardiology*, vol. 39, no. 11, pp. 1852-1858.

Liu, Q. Y., Bei, Y. L., Qi, G. B., & Ding, Y. J. 2008, "Thermal decomposition kinetics of 5-fluorouracil from thermogravimetric analysis", *Korean Journal of Chemical Engineering*, vol. 25, no. 5, pp. 980-981.

Longley, D. B., Harkin, D. P., & Johnston, P. G. 2003, "5-Fluorouracil: Mechanisms of action and clinical strategies", *Nature Reviews Cancer*, vol. 3, no. 5, pp. 330-338.

Lu, Z. R. 2010, "Molecular imaging of HPMA copolymers: Visualizing drug delivery in cell, mouse and man", *Advanced Drug Delivery Reviews*, vol. 62, no. 2, pp. 246-257.

Maren, T. H. 1973, "Observations on the rates of ion movement and hypercapnia in aqueous humor", *Experimental Eye Research*, vol. 16, no. 5, pp. 403-411.

McLaren, J. W. 2009, "Measurement of aqueous humor flow", *Experimental Eye Research*, vol. 88, no. 4, pp. 641-647.

Merkli, A., Heller, J., Tabatabay, C., & Gurny, R. 1994, "Semi-solid hydrophobic bioerodible poly(ortho ester) for potential application in glaucoma filtering surgery", *Journal of Controlled Release*, vol. 29, no. 1-2, pp. 105-112.

Michalopoulos, G. K. & DeFrances, M. C. 1997, "Liver regeneration", *Science*, vol. 276, no. 5309, pp. 60-66.

Mietz, H. 1996, "The toxicology of mitomycin C on the ciliary body", *Current Opinion in Ophthalmology*, vol. 7, no. 2, pp. 72-79.

Mietz, H., Addicks, K., Bloch, W., & Krieglstein, G. K. 1996, "Long-term intraocular toxic effects of topical mitomycin C in rabbits", *Journal of Glaucoma*, vol. 5, no. 5, pp. 325-333.

Mietz, H., Addicks, K., Diestelhorst, M., & Krieglstein, G. K. 1994, "Extraocular application of mitomycin C in a rabbit model: Cytotoxic effects on the ciliary body and epithelium", *Ophthalmic Surgery*, vol. 25, no. 4, pp. 240-244.

Miller, M. H., Grierson, I., Unger, W. G., & Hitchings, R. A. 1990, "The effect of topical dexamethasone and preoperative beta irradiation on a model of glaucoma fistulizing surgery in the rabbit", *Ophthalmic Surgery*, vol. 21, no. 1, pp. 44-54.

Miller, M. H., Grierson, I., Unger, W. I., & Hitchings, R. A. 1989, "Wound healing in an animal model of glaucoma fistulizing surgery in the rabbit", *Ophthalmic Surgery*, vol. 20, no. 5, pp. 350-357.

Millipore. GM6001 MMP Inhibitor Powder. 2010.
Ref Type: Data File

Mohamadi, F., Richards, N. G. J., Guida, W. C., Liskamp, R., Lipton, M., Caufield, C., Chang, G., Hendrickson, T., & Still, W. C. 1990, "MacroModel - An integrated software system for modeling organic and bioorganic molecules using molecular mechanics", *J.Comput.Chem.*, vol. 11, pp. 440-467.

Mollan, S. P., Wolffsohn, J. S., Nessim, M., Laiquzzaman, M., Sivakumar, S., Hartley, S., & Shah, S. 2008, "Accuracy of Goldmann, ocular response analyser, Pascal and TonoPen XL tonometry in keratoconic and normal eyes", *British Journal of Ophthalmology*, vol. 92, no. 12, pp. 1661-1665.

Monnot, E. A., Kindberg, C. G., Johnson, T. S., Riley, C. M., Stobaugh, J. F., & Slavik, M. 1990, "Stability of intravenous admixtures of 5-fluorouracil and spirogermanium, a novel combination of cytotoxic agents", *International Journal of Pharmaceutics*, vol. 60, no. 1, pp. 41-52.

Mora, C. P. & Martinez, F. 2006, "Thermodynamic quantities relative to solution processes of Naproxen in aqueous media at pH 1.2 and 7.4", *Physics and Chemistry of Liquids*, vol. 44, no. 5, pp. 585-596.

Morra, G., Meli, M., & Colombo, G. 2008, "Molecular dynamics simulations of proteins and peptides: From folding to drug design", *Current Protein and Peptide Science*, vol. 9, no. 2, pp. 181-196.

Moura Filho, E. R. & Sit, A. J. 2009, "Advances in glaucoma surgery", *Expert Review of Ophthalmology*, vol. 4, no. 6, pp. 595-605.

Noecker, R. J. 2006, "The management of glaucoma and intraocular hypertension: Current approaches and recent advances", *Therapeutics and Clinical Risk Management*, vol. 2, no. 2, pp. 193-206.

Orlov, A., Imre, A., Csaba, G., Ji, L., Porod, W., & Bernstein, G. H. 2008, "Magnetic quantum-dot cellular automata: Recent developments and prospects", *Journal of Nanoelectronics and Optoelectronics*, vol. 3, no. 1, pp. 55-68.

Palanca-Capistrano, A. M., Hall, J., Cantor, L. B., Morgan, L., Hoop, J., & WuDunn, D. 2009, "Long-term Outcomes of Intraoperative 5-Fluorouracil versus Intraoperative Mitomycin C in Primary Trabeculectomy Surgery", *Ophthalmology*, vol. 116, no. 2, pp. 185-190.

Pedretti, A., Villa, L., & Vistoli, G. 2004, "VEGA - An open platform to develop chemo-bio-informatics applications, using plug-in architecture and script programming",

*Journal of Computer-Aided Molecular Design*, vol. 18, no. 3, pp. 167-173.

Pharmacia. Healon GV Package insert. 2007.
Ref Type: Data File

Picht, G. & Grehn, F. 1998, "Classification of filtering blebs in trabeculectomy: Biomicroscopy and functionality", *Current Opinion in Ophthalmology*, vol. 9, no. 2, pp. 2-8.

Polak, M. B., Valamanesh, F., Felt, O., Torriglia, A., Jeanny, J. C., Bourges, J. L., Rat, P., Thomas-Doyle, A., Benezra, D., Gurny, R., & Behar-Cohen, F. 2008, "Controlled delivery of 5-chlorouracil using poly(ortho esters) in filtering surgery for glaucoma", *Investigative Ophthalmology and Visual Science*, vol. 49, no. 7, pp. 2993-3003.

Pollack, I. P. & Patz, A. 1976, "Argon laser iridotomy: an experimental and clinical study", *Ophthalmic Surgery*, vol. 7, no. 1, pp. 22-30.

Quigley, H. & Broman, A. T. 2006, "The number of people with glaucoma worldwide in 2010 and 2020", *British Journal of Ophthalmology*, vol. 90, no. 3, pp. 262-267.

Rabowsky, J. H., Dukes, A. J., Lee, D. A., & Leong, K. W. 1996, "The use of bioerodible polymers and daunorubicin in glaucoma filtration surgery", *Ophthalmology*, vol. 103, no. 5, pp. 800-807.

Rahman, I., Cannon, P. S., & Sadiq, S. A. 2010, "Tonopen versus goldmann applanation tonometry for detecting restrictive thyroid eye disease", *Ophthalmic Plastic and Reconstructive Surgery*, vol. 26, no. 1, pp. 36-38.

Reinmuller, J. 2003, "Hyaluronic acid", *Aesthetic Surgery Journal*, vol. 23, no. 4, pp. 309-311.

Reiss, G. R., Lee, D. A., Topper, J. E., & Brubaker, R. F. 1984, "Aqueous humor flow during sleep", *Investigative Ophthalmology and Visual Science*, vol. 25, no. 6, pp. 776-778.

Resnikoff, S., Pascolini, D., Etya'ale, D., Kocur, I., Pararajasegaram, R., Pokharel, G. P., & Mariotti, S. P. 2004, "Global data on visual impairment in the year 2002", *Bulletin of the World Health Organization*, vol. 82, no. 11, pp. 844-851.

Reznick, L. G., Noecker, R. J., & Lathrop, K. 2007, "Trabeculectomy - An efficient and successful technique", *Techniques in Ophthalmology*, vol. 5, no. 1, pp. 27-32.

Rodrigues, L. B., Leite, H. F., Yoshida, M. I., Saliba, J. B., Junior, A. S. C., & Faraco, A. A. G. 2009, "In vitro release and characterization of chitosan films as dexamethasone carrier", *International Journal of Pharmaceutics*, vol. 368, no. 1-2, pp. 1-6.

Rolim, D. M. C., Paranhos, A., & Wormald, R. 2007, "Laser trabeculoplasty for open angle glaucoma", *Cochrane Database of Systematic Reviews* no. 4.

Rootman, J., Ostry, A., & Gudauskas, G. 1984, "Pharmacokinetics and metabolism of 5-fluorouracil following subconjunctival versus intravenous administration", *Canadian Journal of Ophthalmology*, vol. 19, no. 4, pp. 187-191.

Roth, S. M., Spaeth, G. L., Starita, R. J., Birbillis, E. M., & Steinmann, W. C. 1991, "The effects of postoperative corticosteroids on trabeculectomy and the clinical course of glaucoma: Five-year follow-up study", *Ophthalmic Surgery*, vol. 22, no. 12, pp. 724-729.

Sanchez-Castillo, F. X., Anwar, J., & Heyes, D. M. 2003a, "Molecular dynamics simulations of granular compaction", *Chemistry of Materials*, vol. 15, no. 18, pp. 3417-3430.

Sanchez-Castillo, F. X., Anwar, J., & Heyes, D. M. 2003b, "Molecular dynamics simulations of granular compaction: The single granule case", *Journal of Chemical Physics*, vol. 118, no. 10, pp. 4636-4648.

Schraermeyer, U., Diestelhorst, M., Bieker, A., Theisohn, M., Mietz, H., Ustundag, C., Joseph, G., & Krieglstein, G. K. 1999, "Morphologic proof of the toxicity of mitomycin C on the ciliary body in relation to different application methods", *Graefe's Archive for Clinical and Experimental Ophthalmology*, vol. 237, no. 7, pp. 593-600.

Schuman, J. S. 2000, "Antiglaucoma medications: A review of safety and tolerability issues related to their use", *Clinical Therapeutics*, vol. 22, no. 2, pp. 167-208.

Seah, S. K. L., Husain, R., Gazzard, G., Lim, M. C. C., Hoh, S. T., Oen, F. T. S., & Aung, T. 2005, "Use of Surodex in Phacotrabeculectomy Surgery", *American Journal of Ophthalmology*, vol. 139, no. 5, pp. 927-928.

Seetner, A. & Morin, J. D. 1979, "Healing of trabeculectomies in rabbits", *Canadian Journal of Ophthalmology*, vol. 14, no. 2, pp. 121-125.

Shen.Y. 2004, *Prolonged ophthalmic release of 5-Fluorouracil*.

Simmons, S. T., Sherwood, M. B., Nichols, D. A., Penne, R. B., Sery, T., & Spaeth, G. L. 1988, "Pharmacokinetics of a 5-fluorouracil liposomal delivery system", *British Journal of Ophthalmology*, vol. 72, no. 9, pp. 688-691.

Singh, B. N., Singh, R. B., & Singh, J. 2005, "Effects of ionization and penetration enhancers on the transdermal delivery of 5-fluorouracil through excised human stratum corneum", *International Journal of Pharmaceutics*, vol. 298, no. 1, pp. 98-107.

Singh, K., Egbert, P. R., Byrd, S., Budenz, D. L., Williams, A. S., Decker, J. H., & Dadzie, P. 1997, "Trabeculectomy with intraoperative 5-fluorouracil vs mitomycin C", *American Journal of Ophthalmology*, vol. 123, no. 1, pp. 48-53.

Singh, P., Tyagi, G., Mehrotra, R., & Bakhshi, A. K. 2009, "Thermal stability studies of 5-fluorouracil using diffuse reflectance infrared spectroscopy", *Drug Testing and*

*Analysis*, vol. 1, no. 5, pp. 240-244.

Siu, C. K., Fox-Beyer, B. S., Beyer, M. K., & Bondybey, V. E. 2006, "Ab initio molecular dynamics studies of ionic dissolution and precipitation of sodium chloride and silver chloride in water clusters, $NaCl(H_2O)_n$ and $AgCl(H_2O)_n$, n = 6, 10, and 14", *Chemistry - A European Journal*, vol. 12, no. 24, pp. 6382-6392.

Skuta, G. L., Assil, K., Parrish 2nd., R. K., Folberg, R., & Weinreb, R. N. 1987, "Filtering surgery in owl monkeys treated with the antimetabolite 5-fluorouridine 5'-monophosphate entrapped in multivesicular liposomes", *American Journal of Ophthalmology*, vol. 103, no. 5, pp. 714-716.

Smith, A. M., Duan, H., Mohs, A. M., & Nie, S. 2008, "Bioconjugated quantum dots for in vivo molecular and cellular imaging", *Advanced Drug Delivery Reviews*, vol. 60, no. 11, pp. 1226-1240.

Smith, S., D'Amore, P. A., & Dreyer, E. B. 1994, "Comparative toxicity of mitomycin C and 5-fluorouracil in vitro", *American Journal of Ophthalmology*, vol. 118, no. 3, pp. 332-337.

Smith, T. J. & Ashton, P. 1996, "Sustained-release subconjunctival 5-fluorouracil", *Ophthalmic Surgery and Lasers*, vol. 27, no. 9, pp. 763-767.

Stamper, R. L. 2011, "A history of intraocular pressure and its measurement", *Optometry and Vision Science*, vol. 88, no. 1, p. E16-E28.

Starita, R. J., Fellman, R. L., & Spaeth, G. L. 1985, "Short- and long-term effects of postoperative corticosteroids on trabeculectomy", *Ophthalmology*, vol. 92, no. 7, pp. 938-946.

Stein, J. D. & Challa, P. 2007, "Mechanisms of action and efficacy of argon laser trabeculoplasty and selective laser trabeculoplasty", *Current Opinion in Ophthalmology*, vol. 18, no. 2, pp. 140-145.

Still, W. C., Tempczyk, A., Hawley, R. C., & Hendrickson, T. 1990, "Semianalytical treatment of solvation for molecular mechanics and dynamics", *Journal of the American Chemical Society*, vol. 112, no. 16, pp. 6127-6129.

Suihko, E., Poso, A., Korhonen, O., Gynther, J., Ketolainen, J., & Paronen, P. 2000, "Deformation behaviors of tolbutamide, hydroxypropyl-beta-cyclodextrin, and their dispersions", *Pharmaceutical Research*, vol. 17, no. 8, pp. 942-948.

Suitchmezian, V., Jess, I., & Nather, C. 2007, "Investigations on the polymorphism and pseudopolymorphism of the glucocorticoid triamcinolone: New findings for a well-known drug", *Crystal Growth and Design*, vol. 7, no. 1, pp. 69-74.

Sunkara, G. & Kompella, U. B. 2003, "Membrane Transport Processes in the Eye," in *Ophthalmic Drug Delivery Systems, Second Edition*, 2nd edition edn, Ashim K.Mitra,

ed., Informa Healthcare, pp. 13-58.

Tahery, M. M. & Lee, D. A. 1989, "Review: Pharmacologic control of wound healing in glaucoma filtration surgery", *Journal of Ocular Pharmacology*, vol. 5, no. 2, pp. 155-179.

Tan, D. T. H., Chee, S. P., Lim, L., & Lim, A. S. M. 1999, "Randomized clinical trial of a new dexamethasone delivery system (Surodex) for treatment of post-cataract surgery inflammation", *Ophthalmology*, vol. 106, no. 2, pp. 223-231.

Theelen, T., Wesseling, P., Keunen, J. E. E., & Klevering, B. J. 2007, "A pilot study on slit lamp-adapted optical coherence tomography imaging of trabeculectomy filtering blebs", *Graefe's Archive for Clinical and Experimental Ophthalmology*, vol. 245, no. 6, pp. 877-882.

Ticho, U. 1977, "Laser application to the angle structures in rabbits, cats, and in human glaucomatous eyes", *Documenta Ophthalmologica*, vol. 43, no. 1, pp. 115-125.

Ticho, U. & Zauberman, H. 1976, "Argon laser application to the angle structures in glaucomas", *Archives of Ophthalmology*, vol. 94, no. 1, pp. 61-64.

Tilleul, P., Denis, P., Maignen, F., Elena, P. P., Nordmann, J. P., Leverge, R., & Rostene, W. 1997, "Effects of different formulations of mitoxantrone (solutions, nanospheres, liposomes) on glaucoma surgery in rabbits", *Ophthalmic Res.*, vol. 29, no. 4, pp. 218-226.

Toris, C. B., Koepsell, S. A., Yablonski, M. E., & Camras, C. B. 2002, "Aqueous humor dynamics in ocular hypertensive patients", *Journal of Glaucoma*, vol. 11, no. 3, pp. 253-258.

Trope, G. E., Cheng, Y. L., Sheardown, H., Liu, G. S., Menon, I. A., Heathcote, J. G., Rootman, D. S., Chiu, W. J., & Gould, L. 1994, "Depot drug delivery system for 5-fluorouracil after filtration surgery in the rabbit", *Canadian Journal of Ophthalmology*, vol. 29, no. 6, pp. 263-267.

Turner, D. T. & Schwartz, A. 1985, "The glass transition temperature of poly(N-vinyl pyrrolidone) by differential scanning calorimetry", *Polymer*, vol. 26, no. 5, pp. 757-762.

Uppal, P., Jampel, H. D., Quigley, H. A., & Leong, K. W. 1994, "Pharmacokinetics of etoposide delivery by a bioerodible drug carrier implanted at glaucoma surgery", *Journal of Ocular Pharmacology*, vol. 10, no. 2, pp. 471-479.

Veeco. HarmoniX Nanoscale Material Property Mapping - exclusively from Veeco. http://www.veeco.com/promos/default.aspx?PromoID=25 . 2010.
Ref Type: Electronic Citation

Wagner, M. S., McArthur, S. L., Shen, M., Horbett, T. A., & Castner, D. G. 2002, "Limits of detection for time of flight secondary ion mass spectrometry (ToF-SIMS) and

X-ray photoelectron spectroscopy (XPS): Detection of low amounts of adsorbed protein", *Journal of Biomaterials Science, Polymer Edition*, vol. 13, no. 4, pp. 407-428.

Wald, J., Muller, C., Wahl, M., Hoth-Hannig, W., Hannig, M., Kopnarski, M., & Ziegler, C. 2010, "ToF-SIMS investigations of adsorbed proteins on dental titanium", *Physica Status Solidi (A) Applications and Materials*, vol. 207, no. 4, pp. 831-836.

Wang, G., Tucker, I. G., Roberts, M. S., & Hirst, L. W. 1996, "In vitro and in vivo evaluation in rabbits of a controlled release 5-fluorouracil subconjunctival implant based on Poly(D,L-lactide-co-glycolide)", *Pharmaceutical Research*, vol. 13, no. 7, pp. 1059-1064.

Washington, C. 1989, "Evaluation of non-sink dialysis methods for the measurement of drug release from colloids: effects of drug partition", *International Journal of Pharmaceutics*, vol. 56, no. 1, pp. 71-74.

Wilmsmeyer, S., Mueller, H., Ness, T., & Funk, J. 2003, "Excimer laser trabeculotomy: A new minimal invasive procedure to reduce intraticular pressure", *Investigative Ophthalmology & Visual Science*, vol. 44, p. U224.

Wilson, C. J., Clegg, R. E., Leavesley, D. I., & Pearcy, M. J. 2005, "Mediation of biomaterial-cell interactions by adsorbed proteins: A review", *Tissue Engineering*, vol. 11, no. 1-2, pp. 1-18.

Wise, J. B. 1981, "Long-term control of adult open angle glaucoma by argon laser treatment", *Ophthalmology*, vol. 88, no. 3, pp. 197-202.

Wise, J. B. & Witter, S. L. 1979, "Argon laser therapy for open-angle glaucoma. A pilot study", *Archives of Ophthalmology*, vol. 97, no. 2, pp. 319-322.

Wollstein, G., Garway-Heath, D. F., Poinoosawmy, D., & Hitchings, R. A. 2000, "Trabeculectomy with intraoperative mitomycin C versus 5-fluorouracil: Prospective randomized clinical trial", *Ophthalmology*, vol. 107, no. 12, pp. 2305-2309.

Wong, T. T., Mead, A. L., & Khaw, P. T. 2005, "Prolonged antiscarring effects of ilomastat and MMC after experimental glaucoma filtration surgery", *Invest Ophthalmol.Vis.Sci.*, vol. 46, no. 6, pp. 2018-2022.

Wong, T. T., Shen, Y., Jing-Jang, C., Ru, Q., Brocchini, S., & Khaw, P. 5-FU Combined With Hyaluronic Acid: Effect on Drug Release Rate. Investigative Ophthalmology and Visual Science 47[E-Abstract 42]. 2006.
Ref Type: Abstract

Wong, T. T. L., Mead, A. L., & Khaw, P. T. 2003, "Matrix metalloproteinase inhibition modulates postoperative scarring after experimental glaucoma filtration surgery", *Investigative Ophthalmology and Visual Science*, vol. 44, no. 3, pp. 1097-1103.

Wong, T. T. L., Sethi, C., Daniels, J. T., Limb, G. A., Murphy, G., & Khaw, P. T. 2002,

"Matrix Metalloproteinases in Disease and Repair Processes in the Anterior Segment", *Survey of Ophthalmology*, vol. 47, no. 3, pp. 239-256.

Wudunn, D., Cantor, L. B., Palanca-Capistrano, A. M., Hoop, J., Alvi, N. P., Finley, C., Lakhani, V., Burnstein, A., & Knotts, S. L. 2002, "A prospective randomized trial comparing intraoperative 5-fluorouracil vs mitomycin C in primary trabeculectomy", *American Journal of Ophthalmology*, vol. 134, no. 4, pp. 521-528.

Yalkowsky, S. & He, Y. 2003, *Handbook of Aqueous Solubility Data* CRC Press.

Yeh, M. K., Tung, S. M., Lu, D. W., Chen, J. L., & Chiang, C. H. 2001, "Formulation factors for preparing ocular biodegradable delivery system of 5-fluorouracil microparticles", *Journal of Microencapsulation*, vol. 18, no. 4, pp. 507-519.

Yong Yang, Sheng Meng, & E G Wang 2006, "A molecular dynamics study of hydration and dissolution of NaCl nanocrystal in liquid water", *JOURNAL OF PHYSICS: CONDENSED MATTER*, vol. 18, no. 45, pp. 10165-10177.

Zahn, D. 2004, "Molecular dynamics investigation of the pressure induced B1 to B2 phase transitions of RbBr", *Journal of Solid State Chemistry*, vol. 177, no. 10, pp. 3590-3594.

Zhang, Y., Lukacova, V., Bartus, V., Nie, X., Sun, G., Manivannan, E., Ghorpade, S. R., Jin, X., Manyem, S., Sibi, M. P., Cook, G. R., & Balaz, S. 2008, "Binding of matrix metalloproteinase inhibitors to extracellular matrix: 3D-QSAR analysis", *Chemical Biology and Drug Design*, vol. 72, no. 4, pp. 237-248.

Zignani, M., Bernatchez, S. F., Le, M. T., Tabatabay, C., Anderson, J. M., & Gurny, R. 1998, "Subconjunctival biocompatibility of a viscous bioerodable poly(ortho ester)", *J.Biomed.Mater.Res.*, vol. 39, no. 2, pp. 277-285.

Zignani, M., Einmahl, S., Baeyens, V., Varesio, E., Veuthey, J. L., Anderson, J., Heller, J., Tabatabay, C., & Gurny, R. 2000a, "A poly(ortho ester) designed for combined ocular delivery of dexamethasone sodium phosphate and 5-fluorouracil: Subconjunctival tolerance and in vitro release", *European Journal of Pharmaceutics and Biopharmaceutics*, vol. 50, no. 2, pp. 251-255.

Zignani, M., Le, M. T., Einmahl, S., Tabatabay, C., Heller, J., Anderson, J. M., & Gurny, R. 2000b, "Improved biocompatibility of a viscous bioerodible poly(ortho ester) by controlling the environmental pH during degradation", *Biomaterials*, vol. 21, no. 17, pp. 1773-1778.

Zignani, M., Merkli, A., Sintzel, M. B., Bernatchez, S. F., Kloeti, W., Heller, J., Tabatabay, C., & Gurny, R. 1997, "New generation of poly(ortho esters): synthesis, characterization, kinetics, sterilization and biocompatibility", *Journal of Controlled Release*, vol. 48, no. 2-3, pp. 115-129.